



Optimization of Dense Medium Cyclone Plant for the Beneficiation of Low Grade Iron Ore with Associated High Proportion of Near-Density Material at Sishen Iron Ore Mine

by

Phakamile Tom (9110806D)

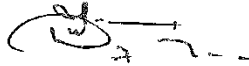
Report submitted to the Faculty of Engineering and the Built Environment, University of the Witwatersrand, Johannesburg in partial fulfilment for the degree of Master of Science in Engineering (Metallurgy and Materials Engineering)

Supervisor(s): Dr Murray M Bwalya

08 July 2015

DECLARATION

I declare that, apart from the acknowledged sources and assistance, this research report for the Master of Science in Engineering (Metallurgy and Materials) degree to the School of Chemical and Metallurgical Engineering, Faculty of Engineering and the Built Environment at the University of the Witwatersrand is my own work and has not been submitted by me or another person for a degree at this university or another institution of higher education.



Phakamile Tom

08 July 2015

ABSTRACT

The research report is premised on three aspects which are critical in the heavy mineral beneficiation. These aspects are classified as (i) understanding the densimetric profile of the available ore body, (ii) understanding the properties of the heavy medium utilised at the plant to beneficiate the ore, and (iii) the automation and modelling of the processing plant in order to maximise plant efficiency.

Ore characterisation is mainly focused on understanding the densimetric profile of the ore body, in order to determine the probability of producing a saleable product as well as predicting the expected yields and quality. This is done to utilise the endowment entrusted upon the operating entity by the government and shareholders to treat the mineral resource to its full potential. Understanding of the beneficiation potential of the ore body will assist the mine planning and processing plant to optimise the product tons and quality. This will ensure the marketing plans are in accordance with the expected product as beneficiation will vary depending on the mining block reserves. The mining blocks have potential to produce varying product grades with different recoveries.

Ore characterisation was conducted on the GR80 mining block, low-grade stockpiles (i.e. C-grade ore reserves & Jig discard and dense medium separation (DMS) run-of-mine (ROM) material. The GR80 material was characterised as having low proportion of near-density material and would be easy to beneficiate as well as produce high volumes of high grade product. Furthermore, it was revealed that the 2014 DMS ROM had an increased proportion of low-density material; however this material also had low proportion of near-density material.

The low-grade stockpiles was characterised by high proportion of near density material, which necessitate the beneficiation process to operate at high density in excess of 3.8 t/m^3 . Maintaining a higher operating density requires more dense medium which leads to viscosity problems and impact performance.

The characterisation of the FeSi medium was imperative to understand its behaviour and potential influence on beneficiation of low-grade stockpiles and mining blocks with elevated proportion of near-density material. As the proportion of near-density waste material increases in the run-of-mine (ROM), it is necessary to beneficiate the material at elevated operating medium densities. However, when cyclones are operated at high densities, the negative influence of the medium viscosity becomes more apparent and thus influences the separation efficiency.

Heavy medium, ferrosilicon (FeSi) characterisation looked at identifying the effects of viscosity

on the FeSi stability and whether there would be a need for a viscosity modifier. Thus, the importance of controlling the stability, viscosity, and density of the medium cannot be underestimated and can very often override the improvements attainable through better designs of cyclones. Furthermore, the slurry mixture of the heavy medium utilised for the purpose of dense medium separation should be non-detrimental to the effectiveness of separation in the DMS Fine cyclone plant. Medium characterisation showed that removal of ultra-fines leads to unstable media as indicated by faster settling rates. This would result in medium segregation in the beneficiation cyclone thereby leading to unacceptable high density differential which will negatively impact the cut-point shift and cause high yield losses to waste.

The overall control of the metallurgical processes at Sishen's Cyclone Plant is still done manually and thus operation still varies from person-to-person and/or from shift-to-shift. This result in some of the process data and trends not being available online as well as being captured inaccurately. Furthermore, this negatively affects the traceability and reproducibility of the production metallurgical key performance indicators (KPI's) as well as process stability and efficiency.

It has been demonstrated that real-time online measurements are crucial to maintaining processing plant stability and efficiency thereby ensuring that the final product grade and its value is not eroded. Modelling and automation of the key metallurgical parameters for the cyclone plant circuit was achieved by installation of appropriate instrumentation and interlocking to the programmable logic control (PLC). This allowed for the control of the correct medium sump level, cyclone inlet pressure, medium-to-ore ratio as well as online monitoring of density differential as "proxy" for medium rheological characteristics.

The benefit of modelling and simulation allows the virtual investigation and optimisation of the processing plant efficiency as well as analysis of the impact of varying ore characteristics, throughput variations and changing operating parameters. Due to the high tonnage for the iron ore cyclone plant a modest increase in plant efficiency such as 1.5% yield increase would have a large impact on plant profitability. Therefore it is imperative that all cyclone operating modules are operated at the same efficiency which can be achieved by optimized process through proper automation and monitoring, thereby improving the total plant profitability.

ACKNOWLEDGEMENT

I would like to express my deepest appreciation to my MSc Eng. supervisor, Dr Mulenga Bwalya, for guiding me in applying my undergraduate knowledge and improving my modelling and simulation skills. This work would not be possible without his intelligent guidance and extraordinary inspiration.

It is my pleasure to thank the plant management of Sishen Mine for entrusting me with managing the optimisation and automation of the DMS cyclone plant. I would also like to thank my sub-ordinates who took my instruction in taking process control samples and ensuring that are delivered to respective laboratories for characterisation and conducting some process monitoring in support of my project.

Special thanks go to my young brother, Zweli Tom, "*an education enthusiast*", for his encouragement and support which have always been a source of inspiration in my work and for lending me his ears in time of doubt.

I would also like to express my sincere appreciation and thanks to my wife, Fikile and dedicate this research report to my precious children Monwabisi, Thobekile, Keabetswe and Sthembiso.

TABLE OF CONTENTS

DECLARATION.....	I
ABSTRACT	II
ACKNOWLEDGEMENT	IV
TABLE OF CONTENTS	V
LIST OF FIGURES	VIII
LIST OF TABLES.....	XII
ACRONYMS AND DEFINITIONS.....	XIII
ACRONYMS	XIII
DEFINITION OF TERMS.....	XIII
CHAPTER 1: INTRODUCTION	- 1 -
1 BACKGROUND.....	- 1 -
1.1 SISHEN DMS CYCLONE PLANT CIRCUIT	- 2 -
1.2 PROBLEM STATEMENT.....	- 5 -
1.3 RESEARCH OBJECTIVE(S):.....	- 6 -
CHAPTER 2: LITERATURE SURVEY	- 8 -
2 LITERATURE REVIEW	- 8 -
2.1 WHAT IS DENSE MEDIUM SEPARATION	- 8 -
2.2 THEORY OF DENSE MEDIUM SEPARATION IN CYCLONE.....	- 8 -
2.2.1 <i>Factors Influencing Dense Medium Beneficiation</i>	- 11 -
2.2.2 <i>Importance of Dense Medium Rheological Characteristics</i>	- 13 -
2.2.3 <i>Cyclone Performance Measure</i>	- 16 -
2.2.4 <i>Online Measurement, Control and Modelling</i>	- 19 -
CHAPTER 3: METHODOLOGY	- 25 -
3 EXPERIMENTAL APPROACH.....	- 25 -
3.1 ORE CHARACTERIZATION	- 25 -
3.2 PROCESS FESi CHARACTERIZATION.....	- 25 -
3.2.1 <i>Coarse FeSi Less Fines</i>	- 28 -
3.2.2 <i>Process FeSi</i>	- 28 -
3.2.3 <i>Process FeSi Less Fines</i>	- 29 -

3.2.4	<i>Viscosity Modifier</i>	- 29 -
3.3	PILOT TESTING OF AUTOMATED CYCLONE MODULE	- 29 -
CHAPTER 4: ORE AND FESI CHARACTERISATION		- 35 -
4	ORE AND FESI CHARACTERISATION RESULTS	- 35 -
4.1	ORE CHARACTERISATION INTRODUCTION	- 35 -
4.1.1	<i>Ore Densimetric and Chemical Analysis</i>	- 35 -
4.1.2	<i>Characterisation Results of DMS Head Grade ROM Composite Samples</i>	- 35 -
4.1.2.1	Impact of cut-density versus Ep	- 37 -
4.1.3	<i>Ore Characterisation Results of GR80 Mining Area Ore body</i>	- 40 -
4.1.4	<i>Interpretation of Data for Samples from the Low Grade Stockpiles</i>	- 44 -
4.1.5	<i>Interpretation of Data for Samples from the Actual Pilot Plant Processing</i>	- 47 -
4.1.6	<i>Summary of Ore Characterisation and Processing Results</i>	- 51 -
4.2	FESI CHARACTERISATION INTRODUCTION.....	- 52 -
4.2.1	<i>FeSi Rheology Test Results</i>	- 52 -
4.2.2	<i>Effect of Viscosity on FeSi Stability</i>	- 54 -
4.2.3	<i>Material Property Test Results</i>	- 54 -
4.2.4	<i>Solids Density Results</i>	- 54 -
4.2.5	<i>Particle Size Analysis</i>	- 55 -
4.2.6	<i>FeSi Stability Tests</i>	- 56 -
4.2.6.1	Stability Test No 1: Static Settling Test Results.....	- 57 -
4.2.6.2	Stability Test No 2: Vertical Pipe Settling Tests.....	- 59 -
4.2.7	<i>Comparison of Static and Vertical Pipe Settling Test Results</i>	- 62 -
4.2.8	<i>Tube Viscometer Test Results</i>	- 63 -
4.2.9	<i>Summary of FeSi Characterisation Tests Results</i>	- 67 -
CHAPTER 5: CYCLONE PLANT AUTOMATION AND CONTROL		- 69 -
5	AUTOMATION AND CONTROL INTRODUCTION	- 69 -
5.1	AUTOMATED MODULE VERSUS TRADITIONAL MODULE	- 72 -
5.2	MODULE 811 PERFORMANCE TRENDS	- 74 -
5.2.1	<i>Monitoring and Control of Medium-to-Ore Ratio</i>	- 75 -
5.2.2	<i>Monitoring and Control of Cyclone Inlet Pressure</i>	- 77 -
5.2.3	<i>Monitoring and Control of Density Differential Measurement</i>	- 81 -

CHAPTER 6: MODELLING OF DENSE MEDIUM CYCLONE CIRCUIT	- 84 -
6 DENSE MEDIUM CYCLONE MODELLING INTRODUCTION.....	- 84 -
6.1 CORRECT MEDIUM SUMP LEVEL MODELLING	- 85 -
6.2 CYCLONE PERFORMANCE MODELLING	- 89 -
CHAPTER 7: CONCLUSIONS AND RECOMMENDATIONS.....	- 96 -
7 CONCLUSIONS AND RECOMMENDATIONS	- 96 -
7.1 CONCLUSIONS	- 96 -
7.1.1 Ore and FeSi Characterisation Conclusions	- 96 -
7.1.2 Automation and Modelling Conclusions	- 97 -
7.2 RECOMMENDATIONS FOR FUTURE WORK.....	- 98 -
REFERENCES AND APPENDICES.....	- 99 -
REFERENCES	- 99 -
APPENDICES	- 102 -
APPENDIX A: ORE CHARACTERISATION	- 102 -
7.2.1 Appendix A.1 – Material Type Classification.....	- 102 -
7.2.2 Appendix A.2 - Densimetric Analysis Results of DMS Head Grade ROM	- 103 -
7.2.3 Appendix A.3 - Densimetric Analysis Results of GR80 Mining Block	- 106 -
7.2.4 Appendix A.4 - Densimetric Analysis Results of ROM from the Low Grade Stockpiles.....	- 108 -
7.2.5 Appendix A.5 - Chemical and Densimetric Analysis Results of Material Treated through the Ultra-High Density DMS	- 111 -
APPENDIX B: FeSi CHARACTERISATION.....	- 113 -
7.2.6 Appendix B.1 - Viscosity Modifier Specification.....	- 113 -
7.2.7 Appendix B.2 - Particle Size Analysis of FeSi	- 114 -
7.2.8 Appendix B.3 - Pipe Loop Settling Data.....	- 118 -
7.2.9 Appendix B.4 - Vertical Pipe loop Test Data	- 128 -
APPENDIX C: CITECT SCADA DISPLAY	- 131 -

List of Figures

FIGURE 1.1: CYCLONE MEDIUM FLOW LINE	- 3 -
FIGURE 1.2: CYCLONE PLANT ORE FLOW LINE MAJOR EQUIPMENT.....	- 4 -
FIGURE 1.3: MATERIAL CLASSIFICATION AND DMS ROM FEED GRADES	- 5 -
FIGURE 2.1: TYPICAL CYCLONE EQUIPMENT SHOWING (A) PARTICLE TRAJECTORY, AND (B) FORCES ACTING ON A PARTICLE IN A CYCLONE. (KING, 2001); (ANON., N.D.),.....	- 9 -
FIGURE 2.2: TOMOGRAM AT FEED DENSITY OF 1.40 G/CM ³	- 10 -
FIGURE 2.3: TOMOGRAM AT ASSUMED DENSITY PROFILE AT FEED DENSITY OF 3.60 T/M ³	- 11 -
FIGURE 2.4: PERFORMANCE INDICATORS AND FACTORS AFFECTING DENSE MEDIUM CYCLONE PERFORMANCE	- 12 -
FIGURE 2.5: TYPICAL RHEOGRAM	- 14 -
FIGURE 2.6: SCHEMATIC EXPLANATION OF VARIABLES ON MEDIUM RHEOLOGY.....	- 16 -
FIGURE 2.7: GRAPHICAL REPRESENTATION OF (A) TROMP CURVE, AND (B) EP VS. PARTICLE SIZE. (WILLS & NAPIER-MUNN, 2006).....	- 17 -
FIGURE 2.8: TYPICAL CYCLONE SPIGOT OPERATING CONDITIONS (I) FLARING AND (II) ROPE DISCHARGE	- 19 -
FIGURE 2.9: DISTRIBUTION OF PRESSURE INSIDE THE DENSE MEDIUM CYCLONE (WANG, 2009) .	- 20 -
FIGURE 2.10: GENERAL STRUCTURE OF THE CONTROL CONFIGURATION (STEPHANOPOULOS, 1984) .	- 21 -
FIGURE 2.11: (A) CAPCOAL AND (B) VENETIA'S CYCLONE INLET PRESSURE INSTRUMENTS.....	- 21 -
FIGURE 2.12: VENETIA'S MEDIUM HEAD BALANCE ACROSS MODULE AND ITS IMPACT OF CYCLONE INLET PRESSURE	- 22 -
FIGURE 3.1: TYPICAL XRF AND QEMSCAN SET-UP IN SISHEN AND ANGLO RESEARCH LABS	- 25 -
FIGURE 3.2: SCHEMATIC DIAGRAM OF VERTICAL TUBE VISCOMETER SET-UP AT P&C LAB	- 27 -
FIGURE 3.3: PHOTOGRAPH OF PIPE LOOP SETTLING TEST EQUIPMENT	- 28 -
FIGURE 3.4: SCHEMATIC DIAGRAM OF PIPE LOOP SETTLING TEST EQUIPMENT.....	- 28 -
FIGURE 3.5: DENSITY DIFFERENTIAL METHODS.....	- 32 -
FIGURE 3.6: INSTALLATION OF DENSITY DIFFERENTIAL MEASURING INSTRUMENTS (DMCT110 UNITS) .	- 34 -
FIGURE 4.1: DENSIMETRIC PROFILE OF THE DMS HEAD GRADE ROM SAMPLES.....	- 36 -
FIGURE 4.2: CHEMICAL QUALITY OF THE DMS HEAD GRADE ROM SAMPLES.....	- 36 -

FIGURE 4.3: EFFECT OF ROM'S DENSIMETRIC PROFILE ON YIELD AT CUT-DENSITY OF 3.6 T/M ³ AND EP~0.17	- 37 -
FIGURE 4.4: PREDICTED YIELD AND QUALITY AS FUNCTION OF EP AND CUT-DENSITY.....	- 38 -
FIGURE 4.5: 2014 DMS ROM COMPOSITIONS SUMMARY	- 39 -
FIGURE 4.6: DETAILED ROM COMPOSITIONS – MATERIAL CLASS	- 40 -
FIGURE 4.7: DETAILED ROM MATERIAL COMPOSITION – MATERIAL BLEND.....	- 40 -
FIGURE 4.8: DENSIMETRIC ANALYSIS OF COMBINED GR80 SAMPLES	- 41 -
FIGURE 4.9: IMPACT OF NEAR DENSITY MATERIAL OF BENEFICIATION (PLANT 1 VS. PLANT 8).....	- 42 -
FIGURE 4.10: DENSIMETRIC PROFILE AS A FUNCTION OF MATERIAL PARTICLE SIZE DISTRIBUTION. -	43 -
FIGURE 4.11: COMBINED DENSIMETRIC ANALYSIS OF SAMPLES FROM LOW-GRADE STOCKPILES... -	45 -
FIGURE 4.12: COMPARISON OF BENEFICIATION POTENTIAL DIFFERENT LOW-GRADE STOCKPILES ORE TYPES	- 46 -
FIGURE 4.13: DENSIMETRIC PROFILE OF FEED MATERIAL PROCESSED THROUGH UHDMS	- 47 -
FIGURE 4.14: YIELD AND PRODUCT GRADE PREDICTION (A) LOW-GRADE STOCKPILE (B) JIG DISCARD -	48 -
FIGURE 4.15: OBSERVED VS. PREDICTED CUT-DENSITY DURING PROCESSING OF LOW-GRADE STOCKPILE MATERIAL	- 49 -
FIGURE 4.16: OBSERVED VS. PREDICTED CUT-DENSITY DURING PROCESSING OF JIG DISCARD MATERIAL	- 50 -
FIGURE 4.17: SUMMARY OF DENSIMETRIC ANALYSIS FOR THE GR80 VS. LOW-GRADE VS. 2014 DMS ROM SAMPLES	- 51 -
FIGURE 4.18: PSEUDO SHEAR DIAGRAM OF SISHEN PROCESS FESi	- 53 -
FIGURE 4.19: FLUID CONSISTENCY INDEX AS A FUNCTION OF DENSITY AND MASS SOLIDS CONCENTRATION FOR THE PSEUDO-PLASTIC MODELLED PROCESS FESi	- 53 -
FIGURE 4.20: ρ_M , CW, ρ_S AND CV RELATIONSHIP FOR THE COARSE FESi.....	- 55 -
FIGURE 4.21: ρ_M , CW, ρ_S AND CV RELATIONSHIP FOR THE PROCESS FESi.....	- 55 -
FIGURE 4.22: ROSIN-RAMMLER REGRESSION OF THE PARTICLE SIZE BY SIEVE ANALYSIS OF THE (A) COARSE FESi AS DELIVERED AND (B) COARSE FESi LESS FINES	- 56 -
FIGURE 4.23: ROSIN-RAMMLER REGRESSION OF THE PARTICLE SIZE BY SIEVE ANALYSIS OF THE (A) PROCESS FESi AS DELIVERED AND (B) PROCESS FESi LESS FINES	- 56 -
FIGURE 4.24: COMPARISON OF THE TWO TYPES OF SETTLING TESTS AND RESULTS	- 57 -
FIGURE 4.25: BENCH TOP SETTLING TESTS FOR COARSE FESi LESS FINES.....	- 58 -
FIGURE 4.26: BENCH TOP SETTLING TESTS FOR PROCESS FESi LESS FINES.....	- 58 -

FIGURE 4.27: BENCH TOP SETTLING TESTS FOR COARSE FeSi WITH VISCOSITY MODIFIER	- 58 -
FIGURE 4.28: COMPARISON OF BENCH TOP SETTLING TEST RESULTS AT A DENSITY OF 4000 KG/M ³ ...	59 -
FIGURE 4.29: PIPE LOOP SETTLING TEST RESULTS FOR COARSE FeSi LESS FINES.....	- 60 -
FIGURE 4.30: PIPE LOOP SETTLING TEST RESULTS FOR PROCESS FeSi.....	- 60 -
FIGURE 4.31: PIPE LOOP SETTLING TEST RESULTS FOR PROCESS FeSi LESS FINES	- 61 -
FIGURE 4.32: PIPE LOOP SETTLING TEST RESULTS FOR COARSE FeSi WITH VISCOSITY MODIFIER	- 61 -
FIGURE 4.33: PIPE LOOP SETTLING TEST RESULTS AT SLURRY DENSITY OF APPROXIMATELY 3900 KG/M ³	- 62 -
FIGURE 4.34: CLEAR WATER TEST RESULTS	- 63 -
FIGURE 4.35: PSEUDO SHEAR DIAGRAM OF COARSE FeSi LESS FINES	- 64 -
FIGURE 4.36: PSEUDO SHEAR DIAGRAM FOR PROCESS FeSi LESS FINES	- 64 -
FIGURE 4.37: PSEUDO SHEAR DIAGRAM COMPARING PROCESS FeSi TO PROCESS FeSi LESS FINES AT APPROXIMATELY 3900 KG/M ³	- 65 -
FIGURE 4.38: PSEUDO SHEAR DIAGRAM COMPARING PROCESS FeSi TO PROCESS FeSi LESS FINES AT APPROXIMATELY 3800 KG/M ³	- 65 -
FIGURE 4.39: PSEUDO SHEAR DIAGRAM COMPARING PROCESS FeSi TO PROCESS FeSi LESS FINES AT APPROXIMATELY 3660 KG/M ³	- 65 -
FIGURE 4.40: PSEUDO SHEAR DIAGRAM OF COARSE FeSi WITH VISCOSITY MODIFIER ADDED.....	- 66 -
FIGURE 4.41: PSEUDO SHEAR DIAGRAM OF COARSE FeSi AT A DENSITY OF APPROXIMATELY 4500 KG/M ³ WITH AND WITHOUT VISCOSITY MODIFIER ADDED.....	- 66 -
FIGURE 4.42: PSEUDO SHEAR DIAGRAM OF COARSE FeSi AT A DENSITY OF APPROXIMATELY 4260 KG/M ³ WITH AND WITHOUT VISCOSITY MODIFIER ADDED.....	- 67 -
FIGURE 4.43: PSEUDO SHEAR DIAGRAM OF COARSE FeSi AT A DENSITY OF APPROXIMATELY 3980 KG/M ³ WITH AND WITHOUT VISCOSITY MODIFIER ADDED.....	- 67 -
FIGURE 5.1: GENERAL MODULE LAYOUT OF WITH INSTRUMENTS FOR MONITORING AND CONTROL (TOM, 2014).....	- 71 -
FIGURE 5.2: GENERIC LAYER OF CONTROLS (DE VILLIERS, ET AL., 2014)	- 72 -
FIGURE 5.3: SUMP LEVEL INDICATORS	- 73 -
FIGURE 5.4: CYCLONE INLET PRESSURE TRANSMITTER	- 73 -
FIGURE 5.5: NON-CONTACT SONARTRAC FLOWMETER INSTALLATION IN CORRECT MEDIA PIPELINE ..	74 -
FIGURE 5.6: MEDIUM-TO-ORE RATIO DISPLAY IN CITECT SCADA.....	- 75 -

FIGURE 5.7: MEDIUM-TO-ORE RATIO TRENDS	- 75 -
FIGURE 5.8: MEDIUM FLOW RATE AS FUNCTION OF MEDIUM SUMP LEVEL	- 76 -
FIGURE 5.9: CONTAMINANT LEVELS IN THE FINE PRODUCT	- 76 -
FIGURE 5.10: LAYOUT OF THE MODULE FEED STREAMS.....	- 77 -
FIGURE 5.11: CYCLONE INLET PIPE ARRANGEMENT	- 77 -
FIGURE 5.12: CYCLONE AND CLUSTER MONITORING DISPLAY IN THE SCADA	- 78 -
FIGURE 5.13: MODULE INLET PRESSURE TRENDS AND SPIGOT FLARE CONDITIONS.....	- 79 -
FIGURE 5.14: CYCLONE CLUSTER BALANCE	- 80 -
FIGURE 5.15: CYCLONE CLUSTER FEED FLOW RATE.....	- 80 -
FIGURE 5.16: FESi MEDIUM DENSITY TRENDS	- 81 -
FIGURE 5.17: ONLINE DENSITY DIFFERENTIAL TRENDS.....	- 82 -
FIGURE 5.18: MANUAL DENSITY DIFFERENTIAL	- 82 -
FIGURE 5.19: RELATIONSHIP OF THE UNDERFLOW MEDIUM DENSITY WITH AND WITHOUT WATER DILUTION	- 83 -
FIGURE 6.1: CYCLONE MODULE MEDIUM FLOW LINE	- 85 -
FIGURE 6.2: SIMPLIFIED REPRESENTATION OF CORRECT MEDIUM TANK.....	- 86 -
FIGURE 6.3: SIMULINK STRUCTURE FOR THE CORRECT MEDIUM TANK LEVEL CONTROL.....	- 87 -
FIGURE 6.4: SIMULATED RESPONSE OF THE CORRECT MEDIUM SUMP LEVEL.....	- 88 -
FIGURE 6.5: PLANT MEASURED CORRECT MEDIUM SUMP LEVEL	- 89 -
FIGURE 6.6: INTERNAL STRUCTURE OF THE SIMULINK MODEL FOR THE MODELLING OF THE CYCLONE UNDERFLOW AND OVERFLOW DENSITY.....	- 90 -
FIGURE 6.7: SUBSYSTEM OF THE INTERNAL STRUCTURE OF MODELLING OF THE CYCLONE UNDERFLOW AND OVERFLOW DENSITY.....	- 91 -
FIGURE 6.8: SUBSYSTEM OF THE INTERNAL STRUCTURE OF MODELLING OF THE MEDIUM SPLIT WITHIN THE DENSE MEDIUM CYCLONE	- 91 -
FIGURE 6.9: SIMULATED RESPONSE INDICATING THE RESULT OF CYCLONE UNDERFLOW & OVERFLOW DENSITY	- 93 -
FIGURE 6.10: MODEL RESPONSE FOR UNDERFLOW AND OVERFLOW DENSITY AS FUNCTION OF MEDIUM FLOW RATE	- 94 -
FIGURE 6.11: MODEL RESPONSE FOR UNDERFLOW AND OVERFLOW DENSITY AS FUNCTION OF OPERATING DENSITY	- 95 -

List of Tables

TABLE 1.1: TYPICAL HEAD GRADE OF A-CLASS ROM IN SISHEN (SRK CONSULTING ENGINEERS, 2006).....	- 1 -
TABLE 2.1: RHEOLOGICAL MODELS	- 13 -
TABLE 2.2: TYPICAL PARTITION CURVE MODELS FOR DENSE MEDIUM SEPARATION.....	- 18 -
TABLE 3.1: TYPICAL VALUES OF DENSITY DIFFERENTIAL FOR DENSE MEDIUM SEPARATORS (KING, 2001).....	- 32 -
TABLE 4.1: GR80 BULK SAMPLES DESCRIPTIONS	- 41 -
TABLE 4.2: YIELD AND QUALITY PREDICTIONS FOR AT 3.6 T/M ³ CUT-POINT AND EP OF 0.11	- 44 -
TABLE 4.3: YIELD AND PRODUCT QUALITY PREDICTIONS FOR LOW-GRADE MATERIAL AT 3.8 T/M ³ CUT-POINT AND EP OF 0.11	- 45 -
TABLE 4.4: MODELLING THE PERFORMANCE UHDMS OPERATION USING PARTITION CURVE MODELS .	- 50 -
TABLE 4.5: RHEOLOGICAL CORRELATIONS FOR PROCESS FESi	- 54 -
TABLE 4.6: MATERIAL PROPERTIES OF COARSE AND PROCESS FESi LESS FINES	- 54 -
TABLE 4.7: COMPARISON OF FESi SETTLING TEST RESULTS	- 62 -

ACRONYMS AND DEFINITIONS

ACRONYMS

ACARP	Australian Coal Association Research Program
BIF	Banded iron formation material type
DMS	Dense medium separation
FeSi	Ferrosilicon
CHPP	Coal Handling and Processing Plant
Ep	Ecart Probable Moyen
JKMRC	Julius Kruttschnitt Mineral Research Centre
KGT	Conglomerate material type
KPI	Key performance indicator
M:O	Medium-to-ore ratio
P&C	Paterson and Cooke
PLC	Programmable Logic Controller
PSD	Particle Size Distribution
RD	Relative density, normally unit less. This can be assumed as t/m ³ .
ROM	Run-of-mine, defined as the feed from the mining area to be beneficiated.
SCADA	Supervisory Control and Data Acquisition
SG	Specific gravity
SK	Shale material type

DEFINITION OF TERMS

Terminology	Description
Coarse FeSi	: Fresh coarse FeSi supplied by Exxaro uncontaminated with iron ore slimes.
Dense media	: Refers to the solids used in creating a suspension with a certain relative density, e.g. such solids is magnetite or FeSi.

Terminology	Description
Dense medium	: Refers to the suspension itself, thus for example, a dense medium is created using water and FeSi.
Densimetric analysis	: Is a procedure whereby the density distribution of a sample is determined. It normally known as “ <i>sink-float analysis</i> ” in coal industry. The term is used to describe the separating material with a range of specific gravities by means of heavy liquids.
Ep	: Is the separation efficiency of the dense media separation process and it is defined as the inverse of the gradient of the tromp curve between 25% and 75 % of the cumulative percentage material to sinks.
PIT	: Mining area where the supply of run-of-mine ore is mined prior dispatch to the processing plant.
Process FeSi	: FeSi sampled from the Sishen DMS circuit that contains a percentage of iron ore slimes
Specific gravity	: A term used to describe the density of a substance. Also referred to as the relative density.
Stability	: Is the inverse of the rate at which a solid media will settle out from a suspension and hence has a common units of second per centimetre (i.e. s/cm)
Rheology	: Rheology is the science dealing with flow and deformation of matter. Within the context of slurry pipeline systems, rheology is defined as the viscous characteristics of a fluid or homogenous solid-liquid mixture. There are two terms in this definition that are important (van Sittert & Malloch, n.d.): <ul style="list-style-type: none"> ▪ The term viscous indicates that laminar flow is being considered (where viscous forces dominate) as opposed to turbulent flow (where inertial forces dominate). Thus, it is important to note that rheology refers to laminar flow phenomenon only. ▪ The term homogenous indicates that the solid particles are uniformly distributed across the pipe section
Rheogram	: A plot of shear stress versus shear rate for laminar flow conditions is called a rheogram.
Pseudo-Shear Diagram	: A pseudo-shear diagram is a plot of pipe wall shear stress versus the bulk or pseudo-shear rate for laminar flow conditions (van Sittert & Malloch, n.d.). The pseudo-shear rate is defined as: $\Gamma = \frac{8 V_m}{D} ,$ where Γ = pseudo-shear rate (s^{-1}); D = internal pipe diameter (m).

Terminology	Description
	In laminar flow if there is no slip, the data will be co-incident irrespective of tube diameter.
Newtonian Fluids and Mixtures	<p>: Isaac Newton, the originator of the science of rheology, postulated that the relationship between shear stress and shear rate in a fluid is linear (van Sittert & Malloch, n.d.), i.e.:</p> $\tau = \mu \gamma$ <p>where τ = shear stress (Pa); γ = shear rate (s^{-1}); and μ = constant of proportionality known as the dynamic coefficient of viscosity (Pa.s).</p> <p>Any fluid or mixture that obeys this relationship in laminar flow is considered Newtonian and the viscosity is sufficient to characterise the flow. Rheogram for Newtonian fluids and mixtures pass through the origin and the slope of the line is the viscosity.</p>
Non-Newtonian Fluids and Mixtures	<p>: A non-Newtonian fluid or mixture has one or more of the following characteristics:</p> <ul style="list-style-type: none"> ▪ a non-linear rheogram ▪ the rheogram does not pass through the origin ▪ the rheogram varies with time (i.e. dependant on the shear history).
Upgrade	: Enhancing the physical and/or chemical quality of the ore in view of increasing its market value.
Yield	: Is defined as the quantity of product obtained from the beneficiation process and it is mass based
	:

CHAPTER 1: INTRODUCTION

1 BACKGROUND

Sishen iron ore processing plant comprises of two beneficiation processes, namely, the Dense Medium Separation (DMS) Plant and the JIG Plant. The DMS plant was designed to beneficiate the high-grade run-of-mine (ROM) typically referred to as “*A-grade material*” whereas the Jig Plant beneficiate a lower grade ROM known as “*B-grade material*”. The historical A-grade ROM material blend had an iron content of approximately 60%Fe, with the typical head grade grades of the DMS plant feed blend comprising of ore types depicted in Table 1.1. These main ore types are:

- ✓ *Laminated and massive ore*: These rocks most probably represent ferruginous mud and chemically precipitated sludge locally derived from the underlying BIF and Thabazimbi-ore. The finely laminated and even structure less massive nature of the deposit indicates slow deposition in calm water over an extended period.
- ✓ *Conglomeratic and gritty ore*: These rock types were subsequently deposited as alluvial fan deposits filling nearby depressions. Rapid changing cycles of mudstone, shale and hematite- conglomerate, and later also BIF conglomerate, followed each other to form the deposits of conglomeratic and gritty ore, inter-bedded with shale and mudstone and higher up also BIF conglomerate.

Table 1.1: Typical head grade of A-class ROM in Sishen (SRK Consulting Engineers, 2006)

Ore type	%	Fe	SiO ₂	Al ₂ O ₃	K ₂ O	P
Conglomeratic and grit	18	62.2	5.3	2.9	0.28	0.055
Breccia	8	63.4	3.9	2.0	0.39	0.078
Massive	20	65.2	3.0	1.4	0.14	0.044
Laminated	54	66.3	2.4	0.8	0.07	0.056

The product from the DMS plant is the high-grade premium product with the historic 66%Fe for the lumpy product and 65%Fe for the fine product. This made the products from Sishen Mine to be sought-after by many steel producers in Asia due to their higher quality and low levels of impurities. However, since year 2012 the pit constraint coupled with the decline in the volume of exposed A-grade ROM posed a threat to the company’s ability to deliver on the volume of a high-grade premium product.

Thus, Sishen DMS plant has to gear itself to be able to beneficiate lower grade run-of-mine material in an efficient manner in order to maintain both the required product specification as well as product volumes. Traditionally, 25% of the feed to the DMS plant was processed through the dense medium cyclone circuit with yields ranging from 75% to 90% for the production of “premium fine product of 65%Fe”. However, with the drop in the grade of run-

of-mine material coupled with elevated proportion of near-density material, the performance of dense medium cyclone plant has been impacted negatively. The current yields hardly reach 70% with the fine product of ranging around 62.5%Fe to 63%Fe.

1.1 SISHEN DMS CYCLONE PLANT CIRCUIT

This section aims to describe the high-level process flow of the Sishen's cyclone plant as illustrated in Figure 1.1 with supporting major equipment depicted in Figure 1.2. As the fine material enters the cyclone plant through the conveyors it is mixed with water as the material is discharged into the feed sump as seen in Figure 1.2a. The ore is further split into two separate lines as seen in Figure 1.2b to feed two prewash screening section of the module on each side of the split. In each section, the stream is further split again into two streams with each stream feeding a single screen module. Unfortunately, the splits causes an uneven split of solids reporting to each screen as seen when Figure 1.2c.

The material being discharged from the screens is mixed with process FeSi from the medium distribution tank. The FeSi in the medium distribution tank (in Figure 1.2c) has to overflow the launder as shown in Figure 1.2d so as to ensure the correct static head is maintained sufficient to generate the correct DMS cyclone pressures. The FeSi – Solids mixture then flows into a distributor as seen in Figure 1.2e and is further split into three streams with each stream flowing into a cyclone as seen in Figure 1.2f. Trial test conducted using pressure gauges installed on some of the cyclones showed that the difference in pressure between individual cyclones of a cluster varied widely. It is suspected that the pressure variation is a result of the static head not being maintained and that the uneven split of solids to each screen and subsequently each cyclone cluster. These challenges cause unstable operation of cyclone plant. Currently the Cyclones do not have pressure gauges installed on them.

The cyclone floats flow over the float screens to separate the solids from the FeSi and likewise the cyclone sinks flow over the sink screen to separate the FeSi from the solids. The separated FeSi from the float screens flows into the dilute sump while the separated FeSi from the sink screens flows into the corrected medium tank. In order to ensure that the correct static head is maintained for the cyclones the level of FeSi medium in the correct medium sump has to be maintained above a certain level so that the FeSi continuously overflows the discharge launder in the medium distribution tank. Furthermore, in order to maintain the desired cut point it is important to accurately control the correct medium density. Dilute medium from both the float and sink screens flows into the dilute sump, is then pumped into the Primary and Secondary magnetic separators, and degrit cyclones to separate the FeSi from the water and any solids associated with the stream.

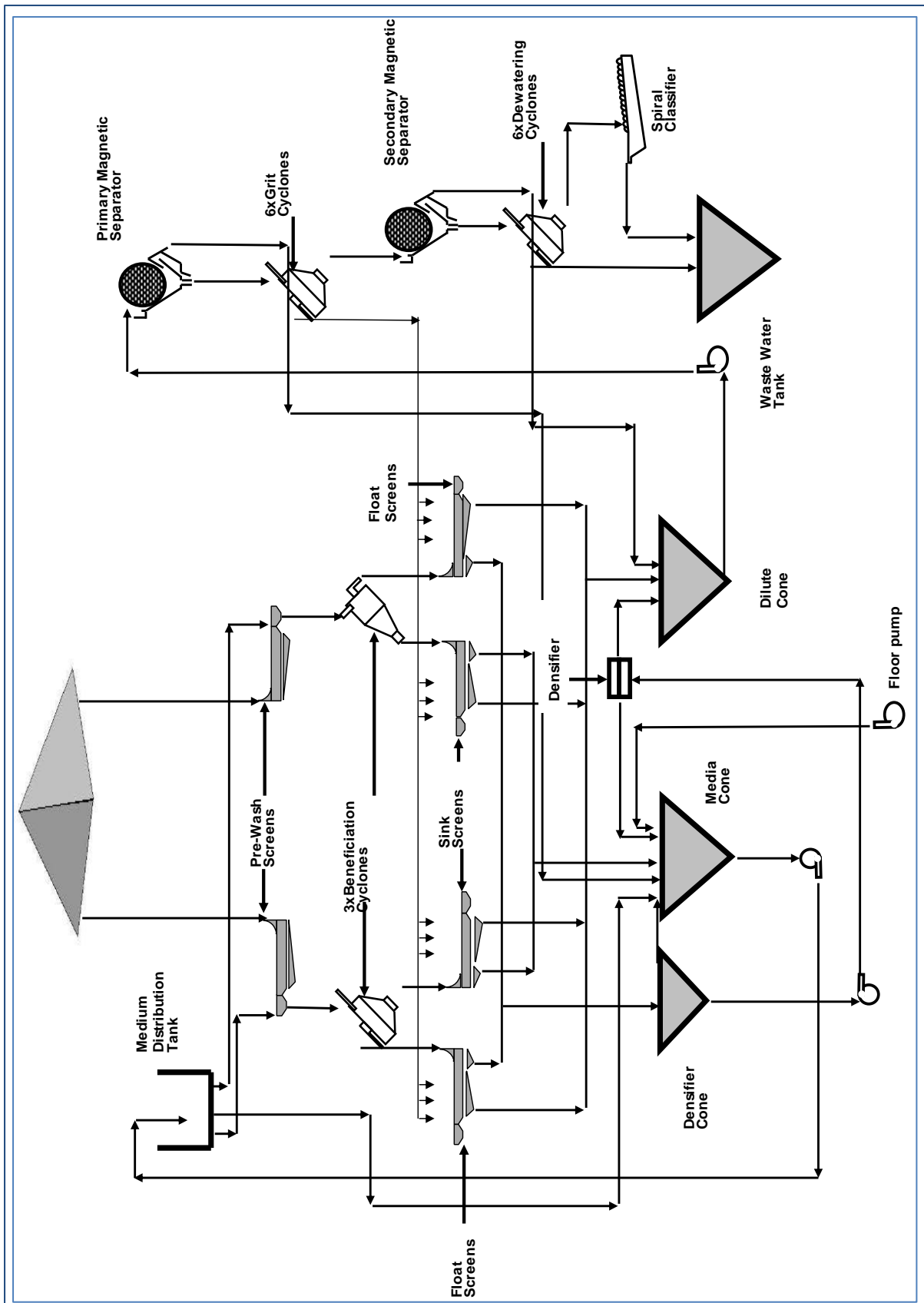


Figure 1.1: Cyclone medium flow line

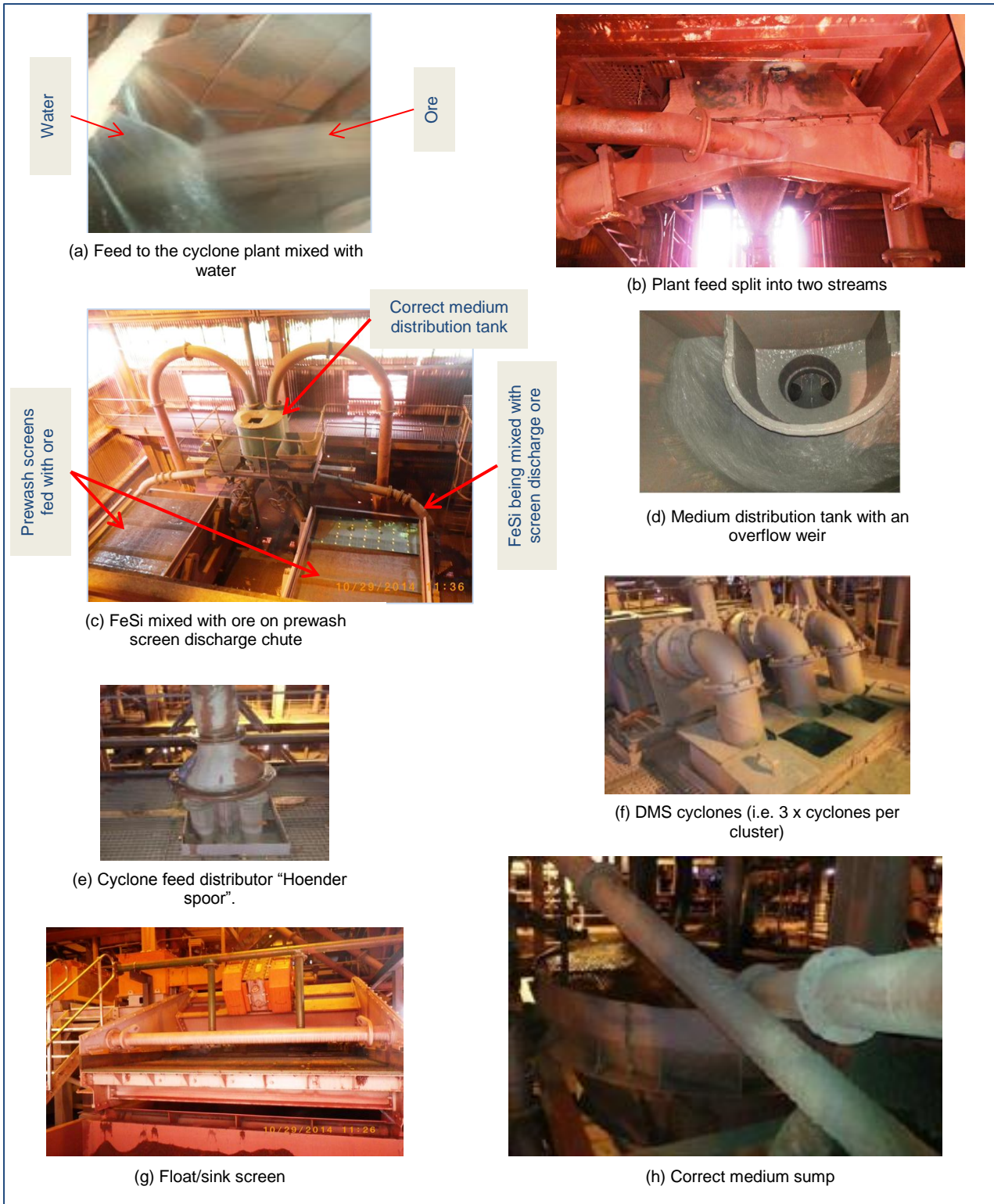


Figure 1.2: Cyclone plant ore flow line major equipment

The medium density, cyclone inlet pressures as maintained by a static head, affects the cyclone performance. In addition, the cyclone feed flow and mechanical availability of feed piping impacts on cyclone performance. The whole circuit is tied up around the flow of corrected medium as seen in Figure 1.1, which is controlled. The controlled variable is currently limited to only correct medium density whilst the sump level and correct medium flow rate is not measured. The corrected media density is controlled by adding dilution water to the correct medium sump when necessary.

1.2 PROBLEM STATEMENT

As the mining of high-grade iron ore becomes depleted, a need arises to beneficiate the low-grade material. Figure 1.3 presents the Sishen Mine material classification as well as the ROM feed grades to the DMS plant. It is evident that post-2010 year, the feed grade to the DMS plant declined drastically, with an increase in the material with less 58%Fe being fed to the plant.

A high proportion of near density waste material, which would necessitate a higher separation density in order to effectively, and efficiently beneficiate this material normally characterizes this low-grade ROM in order to maintain required product specification and volumes. Thus, a much higher operating density of the ferrosilicon (FeSi) medium will be required as well as refining the cyclone geometry and control to achieve the required beneficiation objectives.

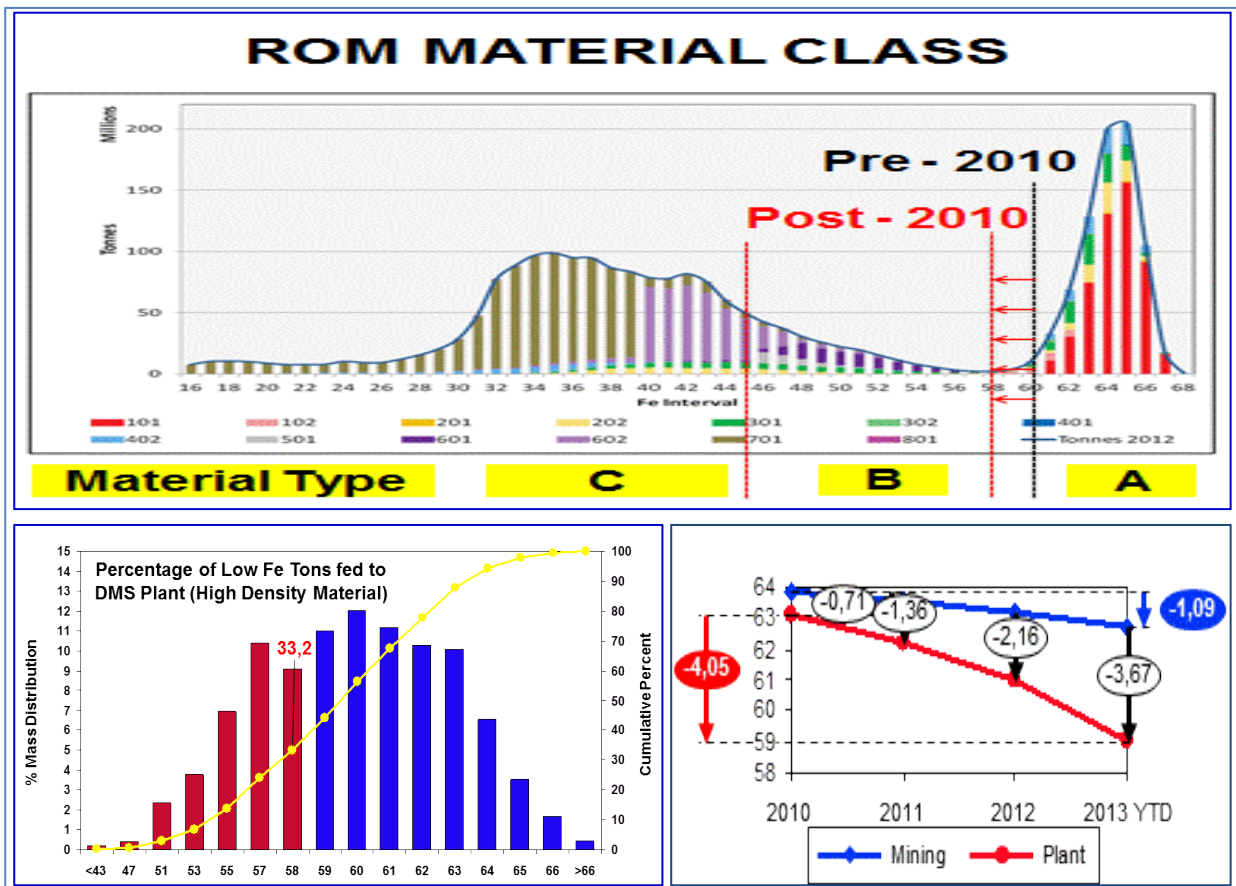


Figure 1.3: Material classification and DMS ROM feed grades

The current Sishen dense medium cyclone process operations is mostly reliant on operator intervention, which include visual inspection of process, control parameter that can easily be tracked by automated instruments. This results in an inconsistent medium balance in circuit thereby influencing the plant efficiency. Thus, high yield losses to waste and poorer product quality are generally noticed.

With the current performance of cyclone plant, an optimisation project has been undertaken to ensure tighter control philosophy of the cyclone unit processes to ensure that it can handle lower grade ROM material with higher near density material. This type of statement is made on the basis that cyclone setup and operation throughout Sishen Mine is in a relatively poor shape. This is due to number of reasons such as:

- i. Incorrectly specified system setup → Sishen's cyclone plant is relatively manual operated with limited automated control.
- ii. Overfeeding
- iii. Variation in medium viscosity
- iv. System changes over time
- v. Poor maintenance

Therefore, consistent system management, measurement and insight are required to maximize the opportunity that the cyclones present. By modelling and simulation, the aim should be to identify the financial benefit to be gained from better operation, automation, and consequently, trade this off against the costs associated with operation. Moreover, it will help to identify how much effort should be placed on this part of the operation.

1.3 RESEARCH OBJECTIVE(S):

One of the major challenges in the plant is trying to stabilise the cyclone operation and equalising the flow of the solids through the parallel streams in the plant. In addition, the ability of the plant to treat run-of-mine of varying grade and changing proportion of near-density material is challenging due to the reliance on human intervention and it being manual operated system. Thus, the main objective of the research project is to:

- i. To investigate the benefit of automated control of the cyclone plant in order to stabilise the process and manage the roping conditions.
- ii. To investigate the operating conditions in order to treat the material of lower grade and still produce product with the current quality specification.
- iii. To characterise the ROM in order to understand and manage the impact of near-density gangue material in the beneficiation of iron ore.
- iv. To analyse process FeSi rheological characteristic and the ability to operate at ultra-high densities in order to beneficiate low grade iron ore material.
- v. To develop algorithms for modelling and simulating the ore and FeSi circuit for the iron ore beneficiation in cyclone unit process.
- vi. The data gathering was around the DMS on the plant and this data was used to compare with the Simulink model.

This part of the cyclone optimisation project is concerned with the effectiveness of the cyclones process and automation in order to improve operating efficiency during beneficiation of lower grade ROM material with higher proportion of near-density material. Furthermore, the optimisation project included the provision of a DMS model that is useful to the personnel at Sishen without being laborious in its use and calibration.

CHAPTER 2: LITERATURE SURVEY

2 LITERATURE REVIEW

2.1 WHAT IS DENSE MEDIUM SEPARATION

Dense medium separation (DMS) can be defined simplistically as the practical commercial application of the use of a fluid of some intermediate relative density to effect the separation of a mixture of solids particles with different specific gravities. DMS as defined by (Gochin & Smith, 1983) is a process utilised to sort particles based on their apparent density relative to that of a carrying medium. Thus, in the DMS process, the lighter particles float on the dense medium whilst the heavier particles sink forming a low SG and high SG fractions respectively.

Dense medium separation has been widely used in mineral processing plants that produce saleable products such as coal, diamonds and iron ore concentrates (Gochin & Smith, 1983). The coal washing plants mainly use magnetite medium and operated at relatively lower densities ranging between 1250 – 1650 kg/m³, whereas the diamond and iron ore industries utilised the ferrosilicon medium. Most of the research work and optimisation studies in the application of DMS cyclones have focused mainly on the application of this technology in the coal washing processes.

2.2 THEORY OF DENSE MEDIUM SEPARATION IN CYCLONE

DMS cyclones are universally standard pieces of equipment for high tonnage density separation duties. They are essentially “plug and play” devices that are perceived to be highly robust, particularly in terms of performance under a wide range of operating conditions. This perception is further entrenched by the use of a single performance indicator, the **cut point density**, which trivializes the complexity of the device.

The principle of operation of dense medium cyclone, as described by (King, 2001) and (http://www.portaclone.co.za/pr_cyclo.htm) is based on the fluid pressure energy that creates a rotational fluid motion as result of tangential feed of the dense medium in the cyclone. There are two main factors influencing the separation efficiency in a cyclone. These are the force ratios in the cyclone and the cyclone geometry. Figure 2.1 graphically presents the particle motion taking place inside the cyclone as well as the forces acting on the particle suspended in the dense medium. There are three major forces (i.e. centrifugal, drag, and gravitational force) acting on the solid particles as they travel radially and helically inside the cyclone body, forcing the heavier particles toward the wall of the body and the lighter particles toward the centre.

The centrifugal field generated by high circulating velocities in the cyclone to creates an air core on the axis that usually extends from the spigot opening at the bottom of the conical

section through the vortex finder to the overflow at the top. The air core creates a force high enough to drag lighter mixture of particles and medium towards the vortex finder. Thus, the fluid leaving via the vortex finder carries the lighter particles with it while the centrifugal force causes heavy and large particles to migrate towards the cyclone wall and there descend to leave via the spigot.

In addition, it has been described that there is an envelope of zero velocity (i.e. $F_c = F_{drag}$) inside the cyclone where the near-density material normally is trapped. This trapped material has equal probability to be misplaced to either the underflow or the overflow. Thus, adjusting the vortex finder and spigot diameter would allow shifting the cut-size to a range where the impact of near-density material is minimised.

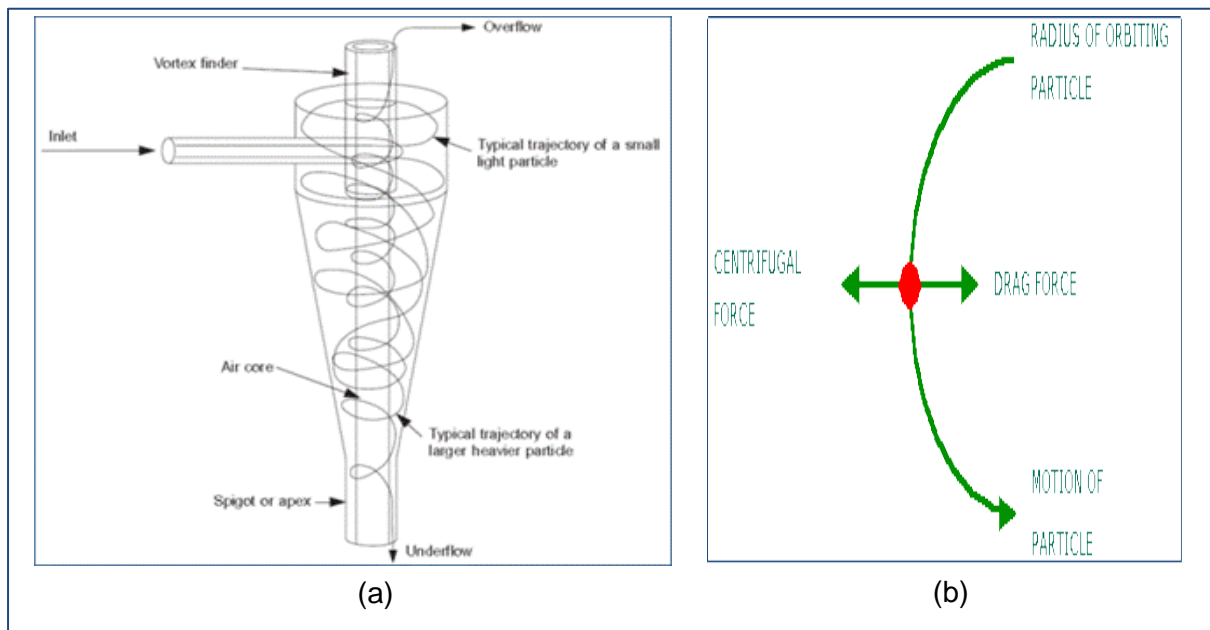


Figure 2.1: Typical cyclone equipment showing (a) Particle trajectory, and (b) Forces acting on a particle in a cyclone. (King, 2001); (Anon., n.d.),

These forces influencing the separation efficiency in a cyclone are being imparted on a particle inside a normal cyclone and summarised as follows:

- i. *Centripetal Force:* Due to the velocity of the material as it enters the cyclone, a centripetal force is exerted on the particles as they change from a linear motion to a circular motion. This force, when dominant, will cause the particles to report to the peripheral of the cyclone and hence to the cyclone spigot. The force is a function of the particle mass and subsequently the density and the tangential velocity in the cyclone.

$$F_{Centrifugal} \propto V^2, \text{ with } V \text{ being the tangential velocity in the cyclone.}$$

- ii. **Drag Forces:** Drag forces are imparted to the particles, primarily by the volumetric flow rate to the cyclone vortex finder. The drag force is dependent on the fluid velocity and particle velocity in the cyclone in the following relationship:

$$F_{Drag} \propto U_f - U_p, \text{ where } U_f \text{ is the velocity of the fluid and } U_p \text{ is the velocity of the particle.}$$

- iii. **Buoyancy Force:** Buoyancy force is a function of the density and stability of the medium. The buoyancy force can be either in the direction of the cyclone wall or the air core depending on the density and size of the particle. The relationship between buoyancy force and tangential velocity in the cyclone is the same as for centripetal forces.

$$F_{Buoyancy} \propto V^2$$

- iv. **Gravity Force:** This force is ignored due to dynamic nature of separation in the cyclone.

To understand the effect that the above mentioned forces will have on the separation efficiency in the DMS cyclone, JKMRRC did some test work showing a density profile in a cyclone (at a feed density of 1.40g/cm³) constructed by means of gamma radiation tomography. Although this experiment was conducted using magnetite, the principle will be similar for a cyclone operating with ferrosilicon. Figure 2.2 is a graphical representation of the tomography results by (Wang, 2009) and (Narasimha, et al., 2006).

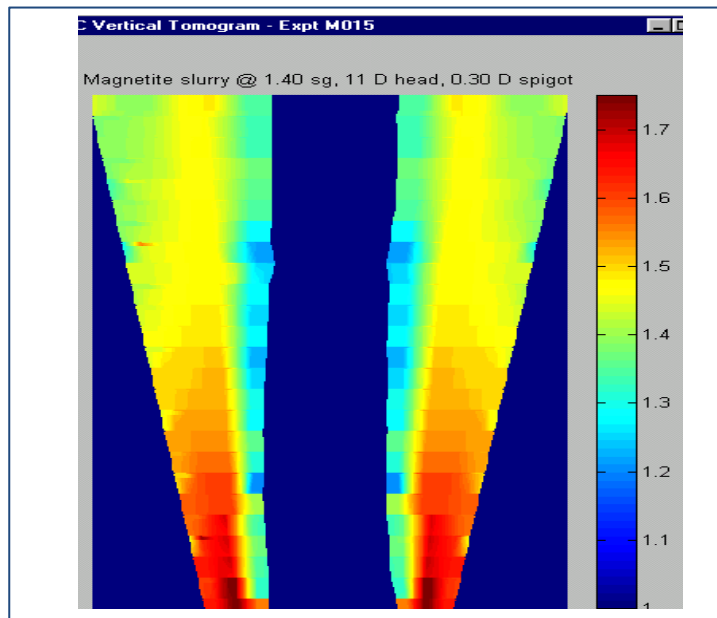


Figure 2.2: Tomogram at feed density of 1.40 g/cm³

Looking at the density profile between the air core and the cyclone wall at the top of the cyclone cone, the differential is no more than 0.02 ranging from 1.30 t/m³ to 1.50 t/m³. It is only in the spigot area that the density profile starts to change, increasing to a density of

1.70 t/m³ and above. Applying this principle to a cyclone operating with ferrosilicon at a feed density of 3.60 t/m³, similar density distributions can be assumed as presented in Figure 2.3. Due to its size, the cyclone spigot can only handle a certain amount of material reporting to the cyclone underflow before inefficiencies will start to occur. In the past it was believed that only the high-density material (+3.60 t/m³) reported to the spigot area while the lower density material (-3.60 t/m³) reports to the cyclone overflow through the vortex finder while still in the cyclone barrel.

From Figure 2.3 it is evident that the +3.40 t/m³ – 3.80 t/m³ material will report to the spigot area where it will encounter medium densities of 3.80 t/m³ and higher. These spigot densities will force the material with densities below 3.80 t/m³ back to the vortex finder to the cyclone overflow with the rest of the low-density material. To ensure efficient separation in the cyclone spigot of the high-density material (+3.80t/m³) to the cyclone underflow and the low-density material (<3.80t/m³) to the cyclone overflow, the material loading in the spigot areas must not exceed 80%.

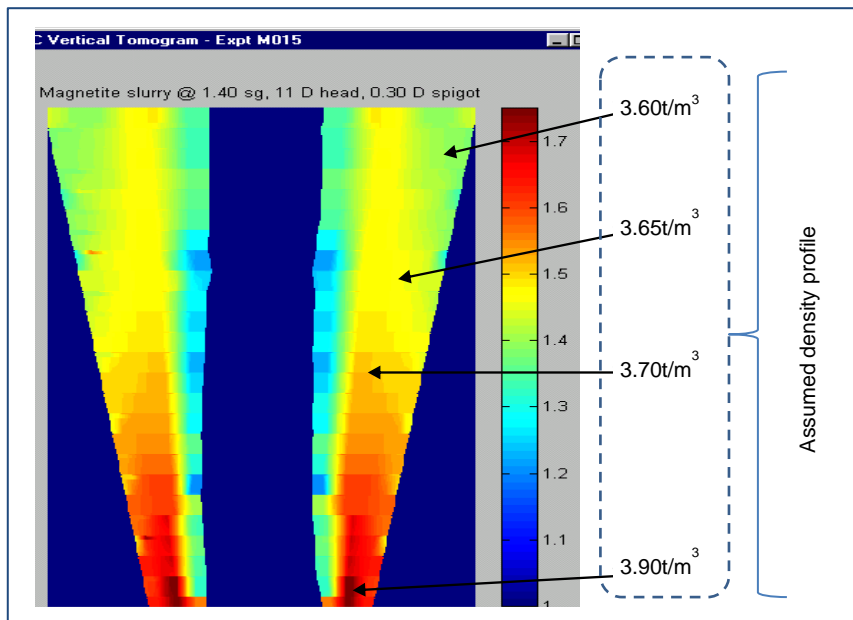


Figure 2.3: Tomogram at assumed density profile at feed density of 3.60 t/m³

2.2.1 Factors Influencing Dense Medium Beneficiation

The summary of major factors that affect the dense medium cyclone performance as well as its performance indicators are explained by He and Laskowski (1995a) as cited by (Sripriya, et al., 2001). The factors that include three groups of variables are illustrated in Figure 2.4 and include the following: (i) *medium composition*, (ii) *feed characteristics*, and (iii) *cyclone operating conditions*.

- i. **Medium composition:** medium composition affects beneficiation process performance by changing its stability and rheology. The impact of medium stability in cyclone performance can be characterised by the density differential between the cyclone overflow and underflow streams.

- ii. **Feed characteristics:** is mainly determined by the particle size, particle shape, proportion of near-density material as well as the feed rate.
- iii. **Operating conditions:** this can be summarised as the (a) *inlet pressure*; (b) *medium density*; (c) *medium flow rate*; (d) *medium split* and (e) *medium-to-ore ratio*.

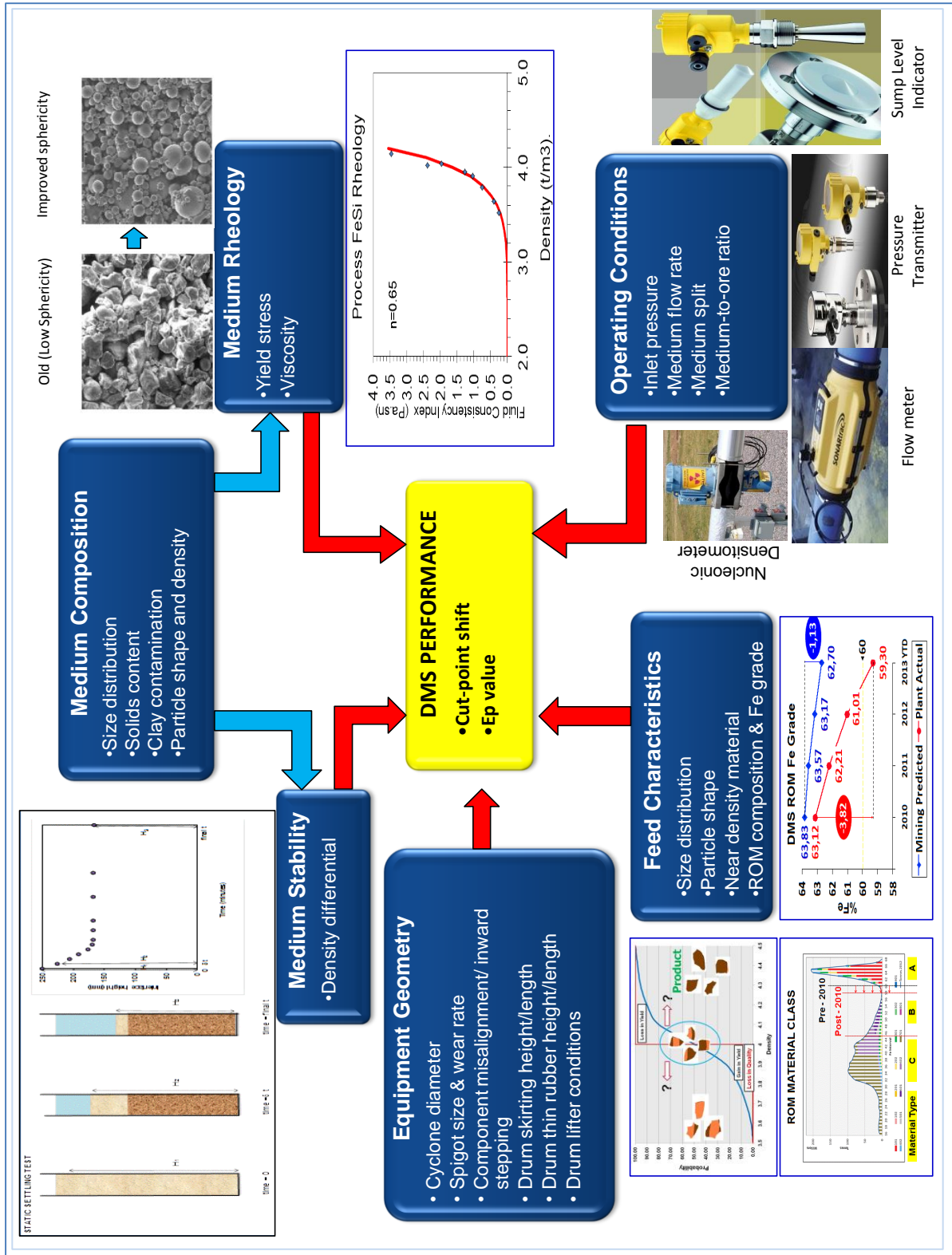


Figure 2.4: Performance indicators and factors affecting dense medium cyclone performance

2.2.2 Importance of Dense Medium Rheological Characteristics

Rheology has been described in literature as the science dealing with flow and deformation of matter. It can be defined as the viscous characteristics of a fluid or homogenous solid-liquid mixture. The term homogenous indicate that the solids particles are uniformly distributed across the medium carrier whilst the viscous indicate that laminar flow condition is considered as opposed to turbulent flow regime.

The heavy liquid medium used for the dense medium is classified as a non-Newtonian slurry mixture and its flow behaviour can be models by various rheological mathematical models. Rheological models are applied on the rheogram in order to transform them to information on the fluid rheological behaviour (Björn, et al., 2012). Non-Newtonian fluid or mixture can be characterised by one of the following characteristics such as (i) a non-linear rheogram; (ii) the rheogram does not pass through the origin; and (iii) the rheogram varies with time, which is, depended on the shear history.

According to van Sittert & Malloch (n.d.) and Bjorn *et al* (2012) the most suitable mathematical models for most of the non-Newtonian fluid or mixture and mineral slurry application is the generalised yield pseudo-plastic or Herschel Bulkley model and Bingham model. Rheological models as found in literature are summarized in Table 2.1 while typical rheogram for different models are graphically illustrated in

Figure 2.5.

Table 2.1: Rheological models

Model	Yield Stress	Fluid Behaviour Index	Constitute Equation
Newtonian	$\tau_y = 0$	$n = 1$	$\tau = \mu\gamma$
Bingham plastic	$\tau_y > 0$	$n = 1$	$\tau = \tau_y + K\gamma$
Pseudo-plastic	$\tau_y = 0$	$n < 1$	$\tau = K\gamma^n$
Yield pseudo-plastic	$\tau_y = 0$	$n < 1$	$\tau = \tau_y + K\gamma^n$
Dilatant	$\tau_y = 0$	$n > 1$	$\tau = K\gamma^n$
Yield Dilatant	$\tau_y > 0$	$n > 1$	$\tau = \tau_y + K\gamma^n$

In addition, the rheological properties of heavy medium can be represented in plotted pseudo shear diagram using a data generated from the vertical loop pipe test. This is a plot of wall shear stress versus pseudo shear rate. The pseudo-shear rate is defined as (van Sittert & Malloch, n.d.):

$$\Gamma = \frac{8 V_m}{D} ,$$

...Equation 2.1

Where, Γ is the pseudo-shear rate (s^{-1}); V_m is the mean mixture velocity (m/s); and D is the internal pipe diameter (m).

The wall shear stress is determined from:

$$\tau_0 = \frac{D\Delta P}{4\Delta L} \quad \dots \text{Equation 2.2}$$

Where, τ_0 is the wall shear stress (Pa); ΔP is the pressure differential over pressure tapping's (Pa/m); ΔL is the distance between pressure tapping's (m).

The rheological characteristics of the heavy medium fluids can be modelled in the form of form of the pseudo-plastic models which are as follows:

$$\tau_0 = k\gamma^n \quad \dots \text{Equation 2.3}$$

Where, τ_0 is the wall shear stress (Pa); K is the fluid consistency index ($Pa \cdot s^n$); γ is the shear rate (s^{-1}); and n is the fluid behaviour index (<1).

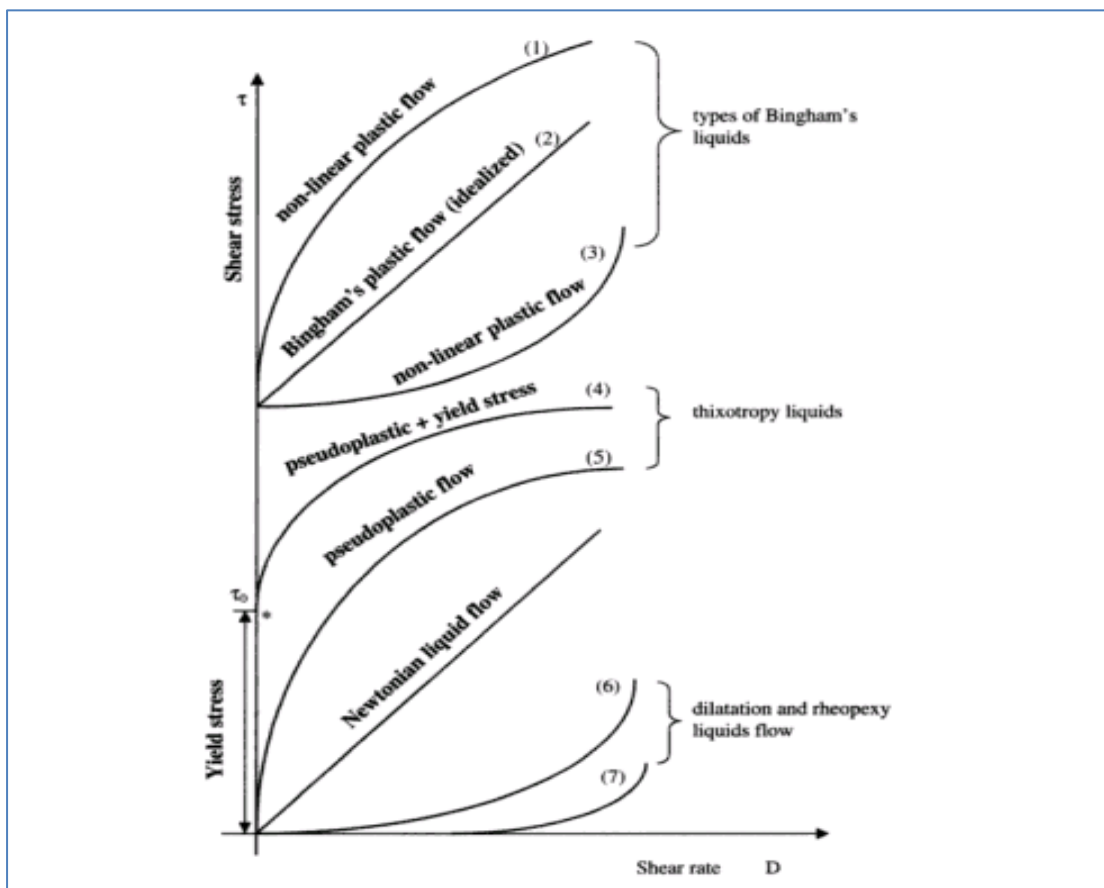


Figure 2.5: Typical rheogram

The important rheological characteristic of the dense medium that influences the performance of dense medium separation are generally classified as the viscosity and stability properties (Gochin & Smith, 1983), (Wang, et al., 2009) and (He & Laskowski,

1994). The viscosity is described as a measure of the resistance to flow of a liquid and influences the movement of ore particles through the dense medium. On the other hand, stability controls the medium segregation in the cyclone that leads to a phenomenon known as cyclone differential. Cyclone differential is defined as the density differential of the medium reporting to the floats stream and that to the sinks stream of the unit process.

In a separating medium (typical of DMS operations) it is determined largely by the concentration, shape and size distribution of the solids making up the medium. Viscosity is measured for particular shear rates in units of cP (centipoise), the SI equivalent being Ns/m^2 . A high viscosity results from high solids concentration, fine particle size distribution, irregular shapes, and presence of low density contaminant solids. A low viscosity results from the converse of the above.

Medium viscosity is an important property, and given the difficulty of measurement, its influence on separation is not always completely understood. In general too high viscosity values are not desirable because of reduced separation velocities, increasing probability of particle misplacement and reduced partition efficiencies.

The literature described that the rheological properties of the dense medium are one of the key factors that influence/affects the separation efficiency cyclone systems. The influence of medium rheological properties on cyclonic dense medium system can be summarised as follows:

- a) Coarser ferrosilicon medium at lower medium densities results in excessive media segregation that leads to a higher density differential due to unstable medium. Higher density differential are responsible for high cut-point shifts and leads to longer retention time of near density material in the cyclone.
- b) According to (Wang, et al., 2009), the density differential was found to decrease as the non-magnetic content of the medium increases.
- c) In order to achieve satisfactory separation in cyclonic systems, (Napier-Munn, et al., 1994) and (He & Laskowski, 1994) recommended that density differential be maintained within 0.2 and 0.5 SG.
- d) Increase in medium density, coupled with the fine particle size distribution of media and presence of low density slimes (contaminating non-magnetics) would result in an increase in medium viscosity.
- e) A summary of factors contributing and influencing media rheology are described by (Myburgh, 2006) which is graphically depicted in Figure 2.6. These included; (i) slime (non-mag) content, (ii) media shape and (iii) ultrafine content (percentage of $-45\mu\text{m}$).

The proportion of the ultra-fine is required to maintain the optimal operating differential for cyclonic system in Sishen averaged around 62%.

- f) High viscosity media is undesirable because they reduce the velocity of mineral particles being separated thereby increasing the probability of particle misplacement and reducing the efficiency of separation.

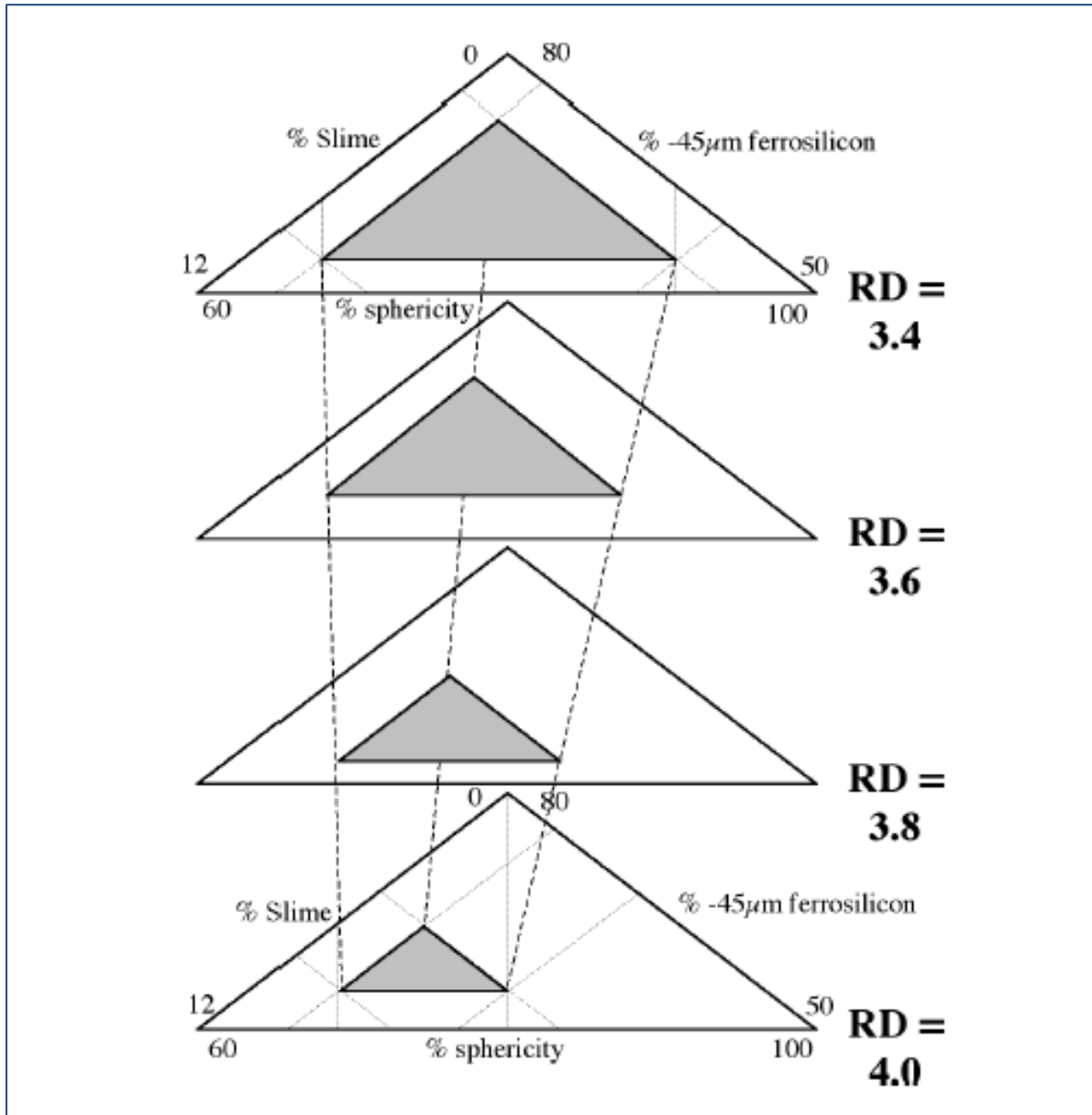


Figure 2.6: Schematic explanation of variables on medium rheology

2.2.3 Cyclone Performance Measure

The performance of the cyclone unit process is generally determined by the Ecart Probable Moyen (Ep-value). The Ep value describes the separating efficiency of the unit process regardless of the quality of feed material (Wills & Napier-Munn, 2006); (Gochin & Smith, 1983). The Ep is determined from the slope of the tromp curve which represents the probability of the percentage of the feed material that will report to either the sinks or floats depending on their relative density distribution.

A typical tromp curve as well as operating E_p values of separating unit processes are graphically presented in Figure 2.7. In addition, Figure 2.7(b) shows the effect of particle size on the efficiency of dense media separating unit process. The lower the E_p value, the better the efficiency of the equipment. Typical acceptable E_p values for the cyclone module range between 0.05 - 0.10 for the iron ore beneficiation. The probability curve (Tromp curve) in conjunction with the Ecart Probable Moyen was used to demonstrate the impact of processing efficiency of material with different densimetric profiles.

The partition curve is determined using the Whitten's equation for beneficiation process without short-circuiting (Wills & Napier-Munn, 2006):

$$PN = \frac{1}{\left[1 + \exp\left(\frac{k(\rho_{50} - \rho_i)}{E_p}\right)\right]} \quad \dots \text{Equation 2.4}$$

With, $k = 1.098$ (constant determined experimentally); ρ_{50} = cut-point density; ρ_i = density fraction and E_p = separation efficiency.

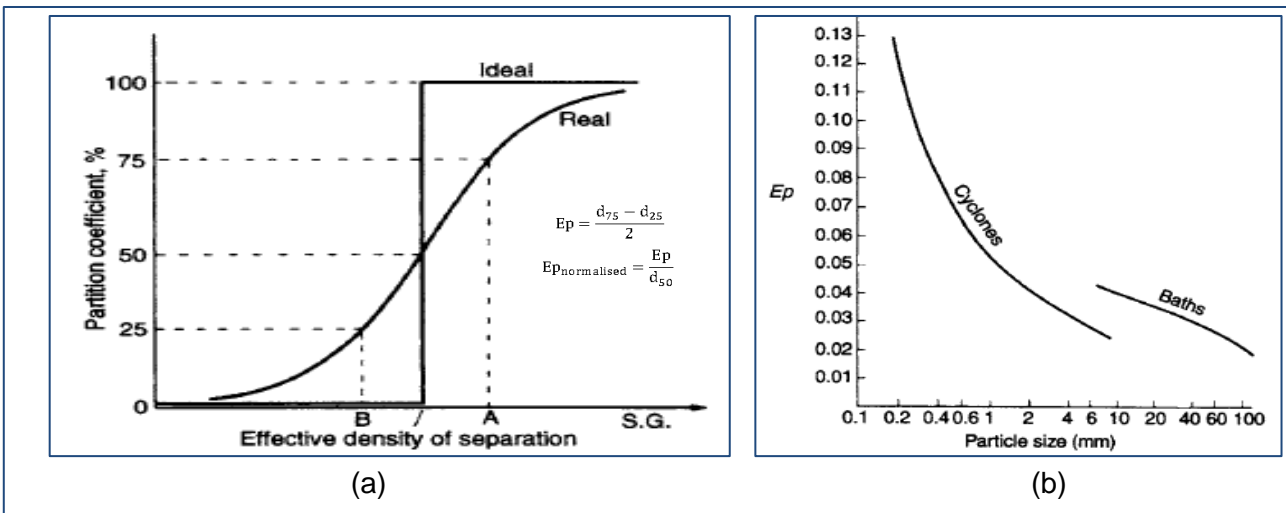


Figure 2.7: Graphical representation of (a) Tromp curve, and (b) E_p vs. Particle size. (Wills & Napier-Munn, 2006)

Some of the critical process and operating parameters that are critical for the efficient operation of dense medium cyclone circuits as described by (Bekker, 2012) and (Atkinson, et al., 2012) includes:

- (i) Washability of material which is related to yield,
- (ii) Feed particle size distribution,
- (iii) Head (D) and head loss, with the normal head for mineral industry is $7 - 20 \times D$. According to (Atkinson, et al., 2012), lower head, (e.g. $<7D$), is not desirable for beneficiation of fine material. In addition, it has been alluded that higher operating head results in high cut-point shift and thus are not recommended in operation where high cut-point densities are not desirable.

- (iv) Percentage of the near density material, which is the material, that lies within 0.05 – 0.1 RD intervals on either side of the separation density. Near density material in excess of 15% is very difficult to beneficiate.
- (v) Medium to ore ratio.
- (vi) Top size (mm).

Typical models for partition curves as applied to the dense medium beneficiation are presented in Table 2.2 below:

Table 2.2: Typical partition curve models for dense medium separation

PARTITION MODELS FOR DMS SEPARATORS						
CHANGE DATA AND SEE THE IMPACT ON THE SEPARATION						
NOTE: CHANGE ONLY DATA IN THE BLACKENED CELLS						
Feed Stream Data				mass%		
	SG Class #	SG Range	Av SG	in class	%Fe	
	1	Float	4.000	3.9	33.063	21.418
	2	4	4.200	4.1	4.872	51.300
	3	4.2	4.400	4.3	6.754	55.699
	4	4.4	4.600	4.5	9.042	60.500
	5	4.6	4.800	4.7	15.514	64.400
	6	4.8	5.000	4.9	20.063	66.772
	10	5	Sink	4.3	10.692	68.439
	Av Particle Size (mm)	3				
	Feed rate (tph)	100				
				RESULTS (For calculations see Spread Sheet <Model 3>)		
		Partition %		Cum %Density Distribution		
				Feed	Floats	Sinks
		100.00		33.06	87.56	45.50
		100.00		4.87	92.44	45.50
		80.70		6.75	97.89	46.80
		19.30		9.04	99.63	54.10
		1.35		15.51	99.84	69.40
		0.08		20.06	99.86	89.45
		1.35		10.69	100.00	100.00
		TPH		100.0	45.5	54.5
		SG		4.158	3.630	4.732
		%Fe		49.52	30.59	65.32
DMS Separator Parameters				MODEL for Partition Curve		
$\rho_m = \text{Medium SG}$				$R(x) = Rc(x)(1 - \alpha - \beta) + \beta$		
4.00				$Rc(x) = 1/(1 + (\exp(\lambda(x-1))))$		
Cut Point Shift = CPS = $\rho_{50} - \rho_m$				$\lambda = 1.099/lc$		
CPS				0.4		
cut density = $\rho_{cut} = \rho_{50}$						
ρ_{50}				4.4		
epm				0.077		
Corrected imperfection = $lc = epm/\rho_{50}$ (Realistic range 0.4 to 0.01)						
lc				0.017		
by-pass to floats: β				0		
by-pass to sinks: α				0		
fluid recovery to sinks = Rf				0		
Density Differential = $\rho_{diff} = \rho_{underflow\ medium} - \rho_{overflow\ medium}$				0.097381407		
ρ_{diff}						

(vii)

In addition, the cyclone geometry, spigot capacity and operating pressures are of paramount importance as well as the particle size distribution of the ore being treated. The visible condition that generally influences the separation efficiency is the type of spigot discharge, which is related to the spigot loading capacity. It was demonstrated by (Magwai & Bosman, 2008) that as the spigot is overloaded, the cyclone tends to produce a rope discharge. This roping has been prevalent in the Sishen cyclone plant operation as depicted in Figure 2.8, and thus would have to be managed with an automated control mechanism. In a cyclonic system that is operating in an efficient manner, the spigot discharge should be flaring.

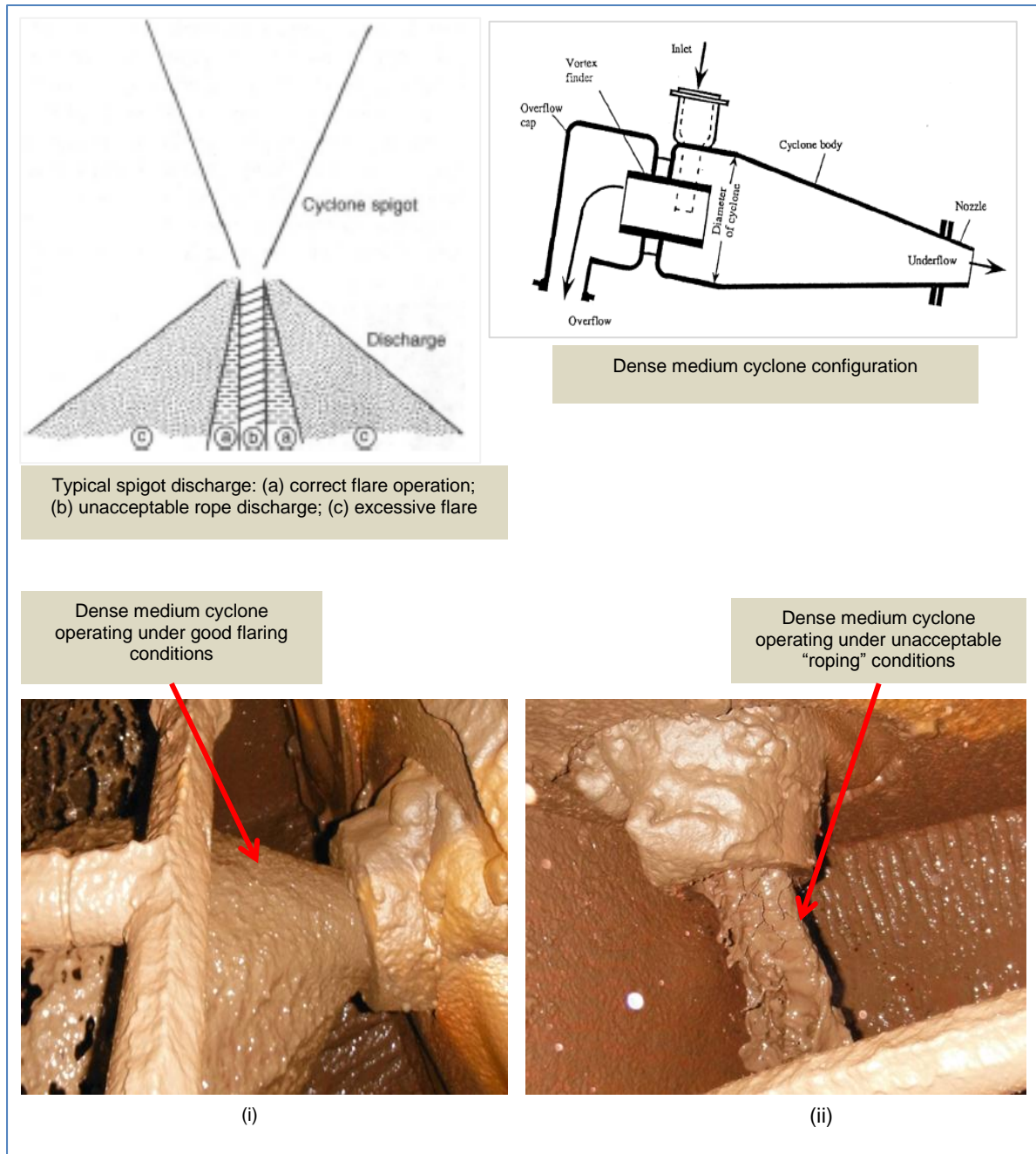


Figure 2.8: Typical cyclone spigot operating conditions (i) Flaring and (ii) Rope discharge

2.2.4 Online Measurement, Control and Modelling

On-line measurements of cyclone operation have been discussed at length for decades. It is understood that in most industrial applications that cyclone stability is key to the overall performance of the business. However, there has been a lack of suitable measurement systems that can provide direct performance measurement insight and secondly, be robust enough to maintain accuracy in a harsh industrial environment.

The most common variable that can be measured online and has a direct influence in the performance of dense medium cyclone as described by (Petersen, 2010) and (Mukherjee, et al., 2003) is the cyclone inlet pressure. The cyclone system is designed to maintain a

specific inlet pressure, which would indicate that the flow rate is then within specification. Thus, inlet pressure measurement is most commonly used for cyclone system stability. Inlet pressure is currently not measured at Sishen due to the harshness of the environment.

The pressure distribution within the cyclone unit process as shown in Figure 2.9 cited from (Wang, 2009)'s thesis indicate that the static pressure decreases rapidly from the cyclone wall to the centre. This is due to the fact that a lot of fluid that is thrown to the wall. It has been indicated that the pressure gradient force on ore particle is high and dominant in the radial direction. Thus, the balance between the pressure gradient force and centrifugal force due to swirling flows determined the destination of the ore particles being beneficiated.

Conclusion on pressure gradient by (Wang, 2009) indicated that when pressure gradients on ore particle is larger than centrifugal force, the particle will reports to the overflow via the vortex finder, otherwise, it is discharged through the spigot to the underflow stream. Thus proving the assertions by (Petersen, 2010) and (Mukherjee, et al., 2003) that understanding the inlet pressure is very important for the dense medium cyclone operation.

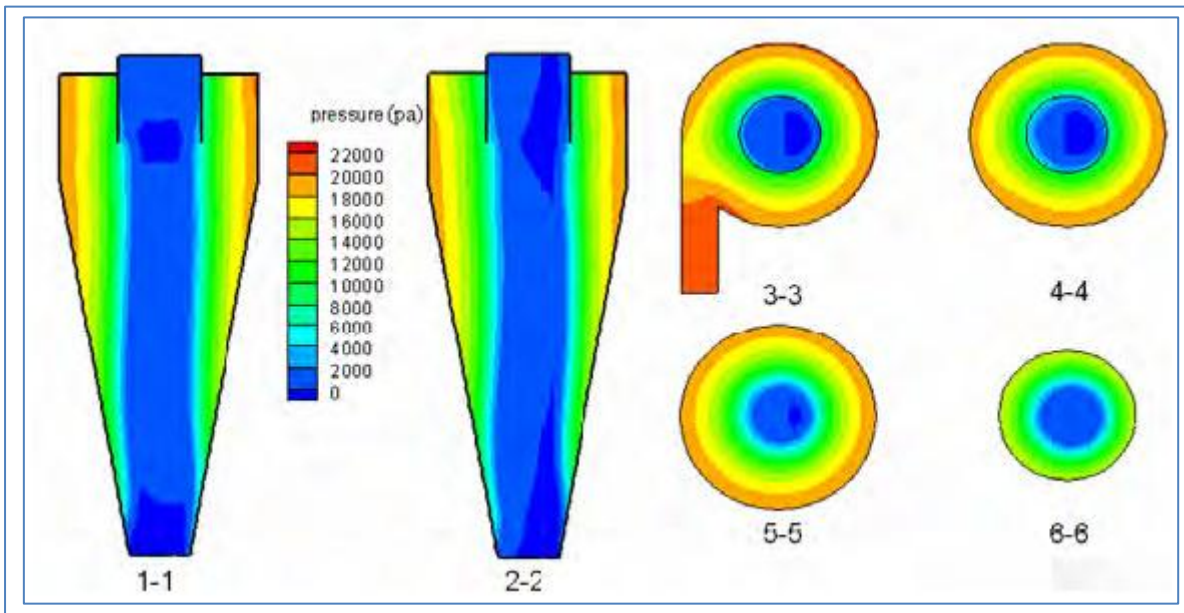


Figure 2.9: Distribution of pressure inside the Dense Medium Cyclone (Wang, 2009)

The generic structure of the configuration is illustrated in Figure 2.10 (Stephanopoulos, 1984). The control systems take into consideration the possible application to large-scale systems by looking at (i) selection of the number of manipulated/measured variables to achieve process stability, and (ii) selection of feedback loops between measured and manipulated variables.

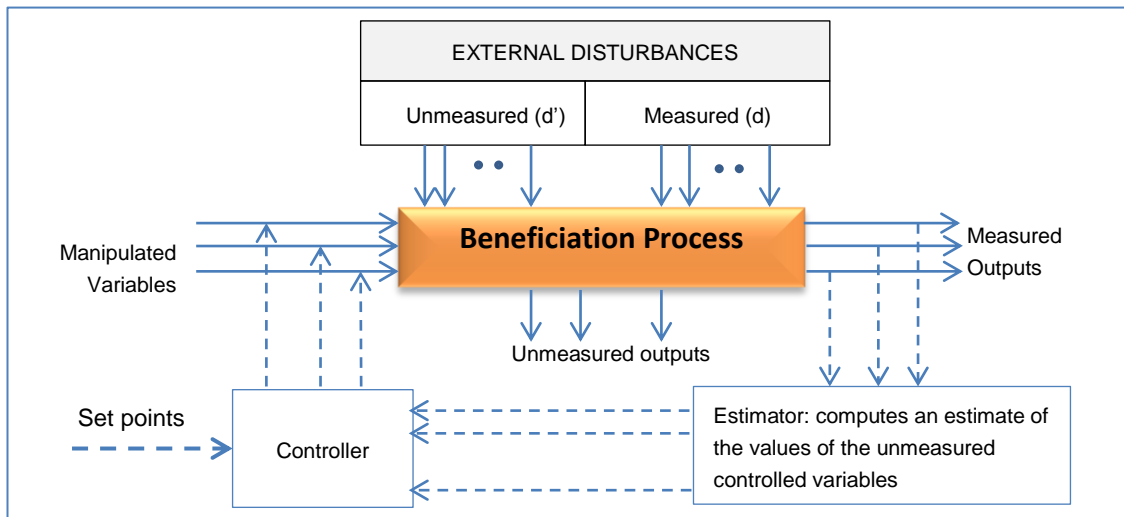


Figure 2.10: General structure of the control configuration (Stephanopoulos, 1984)

Met Coal and Venetia mine’s unit processes have pressure transmitter and gauges installed, which are used for control purpose. Venetia Mine is maintaining a balanced static head across operating modules thereby ensuring stable inlet pressures in all operating cyclones. This showed a great improvement in processing and beneficiation efficiency

Therefore, Sishen Mine can learn from their system of ensuring that all operating cyclones maintain similar feed pressure. Figure 2.11 shows the installation of pressure transmitters at Capcoal and Venetia Mines whilst Figure 2.12 present Venetia’s innovative system to ensure medium balance in the circuit thereby achieving constant cyclone pressure across operating modules for their gravity fed system.

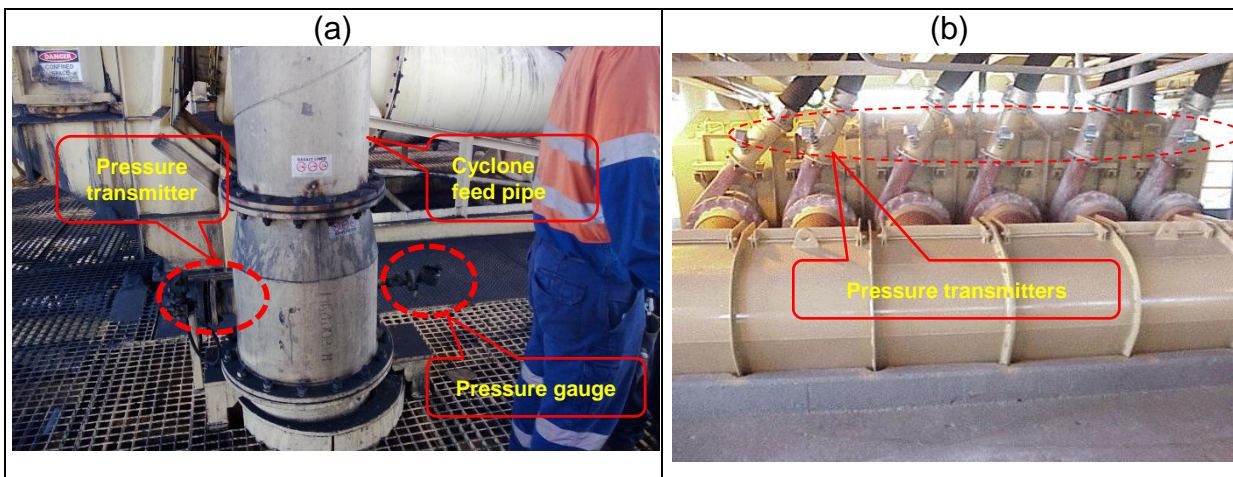


Figure 2.11: (a) Capcoal and (b) Venetia’s cyclone inlet pressure instruments

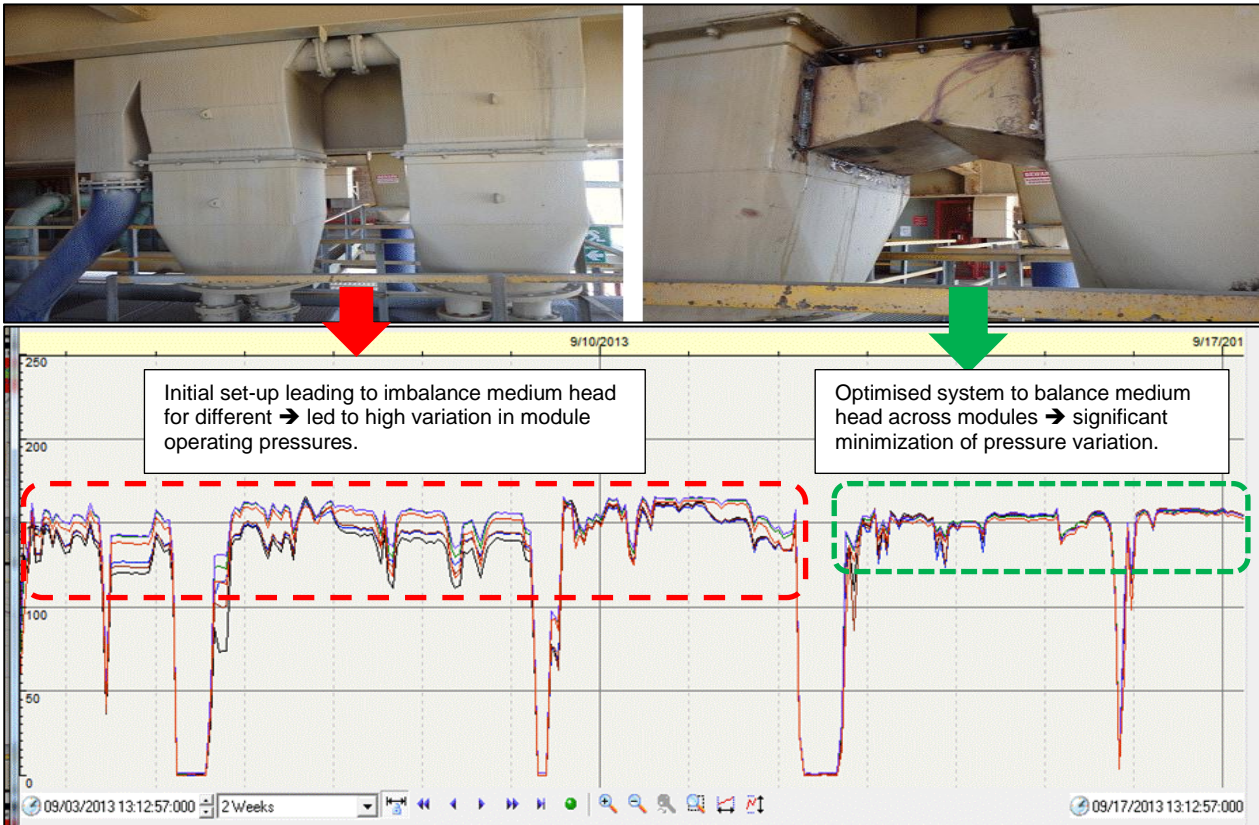


Figure 2.12: Venetia's medium head balance across module and its impact of cyclone inlet pressure

Flow rate measurement is possibly the other most important piece of information that could be obtained from a cyclone system. Magnetic flow rate meters are common equipment in the minerals industry, but can only be used if the material being processed is non-magnetic. Advances that are more recent have shown the development of the ring impulse flow-rate measurement scheme, which attaches approximately eight (8) rings around the inlet of the cyclone and disturbances within the fluid are picked up by all eight (8) rings, which are then correlated to determine the movement of the disturbances, which is then turned into flow-rate estimation. Sishen is considering the installation of SONARtrac flow meters, which are non-slurry contact unit and thus will not be subjected to high abrasive environment in the DMS circuit.

Modelling of the performance of the dense medium separation can be performed using a Simulink program based on the existing models from literature. Such models includes empirical models developed by many researchers on the predictions of performance of the dense medium cyclone are well summarised by (Wang, 2009). The well-known model is the Wood's empirical model with heavy reliance on many fitting factors. The use of the model is to assess the likelihood of the outlet overloading, particle retention as well as surging. The basic structure of the Wood's Model is as follows:

- i. The main state equation is that of flow rate (Q_f) which includes both medium and ore:

$$Q_F = K \cdot D^{1.48} \cdot R^{0.15} \cdot H^{0.45} \quad \dots \text{Equation 2.5}$$

ii. The flow split of medium only:

$$\frac{Q_{uz}}{Q_{fz}} = 0.79Head^{-0.37} \left(\frac{D_u}{D_o}\right)^{4.2} \quad \dots\text{Equation 2.6}$$

The above equation then acknowledges that the presence of ore modifies the medium flow split, via Q_{um} :

$$Q_{um} = 0.97Q_{us} + \frac{Q_{uz}^2}{Q_{us} + Q_{uz}} \quad \dots\text{Equation 2.7}$$

Percentage of medium split to overflow can also be determined by the following equation:

$$Over \% = K \cdot \left(\frac{D_o}{D_u}\right)^2 \cdot \rho_{fm}^{-1} \cdot P \cdot (M:O)^{0.25} \quad \dots\text{Equation 2.8}$$

iii. Now the density of the spigot medium is calculated, ρ_{um} :

$$\rho_{um} = 0.459\rho_{fm} \left(\frac{Q_{um}}{Q_{fm}}\right)^{(0.194(\rho_{fm}-2.04))} P_{RR}^{0.17} Head^{0.082} D_c^{0.010} \quad \dots\text{Equation 2.9}$$

iv. Overflow density, ρ_{om} :

$$\rho_{om} = \rho_{fm} \left[\frac{\left(1 - \frac{Q_{um} \cdot \rho_{um}}{Q_{fm} \cdot \rho_{fm}}\right)}{\left(1 - \frac{Q_{um}}{Q_{fm}}\right)} \right] \quad \dots\text{Equation 2.10}$$

Where Q_{fm} ; Q_{um} ; is the flow rate feed and underflow medium respectively;

Q_{fz} ; Q_{uz} is flow rate of feed; underflow with non-medium solids respectively;

Q_{us} is the solids flow rate of underflow;

“Head” is the inlet pressure head in meters of medium;

P_{RR} is the intercept (63.2%) of a Rosin-Rammler medium size distribution

D_u is the inside diameter of the spigot;

D_o is the inside diameter of the vortex finder;

K is the constant;

ρ_{fm} ; ρ_{um} ; ρ_{om} is the feed, underflow and overflow density of medium respectively;

The control of the correct medium sump and/or tank is one of the critical part in the dense medium separation. In most cases, these sumps/tanks tank design are truncated conical tank. Thus, the equations 2.11 to 2.13 are applicable for determining the capacity of the correct medium tank for a cyclone module:

$$\text{Slant height: } s = \sqrt{(R - r)^2 + h^2} \quad \dots \text{Equation 2.11}$$

$$\text{Total surface area: } A = \pi[(R + r)s + R^2 + r^2] \quad \dots \text{Equation 2.12}$$

$$\text{Volume: } V = \frac{1}{3}\pi h(Rr + R^2 + r^2)$$

... Equation 2.13

To simplify the modelling of the tank height in order to determine when manual “fresh FeSi addition” must happen, it was assumed that the effective area of the medium tank does not change with change in medium height in the tank. Thus, the modelling of rate of change of medium level in the tank can be simulated utilising the conservation of mass taking into account the rate of medium flow in and out of the tank as follows:

$$A_t \frac{dh_t}{dt} = Q_{t,med} + Q_{t,dis} - Q_t$$

... Equation 2.14

CHAPTER 3: METHODOLOGY

3 EXPERIMENTAL APPROACH

The experimental procedure was sub-divided into three parts: (i) ore characterisation, (ii) characterisation of process FeSi and (iii) automation of one cyclone plant module and processing of ROM of varying grades and evaluating performance and efficiency.

3.1 ORE CHARACTERIZATION

Ore characterisation entailed testing of various ore types and ROM blends of varying quality for densimetric analysis; mineralogical and chemical analysis. This characterisation work was conducted at Sishen Mine, with some of the samples dispatched to external laboratories such as Anglo Research, Mintek and UIS Analytical Services. The equipment that was used for the densimetric analysis of the ore material is discussed briefly below:

- i. Semi-automated sink-float column and static bath sink-float set-up located at Sishen Met Lab and Anglo Research Laboratories. Drawing and pictures of the automated sink-float column as not shown as they might be violating the intellectual property of the designer.
- ii. XRF & QEMSCAN: Anglo Research. Figure 3.1 illustrates pictures of the XRF and QEMSCAN machines used for chemical in Sishen and Anglo Research Labs.



Figure 3.1: Typical XRF and QEMSCAN Set-up in Sishen and Anglo Research labs

3.2 PROCESS FeSi CHARACTERIZATION

Process FeSi sample was characterised at Paterson & Cooke Consulting Engineers (P&C) Laboratories in Cape Town for rheological properties for application at ultra-high density set-up. The schematic diagram of vertical tube viscometer set-up at P&C Labs illustrated in Figure 3.2. A Warman 2 × 1½ AH pumps slurry through a vertical pipe of 19.6 mm internal diameter to form a re-circulating pipe loop. Differential pressure transducers measure the

pressure difference across sections on the up and down legs of the pipes. A cooling jacket cools down the slurry temperature during testing. The loop is fitted with a coriolis mass flow meter for measuring flow rate, slurry density and temperature. The pump is fitted with a mechanical seal to prevent dilution of the slurry.

The FeSi characterisation was subdivided as follows:

- i. **Medium stability test:** The medium stability test measure the rate at which the heavy medium liquid settles in a bench top scale settling test procedure. The procedure is similar to the test conducted for determining the slurry settling rate as well as the design of slurry thickening system. The aim of the static bench top settling tests provides an indication of the rate at which surface water separates from the solids for a given slurry mixture. The rate at which the slurry/water interface settles is recorded as a function of time. During static settling test a 500 ml of sample, made up to the correct density, is shaken vigorously and allowed to settle in a 500 ml measuring cylinder. A plot of the interface height of the supernatant water above the suspended solids over time is recorded.
- ii. **Rheology test work:** Sishen Mine supplied P&C with a sample of the “ideal” FeSi, which was tested to characterise the rheology of the FeSi. The viscosity is problematic to measure as the solids settles out in conventional viscometers. It was proposed to measure the viscosity in a re-circulating vertical tube viscometer using small bore pipelines. The FeSi was tested over a range of concentrations to determine the change in viscosity as a function of slurry concentration. Once the flow behaviour of the FeSi was benchmarked, a number ways of maintaining lower viscosities at high FeSi densities were investigated which are discussed below.
- iii. **Changing FeSi material properties to improve rheological flow behaviour:**
 - o *Particle Size Distribution:* Changing the particle size distribution of the FeSi can result in improved “lower” viscosity values and better stability at high FeSi densities. Changes to the FeSi particle size was conducted by removing of the finer fraction for both the dry coarse FeSi as well as the process FeSi. The influence of finer fraction removal is then mathematically modelled using the Rosin-Rammler equation so as to quantify the difference observed as follows (Doll, 2014):

$$Y = nX - n \ln(D_n) \quad \dots \text{Equation 3.1}$$

Where, $Y = \ln(-\ln R)$ and $X = \ln(D)$; D_n and n are fitting parameters.

The general Rosin-Rammler equation is as follows:

$$R = e^{-\left(\frac{D}{D_n}\right)^n} \quad \dots \text{Equation 3.2}$$

- *Viscosity Modifiers*: viscosity modifiers were investigated to check their impact on high density FeSi slurry. High density FeSi medium was then be dosed with viscosity modifiers and tested to investigate the change is FeSi viscosity and stability.

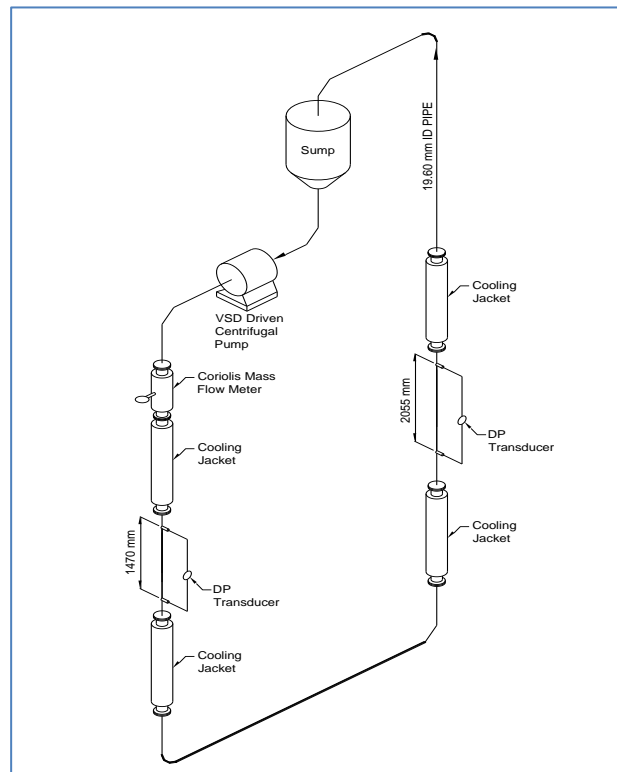


Figure 3.2: Schematic diagram of vertical tube viscometer set-up at P&C lab

Figure 3.3 shows a photograph of the equipment used for the pipe loop settling tests whilst a schematic diagram of the pipe loop settling test equipment is presented in Figure 3.4. The test measures the rate at which FeSi settles in a one-metre vertical column of slurry mixture. The test procedure is as follows:

- Circulate the slurry in the loop to form a homogeneous mixture at a constant density.
- While the slurry circulates at a constant flow rate and density, a valve at the bottom of a vertical pipe section is closed and the pump switched off so the slurry in the vertical pipe becomes stationary.
- Allow the slurry to settle in the vertical pipe and measure the change in pressure across the vertical settled bed with time using pressure transmitters (as shown) across a one-metre section of the vertical pipe.

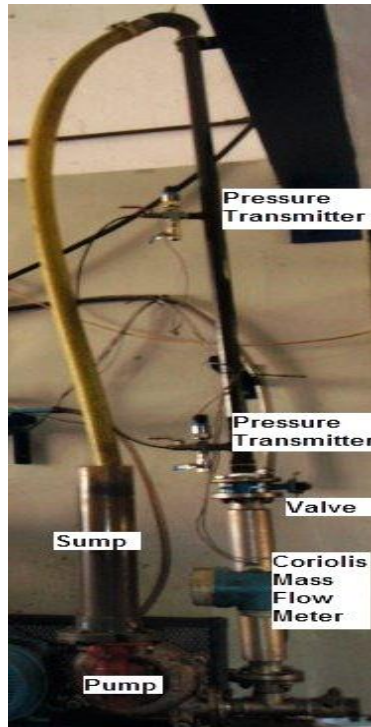


Figure 3.3: Photograph of pipe loop settling test equipment

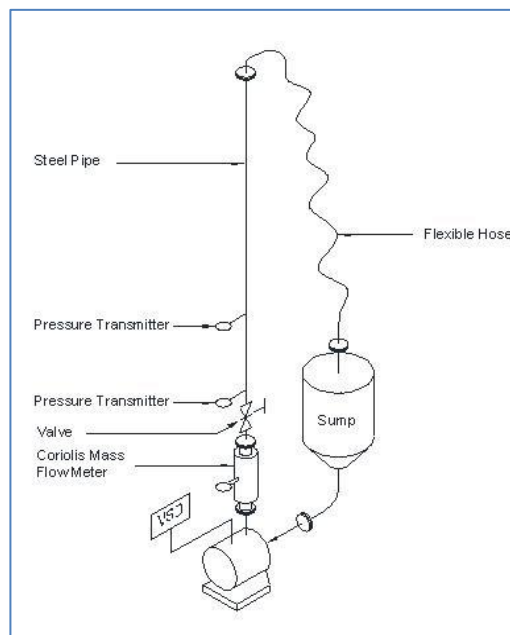


Figure 3.4: Schematic diagram of pipe loop settling test equipment

3.2.1 Coarse FeSi Less Fines

The “coarse FeSi less fines” was made up by blending a 1-tonne bag labelled “Coarse FeSi” and removing a percentage of the 40 μm fraction by sieving and using Cape Town potable tap water to make up the slurry.

3.2.2 Process FeSi

P&C tested a sample of process FeSi by blending the remains of the three drums of damp process FeSi with the sample as received to generate one process FeSi sample. Process FeSi was made up using the process water supplied by Kumba Iron Ore Sishen Mine.

3.2.3 Process FeSi Less Fines

The process FeSi, with a percentage of the 40 µm fraction removed by screening, was made up using the process water supplied.

3.2.4 Viscosity Modifier

The viscosity modifier used for this test work was the DP 725 from Lignotech. It is a purified grade calcium lignosulphonate product with low insoluble content and near neutral pH. Appendix B.1 shows the specifications for DP 725. The modifier was added at a rate of 100 ml/dry tonne FeSi.

3.3 PILOT TESTING OF AUTOMATED CYCLONE MODULE

The aim of the automated pilot testing was to evaluate the benefit of managing metallurgical variables through installation of instruments that would maintain tight control over the process variables and thus improve performance. Such process variables that had to be controlled include among others the following:

- *Medium-to-Ore ratio*: it has been demonstrated that the optimum M:O in spite of the amount of near density material ensures good separation efficiencies. Therefore, the “automation of the M:O ratio” is a critical aspect that must be explored further.
- *Medium viscosity*: it is a known fact that a viscous media is one of the critical factors in dense medium separation process. Thus, viscosity measurement and their control are beneficial to the dense media separation circuit.
- *Ep (E-cart probable)*: understanding the plant controls that would allow operation to control the Ep is also a key factor that the BU's has to consider.
- *Operating pressure*: it is important to understand what the optimum operating pressure for a particular commodity is. Therefore, a clear understanding of what test work methodology will prove this is also critical and how to automatically manage its influence on plant performance.

In addition, the pilot testing will unpack the factors influencing the M:O ratio and how to mitigate the negative impact on beneficiation process. Intensive effect of M:O ratio on dense medium separation was studied by (Chu, et al., 2009) and the following was established:

- ✓ At low M:O ratio, there are heavy particles that reports to the overflow stream,
- ✓ Decrease in M:O ratio increase the intensity of the inter-particle interaction thereby affecting the partition performance of the dense medium cyclone.
- ✓ As the M:O ratio decreases, the total inter-particle force, particle-wall contact force, fluid drag force and pressure gradient force increases. This will result in an increase

random movement of particles thereby leading to deterioration of the partition performance.

- ✓ Lower M:O will also result in surging phenomenon, thereby misplacing the lighter material onto the cyclone underflow streams. Thus, for the iron ore beneficiation, this will be detrimental to the product quality.

The cyclone inlet pressure and the factors influencing the cyclone inlet pressure as well as how they impact on the performance of the plant will be reviewed. (Petersen, 2010) alluded to the fact that the cyclone inlet pressure has been historically used as a diagnostic measure that work is done within the cyclone and not the actual energy doing the work. Sufficient inlet pressure and inlet velocity lead to tangential rotation of the fluid mixture within the cyclone as it move towards the vortex finder or the spigot (Atkinson, et al., 2012).

Cyclone inlet pressure is normally equated to gravity with the level of the head from the mixing box from gravity fed systems. Furthermore, the inlet is proportional to the operating medium density and incorporate:

- i. Static pressure → that is potential energy related on head (height of the mixing box above the cyclone inlet);
- ii. Dynamic pressure → kinetic pressure that is related on the movement of the fluid (that is ore and medium mixture);
- iii. Pressure loss due to viscosity and feed pipeline arrangement.

Density differential is one of metallurgical performance indicator (KPI) for the performance of the dense medium cyclone. In addition, it can be utilised as the “proxy” measure of the medium stability and rheology in the cyclone unit process. Measurement of on line medium viscosity in a DMS (Dense Medium Separation) circuit remains as elusive today, as was the case twenty years ago. Development of suitable instrumentation has been limited; despite industry wide acceptance, that medium rheology is a critical aspect for efficient density separation.

The separation efficiency can go off specification despite all first line measurements being within range, as a result of changes in medium rheology. The latter can only be inferred by the secondary off line laboratory measurements and may not always be immediately obvious given the time lag and probabilistic nature of DMS separation. A better way to make the same inference online in real time, is by measuring the density differential between the overflow and underflow streams.

It has been alluded by (Atkinson, et al., 2012) that when the density differential between the overflow and underflow is too large (i.e. >0.5), then there is the potential for recirculating material to be excessive. When this phenomenon happens, the cyclone is seen to ‘surge’ material through the cyclone spigot, thus leading to poor cyclone efficiency. Density differential can be classified as (i) feed to underflow differential, (ii) feed to D_{50} differential,

(iii) feed to overflow differential or (iv) underflow to overflow differential. The most common methods utilised are:

- ✓ **Method 1:** The density differential of the cyclone is measured by the medium density of the cyclone under flow and overflow, which has been detailed in (Napier-Munn, et al., 1994) and (Atkinson, et al., 2012) technical papers.

That is, Density differential = $RD_{\text{underflow}} - RD_{\text{overflow}}$

- ✓ **Method 2:** In this method, the density differential is measured as percentage of the difference in the medium feed density and cyclone overflow density. This method is adopted from Multotec and described in detail in (Bekker, 2012) course material.

That is, %Density Differential = $\frac{RD_{\text{feed}} - RD_{\text{overflow}}}{RD_{\text{feed}}} \times 100$

Density inversion occurs when the overflow density exceeds that of the underflow, and indicates that minimal classification takes place in the cyclone (Napier-Munn, et al., 1994). This might be due to high medium viscosity and operating feed density. It can also be an indication of the cyclone “back-pressure”, which is not desirable and the percentage minus 45microns FeSi in circulating medium. Other factors affecting differential include among others:

- ✓ medium viscosity/stability,
- ✓ feed head (pressure),
- ✓ cyclone diameter,
- ✓ inlet, barrel section design,
- ✓ spigot size,
- ✓ medium density, and
- ✓ Percentage of -45µm FeSi in circulating medium.

Table 3.1 indicates typical density differential for the dense medium separators, whilst the interpretation of the Method 1 and 2 measure of density differential is graphically summarised in Figure 3.5 as follows:

- ✓ Most common differential is 3% - 12%. A differential in excess of 12% might indicate medium stability problems and the one below 3% is indicative of viscosity problems.
- ✓ For good stable dense medium cyclone operation, density differential should be between 0.2 and 0.4.

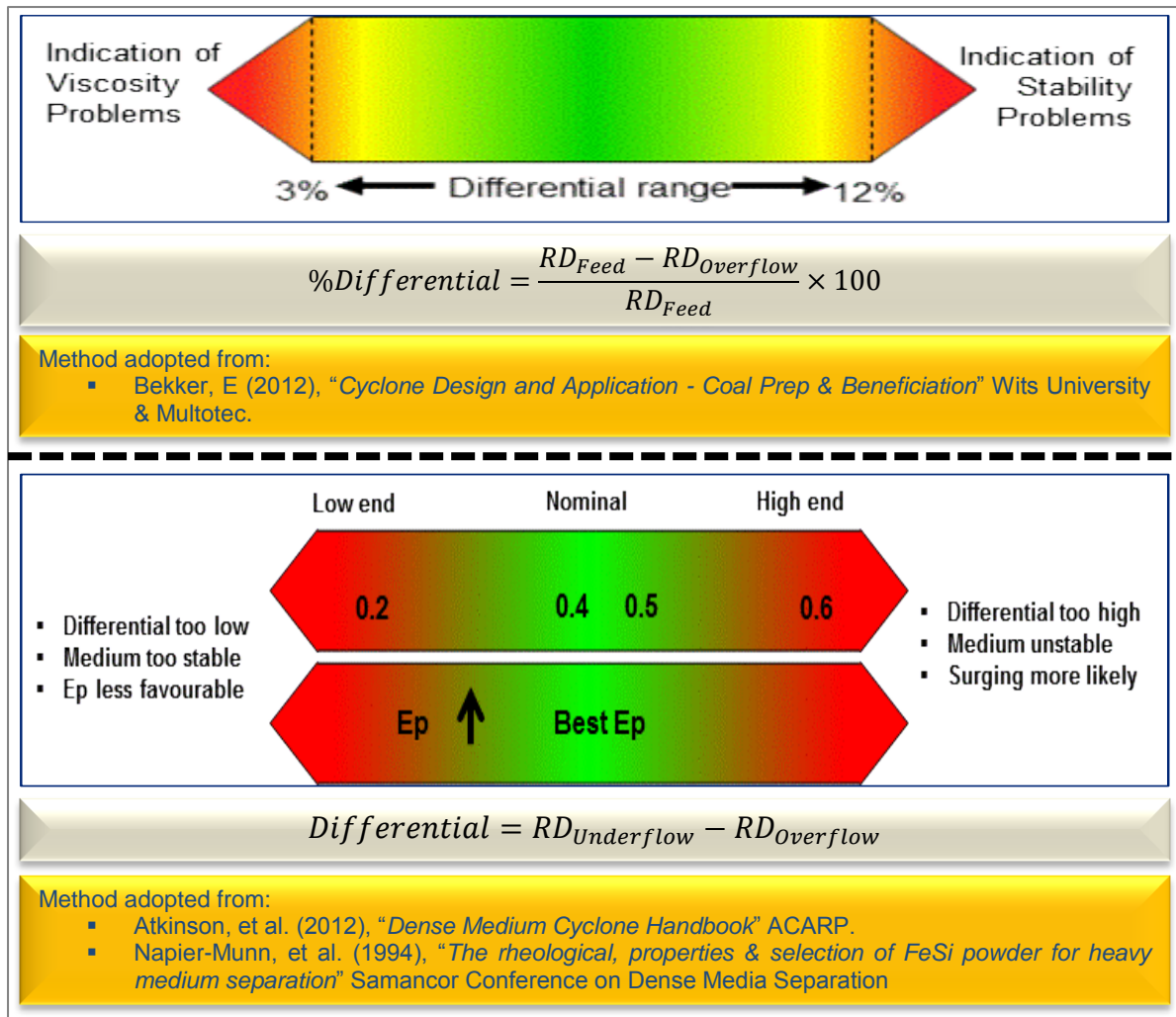


Figure 3.5: Density differential methods

Table 3.1: Typical values of density differential for dense medium separators (King, 2001)

Separator type	Cut point	Cut point shift	Sp. Gr. differential	Imperfection	Particle size	Reference
Chance cone	1.54			0.021		Coal Leonard (1979)
	1.37			0.01	+ 50 mm	
	1.37			0.03	12.5 6.5 mm	
		0.033		0.015		
Dense-medium vessel	1.41			0.020		Coal Leonard (1979)
	1.35			0.018	50 25 mm	
				0.033	12.5 6.3 mm	
Dense-medium cyclone	1.49			0.019	1/2 3/8	Coal Weiss (1985)
	1.50			0.017	3/8 1/4	
	1.51			0.021	1/4 8#	
	1.53			0.025	8# 14#	
	1.57			0.051	14# 28#	
Dense-medium cyclone	1.325	0.045		0.014	1 28#	Coal Weiss (1985)
	1.488	0.142		0.015	1 28#	
Dense-medium cyclone	3.65	0.59	0.39	0.043	3/16 28#	Iron ore Weiss (1985)
	3.385	0.54	0.51	0.028	3/16 28#	
Dense-medium cyclone	3.065	0.455	0.41	0.036	3/16 65#	Chromium ore Weiss (1985)
	3.095	0.345	0.27	0.045	3/16 65#	
	2.907	0.217	0.28	0.018	3/16 35#	
	3.065	0.215	0.25	0.027	3/16 35#	
Dense-medium cyclone	2.82	0.42	0.41	0.028	3/16 28#	Magnesite Copper ore Davies et al. (1963)
	2.4	0.55	0.58	0.037	3/16 28#	

Part of the cyclone automation project, was to install instruments for the real-time measure of the density differential. Historically, the unit operation conditions were manually monitored on an ad-hoc basis by sampling the cyclone overflow and underflow stream for density differential. This practice requires the feed to a particular unit process to be stopped for a period of at least 30 minutes and thus influencing negatively on production. Furthermore, the manual measurement varies from operator-to-operator and thus introduces an error in the accuracy of the measured density differential. Figure 3.6 shows the installation of the instruments (De Beers' DMCT110 units) utilised for the real-time density differential measurement. The on-line measurement method does not require the ore feed to the unit process to be stopped, as the units are installed on the drain section of the cyclone overflow and underflow drain-rinse screens.

The DMCT110 units works on the principal of measuring the inductance of a coil winded around a pipe. This is achieved via an oscillating circuit producing a frequency. Discussion with the supplier (Anglo American's De Beers Group) indicated that during development of the unit's standard (default) equations are derived for most of the different sizes and types of mediums (Atomised FeSi, Milled FeSi or Magnetite). This will in return convert the frequency to a given S.G.

The default equation acts as a starting point for calibration. A full calibration consist of two points; high point above average SG and low point below average SG (not in air or water) within the required measuring range (Nabbie, 2012). The wider apart and consistency of the hand samples the more accurate calibration will be. Since the low and high point can be saved, it is recommend that the density be monitored over a period if the over and underflow drifts higher/lower than normal go to the unit take a manual sample and capture the high/low point. Once both the values has being captured execute the calculate variables. This will in return recalculate the equation.

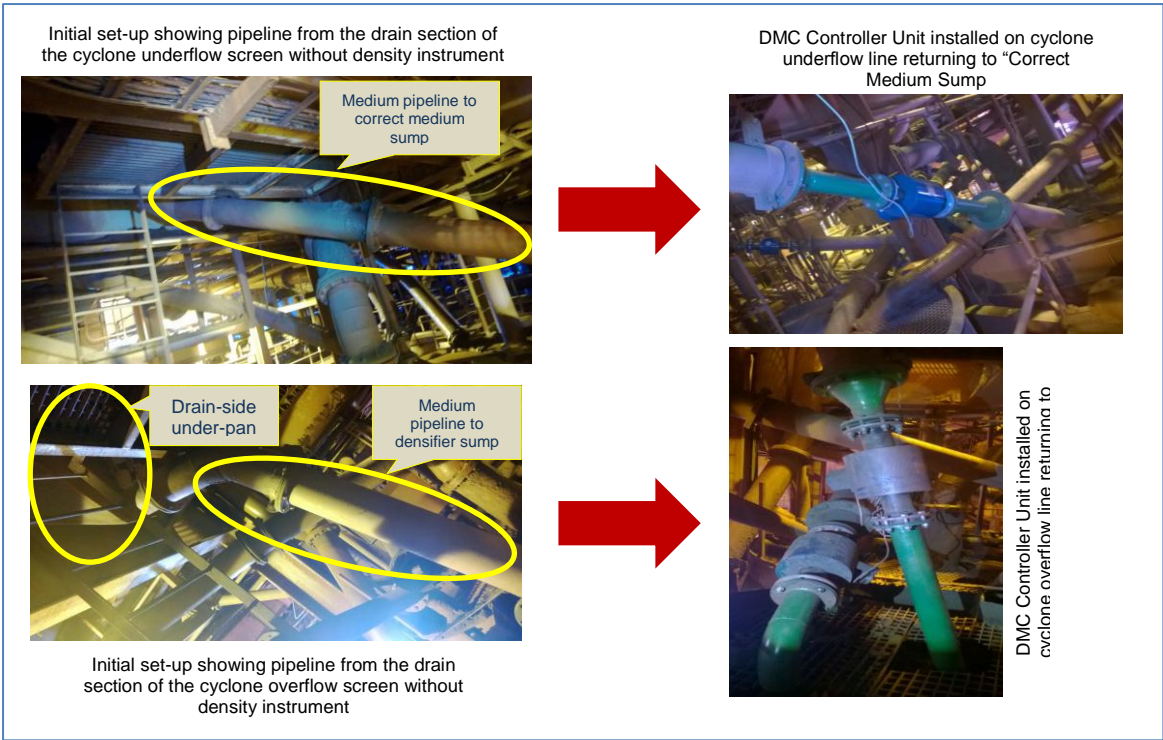


Figure 3.6: Installation of density differential measuring instruments (DMCT110 units)

CHAPTER 4: ORE AND FESI CHARACTERISATION

4 ORE AND FESI CHARACTERISATION RESULTS

4.1 ORE CHARACTERISATION INTRODUCTION

Ore characterisation entailed testing of various ore types and ROM blends of varying quality for densimetric analysis; mineralogical and chemical analysis. The Dense Medium Separation characterisation is based on densimetric (washability) analysis and shaking table tests. These tests were conducted on different particle size ranges. Chemical analysis of the material in the respective density fractions was conducted to predict the individual ore grades as well as prediction of expected product qualities. The material size fraction that is beneficiated in the cyclone plant at Sishen Mine is currently limited to the -8+5mm in the Coarse Cyclone Plant and -5+2mm material in the Fine Cyclone Plant. The proportion of the undersized misplaced to the Coarse Cyclone Plant varies between 5 to 10% minus 5mm material in the feed, whilst the misplacement to the Fine Cyclone Plant can reach up to 20% minus 2mm fraction.

4.1.1 Ore Densimetric and Chemical Analysis

Densimetric (washability) analysis is done to provide an indication of the theoretical mass percentage of the head feed (ROM) that will report to the concentrate stream (product stream) of the beneficiation processes, taking into account the blending requirements of different mining areas. Detailed densimetric and chemical analysis data for the Sishen ROM material is presented in Appendix A. By taking into account typical DMS process inefficiencies, the beneficiation process yields are then predicted for individual ore types.

The samples characterised for beneficiation ability are comprised of:

- i. DMS head grade ROM composite samples
- ii. GR80 bulk samples, since the majority of the feed to the DMS will be from the GR80 location in the pit.
- iii. Low grade stockpiles samples.
- iv. Samples taken during shifts when low-grade material was processed in the plant.

4.1.2 Characterisation Results of DMS Head Grade ROM Composite Samples

Samples comprising three (3) ROM head grade batches were taken from the ROM fed to the plant between the 19th May and 4th July 2014. The samples were composite material fed to the plant sampled hourly using the automated hammer sampler and these samples were as follows:

- i. Batch 1: Hourly composite sample for the period of 19th – 30th May 2014;
- ii. Batch 2: Hourly composite sample for period of 31st May – 13th June 2014;
- iii. Batch 3: Hourly composite sample for the period of 14th June – 4th July 2014.

Figure 4.1 shows the densimetric profile and chemical analysis of the DMS plant ROM Head Grade composite samples for the combined size fractions. The results show that the ROM for all the three batches collected between the 19th May 2014 and 4th July 2014 had relatively lower proportion of near-density material.

Figure 4.2 shows the chemical analysis of the DMS plant ROM Head Grade composite samples for the -5+2 mm size fraction of the three batches. The weighted average SiO₂ contaminant levels of ROM ranges between 7.3 to 9.4%; while the Fe grade range is 61.0 to 62.3% Fe. Thus, this ROM material can be classified as high-grade ore.

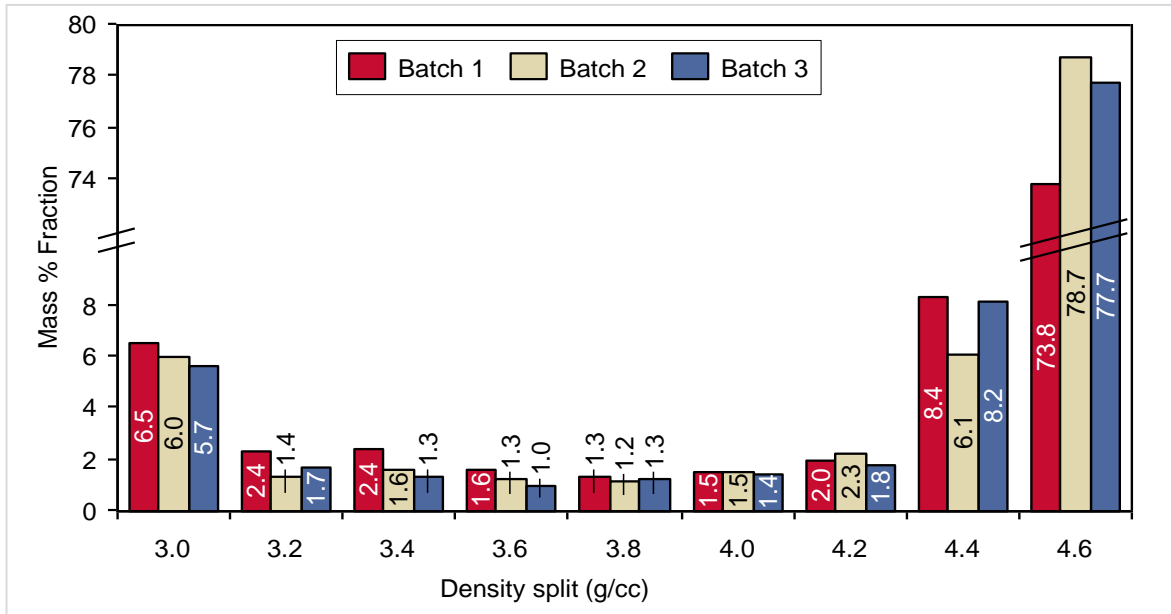


Figure 4.1: Densimetric profile of the DMS head grade ROM samples

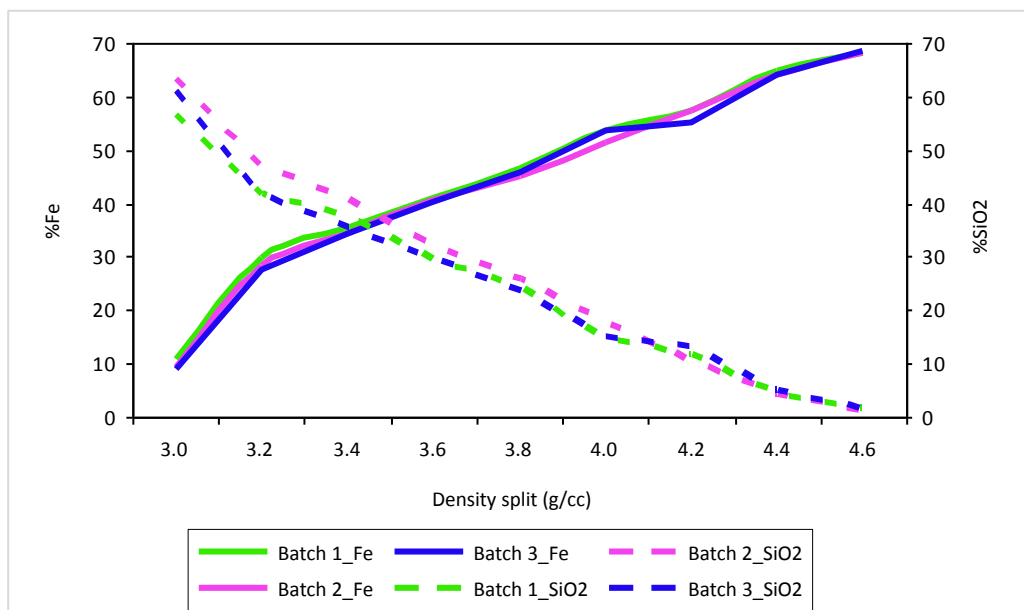


Figure 4.2: Chemical quality of the DMS head grade ROM samples

The probability curve in conjunction with the Ecart Probable Moyen was used to demonstrate the impact of processing efficiency of material with different densimetric profiles. The

partition curve is determined using the Whitten's equation as described in Section 2. Each partition number calculated reflects the fraction of material, per density fraction, that will report to the cyclone concentrate stream.

The beneficiation ability of the DMS head grade material processed through the DMS plant during the 19th May 2014 to 4th July 2014 is presented in Figure 4.3. The result indicated the expected yield for the beneficiation plant operating at cut-density of 3.6 t/m³ with an Ep of 0.17, is 89.78%. When the slimes and -2mm material of the ROM that are fed to thickeners and Up-current Classifier are also considered, the expected yield from the material is **81.25%**. However, the actual plant realised yield for the same period was 79.9%, which is indicative of inefficiency within the plant. Thus, during this period, the beneficiation plant was 98.3% efficient. With a conservative Ep of 0.17, the current operation practice could not achieve the required yield, thus necessitating proper control and automation to ensure stability and good processing efficiency.

When the plant operates at lower EP, such as best practice of 0.05 – 0.10, an improved performance would be realised with approximately 17 – 19% reduction of the contaminant levels in the product. Iron ore product with high contaminant levels are not sought after and results in penalty payment as high as \$1.8m/annum. In addition, a 1.5% yield increase in a plant producing 2.748Mt fine iron ore at a market price of \$65/dmt would result in additional revenue of \$2.679m.

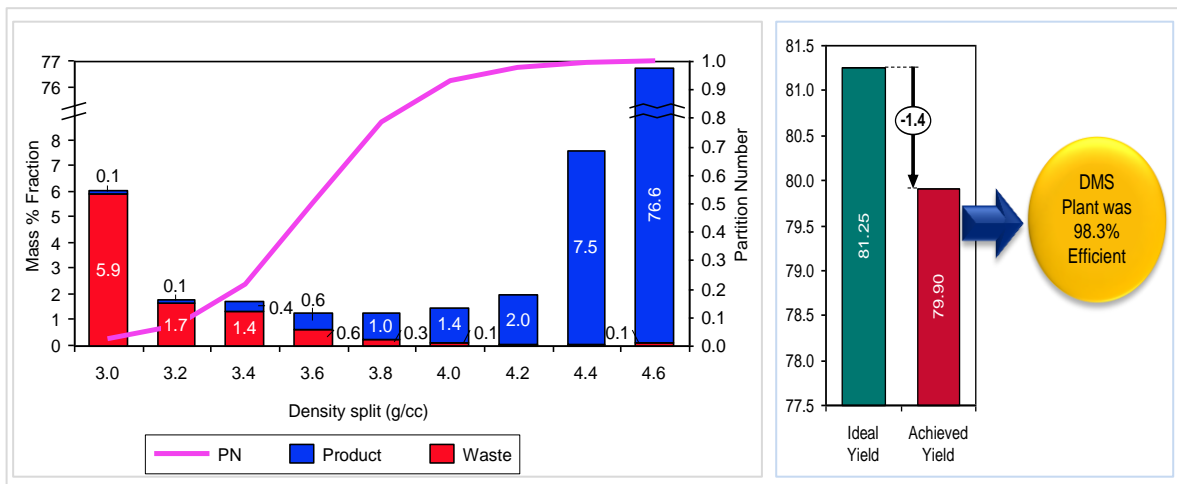


Figure 4.3: Effect of ROM's densimetric profile on yield at cut-density of 3.6 t/m³ and Ep~0.17

4.1.2.1 Impact of cut-density versus Ep

Ep and cut-density are the important performance factors for the dense medium separation process. Ep, that is, Ecart probable error measures the deviation of the actual curve from the ideal curve, with higher Ep indicative of poorer separation. Cut-density is the relative density corresponding to the 50% of the feed material reporting to either overflow or underflow. Sensitivity analysis on the effect of Ep and cut-density was applied to the 2014 DMS ROM

densimetric profile data. The objective was to evaluate which parameter has the greatest impact on the expected yield, product grade as well as contaminant levels in the product.

Figure 4.4 shows the effect of Ep and cut-density on the expected product yield and quality on batch 1 and batch 2. It can be seen by steep slope that the cut-density has the greatest impact either positive or negative. The graph shows that as the operating Ep increases, there is a slight increase in expected yield whereas the product Fe-grade decreases. Furthermore, the graph shows an increase in %SiO₂ contaminant as the Ep increases.

The cut-density showed opposite effect to the Ep, where an increase in cut-density would result in drastic decrease in yield. However, increase in cut-density favours the product quality thereby increasing the Fe-grade of the product while decreasing the levels of SiO₂ contaminant. It can thus be concluded that in order to effect a quick change and response during beneficiation of iron ore, the metallurgical parameter to manipulate is the cut-density.

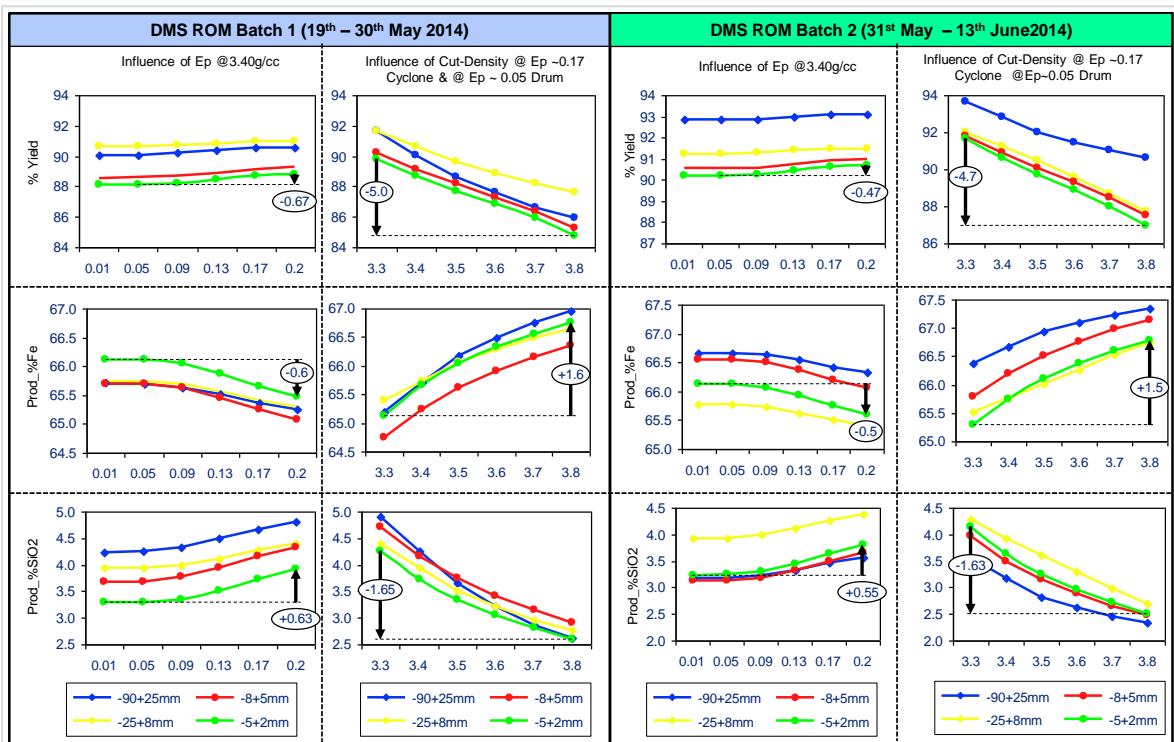


Figure 4.4: Predicted yield and quality as function of Ep and cut-density

Densimetric profile of the ROM is influenced by the material composition in the blend, of which it is summarized in Figure 4.5, whereas detailed daily material class and material blend is illustrated in Figure 4.6 and Figure 4.7 respectively. The description of the material type classification for Sishen Mine ores is presented in Appendix A.1 in order to give a holistic understanding of interpretation linked to material class.

The ROM blend for the period under review is composed mostly of the A-material and the Bruce-A ore. The A-material is defined as the high grade iron ore which occurs mainly in the laminated, massive and conglomeratic stratigraphic formations. It also contains gritty iron ore inter-bedded with shale. Bruce-A is the stockpile with material destined for the DMS plant

which is utilised to dump high-grade ore while the processing plant is not available to accept ore from the mining areas.

The material composition of the ROM blend was composed of 101 material classes which is characterised as high grade full bench ore with the head grade in excess of 64.5% Fe. The overall 101 composition of the ROM blend for the period under review was 73.72%. The 101 material classes is further classified in 101L and 101H categories, where the 101H is indicative of high grade full bench ore with high proportion of phosphorus. The phosphorus content in the iron ore body bears no relations to the percent Fe-content of the ore. The main phosphorus bearing mineral is apatite $[Ca_5F(PO)_4]_3$.

The 102 material classes is a high grade full bench with intermediate waste, whereas the 201 and 301 material classes are the ore bodies with high density waste. The in-situ head grades of the 201 and 301 material classes are greater or equal to 61% Fe. The proportion of 201 and 301 material classes in the blend averaged 7.53 and 5.11% respectively.

The 302 material classes are characterized as B-grade material with the in-situ head grade averaging 58.5% Fe. This material is characterized as ore with high density waste from less than full bench.

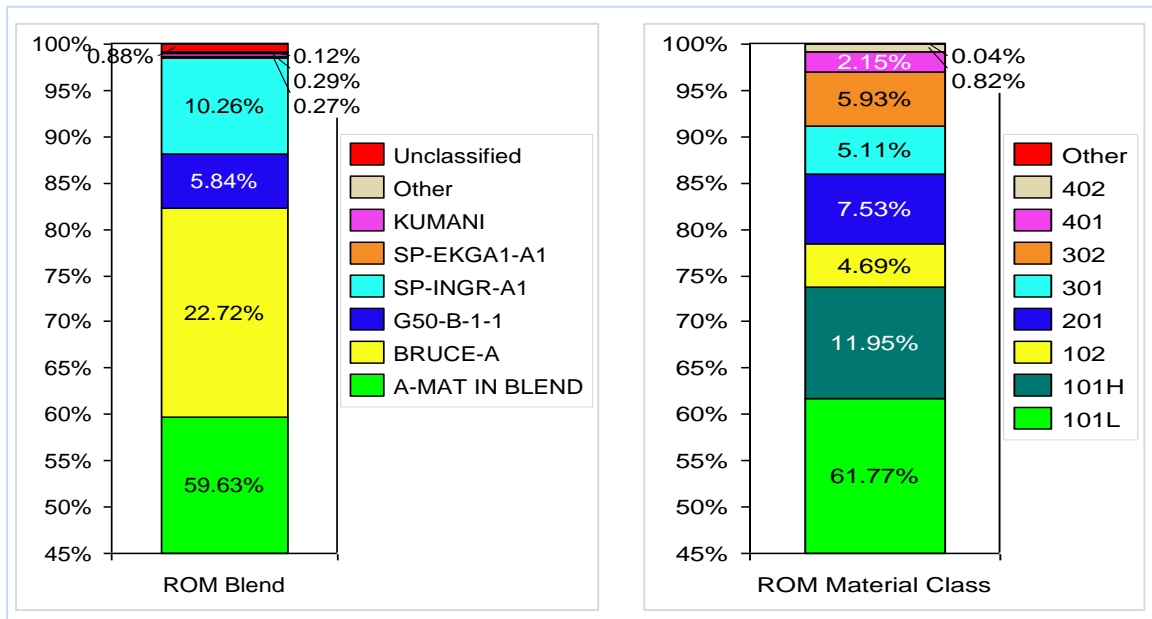


Figure 4.5: 2014 DMS ROM compositions summary

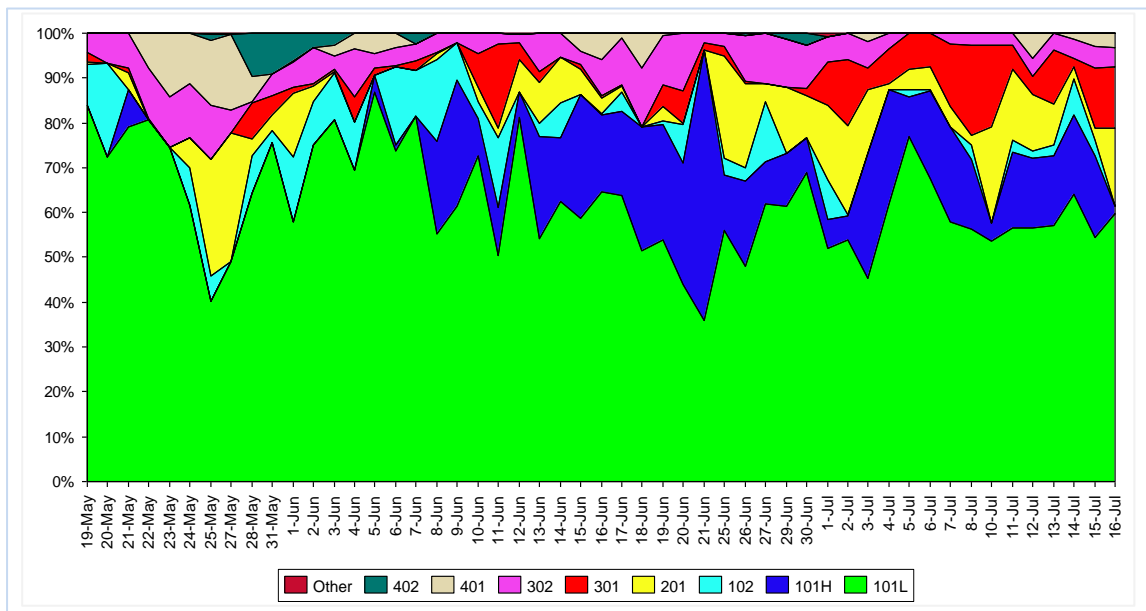


Figure 4.6: Detailed ROM compositions – material class

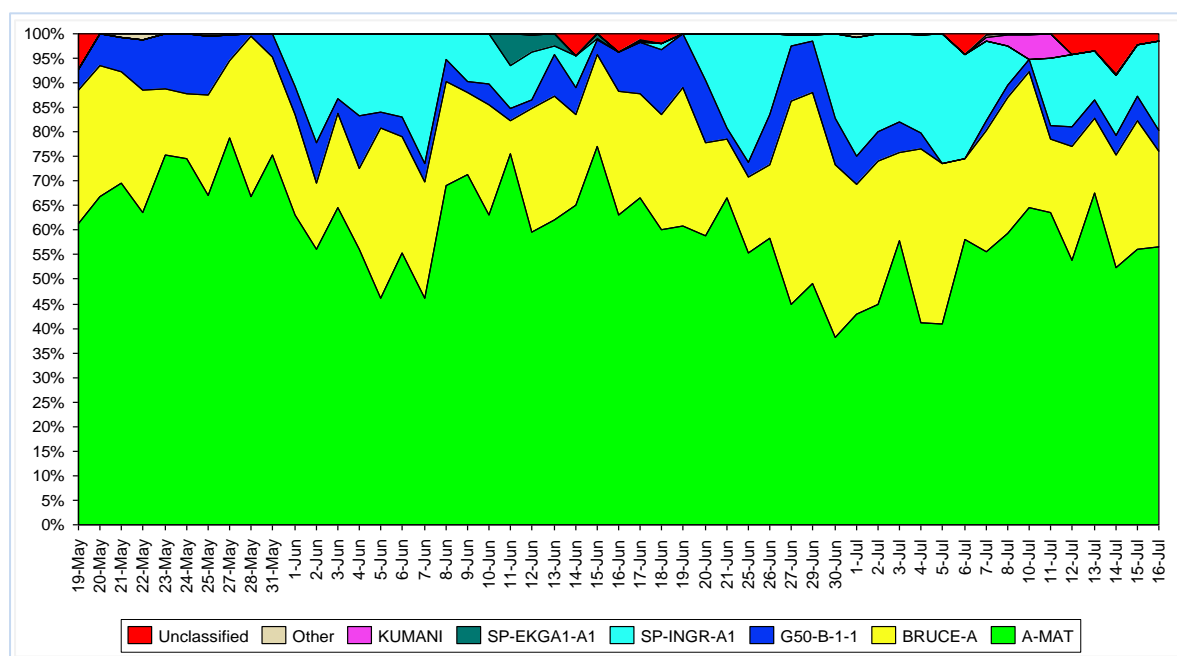


Figure 4.7: Detailed ROM material composition – material blend

4.1.3 Ore Characterisation Results of GR80 Mining Area Ore body

A total of eleven (11) bulk samples were taken from the blasted pit ore that resembles feed grade to the DMS plant. The compositions of these samples were classified by the Production Geologist as to the main ore types comprising the blend. Table 4.1 presents the sample identification number, geological description and the corresponding location within the GR80 mining area. Material type classification for Sishen Mine ores is presented in Appendix A.1 in order to give a holistic understanding of interpretation linked to material class.

Table 4.1: GR80 bulk samples descriptions

Sample Number		Geological Description	Sample Number		Geological Description
Plant 1	851614A1	HL + BIF (Laminated ore + Banded iron formation)	Plant 7	370422A2	201.1 Laminated ore and Banded iron stone
Plant 2	931614A1	101 EL Laminated ore	Plant 8	090419A1	101.1 Laminated ore
Plant 3	231032A1	102.1 Conglomeratic ore	Plant 9	851614A2	HL + BIF (Laminated ore + Banded iron formation)
Plant 4	851613A2	101.2 EL - Laminated ore			
Plant 5	851613A3	201.1 EL+ LY (Laminated ore + banded iron formation)	Plant 10	931614A1	101 EL Laminated ore
Plant 6	1021307A2	301 HL + SH (Laminated + shale)	Plant 11	931614A1	101 EL Laminated ore

Figure 4.8 shows the densimetric analysis results of the combined size fractions, whilst Appendix A.2 present detailed chemical and densimetric results for GR80 samples. The results indicated that most of the bulk samples from GR80 area can be classified as “*forgiving*” due to relatively low proportion of near density material. However, Plant 1, 7 and 9 samples had relatively higher proportions of the near density and lower density fractions compared to other ore blends. These samples comprised of class 201 laminated ore with banded iron formation (BIF). The class 201 ore is characterised as ore with high density BIF.

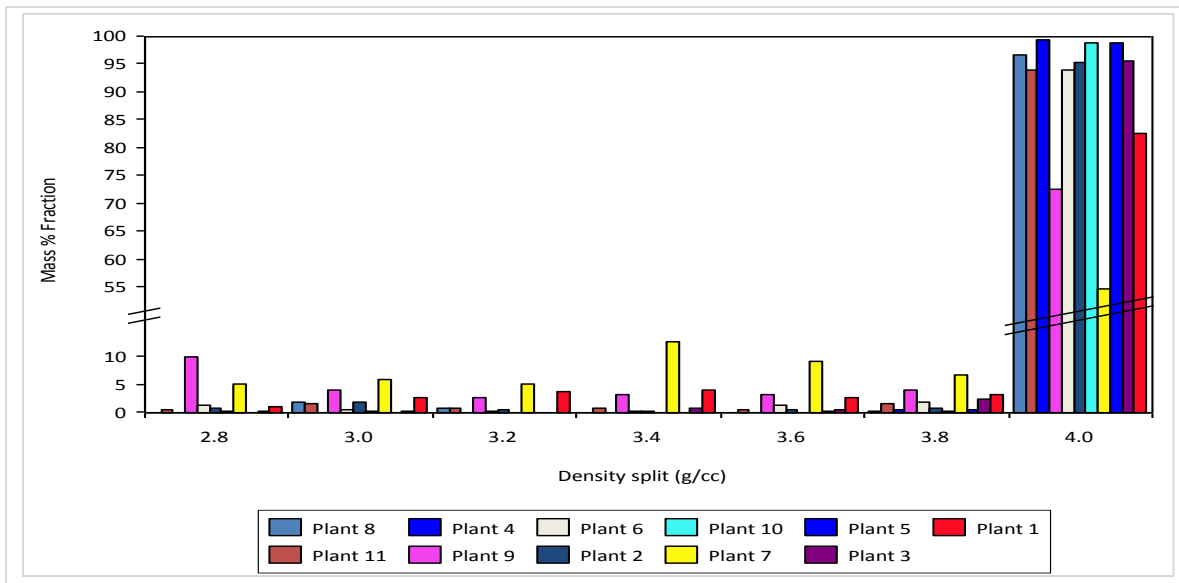


Figure 4.8: Densimetric analysis of combined GR80 samples

The impact of near density material on the beneficiation efficiency of GR80 material is demonstrated in Figure 4.9, which compares the processing ability of Plant 1 versus Plant 8 material.

The results indicated that the yield and quality prediction for ROM with high proportion of near density material would be worse than the ROM with low near density material. It can be seen in Figure 4.9 that Plant 1 material would produce lower product yield and quality versus that the Plant 8 material. The predicted yield for Plant 1 and Plant 8 are 85.90% and 95.31%

respectively, whilst the expected product quality would be 65.25% Fe and 67.76% Fe for Plant 1 and Plant 8 respectively.

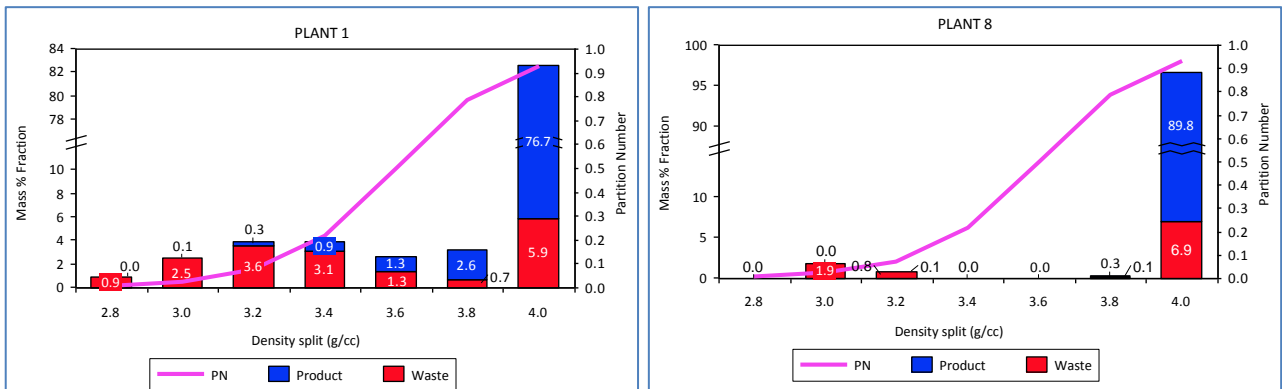


Figure 4.9: Impact of near density material of beneficiation (Plant 1 vs. Plant 8)

Figure 4.10 presents the densimetric profile of the GR80 material at various size fractions. The graphs show that different size fractions of the same sample have different densimetric profile. This is the influence of ore liberation of less dense minerals as the ore is crushed to finer size. Thus, it would be expected that smaller size fraction would have lower yields. This has been experienced in the processing plant where Fine Cyclone Plant yields are generally lower than the Coarse Cyclone Plant. The Fine Cyclone Plant treats the -5+2mm material whereas the Coarse Cyclone Plant treats the -8+5mm material. The -90+8mm material is treated on the Wemco Drum unit process.

From the data, it can be concluded that the Plant 7 and Plant 9 run-of-mine material would pose processing challenges in the Cyclone Plant. Table 4.2 shows simulated yield and product quality when operating at a cut-density of 3.6 t/m³ and Ep of 0.11. These results show that as the size fraction decrease lower yields are expected as well as lower product Fe grades. In addition, the contaminants in the product, that is, SiO₂ increases with a decrease in size fraction. Plant 7, which had high proportion of near-density material, showed the lowest predicted yields and product Fe grade while the SiO₂ grade was the highest of all samples.

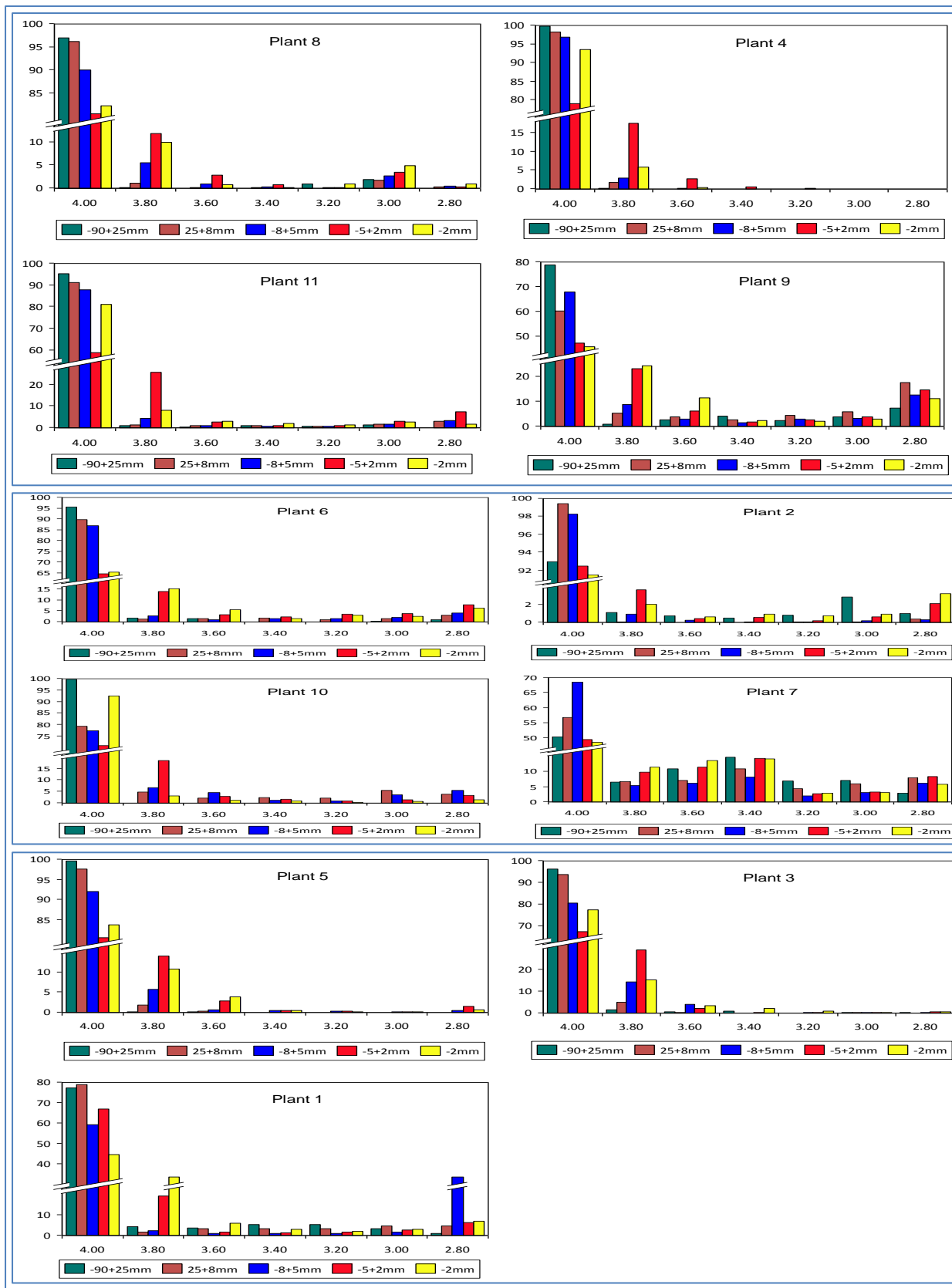


Figure 4.10: Densimetric profile as a function of material particle size distribution

Table 4.2: Yield and quality predictions for at 3.6 t/m³ cut-point and Ep of 0.11

% Yield	PLANT 8	PLANT 11	PLANT 4	PLANT 9	PLANT 6	PLANT 2	PLANT 10	PLANT 7	PLANT 5	PLANT 3	PLANT 1
Total Split	95.31	94.17	98.05	76.77	94.69	94.50	97.46	66.05	97.87	96.33	85.90
-8+5mm	93.69	90.64	97.62	76.20	88.52	97.36	84.35	76.25	95.94	93.80	61.00
-5+2mm	90.97	81.98	94.46	70.24	77.87	94.29	87.56	64.83	92.98	92.76	83.79
-2mm	89.94	88.55	97.21	72.52	80.77	92.05	94.14	66.41	93.75	91.44	77.46
ROM Density	3.97	3.96	4.00	3.78	3.96	3.96	3.99	3.71	4.00	3.98	3.89
ROM %Fe	66.79	64.51	66.42	55.75	65.14	64.65	66.04	53.21	67.91	64.27	60.89
Product %Fe	PLANT 8	PLANT 11	PLANT 4	PLANT 9	PLANT 6	PLANT 2	PLANT 10	PLANT 7	PLANT 5	PLANT 3	PLANT 1
Total Split	67.76	66.21	66.43	65.45	66.56	66.36	66.33	61.77	67.97	64.81	65.23
-8+5mm	67.34	65.82	66.17	65.17	66.37	66.40	64.47	62.71	67.82	64.03	65.55
-5+2mm	66.75	62.78	64.18	63.27	63.55	65.85	62.80	60.95	67.48	63.65	62.65
-2mm	66.98	65.01	65.82	62.48	63.10	66.08	65.73	60.54	67.45	63.94	58.78
ROM %SiO ₂	2.89	4.02	2.78	18.46	3.88	3.97	3.23	24.20	1.86	4.31	11.59
Product %SiO ₂	PLANT 8	PLANT 11	PLANT 4	PLANT 9	PLANT 6	PLANT 2	PLANT 10	PLANT 7	PLANT 5	PLANT 3	PLANT 1
Total Split	1.94	2.92	2.77	4.56	2.91	2.86	3.06	10.68	1.83	3.74	5.35
-8+5mm	2.19	3.17	2.94	4.88	3.03	2.84	3.80	9.04	1.90	4.65	4.90
-5+2mm	2.56	5.09	4.20	7.32	4.82	3.20	4.35	12.03	2.06	5.04	9.16
-2mm	2.42	3.68	3.16	8.45	5.11	3.05	3.29	12.70	2.08	4.74	14.84

4.1.4 Interpretation of Data for Samples from the Low Grade Stockpiles

Sample taken from low-grade stockpiles comprised of *banded iron formation*, *conglomeratic* and *shale* mineral types. Detailed ore characterisation of results of the low-grade stockpiles samples is presented in Appendix A.3, while Figure 4.11 shows the overall densimetric analysis of the material from low-grade stockpiles. The results showed that the samples from low-grade stockpiles have elevated proportion of near-density material. In addition, the results indicate that the low-grade stockpile had high proportion of near-density material compared to GR80 material from the mining pit. Thus, it is expected that ROM material from stockpiles would be difficult to beneficiate compared to the GR80 material, which would necessitate the beneficiation process to operate at relatively higher density.

Table 4.3 presents the predicted yield and product grade when operating the beneficiation unit process at a cut-point of 3.8 t/m³ and Ep of 0.11. The results indicates that when the low grade stockpile material is fed to the cyclone plant as blended head-feed would produce a product yield of 46.5% which the product grade of 62.60% Fe and the contaminant levels of 6.75% SiO₂.

However, if the material were to be treated in isolation, the banded iron formation material would result in the lowest yield estimated at 40.39%. The predicted product quality from the low grade banded iron formation will be 62.10% Fe with the contaminant levels as high as 8.17 to 10.9% SiO₂.

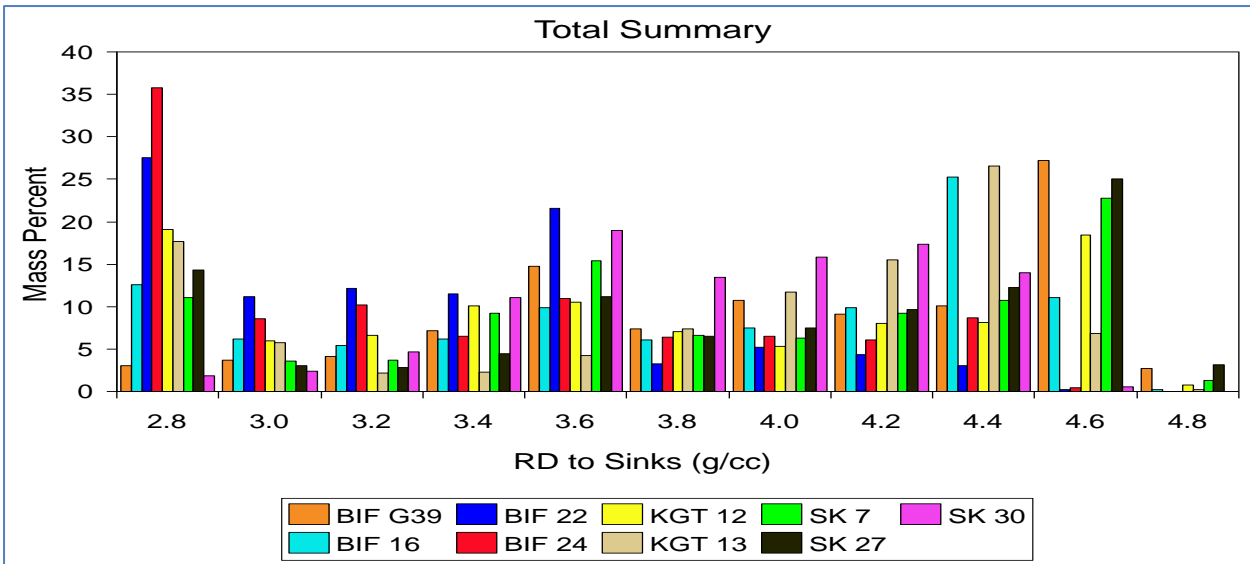


Figure 4.11: Combined densimetric analysis of samples from low-grade stockpiles

Table 4.3: Yield and product quality predictions for low-grade material at 3.8 t/m³ cut-point

DMS Cut-point: 3.80

DMS Ep-Value: 0.11

Key: Yield & Quality Based on Densimetric Analysis

Inputs

Weighted average of all tested samples from low grade stockpiles

Weighted average of combined BIF

	Banded Iron Formation				Conglomerate		Shale			Combined BIF Data	
	BIF G39	BIF 16	BIF 22	BIF 24	KGT 12	KGT 13	SK 7	SK 27	SK 30		
Average Yield	46.5%				52.35		62.60		6.75		
% Yield											
Total Split	64.01	57.01	16.63	25.49	44.90	63.09	54.73	61.23	54.58	40.39	
-90+25mm											
-25+6mm	72.32	64.42	19.00	25.56	50.93	80.32	66.29	70.39	70.67	45.20	
-6+2mm	66.87	57.18	16.80	28.88	43.31	69.34	61.70	63.31	55.18	42.70	
-2+1mm	38.90	37.93	11.70	19.39	37.18	20.17	26.82	39.98	21.76	25.61	
-1mm											
ROM Density	4.02	3.84	3.32	3.36	3.71	3.85	3.88	3.93	3.84	3.63	
ROM %Fe	55.94	57.71	40.09	45.60	53.33	57.11	57.22	59.70	53.00	50.53	
Product %Fe											
Total Split	62.38	65.64	55.49	58.64	63.31	62.03	64.13	64.88	58.17	62.10	
-90+25mm											
-25+6mm	61.84	65.64	52.11	57.52	63.85	61.40	63.80	64.50	58.04	61.32	
-6+2mm	62.57	65.40	57.96	60.64	64.37	62.70	64.71	65.04	58.52	62.80	
-2+1mm	64.37	66.44	61.83	56.73	60.31	63.70	63.40	65.59	57.06	63.22	
-1mm											
ROM %SiO₂	18.80	15.08	24.39	23.31	10.37	8.84	13.02	8.82	10.57	18.92	
Product %SiO₂											
Total Split	8.62	5.06	19.75	15.25	4.74	2.13	5.23	3.68	7.28	9.72	
-90+25mm											
-25+6mm	9.41	5.20	24.73	17.22	4.20	0.12	5.56	3.98	7.60	10.90	
-6+2mm	8.23	5.25	16.11	12.03	4.07	4.89	4.75	3.60	6.82	8.58	
-2+1mm	6.10	3.74	10.47	17.86	7.10	4.22	5.57	3.01	7.66	8.17	
-1mm											

and Ep of 0.11

Figure 4.12 presents the beneficiation potential of different ore types from the low-grade stockpiles. The results indicated that the shale (SK) ore types would have the highest yields of 56.98%, followed by the conglomeratic (KGT) ore with 54.29% yields whilst the banded

iron formation (BIF) would result in the lowest yield of 40.39%. The predicted product grades for the different ore types would be 63.1% Fe, 62.7% Fe and 62.1% Fe for the SK, KGT and BIF material respectively.

In addition, SK and KGT would produce a product with low content of contaminant, which would be lower than 8% SiO₂. The product specification for the low-grade product specifies that the contaminant should be below 8% SiO₂. Thus, if the ore types were to be treated in isolation, only the product produced from SK and KGT would meet the customer specification. This shows that if product volumes and quality spec were critical, it would be advisable to process these ore types in isolation since the blended head-feed generate lower yield of 10% less than individual ore types though the contaminant level is much lower than specification.

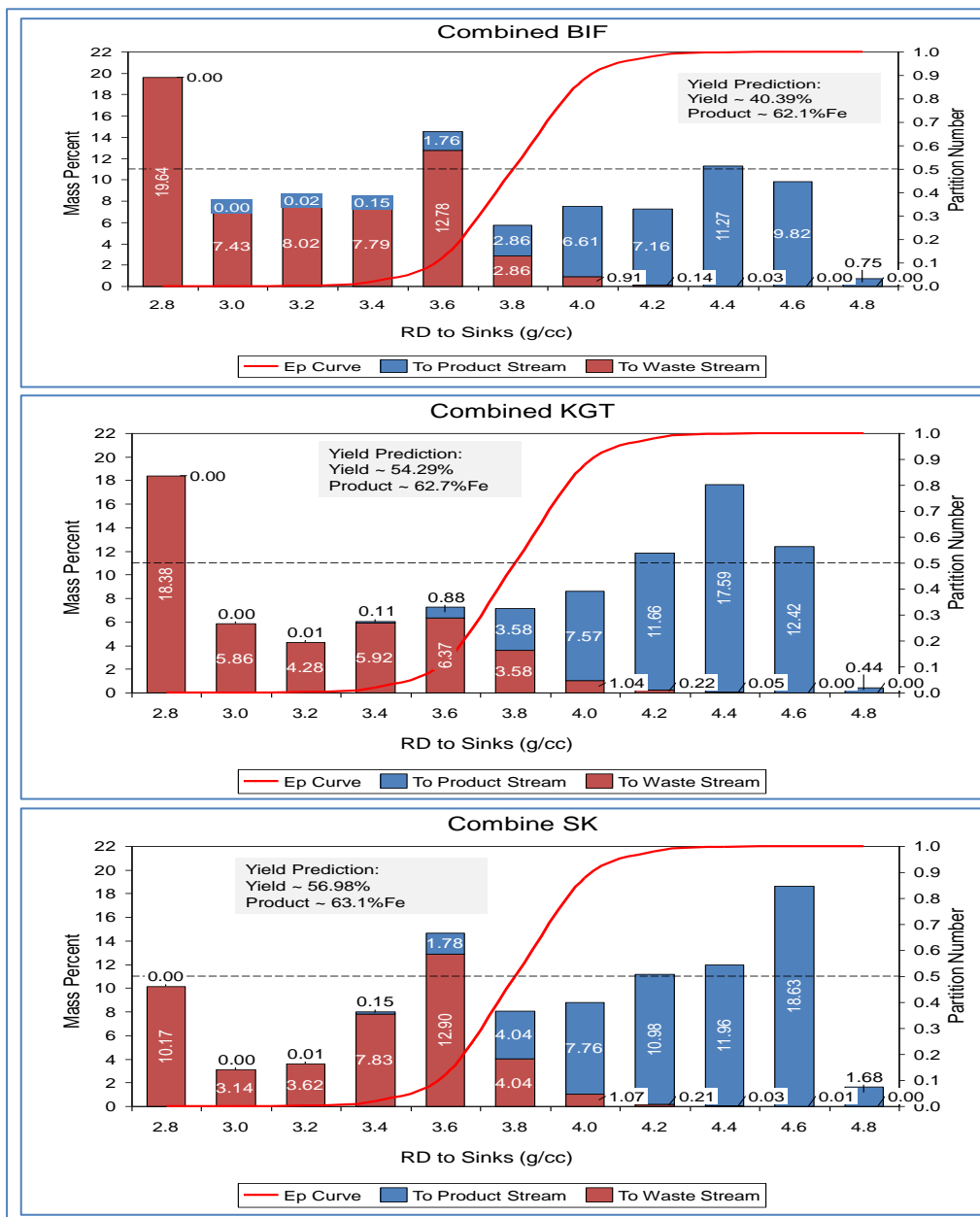


Figure 4.12: Comparison of beneficiation potential different low-grade stockpiles ore types

4.1.5 Interpretation of Data for Samples from the Actual Pilot Plant Processing

Samples comprising the product, waste and feed were taken for the material that was processed through the Ultra-High Density DMS (UHDMS) Pilot Plant. The samples processed through UHDMS comprised of two sets of samples, that is, (i) *material from low-grade stockpiles* and (ii) *waste material from the JIG plant*. Tabulated data of the densimetric material from these samples is presented in Appendix A.4, while graphical presentation of the data is depicted in Figure 4.13. The material from low-grade stockpile showed a similar densimetric profile while the JIG waste material was characterised with a high proportion of low-density material. However, similar Fe grade can be seen for the same density splits for all samples tested.

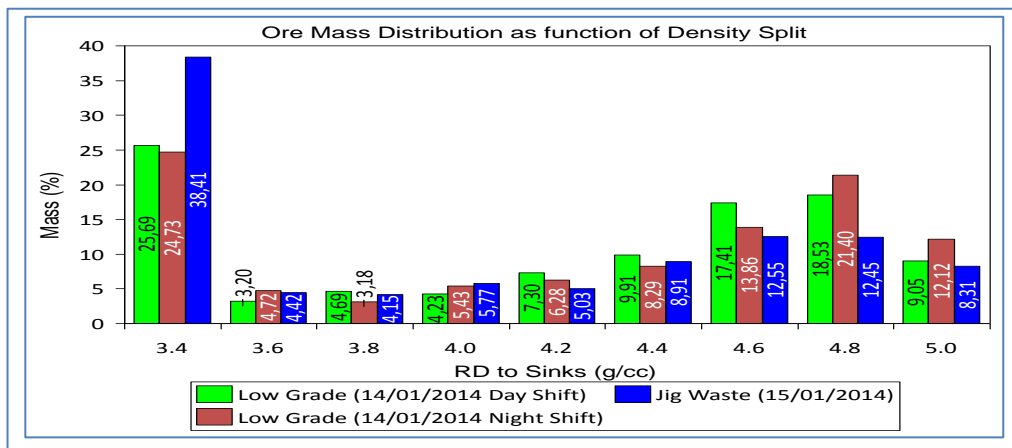


Figure 4.13: Densimetric profile of feed material processed through UHDMS

The theoretical prediction of the expected yield and product grade for the low-grade stockpile and JIG waste material is presented in Figure 4.14. The low-grade material had a weighted ROM grade of 49.34%Fe whereas the JIG waste material has a ROM grade of 43.58% Fe. The predicted yields were 57.59% and 44.19% for the low grade stockpile Jig waste material respectively, whereas their respective product quality is estimated as 64.6% Fe and 64.8% Fe.

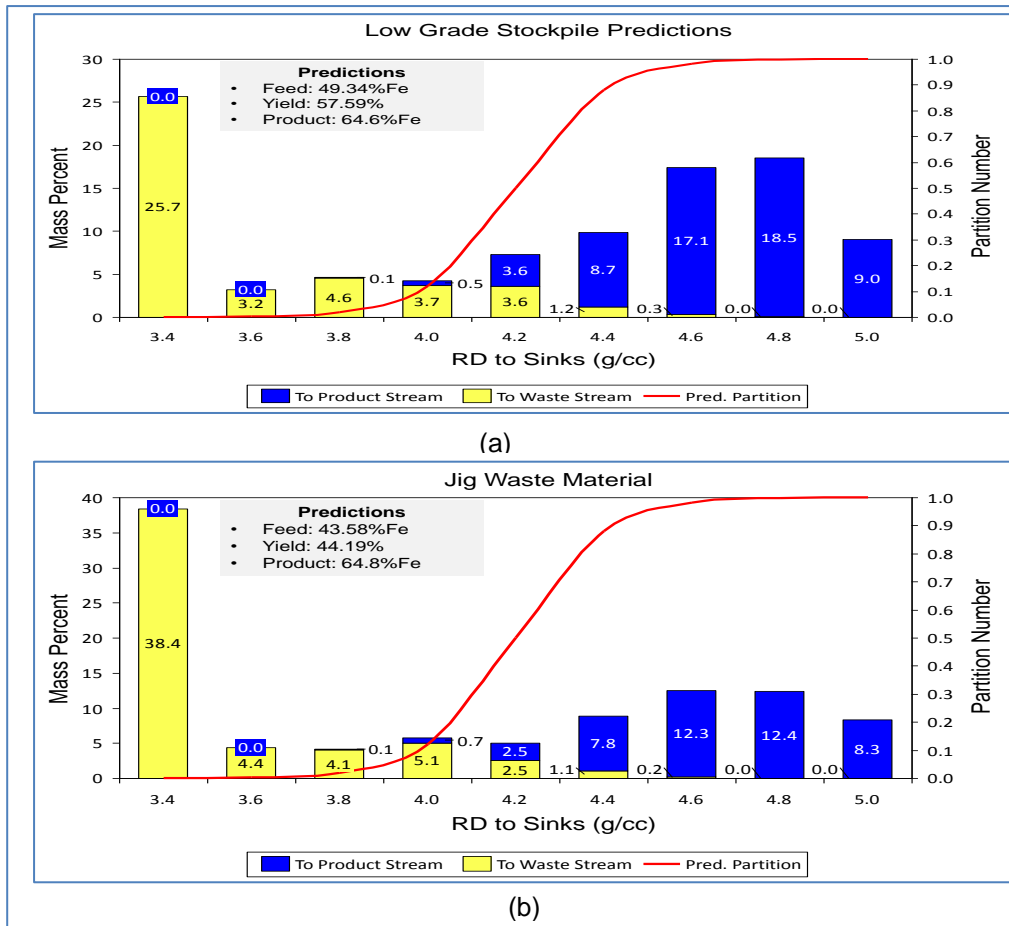


Figure 4.14: Yield and product grade prediction (a) Low-grade stockpile (b) Jig discard

Figure 4.15 presents the comparison of the “*observed partition curve*” versus the “*theoretical predicted partition curve*”. The “observed partition curve” is constructed using the low-grade stockpile material. The density of the circulating medium was set at density of 4.00 t/m³ in order to give an expected cut-point of 4.20 t/m³. However, the results for the cut-points while processing low-grade material during the **day shift** and **night shift** operation were 4.51 t/m³ and 4.44 t/m³ respectively. Coarse ferrosilicon was used for preparation of the heavy dense medium, thus the high offset (i.e. cut-point shift) might be related to relatively high-density differentials that were measured during material processing. The achieved yield was averaging 54.5% with product grade of higher than 66.11% Fe. The yield was 3.09% lower than the predicted yield whilst the product quality was 1.51% higher than prediction. Thus, producing a product with higher product quality would be expected to have a negative impact on yield.

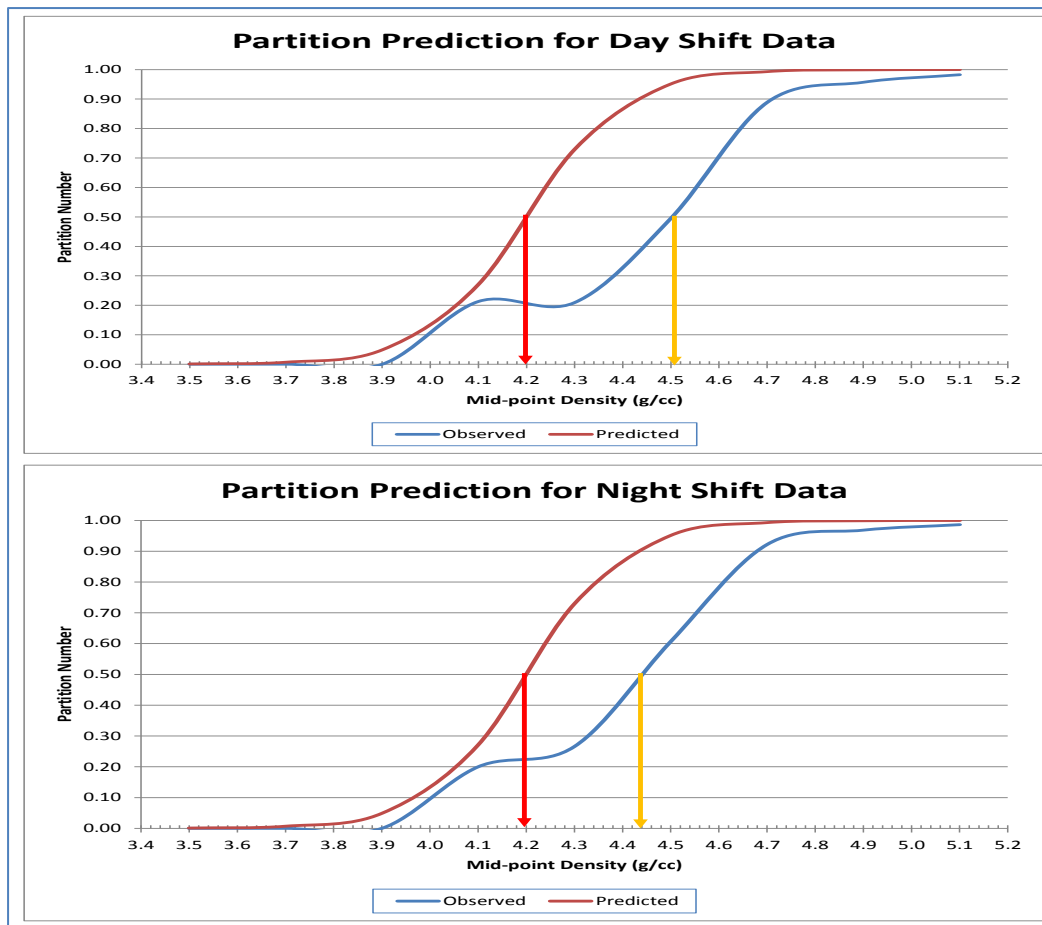


Figure 4.15: Observed vs. Predicted cut-density during processing of low-grade stockpile material

Figure 4.16 shows the observed partition curve when processing the Jig waste material. The results while processing the Jig waste material showed that the cut-point was 4.46 t/m^3 . The “*kink*” displayed in around density 4.1 to 4.3 t/m^3 , during the Jig waste processing might be due to medium rheology influencing the particle separation of material near the operating density. This effect is normally observed when misplacement due to medium viscosity or unstable medium during dense medium separation. The achieved yield was averaging 40.38% with product grade of higher than $66.16\% \text{ Fe}$. The yield was 3.81% lower than the predicted yield whilst the product quality was 1.36% higher than prediction.

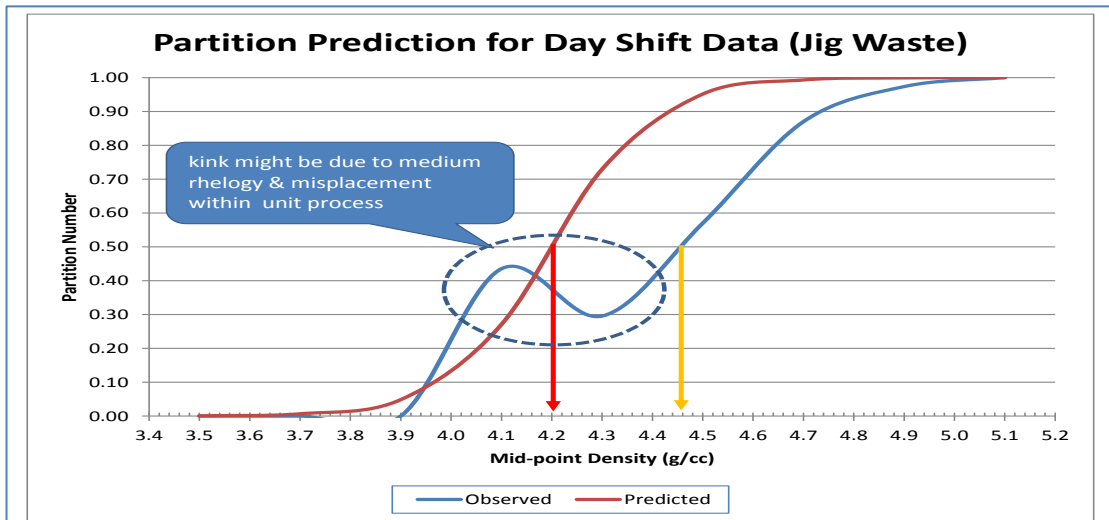


Figure 4.16: Observed vs. Predicted cut-density during processing of Jig discard material

Densimetric analysis of the feed sample was utilised to model the performance of the UHDMS as depicted in Table 4.4 when operating at the circulating medium density of 4.0 t/m³. Whitten's model with no by-pass to either the sinks or overflow was utilised to model the performance of UHDMS in order to achieve a yield of 54.5%. This indicated that the UHDMS operated at a cut-point shift of approximately 0.4 and E_{pm} of 0.077.

Table 4.4: Modelling the performance UHDMS operation using partition curve models

PARTITION MODELS FOR DMS SEPARATORS							
CHANGE DATA AND SEE THE IMPACT ON THE SEPARATION							
NOTE: CHANGE ONLY DATA IN THE BLACKENED CELLS							
Feed Stream Data				mass%			
SG Class #		SG Range	Av SG	in class	%Fe		
1	Float	4.000	3.9	33.063	21.418		
2		4.200	4.1	4.872	51.300		
3		4.400	4.3	6.754	55.699		
4		4.600	4.5	9.042	60.500		
5		4.800	4.7	15.514	64.400		
6		5.000	4.9	20.063	66.772		
10	Sink		4.3	10.692	68.439		
Av Particle Size (mm)	3						
Feed rate (tph)	100						
				RESULTS (For calculations see Spread Sheet <Model 3>)			
				Partition %	Cum %Density Distribution		
				Feed	Floats	Sinks	
				100.00	33.06	87.56	45.50
				100.00	4.87	92.44	45.50
				80.70	6.75	97.89	46.80
				19.30	9.04	99.63	54.10
				1.35	15.51	99.84	69.40
				0.08	20.06	99.86	89.45
				1.35	10.69	100.00	100.00
				TPH	100.0	45.5	54.5
				SG	4.158	3.630	4.732
				%Fe	49.52	30.59	65.32
DMS Separator Parameters				MODEL for Partition Curve			
ρ_m = Medium SG	4.00			$R(x) = Rc(x)(1 - \alpha - \beta) + \beta$			
Cut Point Shift = CPS = $\rho_{50} - \rho_m$	0.4			$Rc(x) = 1/(1 + (\exp(\lambda(x-1))))$			
CPS	0.4			$\lambda = 1.099/lc$			
cut density = $\rho_{cut} = \rho_{50}$							
ρ_{50}	4.4	<<DO NOT CHANGE THIS DIRECTLY !!					
e_{pm}	0.077						
Corrected imperfection = $lc = e_{pm}/\rho_{50}$ (Realistic range 0.4 to 0.01)							
lc	0.017						
by-pass to floats: β	0			0.097381407			
by-pass to sinks: α	0						
fluid recovery to sinks = R_f							
R_f	0						
Density Differential = $\rho_{diff} = \rho_{underflow\ medium} - \rho_{overflow\ medium}$							
ρ_{diff}							

4.1.6 Summary of Ore Characterisation and Processing Results

- ✓ The summary of the weighted average densimetric profile for the GR80, Low-grade stockpile material and 2014 DMS ROM are shown in Figure 4.17:
 - ✓ GR80 and 2014 DMS ROM comprises very low near-density material.
 - ✓ Low-grade stockpiles comprise a high proportion of near-density material.
 - ✓ The 2014 DMS ROM shows an increase in low-density material in the feed compared to GR80. This can be seen from a higher proportion of 2.8 t/m³ material for 2014 DMS ROM (i.e. 5.8%) compared to 1.78% for the GR80 ore body.

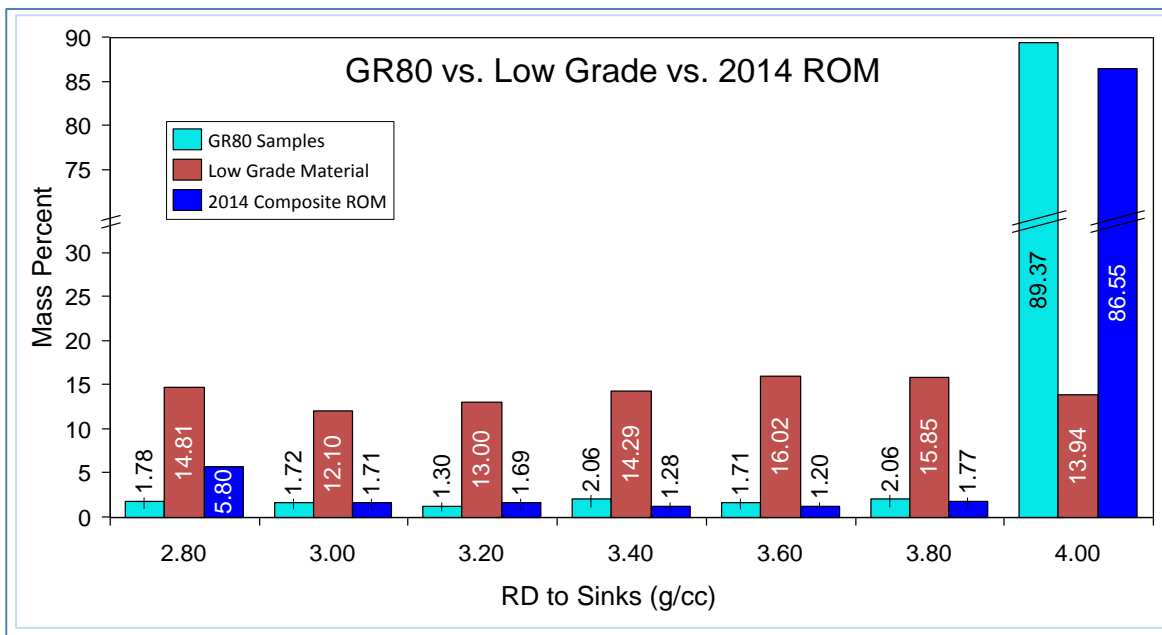


Figure 4.17: Summary of densimetric analysis for the GR80 vs. Low-grade vs. 2014 DMS ROM samples

- ✓ In spite of increased low-density material in the 2014 DMS ROM, this material is characterised as having low near-density material and thus easy to beneficiate in the dense medium process.
- ✓ The densimetric analysis of the GR80 material show that the high-grade ore from the mining area has low proportion of near-density material and can be classified as “forgiving” and easy to beneficiate. This material will produce high yields when processed through the dense medium beneficiation circuit. In addition, qualities expected from these samples would be high, that is, 65.2% Fe.
- ✓ Characterisation of the low-grade stockpiles indicated that the material from these stockpiles is characterised by elevated proportions of near-density material. Thus, in order to beneficiate these material relatively high operating densities are required for the dense medium separation process. However, these material can be beneficiated

at operating density of at least 3.80 t/m^3 in the dense medium process to produce expected yield of ranging between 40 to 60%, which an low grade products with an average Fe grade of 62.60% Fe.

- ✓ Pilot testing at operating density of 4.00 t/m^3 showed that the yields of 54.5% with product grades of 66.11% Fe could be achieved for the low-grade stockpile material. In addition, waste material from the current Jig processing plant can be efficient processed to generate further product at yields of 40.38% with product grades of 66.18% Fe.
- ✓ The ability to operate the dense medium slurries at high density as well as ultra-high density brings an added benefit to whole value chain. This is through producing additional product from material that was historically classified as being difficult to beneficiate and not economic viable for the mine.

4.2 FESI CHARACTERISATION INTRODUCTION

The physical properties of ferrosilicon are critical for both separation efficiency and recovery depending on application. In 1996 Sishen stopped using milled and water atomised FeSi for dense medium separation. This is based on the issues of the FeSi that could arguably be described as being “too stable”, causing difficulty in pumping and the tendency to retain non-magnetic slimes in the medium, which further complicate pumping. The high stability is partnered by high viscosity, which apart from being the cause for pumping issues also prevents the natural migration of ore particles toward the expected product stream.

4.2.1 FeSi Rheology Test Results

The objective of the vertical tube viscometer is to collect pipeline pressure gradient data that can be used to determine the rheological behaviour of the process FeSi. The data from the pipe loop is plotted on a pseudo shear diagram with the application of equations described in section 2.2.2.

The process FeSi sampled from the plant contained some particles bigger than 5mm in diameter, which would block the pipe loop, used for testing the viscosity and so it was screened to -500 microns for the test work. The specific gravity was found to be 6392 kg/m^3 .

The wall shear stress versus pseudo shear rate for the process FeSi tested over a range of slurry densities ranging from 3440 kg/m^3 to 4150 kg/m^3 is presented in Figure 4.18. The FeSi was too viscous to test at densities greater than 4150 kg/m^3 . The pseudo shear diagram only presents laminar flow data for pseudo-shear rates less than 500 s^{-1} . Thus the process FeSi is best modelled as a pseudo-plastic slurry, however, detailed analysis of the process FeSi rheogram a Bingham behaviour is also observed at shear rate higher than 200 s^{-1} for other medium density.

For the process-FeSi, a value of 0.65 was selected for the flow behaviour index, which was based on historic model fitting of similar heavy medium slurries tested in the pipe loop set-up. The relationship between the fluid consistency index and the process FeSi density as well as the mass solids concentration is presented in Figure 4.19. It can be seen that at FeSi slurry density higher than 3.90 t/m^3 , the viscosity of the process FeSi increases exponentially. Thus, when operating the cyclone plant at medium density in excess of 3.90 t/m^3 , it is expected that the viscosity impact would be highly pronounced.

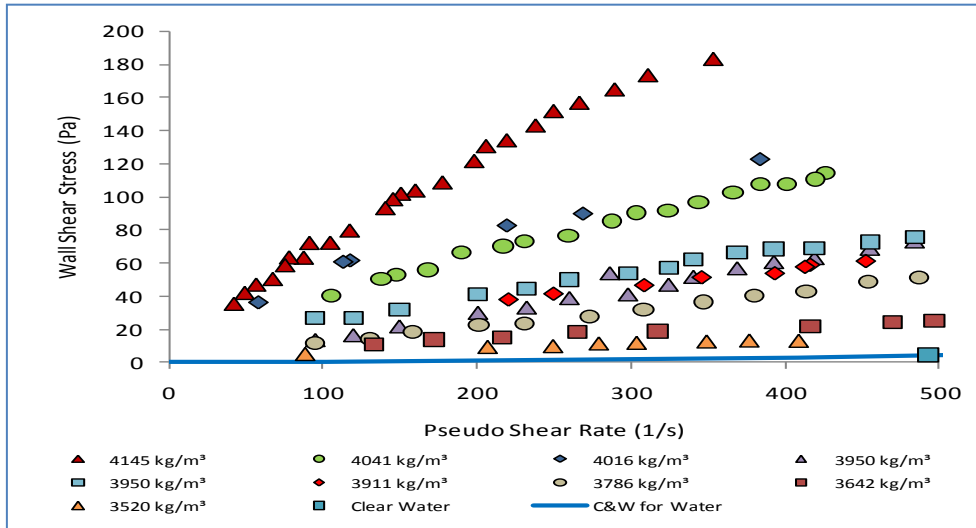


Figure 4.18: Pseudo shear diagram of Sishen process FeSi

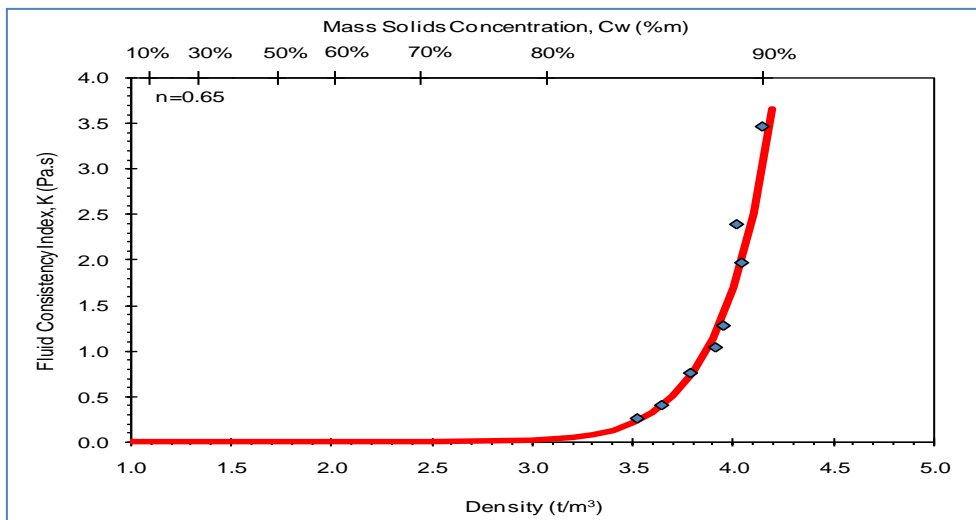


Figure 4.19: Fluid consistency index as a function of density and mass solids concentration for the pseudo-plastic modelled process FeSi

The correlations to predict the rheological characteristics of the process FeSi as a function of density (ρ , t/m^3) is presented in Table 4.5 below.

Table 4.5: Rheological correlations for process FeSi

Pseudo-plastic Model	
Applicable concentration range	$3.4\text{t/m}^3 < \rho < 4.2\text{t/m}^3$
Fluid consistency index	$K = \mu_w + 0.6 \times 10^{-9} \rho^{15.7}$
Flow behaviour index	$n = 0.65$

4.2.2 Effect of Viscosity on FeSi Stability

An efficient dense media separation process requires high-density ferrosilicon (FeSi) slurry (3800 kg/m^3 to 4400 kg/m^3) with a low viscosity that is stable. Stable means that the slurry will remain homogeneous for a reasonable time (approximately 60 to 120 seconds) when in a quiescent state. The objective of this study was to determine the effect of viscosity on the stability of FeSi slurry by using a viscosity modifier and by varying the fine fraction of the FeSi.

The test work scope entailed a vertical pipe loop tests, bench top and pipe loop stability tests were conducted on the following samples:

- i. Coarse FeSi with a portion of the fines removed,
- ii. Process FeSi with a portion of the fines removed,
- iii. Coarse FeSi with viscosity modifier DP 725, from Lignotech.

4.2.3 Material Property Test Results

Table 4.6 summarises the material properties of the different FeSi slurries tested.

Table 4.6: Material properties of coarse and process FeSi less fines

Property Tested	Coarse FeSi	Coarse FeSi Less Fines	Process FeSi	Process FeSi Less Fines
Solids density (kg/m^3)	7 060	7 060	6 501	6 501
d_{90} particle size (μm)	160	166	167	2
d_{50} particle size (μm)	68	71	40	51
% passing $25 \mu\text{m}$	17.7	9.8	12.1	3.7
% + $75 \mu\text{m}$	47.3	48.3	21.3	29.6

4.2.4 Solids Density Results

P&C used a volumetric flask to determine the solids density of the FeSi material. The process FeSi has a solids density of $6\,501 \text{ kg/m}^3$ and the coarse FeSi a solids density of $7\,060 \text{ kg/m}^3$. The process FeSi contained small amounts of iron ore fines, which resulted in the lower average solids density compared to the solids density measured for the coarse FeSi.

Figure 4.20 and Figure 4.21 below shows the relationship between slurry densities, solids mass concentration and solids volume concentration for the coarse FeSi and process FeSi respectively.

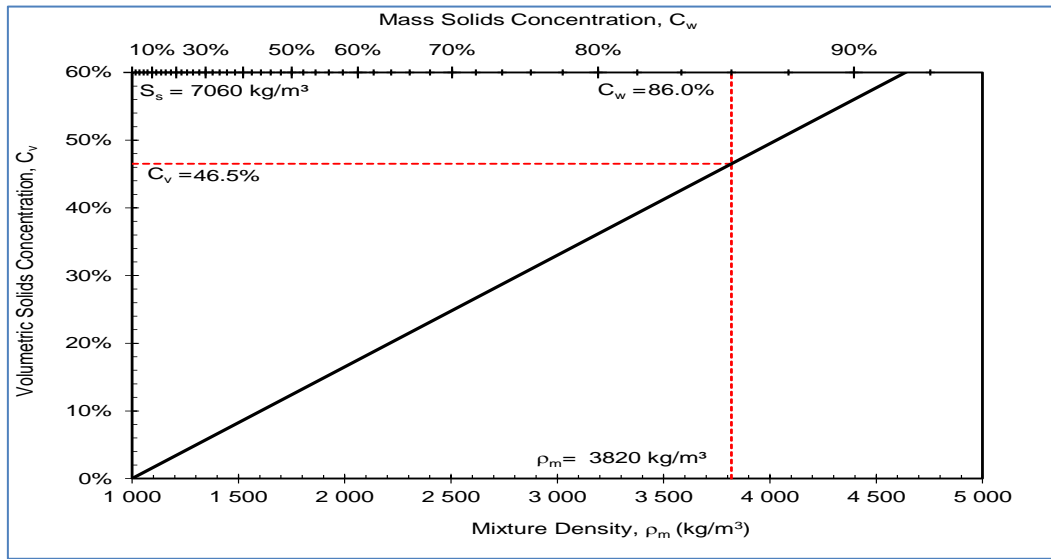


Figure 4.20: ρ_m , C_w , ρ_s and C_v relationship for the coarse FeSi

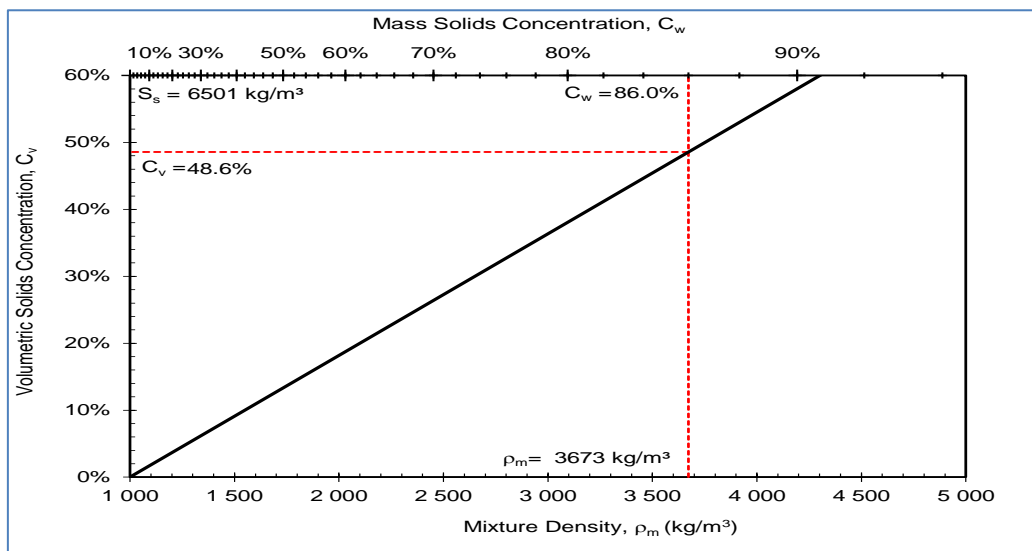


Figure 4.21: ρ_m , C_w , ρ_s and C_v relationship for the process FeSi

4.2.5 Particle Size Analysis

Detailed particle size distribution of the coarse FeSi and process FeSi less fines were measured by wet sieving is presented in Appendix B.2. In order to quantify the difference observed in the size distribution, the measured data was fitted to a Rosin-Rammler model (equations 3.1 and 3.2) as described in section 3.2 of this document.

Figure 4.22 presents the Rosin-Rammler regression for the coarse FeSi with and without fines measured using the wet sieving method. The D_n fitting parameter of the coarse FeSi and coarse FeSi less fines were 229.32 and 442.5 respectively, whilst the n parameter were 0.967 and 0.829 respectively.

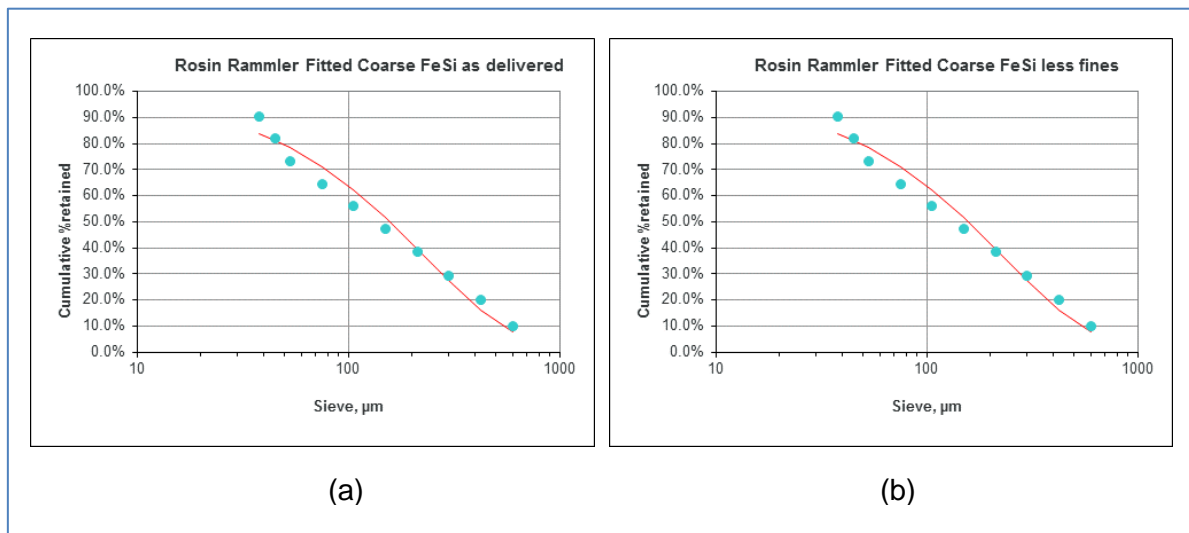


Figure 4.22: Rosin-Rammler regression of the particle size by sieve analysis of the (a) coarse FeSi as delivered and (b) coarse FeSi less fines

Figure 4.23 presents the PSD for the process FeSi with and without fines measured by the wet sieving method. Both figures show the fraction of fines removed for the test work. The D_n fitting parameter of the coarse FeSi and coarse FeSi less fines were 549.93 and 445.43 respectively, whilst the n parameter were 0.805 and 0.822 respectively.

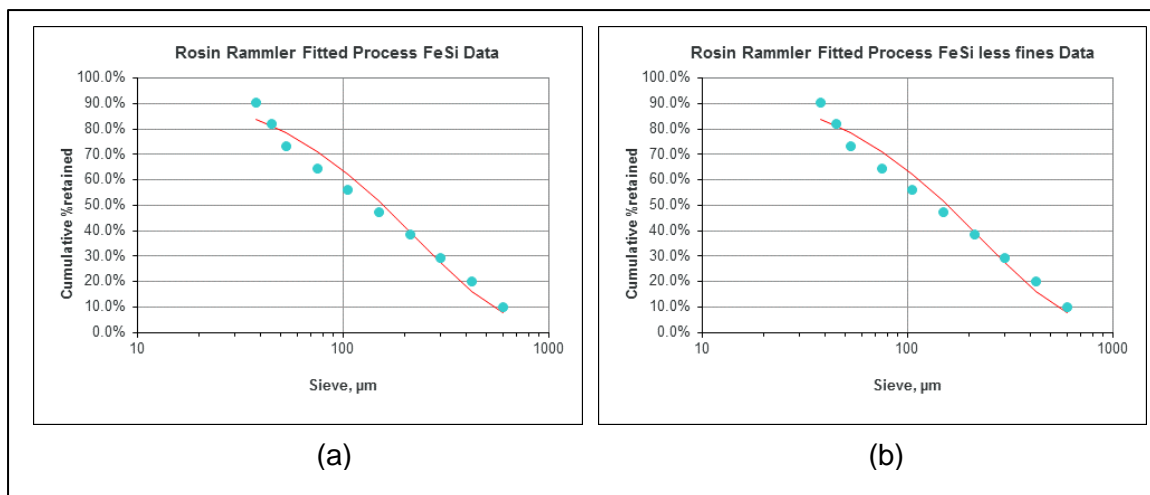


Figure 4.23: Rosin-Rammler regression of the particle size by sieve analysis of the (a) process FeSi as delivered and (b) process FeSi less fines

4.2.6 FeSi Stability Tests

Two sets of “stability” tests were conducted to assess the impact of the fine fraction and viscosity modifier on the different samples. Figure 4.24 schematically shows the differences between the two tests.

Static settling test - this test measures the rate at which the interface of the slurry and the supernatant water changes. A known volume of solids is placed in the measuring cylinder.

Vertical pipe settling test - this test measures the density of the suspended medium as a function over time in a 2 m high column of slurry. It provides an indication of the rate at which solids settle out of the slurry suspension.

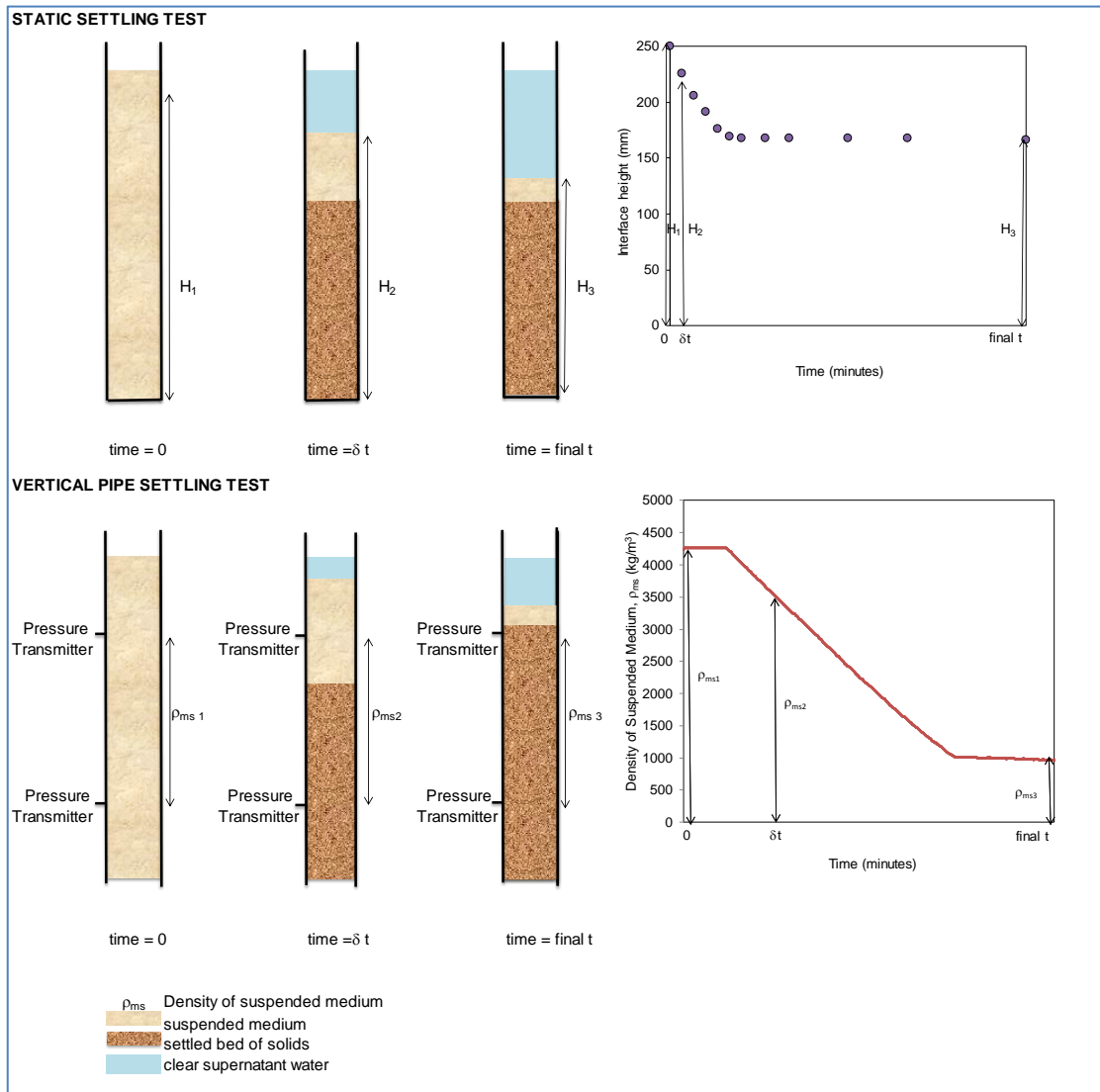


Figure 4.24: Comparison of the two types of settling tests and results

4.2.6.1 Stability Test No 1: Static Settling Test Results

The aim of the static bench top settling tests provides an indication of the rate at which surface water separates from the solids for a given slurry mixture. The medium with high settling rate is regarded as unstable and thus expected have lower viscosity.

Figure 4.25 shows the Coarse FeSi less fines settling rate decreases (becomes more stable) with an increase in slurry density. At low densities, the initial settling rate is high as solids separate quickly, and at high densities, the settling rate decreases, shown by the slope of the initial data points. Figure 4.26 also shows that the Process FeSi less fines settling rate decreases with an increase in density. Figure 4.27 show that the coarse FeSi with viscosity modifier settles in a very similar manner to the coarse FeSi fewer fines.

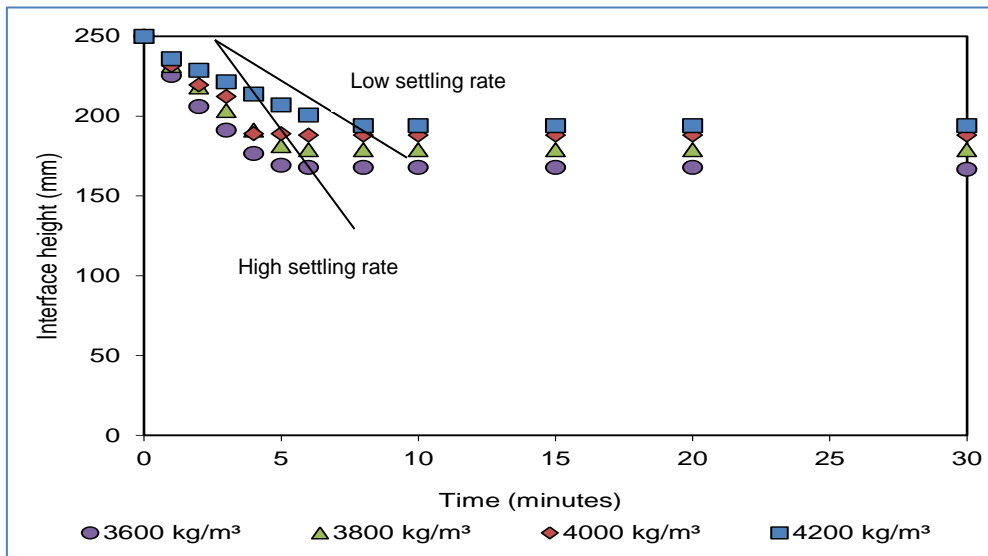


Figure 4.25: Bench top settling tests for coarse FeSi less fines

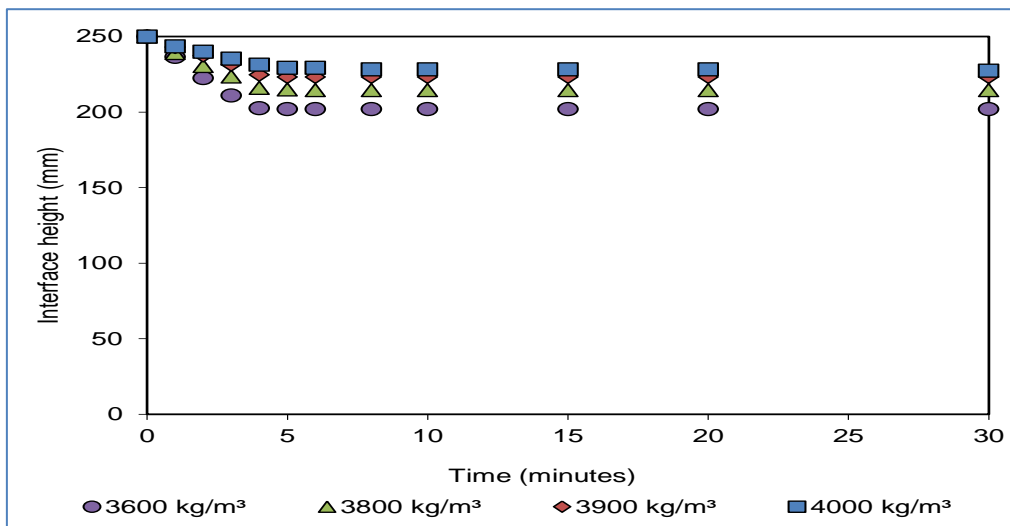


Figure 4.26: Bench top settling tests for process FeSi less fines

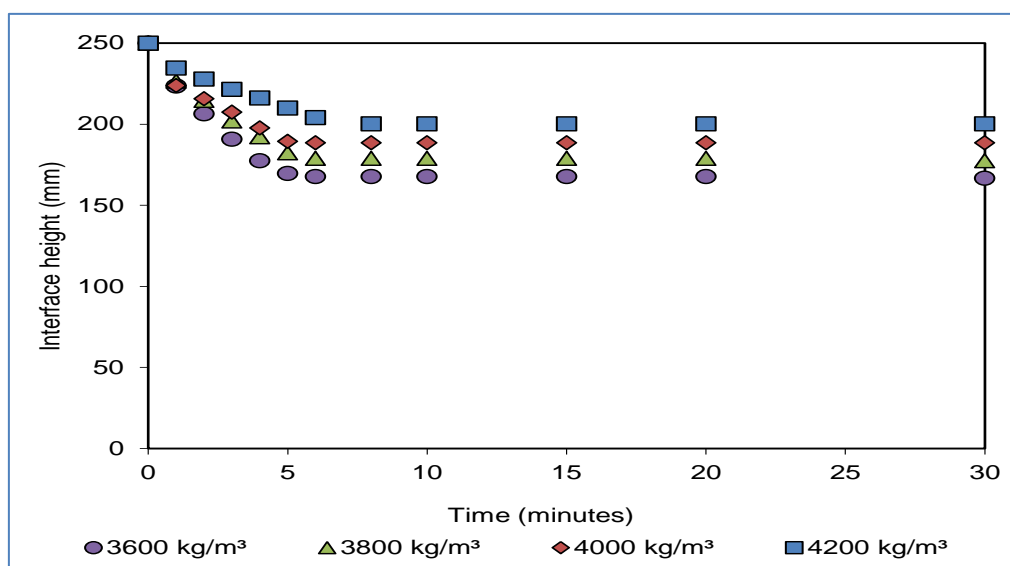


Figure 4.27: Bench top settling tests for coarse FeSi with viscosity modifier

To summarise the results, Figure 4.28 shows a comparison of the bench top test results for different FeSi samples at a density of approximately 4000 kg/m³. From the data, it can be seen that the Coarse FeSi settles fastest with the viscosity modifier added. With the fines removed, it settles slightly faster than the coarse FeSi sample. The process FeSi less fines also settles slightly faster than the full process FeSi sample.

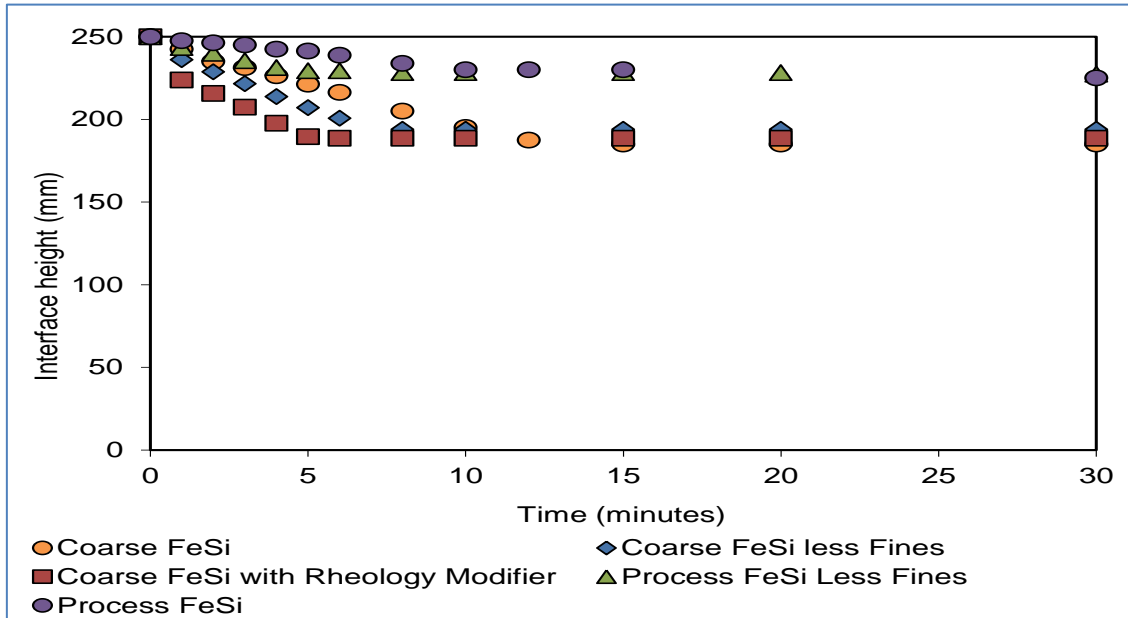


Figure 4.28: Comparison of bench top settling test results at a density of 4000 kg/m³

4.2.6.2 Stability Test No 2: Vertical Pipe Settling Tests

The pipe loop settling tests provide an indication of the rate at which the FeSi mixture density changes while at rest in a vertical pipe. The rate at which the FeSi mixture density changes is an indication of the rate at which a solid bed of FeSi particles settles out of the slurry, forming a self-supporting structure in the slurry. Conversely, it can be considered a measure of rate of settled bed formation. The test records the density of the suspended medium as a function over time.

Appendix B.3 presents detailed test results of vertical pipe settling tests whilst Figure 4.29 Figure 4.30, Figure 4.31 and Figure 4.32 show plots of density of suspended medium versus time for “coarse less fines”, “process FeSi”, “process FeSi less fines” and “coarse FeSi with viscosity modifier” respectively over ten minutes. The first minute is of particular significance as the residence time of FeSi slurry in the DMS drum and cyclone was determined as 58 seconds for Sishen operation. However, in the first few minutes of this test the slurry is forming a bed between the closed valve and the bottom pressure transmitter during which time the density remains almost constant. After this, as the bed is formed in the pipe section between the pressure transmitters, the change in density of suspended medium with time shows a constant settling rate in the pipe. All of these tests, if continued long enough reach a constant density of that of water. This is when all the FeSi particles have settled out of the slurry and are supporting each other by direct particle-particle contact; analogous to a stack

of marbles in a pipe, and only the density of the suspended medium surrounding the particles is detected by the pressure transmitters.

Figure 4.29 shows that it takes longer for the high density FeSi to form a packed bed between the valve and the lower pressure tapping than for the low density FeSi. This is presumably due to the hindered settling phenomena at high density. The actual settling rate in the pipe is highest for the lowest density and decreases with increase in density.

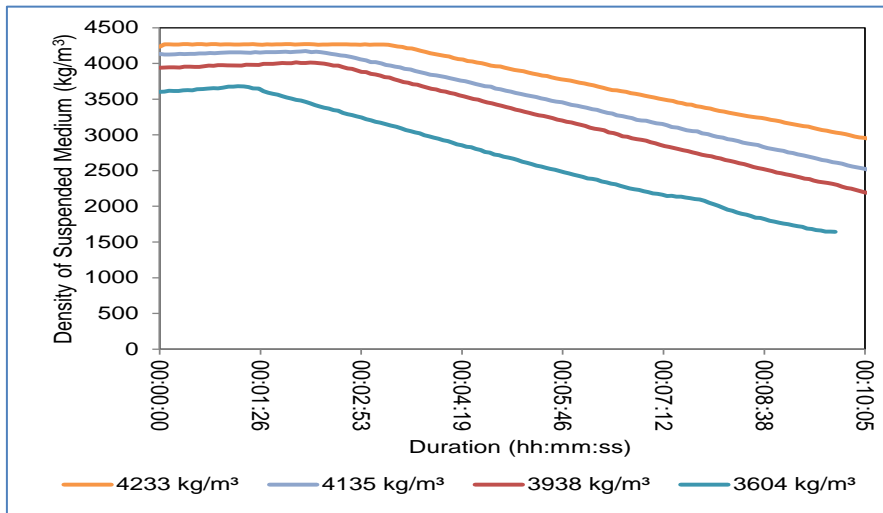


Figure 4.29: Pipe loop settling test results for coarse FeSi less Fines

Figure 4.30 shows that in the first 10 minutes the samples are only just beginning to have packed the bed between the valve and pressure transmitter. The high density FeSi is settling faster than the lower density samples.

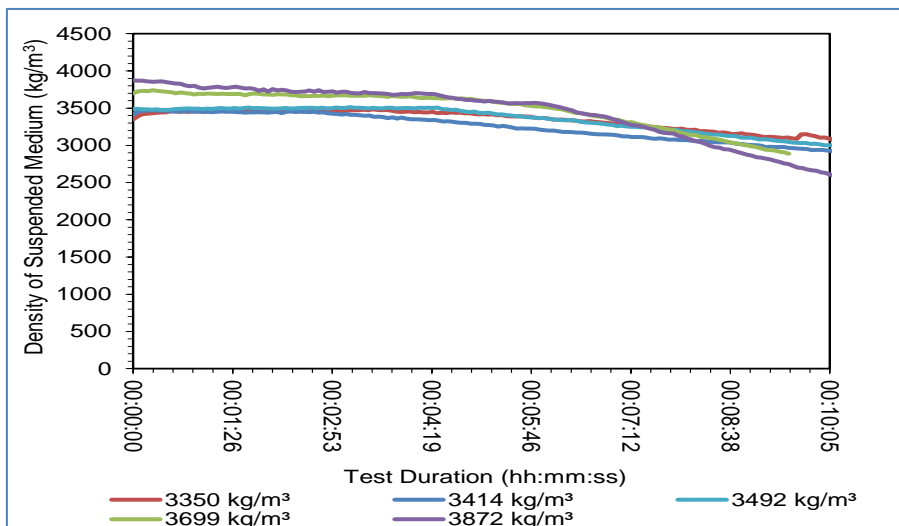


Figure 4.30: Pipe loop settling test results for process FeSi

Figure 4.31 shows that removing the fines from the Process FeSi results in a significant increase in the settling rate of the FeSi. As for the previous data, the highest density FeSi is settling faster than the lower densities.

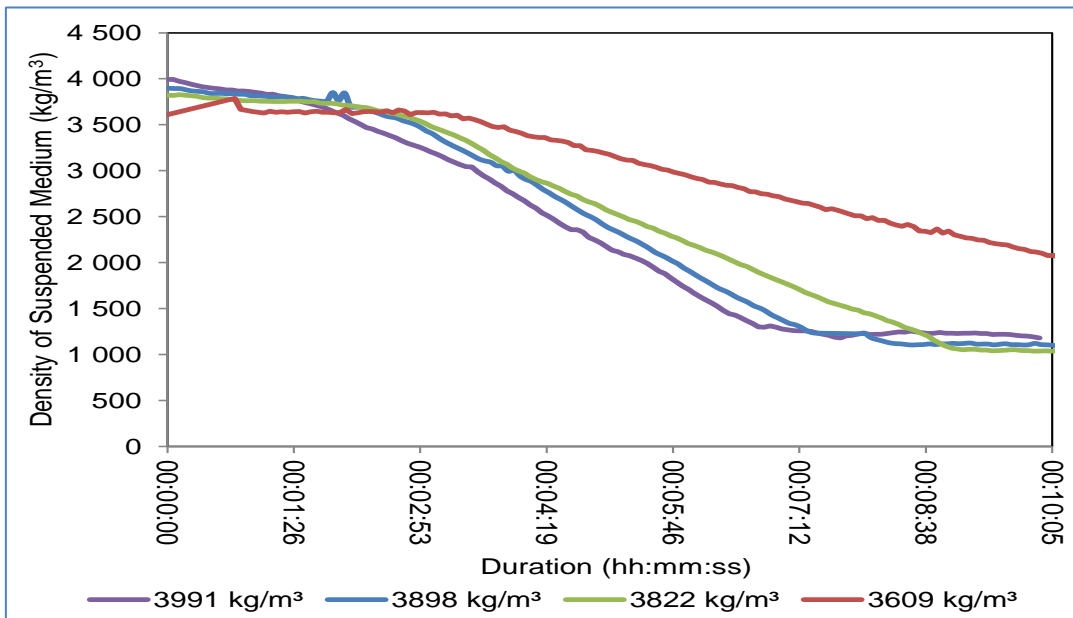


Figure 4.31: Pipe loop settling test results for process FeSi less fines

Figure 4.32 shows that the viscosity modifier dispersed the slurry and held it in suspension so that in the first 10 minutes a bed did not get a chance to form. This is the most stable FeSi tested as it takes the longest to build a bed of settled particles in the pipe.

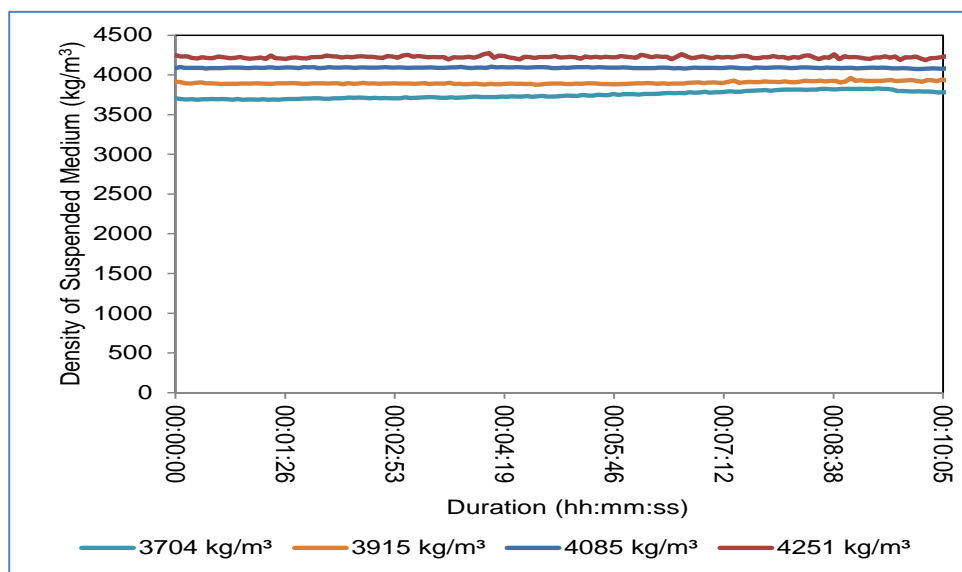


Figure 4.32: Pipe loop settling test results for coarse FeSi with viscosity modifier

Figure 4.33 shows a comparison of the different FeSi slurries at an initial slurry density of approximately 3 900 kg/m³. This shows that both the Process and Coarse FeSi slurries are less stable and settle faster when the fines fraction is removed. It also shows that the viscosity modifier makes the Coarse FeSi settle even more slowly and it is thus more stable.

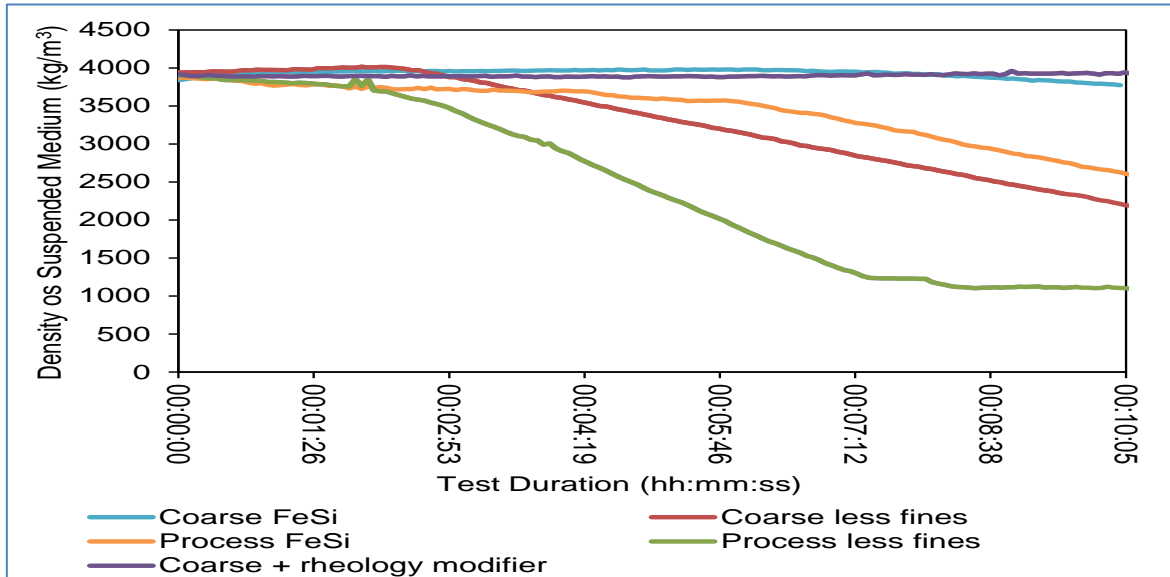


Figure 4.33: Pipe loop settling test results at slurry density of approximately 3900 kg/m³

4.2.7 Comparison of Static and Vertical Pipe Settling Test Results

Table 4.7 shows a comparison of the results of the two different sets of settling tests. The static settling test measures the rate at which the interface of the slurry and the supernatant water changes. The vertical pipe-settling test measures the rate at which the slurry settles into a bed of solids supporting each other and thereby “settling out” of the slurry.

Table 4.7: Comparison of FeSi settling test results

Sample	Static Settling Test	Vertical Pipe Settling Test
Coarse FeSi	3	4
Coarse FeSi less fines	2	2
Coarse FeSi with viscosity modifier	1	5
Process FeSi	5	3
Process FeSi less fines	4	1
Where 1 = settles fastest; 5 = settles slowest		

For the Dense Medium Separator it is desirable to have a FeSi that remains suspended as long as possible. For the FeSi samples tested this is the coarse FeSi with viscosity modifier as the FeSi particles form a settled bed more slowly in that sample than in any of the others, in other words they stay suspended in the water for longer. However, it is the fastest settling (i.e. least stable) in the bench top settling test.

The vertical pipe settling test shows an interesting trend in that all the coarse FeSi samples show hindered settling as the settling rate decreases with increase in density. Conversely, the process FeSi samples show an increased settling rate as density increases. This trend was not evident in the static settling tests that all settled slower as the density increased.

4.2.8 Tube Viscometer Test Results

Tube viscometer test was done to determine the viscous properties of the samples, as these materials could not be tested in a rotational viscometer. The objective of the vertical tube viscometer is to collect pipeline pressure gradient data that can be used to determine the rheological behaviour of Coarse and Process FeSi with a portion of fines removed and of Coarse FeSi with viscosity modifier added.

Clear water tests before and after the slurry test series were conducted to confirm the proper operation of the flow meter, differential pressure transducers and pressure tapping's as shown in Figure 4.34. The average pipe roughness is calculated from the measured water test data points using the Colebrook-White friction factor formulation and the Darcy equation. The measured pipe roughness is 2 μm , which is within the range expected for the stainless steel test pipes.

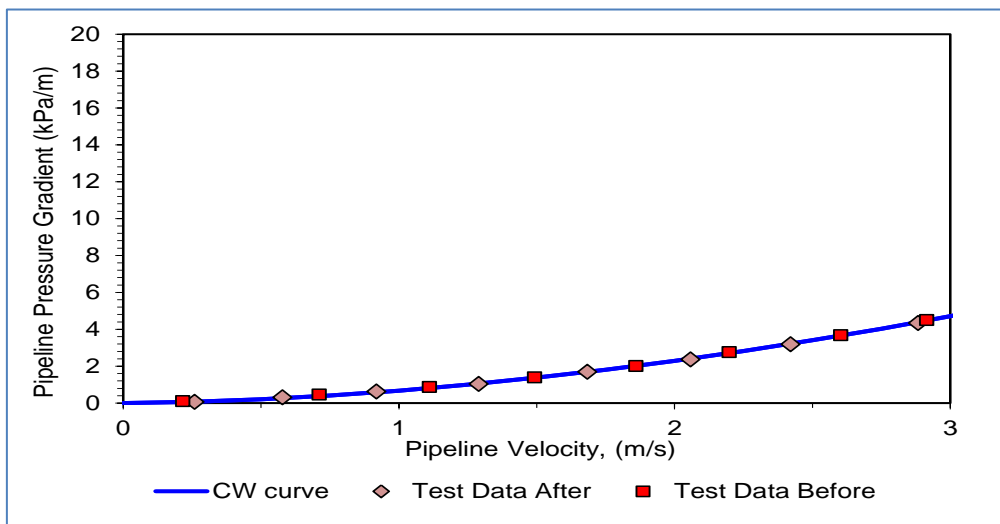


Figure 4.34: Clear water test results

The vertical pipe loop test data which shows the measured pipeline pressure gradient and velocity data is presented in Appendix B.4. Each test data file contains a table of average FeSi slurry density, pseudo shear rate, wall shear stress and temperature. The pseudo shear rate and wall shear stress (τ) were calculated using equation 2.1 and 2.2 as described in section 2.2.2 respectively.

The laminar flow pipe loop data was graphically presented in a pseudo shear diagram. Figure 4.35 presents the pseudo shear diagram for the coarse FeSi less fines over a range of slurry densities varying from 4 277 kg/m^3 to 4 665 kg/m^3 at an average temperature of 22°C. For slurry densities lower than 4 227 kg/m^3 only turbulent flow data were recorded which are not shown on the pseudo-shear diagram.

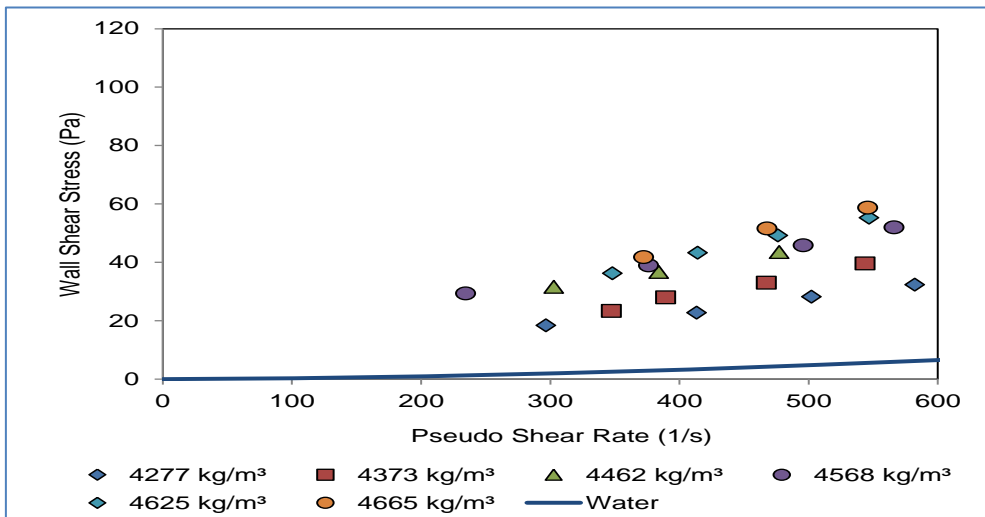


Figure 4.35: Pseudo shear diagram of coarse FeSi less fines

Figure 4.36 presents a pseudo shear diagram for the process FeSi less fines at slurry densities ranging from 3 670 kg/m³ to 3 994 kg/m³ at an average temperature of 29.5°C.

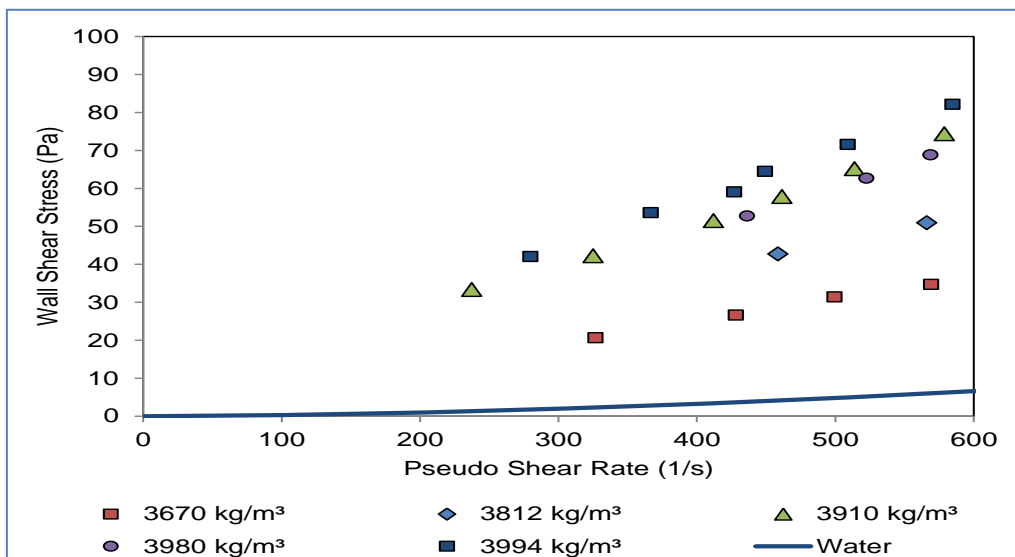


Figure 4.36: Pseudo shear diagram for process FeSi less fines

Figure 4.37, Figure 4.38 and Figure 4.39 depict a comparison between process FeSi and process FeSi less fines at densities of approximately 3900, 3800 and 3660 kg/m³ respectively.

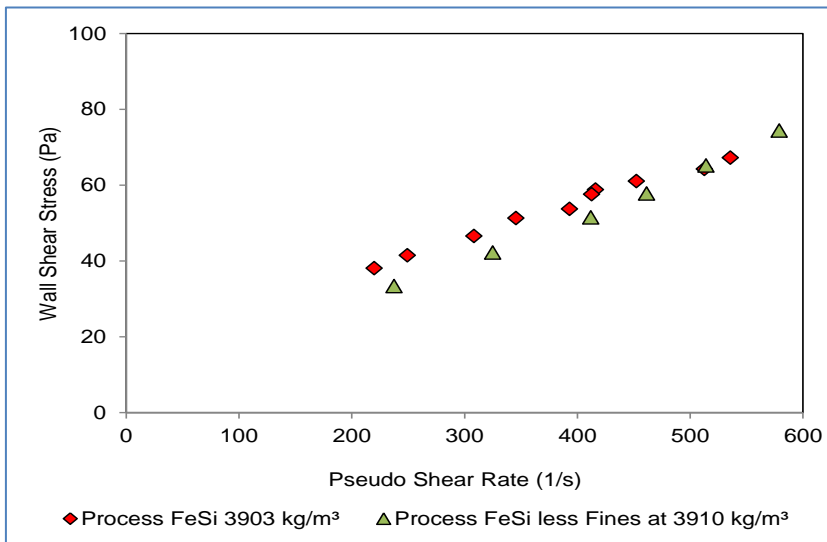


Figure 4.37: Pseudo shear diagram comparing process FeSi to process FeSi less fines at approximately 3900 kg/m³

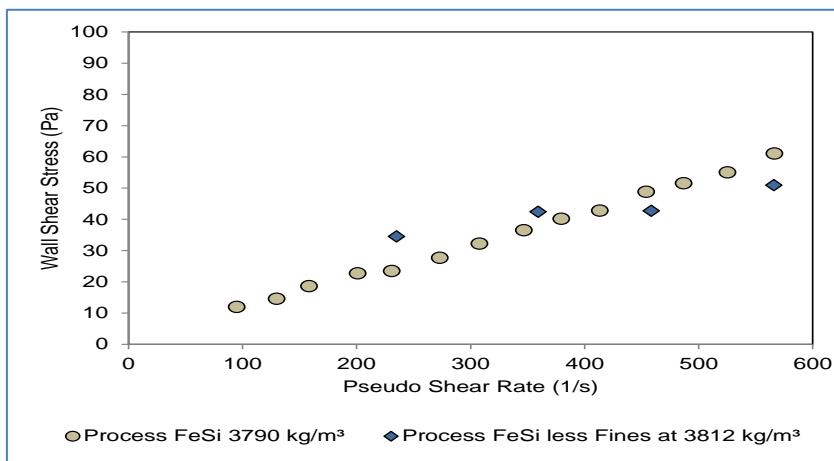


Figure 4.38: Pseudo shear diagram comparing process FeSi to process FeSi less fines at approximately 3800 kg/m³

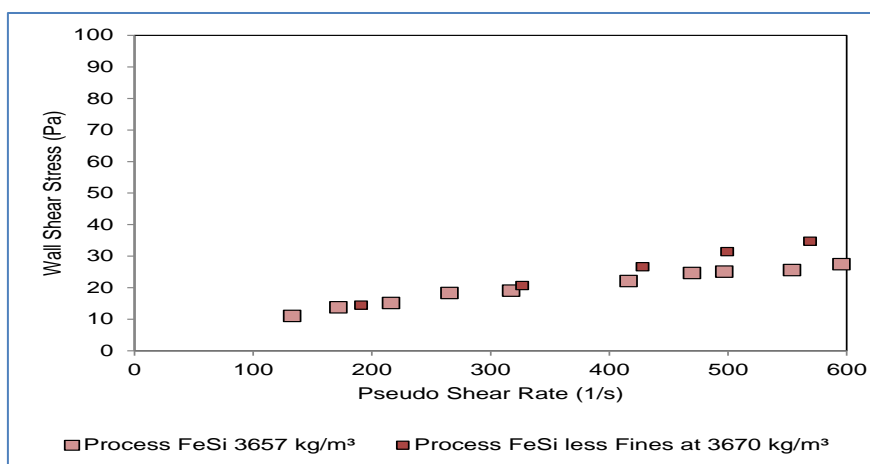


Figure 4.39: Pseudo shear diagram comparing process FeSi to process FeSi less fines at approximately 3660 kg/m³

High density coarse FeSi slurry was circulated in the vertical pipe loop in laminar flow and viscosity modifier was gradually added until a ten percent drop in pressure gradient was

measured in the laminar flow region. The amount of dry FeSi in the loop was determined and the dose of 100 ml per dry tonne of FeSi was determined as a suitable dose of viscosity modifier to test. Figure 4.40 shows the pseudo shear diagrams of coarse FeSi with 100ml viscosity modifier per dry tonne of FeSi over a range of densities from 3947 kg/m³ to 4500 kg/m³. The tests were conducted at an average temperature of 22.8°C.

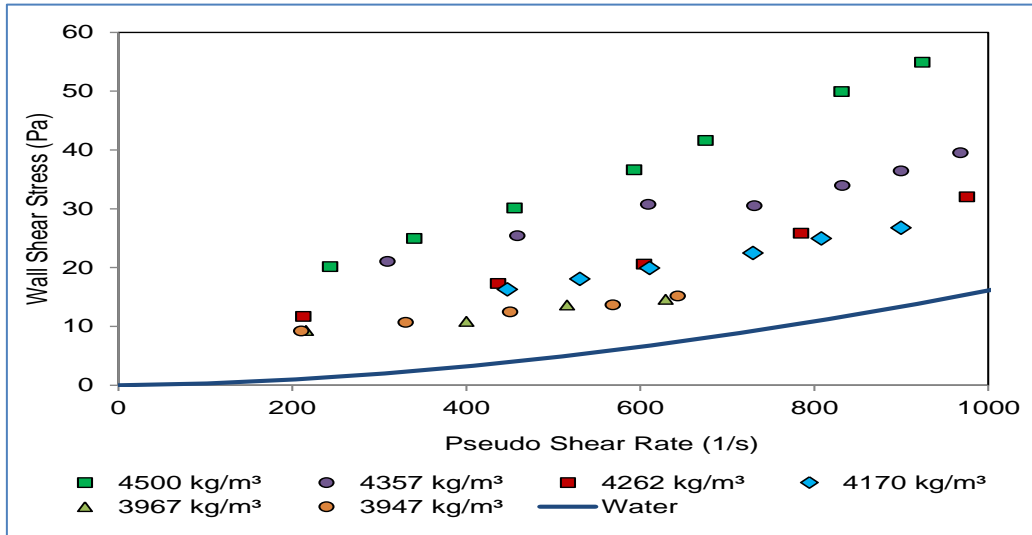


Figure 4.40: Pseudo shear diagram of coarse FeSi with viscosity modifier added

Figure 4.41, Figure 4.42 and Figure 4.43 show pseudo shear diagrams of coarse FeSi with and without viscosity modifier at densities of 4500 kg/m³, 4260 kg/m³ and 3980 kg/m³ respectively. The test data shows that the viscosity modifier decreases the flow curve of the coarse FeSi at a dose of 100ml per dry tonne. The change in flow behaviour is more pronounced for the higher density tests.

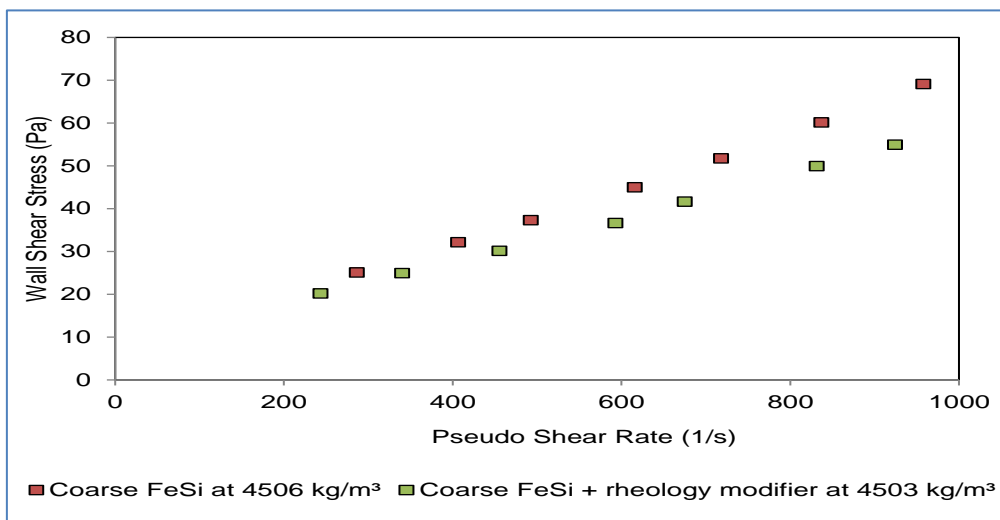


Figure 4.41: Pseudo shear diagram of coarse FeSi at a density of approximately 4500 kg/m³ with and without viscosity modifier added

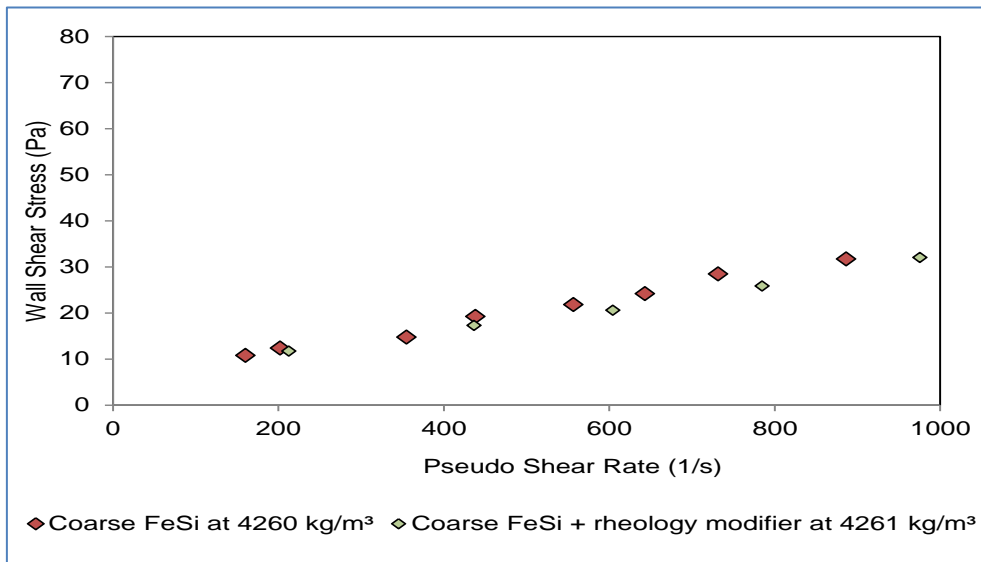


Figure 4.42: Pseudo shear diagram of coarse FeSi at a density of approximately 4260 kg/m³ with and without viscosity modifier added

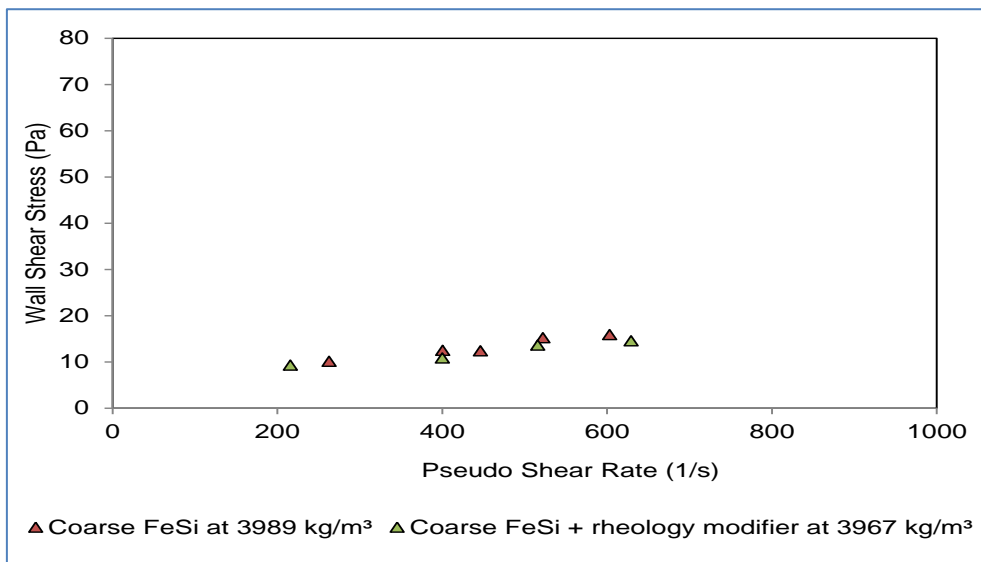


Figure 4.43: Pseudo shear diagram of coarse FeSi at a density of approximately 3980 kg/m³ with and without viscosity modifier added

4.2.9 Summary of FeSi Characterisation Tests Results

- ✓ The viscosity of the minus 500-micron process FeSi was measured in a vertical pipe loop that was characterised using the pseudo-plastic model with the correlations given in the table below. For slurry densities above 3.90 t/m³, the process FeSi slurry viscosity increases exponentially.

Pseudo-plastic Model	
Applicable concentration range	$3.4\text{t/m}^3 < \rho < 4.2\text{t/m}^3$
Fluid consistency index	$K = \mu_w + 0.6 \times 10^{-9} \rho^{15.7}$
Flow behaviour index	$n = 0.65$

- ✓ The static bench top settling stability tests show that the coarse FeSi settles fastest with viscosity modifier added. With fines removed, it settles slightly faster than the coarse FeSi sample. The Process FeSi less fines also settles slightly faster than the full Process FeSi sample.
- ✓ The pipe loop settling tests showed that the coarse FeSi with viscosity modifier was significantly more stable than the other slurries tested. The coarse FeSi less fines and the process FeSi less fines both settled significantly faster (i.e. are more unstable) than the coarse and process FeSi samples without fines removed.
- ✓ The vertical pipe loop tests showed that removing the fines made no significant difference to the rheology of the coarse FeSi and the process FeSi. The viscosity modifier at a dosage of 100 ml per tonne of dry FeSi reduced the viscosity of the coarse FeSi.
- ✓ The removal of the fines in the coarse and process FeSi does not significantly change the rheology of the slurries although both settling tests show the FeSi settles faster without fines.
- ✓ The viscosity modifier makes the slurry settle faster in the static settling tests and slower in the vertical pipe settling tests. It results in a lower pseudo shear diagram than the coarse FeSi without viscosity modifier, reducing the viscosity of the coarse FeSi, presumably by dispersing the particles in the slurry. The static settling test probably settled faster due to the reduced viscosity of the FeSi and the particle dispersion caused the vertical pipe settling test to show greater stability or slower bed formation.

CHAPTER 5: CYCLONE PLANT AUTOMATION AND CONTROL

5 AUTOMATION AND CONTROL INTRODUCTION

Sishen DMS plant process produces approximately 25% of the product through the cyclone plant, with yields ranging from 70% to 80%. A tighter control philosophy can improve yield consistency by 5%, which would deliver at least **1.25%** additional product to Sishen. This type of statement is made on the basis that cyclone setup and operation throughout all mineral industries is in a relatively poor shape. This is due to any number of reasons such as:

- (i) Incorrectly specified system setup
- (ii) Overfeeding
- (iii) Variation in viscosity
- (iv) System changes over time
- (v) Poor maintenance

Therefore, consistent system management, measurement and insight is required to maximize the opportunity that the cyclones present. Through the use of modelling and simulation, the aim was to identify the financial benefit to be gained from better operation, and consequently, trade this off against the costs associated with operation. Moreover, it has helped in identifying how much effort should be placed on this part of the operation.

The main aim of the automation of the cyclone modules is aimed at maintaining the process stability thereby improving the metallurgical efficiency during the beneficiation of iron ore material. This is premised on the fact that, as the head grade of ROM declines, the level of near-density material increases thereby required the dense medium beneficiation circuit operating at optimum efficiency relating to E_p values within best practice range of between 0.02 – 0.05.

The operational objectives of the automated control of dense media system for the cyclone plant are called upon to: (i) ensuring stability of process, (ii) suppressing the influence of external disturbances, and (iii) optimizing the economic performance of the cyclone plant, that is, minimize yield losses to waste.

Thus, the automation focuses on maintaining the following process parameters:

- a) Dense medium in the correct and dilute medium sumps level is controlled to a minimum of 25%.
- b) Correct medium flow rate to be controlled at an absolute minimum of 150 m³/h.
- c) Maintaining the medium to ore (M:O) ratio at a minimum levels of 5:1.
- d) Ensure sufficient cyclone inlet pressure as well as maintaining the variation in pressure differential between cyclone clusters to below 10%.
- e) Monitor and control the cyclone density differential to within the 0.02 – 0.05 range.

Based on current and past conditions, a soft sensor will be used to identify possible problem areas in the near future. This information will then be communicated to the operators and advice given on action steps to take to avoid problems occurring. This soft sensor will thus be employed to act as a pro-active decision management tool.

The expected solution of the control is to ensure that the feed to a particular module is interlocked to the FeSi medium condition. Thus, interlocking correct medium flow with the module ore feed rate will ensure that minimum medium-to-ore (M:O) ratio is maintained.

(Petersen, 2010) in addition (Mukherjee, et al., 2003) indicated that the stability of the dense medium cyclone system can be monitored through the inlet pressure measurement. Thus, one of the primary objectives of the automated control is maintaining cyclone inlet pressure across all operating cyclones constant. The monitoring of cyclone inlet pressure would indicate that a constant head is maintained across cyclone cluster as well as indication of system imbalances and the blockages. Should there be a constant increase in pressure differential between cyclones in a cluster (e.g. 5100 cyclones) or ΔP between clusters of a particular module (e.g. 5100 vs. 5200 set), then the system should warn the control room operator that a particular module is not in balance. Corrective action might be manual flow balance through the “Jacko-Sleeve” valves or unblocking the blocked feed line.

Figure 5.1 shows the flow sheet for the automated module and indicates the critical measuring instruments that have been installed.

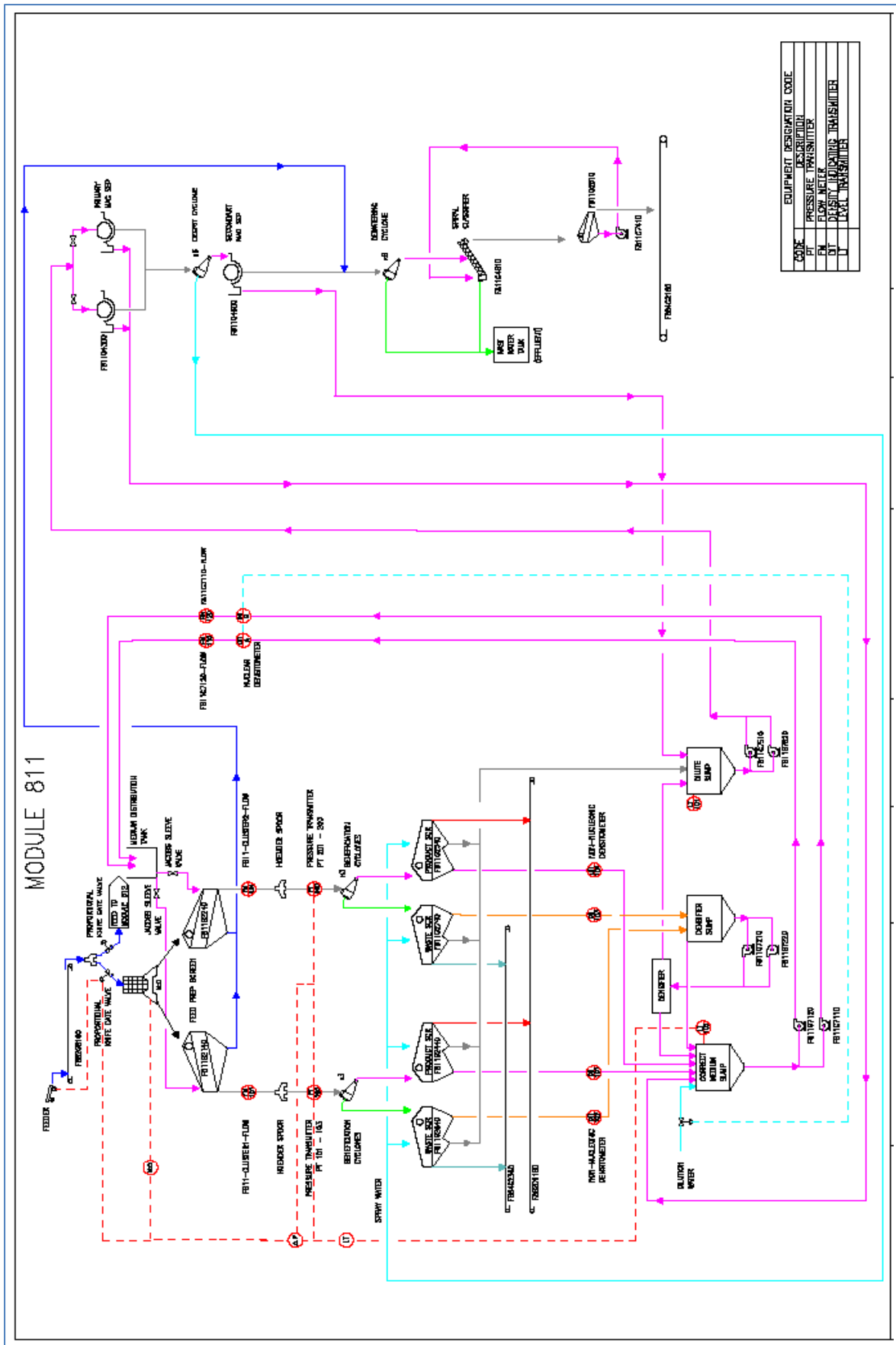


Figure 5.1: General module layout of with instruments for monitoring and control (Tom, 2014)

5.1 AUTOMATED MODULE VERSUS TRADITIONAL MODULE

The current cyclone plant set-up is manual operation, with only automated control being for the medium density. This section aim to indicate the traditional un-instrumented module with the instrumented module to satisfy what is termed level 1 & 2 regulatory controls in terms of layers of controls. Typical layers of control are presented in Figure 5.2 below.

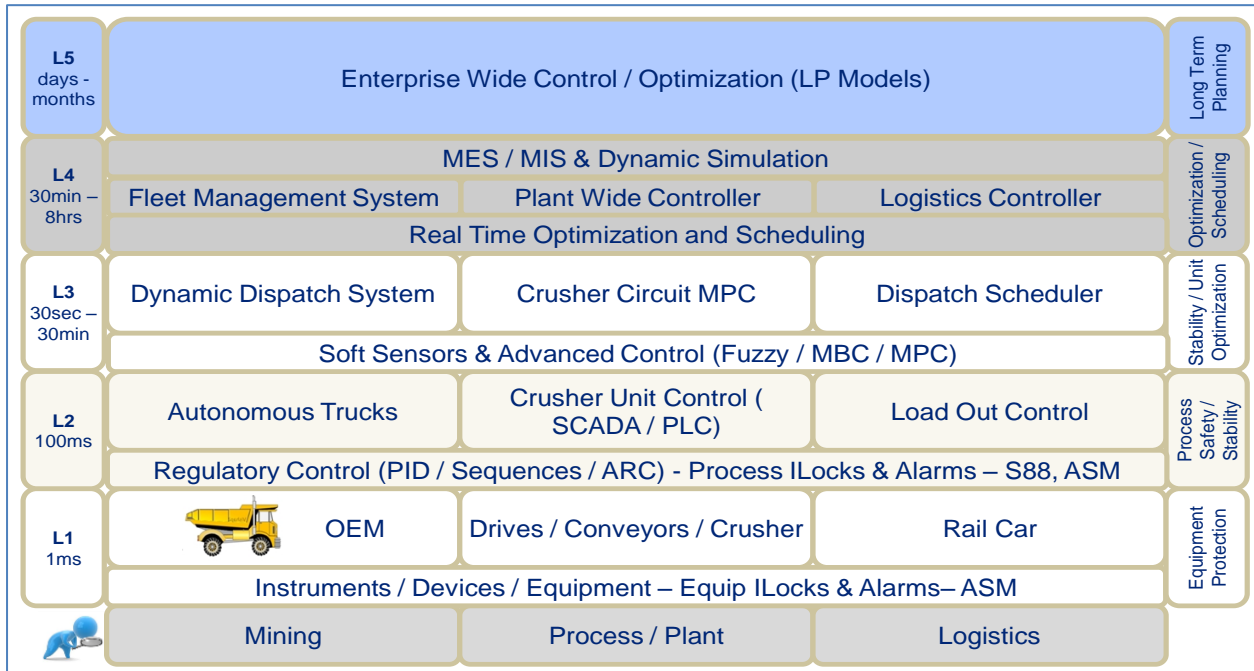


Figure 5.2: Generic layer of controls (de Villiers, et al., 2014)

Automation of the cyclone plant module involved installation of the followings instruments:

- (i) Acoustic level indicators for the monitoring and control of both correct and dilute media sumps. This is critical to ensure enough medium is maintained in the sump to ensure correct flow to the beneficiation cyclone as well as feed to the magnetic separation stream
- (ii) Non-contact, SONARtrac flowmeters for the measurement of the medium flow rates to the cyclone circuit. This is required in order to determine the medium-to-ore ratio for the module. SONARtrac monitoring systems do not utilize ultrasonic; they employ patented sonar array processing techniques to listen to, and interpret, flow turbulence and sound fields generated by the machinery, piping and process flow. This passive listening approach results in measurement of the flow rate and amount of entrained air/gas with a high degree of accuracy and repeatability.
- (iii) Non-contact SONARtrac flowmeter for the measurement of the mixture of ore and dense medium after mixing box to ensure constant flow is maintained between cyclone clusters. This was preferred as the new mixing box similar to Venetia mine would require major structural change and thus impractical for the current set-up.

(iv) Cyclone in-let pressure transmitters for all cyclones in the cyclone-cluster.

Figure 5.3, Figure 5.4 and Figure 5.5 show the instruments installed in cyclone module as part of the automation project, which includes sump level indicator, non-contact medium flowmeter, cyclone inlet-pressure transmitters and cyclone cluster balance respectively.

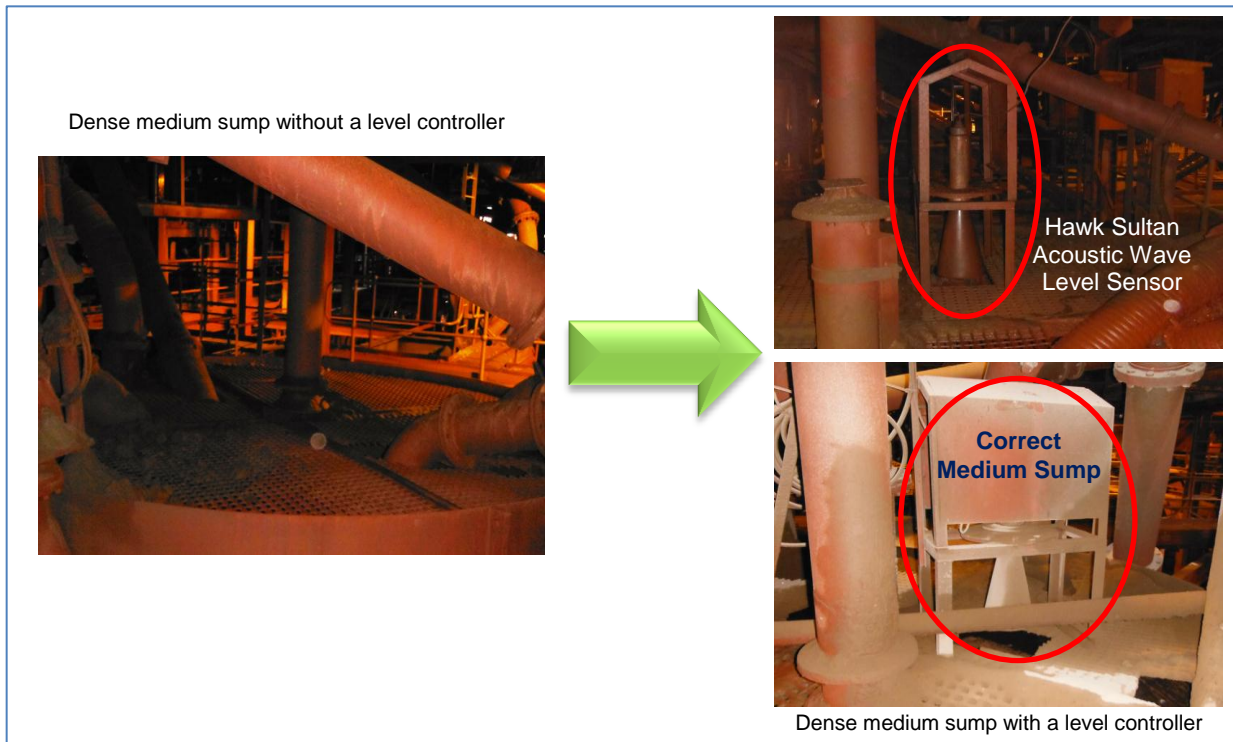


Figure 5.3: Sump level indicators

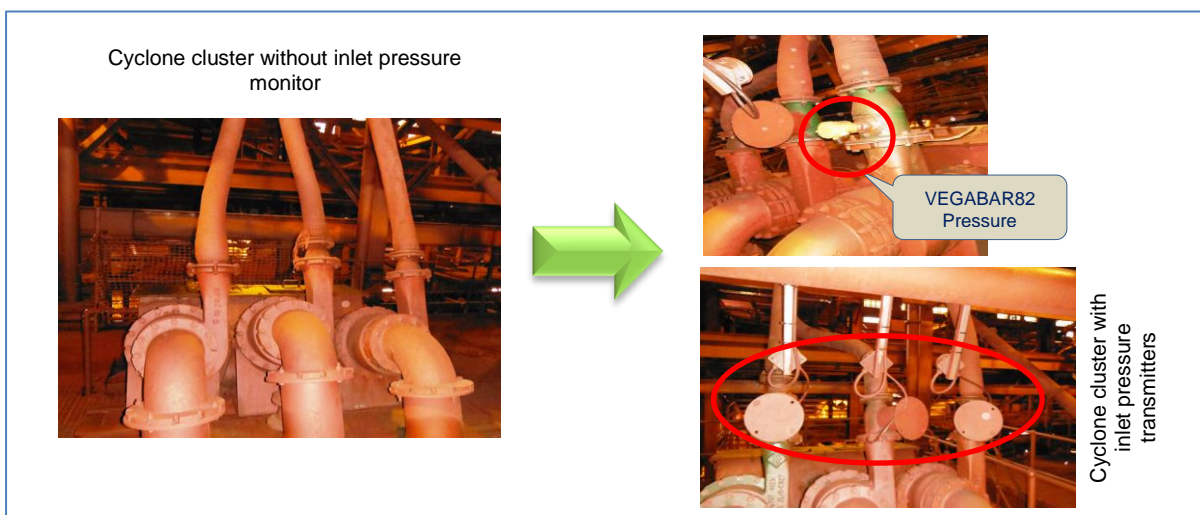


Figure 5.4: Cyclone inlet pressure transmitter

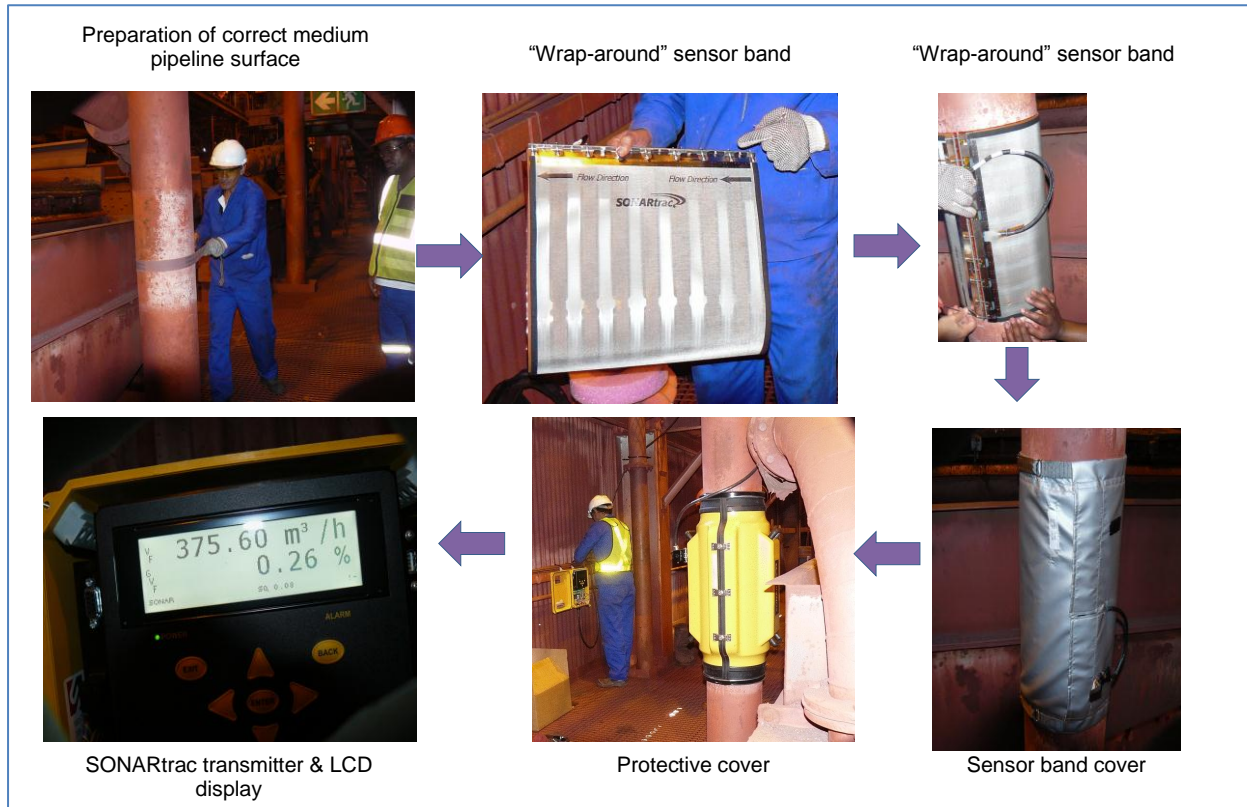


Figure 5.5: Non-contact SONARtrac flowmeter installation in correct media pipeline

5.2 MODULE 811 PERFORMANCE TRENDS

The automation project resulted in the real-time monitoring of the metallurgical key performance indicators (KPI's) and real-time on the CITECT SCADA. The PLC/SCADA display in the control room monitors and office network computers is presented in Appendix C. The process signals from the monitoring instrument gauges representing the process (metallurgical) variables for the streams were connected to the plant PLC control system via the 4 – 20 mA analog inputs. A dedicated data monitoring and logging system was developed to enable the retrieval of the relevant process information trends from the plant PLC control system historian.

The process interlock and alarms allows the control room operator to view unstable plant operating conditions in order to take an appropriate remedial action. In addition, the automation allows the Production Superintendent and Metallurgical Engineers to diagnose the plant conditions that influence the metallurgical process efficiency.

Currently the system is utilised for the monitoring and trending of process data. The control and interlocking described in this document has not been activated, however SCADA status indications have been defined that warn the operator that the system is "out of spec" and if these conditions are allowed to persist then an alarm indication is displayed to indicate to the operator that the system would have cut feed or switched over to an alternate module.

5.2.1 Monitoring and Control of Medium-to-Ore Ratio

This section aims to present the operational trends of the medium-to-ore ratio and its impact on the performance of the plant as well as the factors influencing the M:O ratio and how to mitigate the negative impact on beneficiation process.

Figure 5.6 shows the actual M:O ratio as depicted on the CITECT module overview page. If the M:O ratio is out of limits then a yellow flashing [M:O Ratio] “out of limit” warning indication is displayed to the operator. If this condition is allowed to persist for more than 10 minutes then the SCADA [M:O Ratio] Status display will flash red indicating that feed to the plant will be cut/diverted.

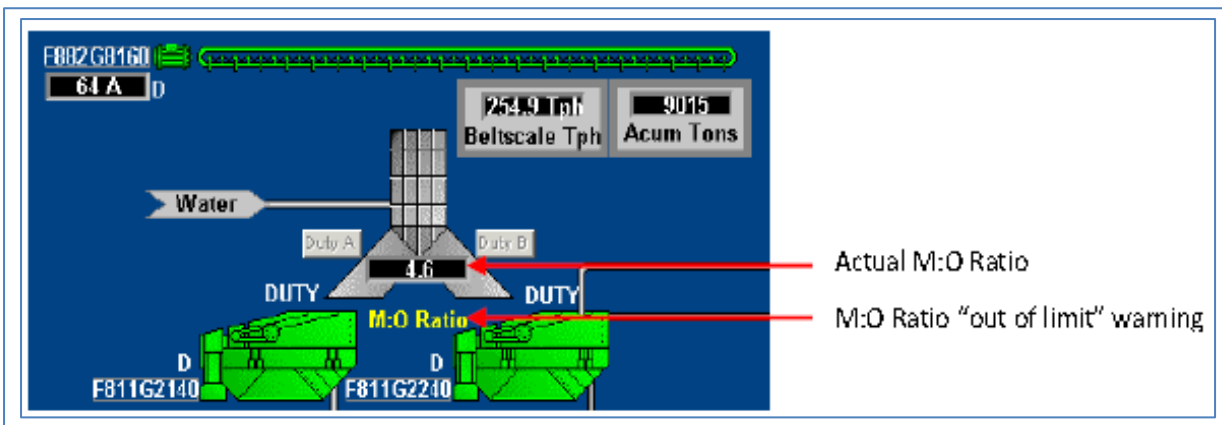


Figure 5.6: Medium-to-ore ratio display in CITECT SCADA

Figure 5.7 shows the medium-to-ore ratio trends for the period of 17Jul 2014 until 06 Aug 2014. As shown in the trends, Module 811 operated at M:O ratio on the border of the absolute minimum target of 5:1, which poses threat to the beneficiation efficiency of the cyclone plant. However, the trends show positive improvement in the M:O ratio in Aug ‘14.

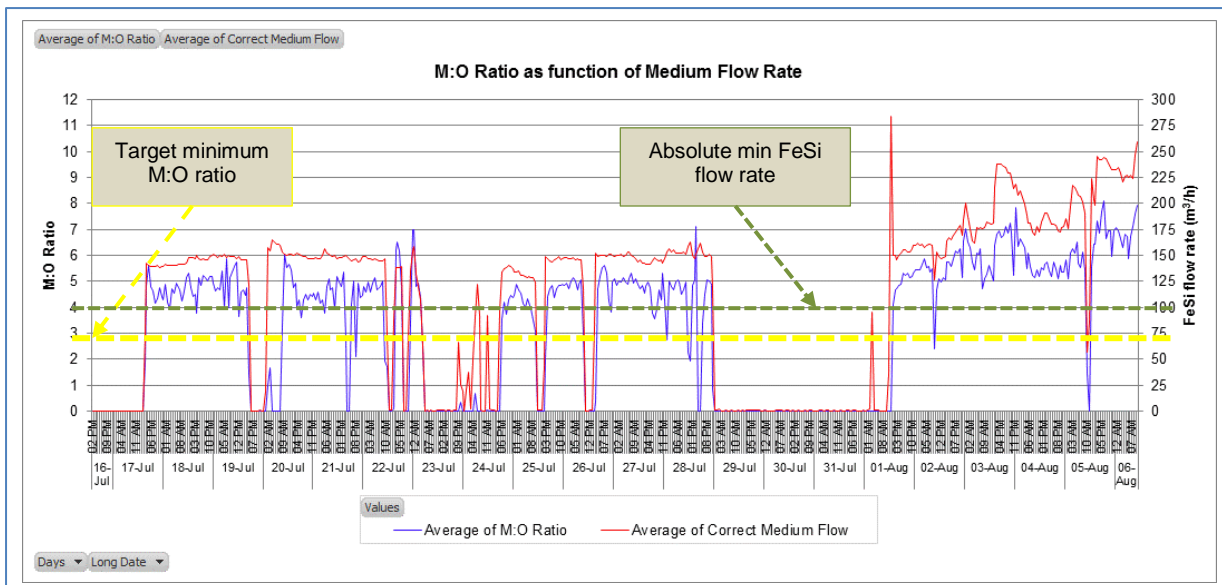


Figure 5.7: Medium-to-ore ratio trends

The other factor that influences the M:O ratio is the correct medium flow rate to the

beneficiation cyclone. The flow rate is directly influenced by the availability of the medium in the the correct medium tank. Thus, Figure 5.8 shows the trends of the FeSi flow rate to the beneficiation circuit as a function of medium level in the correct medium sump. Under normal operating conditions, the correct medium sump is controlled at a minimum level of 25%. This is to ensure enough NPSH for the pump and to avoid cavitation as well as ensuring correct medium flow to the beneficiation cyclone.

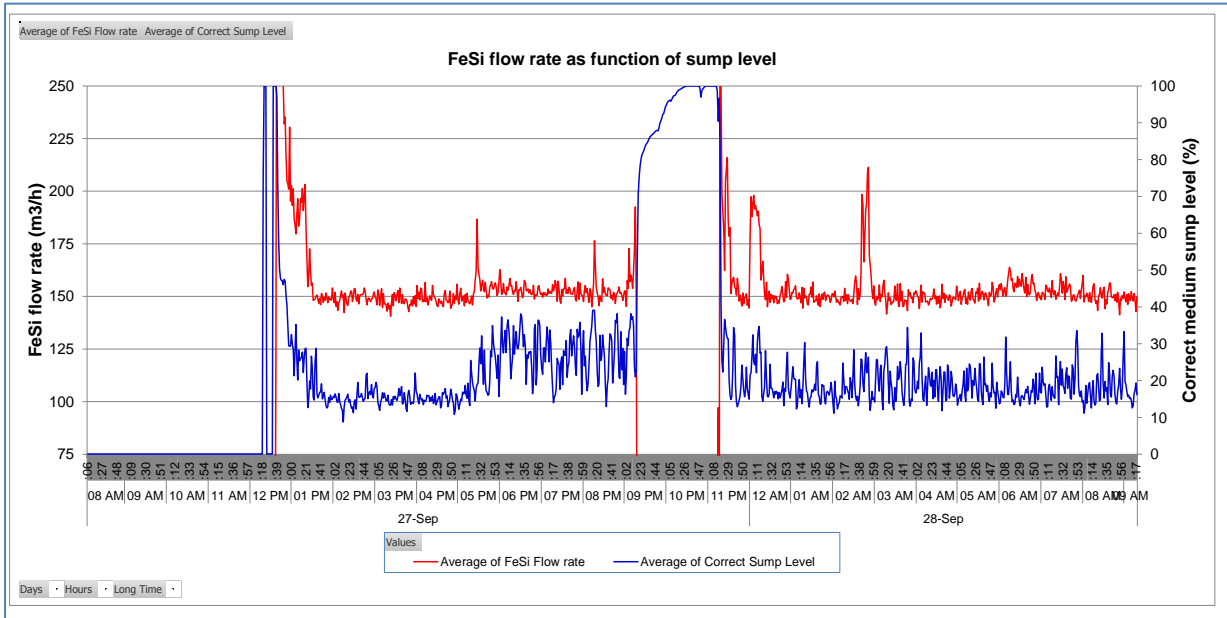


Figure 5.8: Medium flow rate as function of medium sump level

The product quality for the period under review is illustrated in Figure 5.9, which shows that the alumina (Al_2O_3) contaminant level in the product decreases as the M:O ratio increases. However, the level of silica (SiO_2) showed an increasing trend with an increase in M:O ratio. This might be linked to the quality of the quality of the ROM during the period under review. Thus the performance of the fine cyclone plant during the period under review correlate well with the assertion of (Chu, et al., 2009) on effect of M:O on dense medium cyclone.

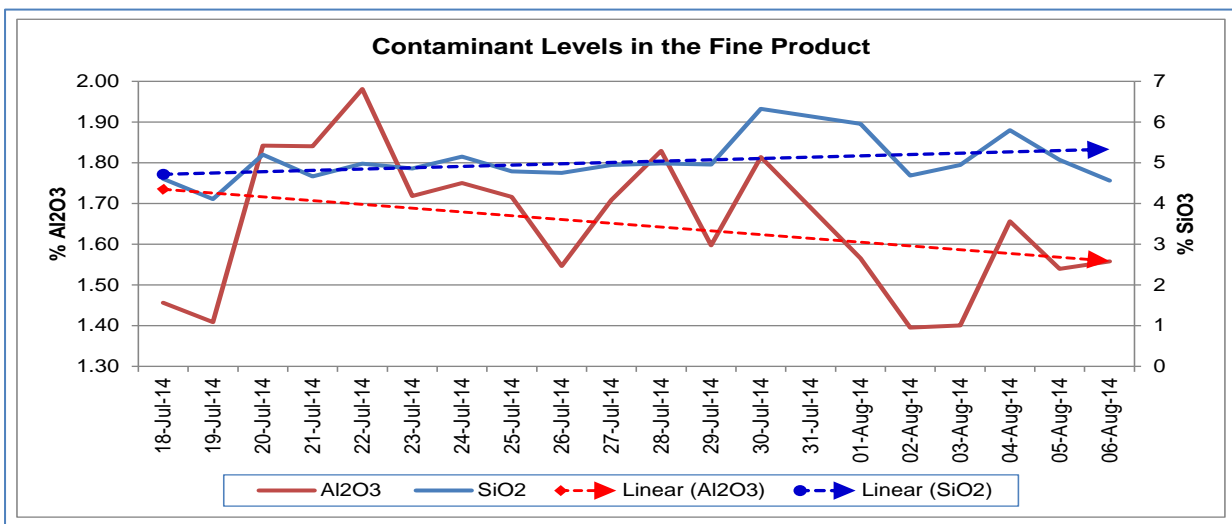


Figure 5.9: Contaminant levels in the fine product

5.2.2 Monitoring and Control of Cyclone Inlet Pressure

This section aims to present the operational trends of the cyclone inlet pressure and their impact on the performance of the plant. Figure 5.10 and Figure 5.11 illustrate the module arrangement and feed pipeline for cyclone plant module in Sishen. The graphs depict designs that will have an impact on the cyclone inlet pressure as well as inlet velocity.

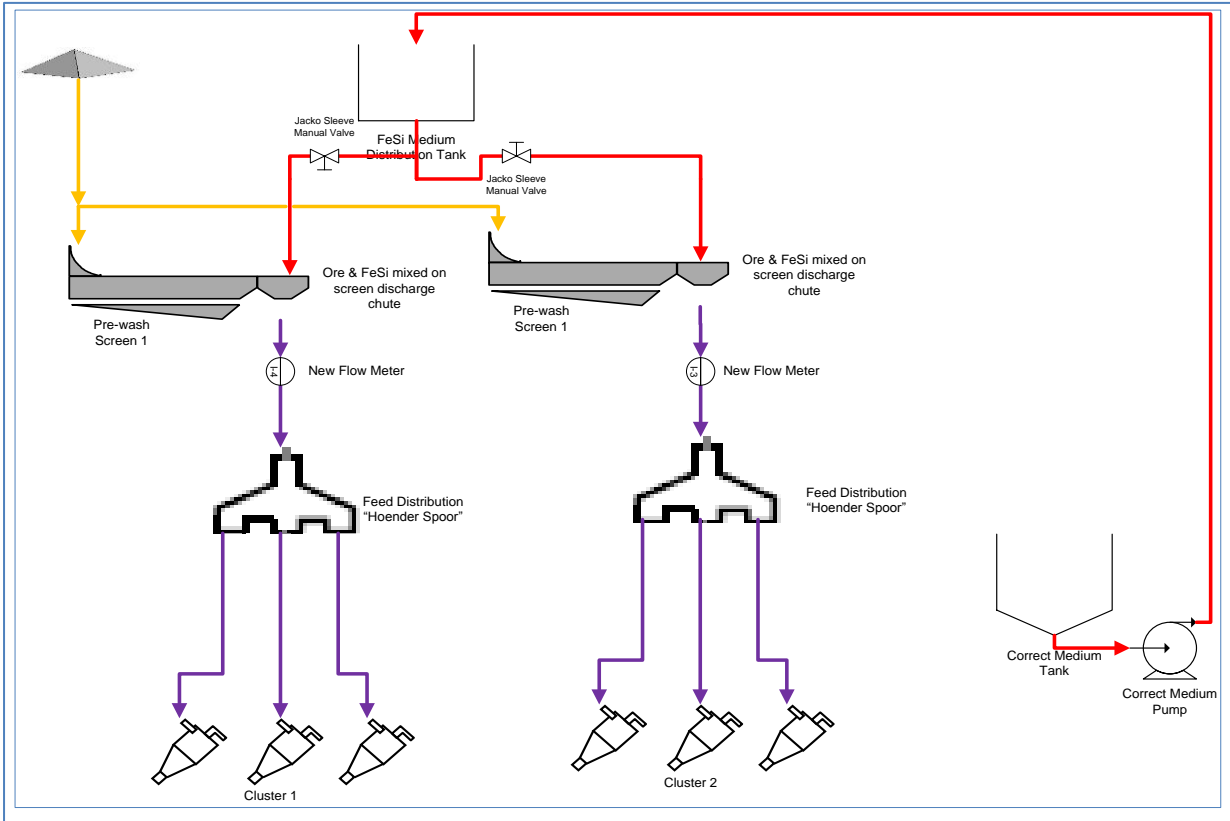


Figure 5.10: Layout of the module feed streams

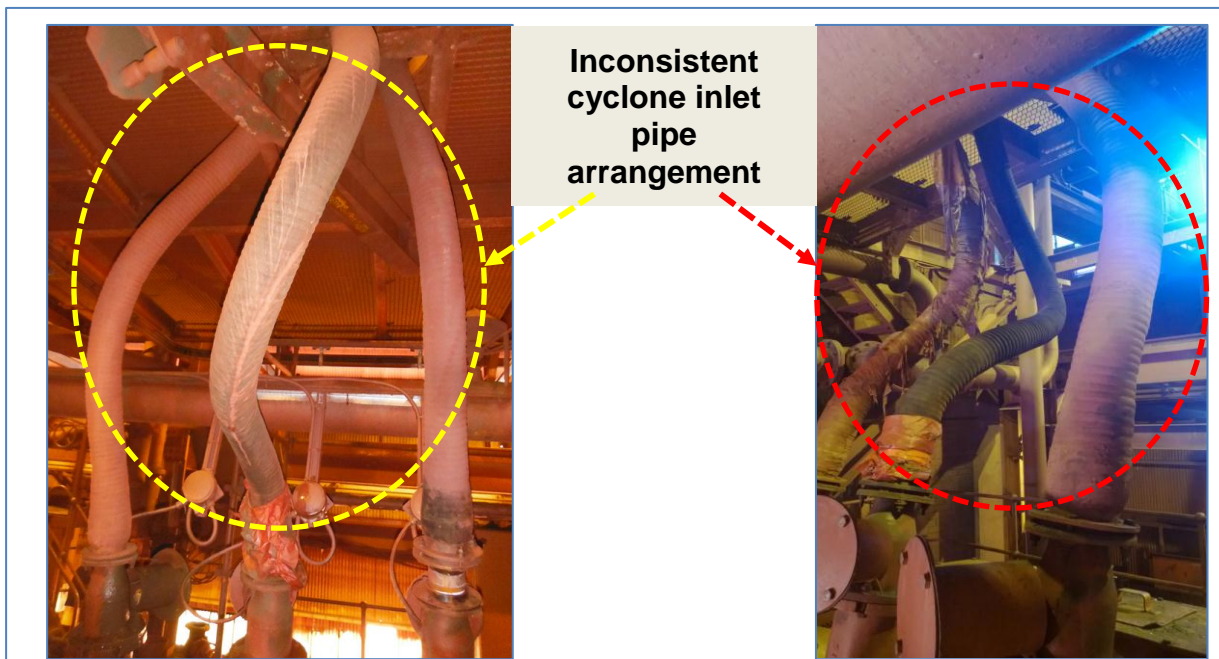


Figure 5.11: Cyclone inlet pipe arrangement

The purpose of the cyclone inlet feed monitoring and control is to ensure that the inlet pressure to respective feed cyclones in cluster is constant. The cyclone inlet pressure should remain as stable as possible under feed conditions. An ideal operating pressure ranges from 8D to 12D. The pressure differential within a cluster can undergo a 5 – 10% variation. However, should the variation be high is an indication of system imbalances and either one set is blocked. The inlet pressure is also been linked to the performance of the beneficiation cyclone, where lower pressures are indicative of cyclone being prone to roping.

Pressure transmitters have been installed on each of the cyclone within a cluster. These pressure transmitters monitor the pressure in each cyclone of a particular cluster and if there is a difference in pressure between any of the cyclones within a cluster, then a SCADA Cyclone Delta P “out of limit” warning will be displayed (Figure 5.12).

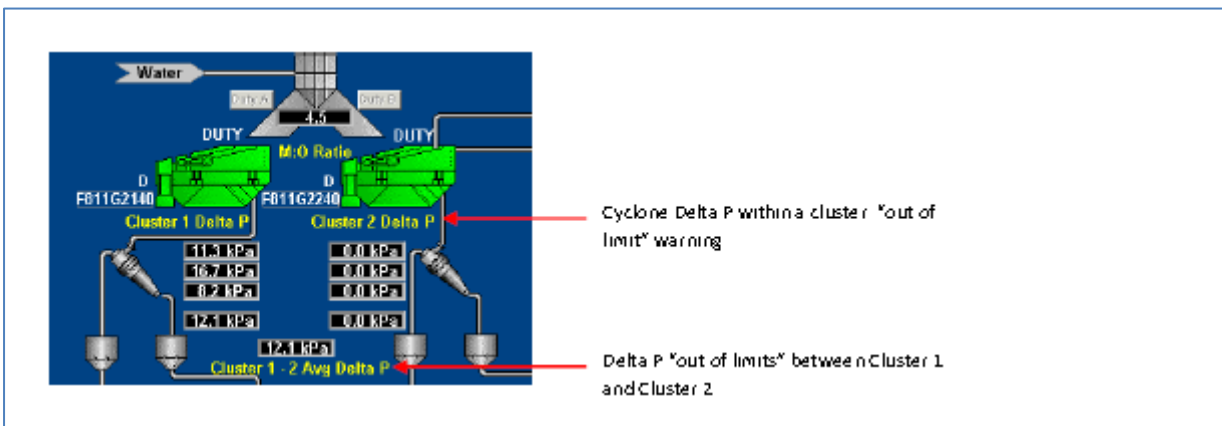


Figure 5.12: Cyclone and cluster monitoring display in the SCADA

Figure 5.13 shows the inlet pressure trends for the Module 811 cyclone clusters. The graph also shows the pictorial view of the cyclone spigot operating condition for the cluster 1 cyclones taken on the 10th August 2014. This was monitored to illustrate the influence of inlet pressure on cyclone operating condition. It can be seen that cyclone 5120 showed excellent flaring condition and this cyclone had the highest inlet pressure indicated by pressure transmitter PT102 trends. Similarly the 5110 cyclone that had the lowest pressure (PT101 trends) showed poorer flaring condition.

The area of concern identified for the possible inaccuracies and variation in inlet pressure of the same cyclone cluster is the flexible feed pipe arrangement depicted in Figure 5.11. This leads to varying flow profile to cluster’s cyclones, thereby having preferential flow for feed pipeline with less restriction. Thus, it is imperative to have similar cyclone feed pipeline profile to limit the impact of preferential flow as well as prevent addition pressure drops prior slurry inlet in the cyclone.

Cyclone inlet pressure can also be influence by the medium flow balance between the two clusters as they are fed from a common medium distribution tank. The medium flow to clusters is control by manual “Jacko-sleeve” screw type valve on a flexible rubber spool

piece. Distinct variation in inlet pressure necessitated the automation project to install non-contact SONARtrac flow meters to measure the flow after mixing ore and dense medium as illustrated in Figure 5.14.

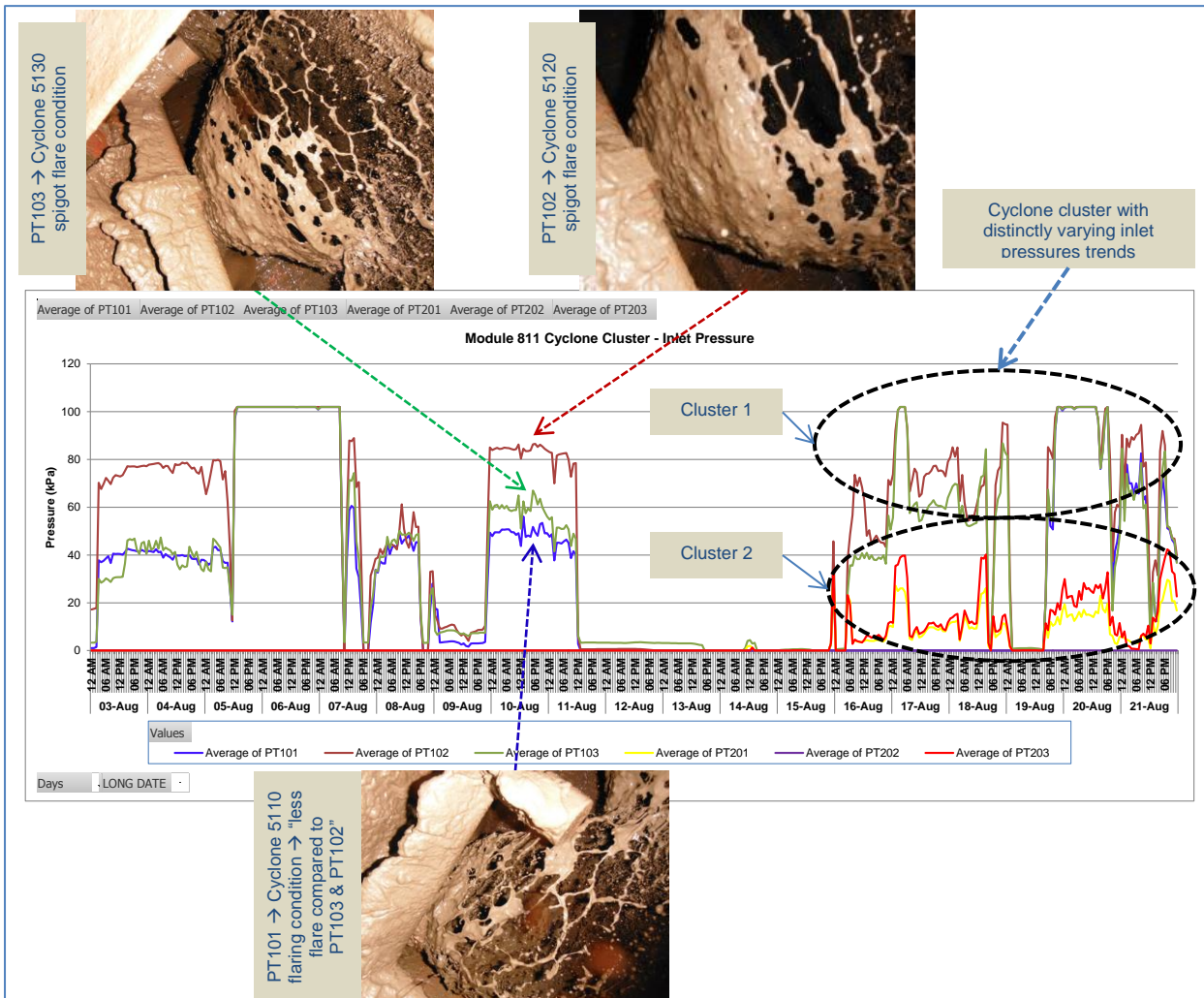


Figure 5.13: Module inlet pressure trends and spigot flare conditions

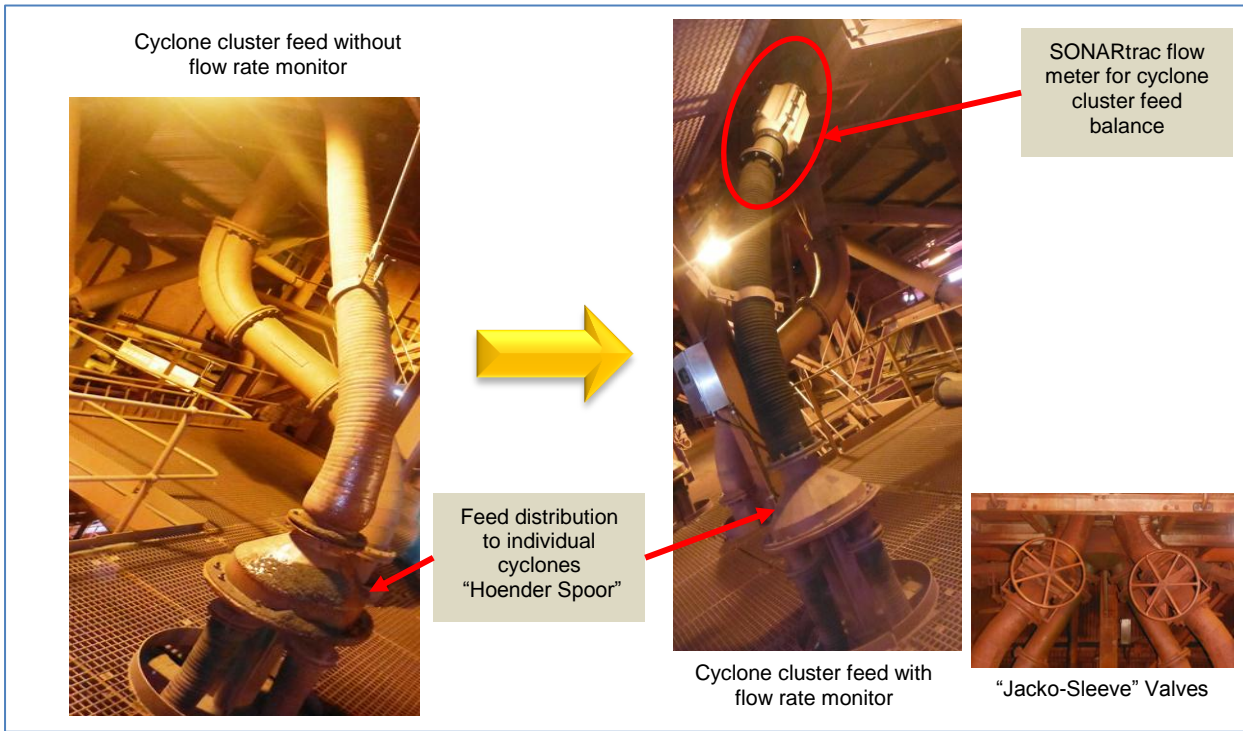


Figure 5.14: Cyclone cluster balance

Cyclone feed flow rate is presented in Figure 5.15. Flow rate variation greater than 15% is regarded as having drastic impact on the system balance. (Mukherjee, et al., 2003) indicated that higher flowrates to the cyclone would result in lower E_p , that is, high flow rates ensures better sharpness of separation. In addition, it was found that medium stability is not affected at high flow rates for the fine dense media. Thus, with the cyclone cluster monitoring would ensure better control of cyclone performance thereby eliminating the effect poorer E_p in another cluster.

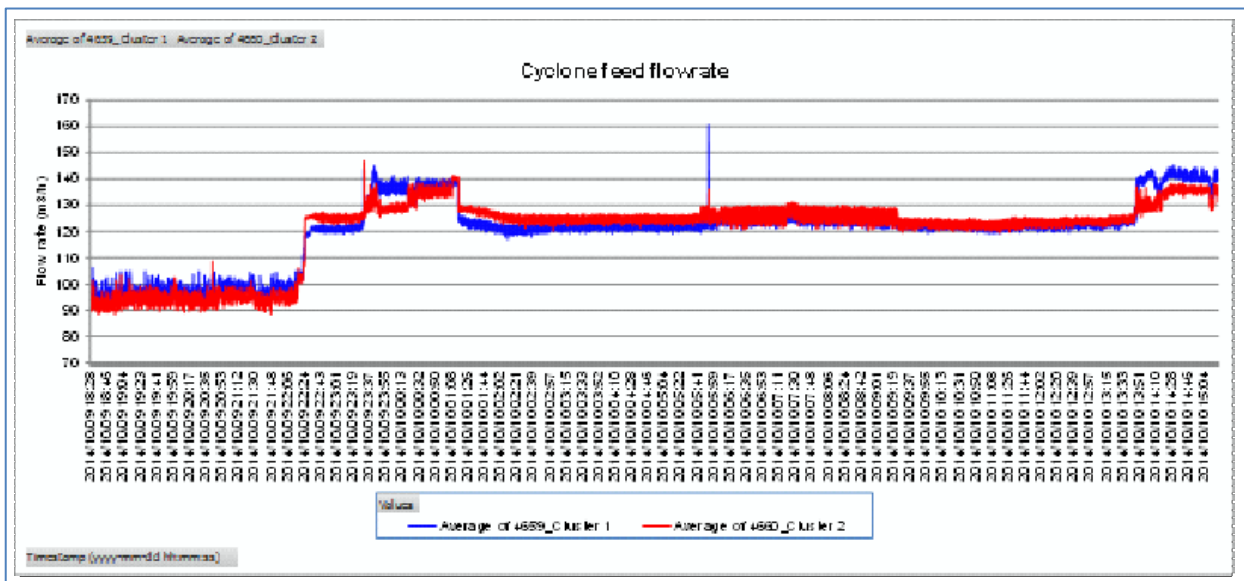


Figure 5.15: Cyclone cluster feed flow rate

5.2.3 Monitoring and Control of Density Differential Measurement

Figure 5.16 illustrates the density trends of the feed medium and the cyclone overflow and underflow medium during the commissioning of the DMCT110 unit. The trends present data after quick calibration of the units using one point measure in order to validate the operability of the instrument from default values. Apart from optimisation and full calibration, the trends show that the system is functioning properly with the values of the underflow stream being higher than the feed and ditto for value of overflow stream being lower than the feed density.

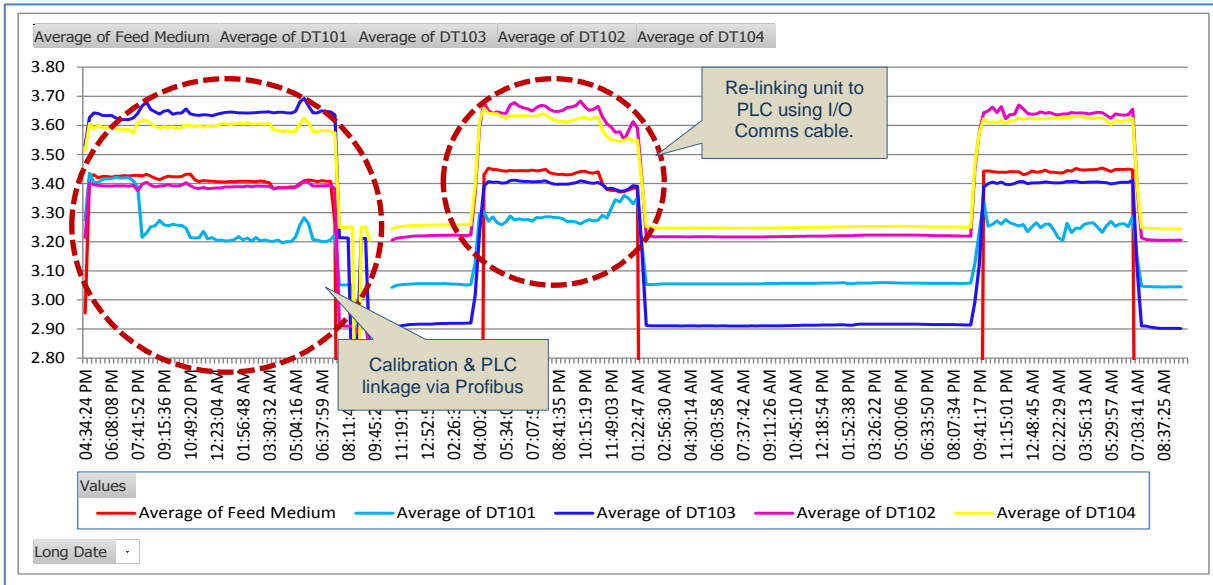


Figure 5.16: FeSi Medium density trends

Figure 5.17 illustrates the density differential trends determined from online measurement during commissioning and quick calibration phase. The density differential trends show some very positive and encouraging results that are worth a mention. It can be seen that point A in the graph during the period of 30th Sept is indicative of medium instability with the overflow and underflow densities diverging from each other while the feed medium density remained relatively constant. This can be attributed to dense medium segregation in the cyclone, where the overflow stream comprises of finer size fraction. In addition, the trends show steady state operations during period 5th Oct 2014 until 7th Oct 2014 as indicated by point B where the underflow and overflow densities are trending relative to the feed control density.

The manual density differential measurements are shown in Figure 5.18. The trends illustrate that the density differential is within the allowable metallurgical best practice. However, the online trends showed a slightly high differential which might be attributed to medium instability.

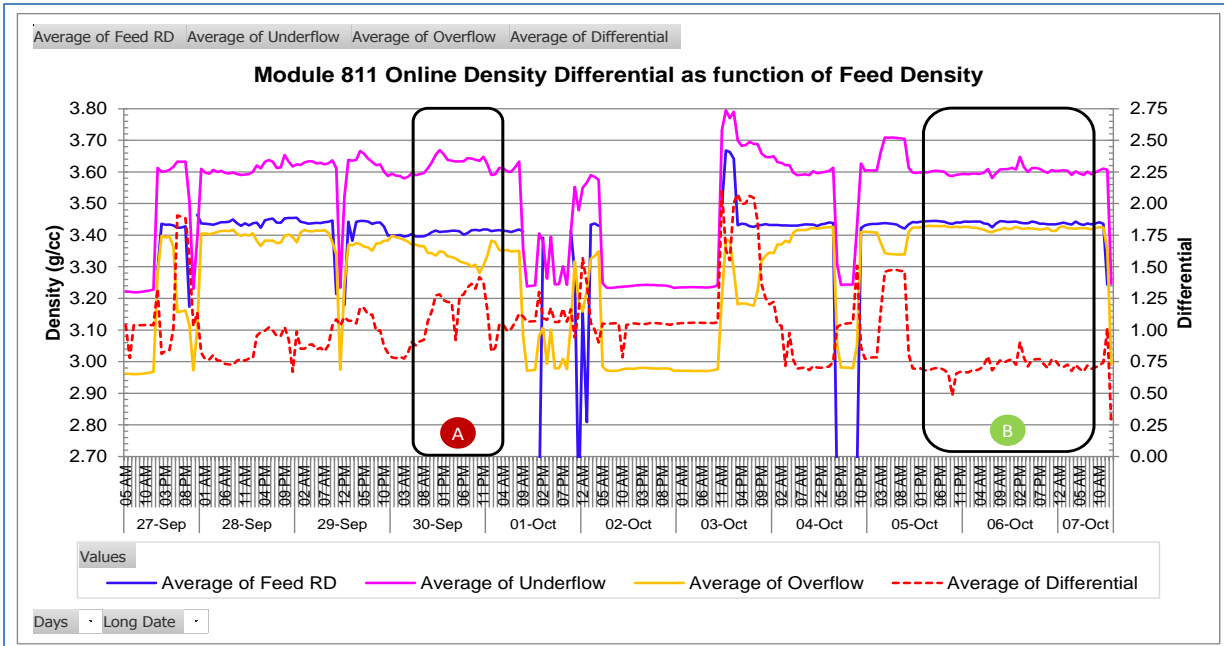


Figure 5.17: Online density differential trends

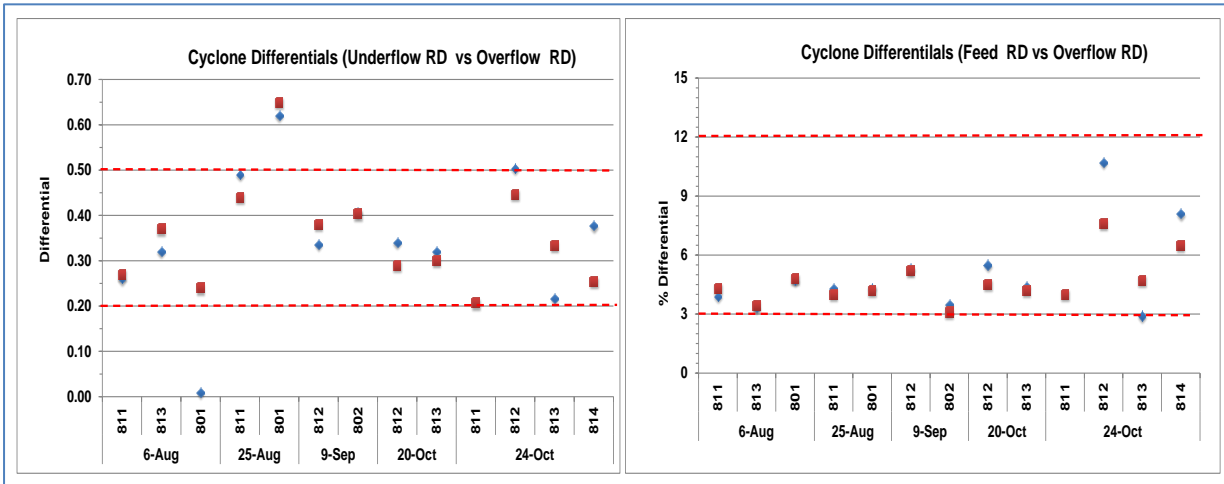


Figure 5.18: Manual density differential

The online differential is measured from the streams of the drain and rinse screen underpan. However, during the normal operation in Sishen cyclone plant, water is added on the spigot underflow flow to ensure proper drainage from the sieve bend prior rinsing in the product screen. Thus the real-time measure underflow medium density has to be corrected to take into account the water addition. Figure 5.19 illustrates the relationship between the underflow density readings with water fully closed and open. Thus a correction factor of 0.081SG will have to be added to the underflow density stream to show the actual medium density from the cyclone spigot.

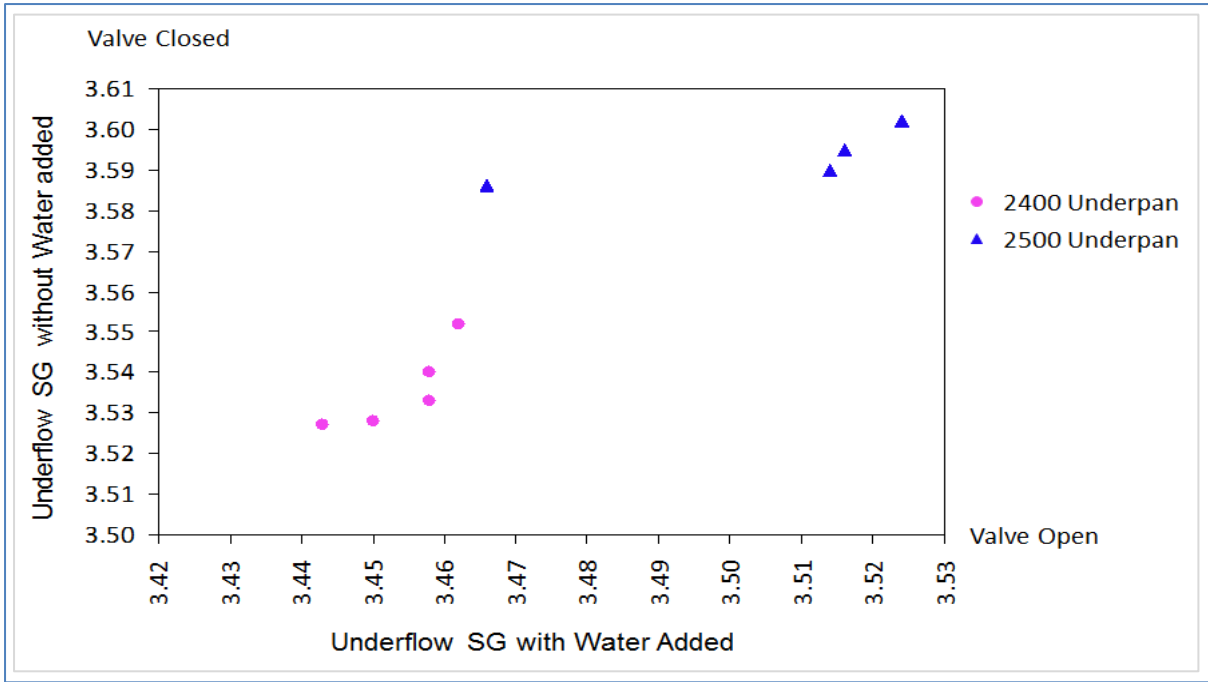


Figure 5.19: Relationship of the underflow medium density with and without water dilution

CHAPTER 6: MODELLING OF DENSE MEDIUM CYCLONE CIRCUIT

6 DENSE MEDIUM CYCLONE MODELLING INTRODUCTION

A Simulink program was utilised to simulate the performance of the cyclone module based on the existing models from literature such as the well-known Wood's empirical model described in section 2.2.4. This was also complemented by use of equations derived by (Meyer, 2010) to model the dense medium circuit and supplementary unit processes is derived from the principle of conservation that is obeyed by all physical systems as cited by (Stephanopoulos, 1984). Thus, the principle of conservation for mass into a system can be summarised as follows:

$$\frac{\text{Accumulation of } M}{\text{time period}} = \frac{\text{Inlet Flow of } M}{\text{time period}} - \frac{\text{Outlet Flow of } M}{\text{time period}} + \frac{M \text{ generated}}{\text{time period}} - \frac{M \text{ consumed}}{\text{time period}} \quad \dots \text{Equation 6.1}$$

The above conservation of mass principle described in Equation 6.1 was used by (Meyer, 2010) to develop mathematical models for the dense medium cyclone and heavy medium make-up tank. With the development of this process models, it was assumed that the rates of change for the mass splits to the cyclone overflow and underflow is proportional to the dense medium densities in cyclone underflow and overflow. Thus, equation 6.2 to 6.4 was derived while assuming the steady state volumetric flows, that is, $Q_{inlet} = Q_{off} + Q_{uf}$.

$$V_{c,o} \frac{d\rho_{c,o}}{dt} + V_{c,u} \frac{d\rho_{c,u}}{dt} = W_{c,i} - Q_{c,o}\rho_{c,o} - Q_{c,u}\rho_{c,u} \quad \dots \text{Equation 6.2}$$

By assuming that the rate of change in mass to the overflow and underflow to be proportional to the medium density differential in underflow and overflow stream, (Meyer, 2010), deducted that the conservation of mass would results in the following relationship:

$$V_{c,o} \frac{d\rho_{c,o}}{dt} = K_{c,o}(\rho_{c,i} - \rho_{c,o}) \cdot \text{waste} \quad \dots \text{Equation 6.3}$$

$$V_{c,u} \frac{d\rho_{c,u}}{dt} = K_{c,u}(\rho_{c,i} - \rho_{c,u}) \cdot \text{product} \quad \dots \text{Equation 6.4}$$

While the above mentioned models are relatively easy to follow and contains all of the components that provide sensitivity to changes in operation, i.e. ore feed rates, cyclone inlet density, cyclone size, particle sizes, FeSi size etc. However, these models come with the disclaimer that it is relevant to a specific cyclone setup and operating conditions. Both (Wang, 2009) and (Petersen, 2010) conceded that this takes the model out of the hands of anyone who wants to use it independently in an applied fashion. Thus in order for the user to apply this in their operational environment, the model has to be "re-engineered" for their own conditions, particularly determining constants and other fitting parameters.

6.1 CORRECT MEDIUM SUMP LEVEL MODELLING

The FeSi used in the beneficiation process is recirculated back to correct medium sump via drainage from the waste and product screen. The FeSi medium recovered from the drain section of the product screen is fed directly to the correct medium tank whereas that recovered from the drain section of waste screen is pumped through densifier sump. The denser stream from the densifier is fed to the correct medium sump whilst the dilute stream goes to the dilute sump. In addition, the FeSi from the rinse section of the product and waste screens as well as plant spillage is collected into the dilute sump. The dilute medium is pumped into the magnetic separator circuit where further FeSi recovery is collected back to the correct medium sump.

The addition of “fresh FeSi” is via the break tank of FeSi powder directly into the correct medium. This stream is done when the level in the correct medium sump is below absolute minimum of 15% as well as when the operating density has to be increased to higher values. Figure 6.1 show a schematic layout of the cyclone plant module medium flow line which indicate all streams following back to the correct medium sump. The major metallurgical KPI for cyclone plant is to maintain the level in the correct medium sump to 25% as well as to operating density to the required set-point.

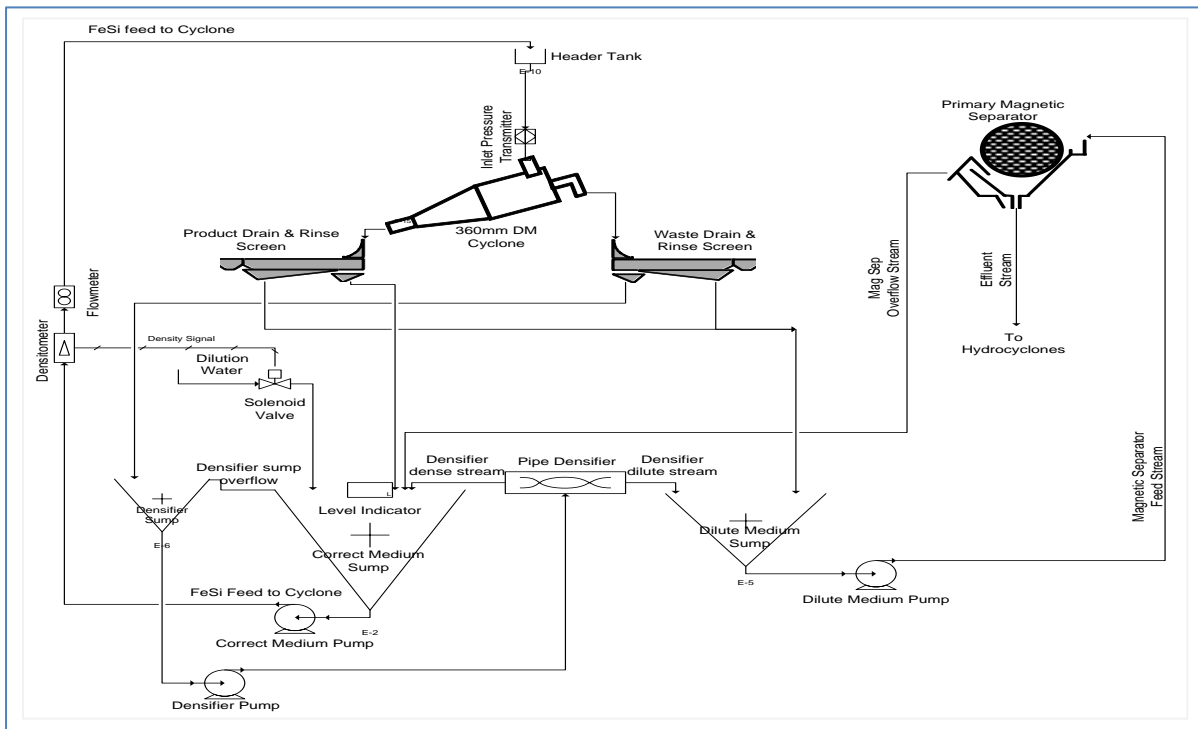


Figure 6.1: Cyclone module medium flow line

Thus in order to simplify the correct medium tank modelling, only the combined streams collected to the tank and “fresh FeSi” addition will be modelled. This is done, in order to model the drop in the correct medium sump level and determine the cycle time for the addition of a new batch of fresh FeSi. Figure 6.2 shows a simplified representation of the

correct medium tank system utilised for modelling purposes. The current medium tank design is a truncated conical tank. Thus, the equations 2.11 to 2.13 as described in section 2.2.3 are applicable for determining the capacity of the correct medium tank for a cyclone module.

The dimensions of the correct medium tank are as follows:

- ✓ Bottom diameter = 610 mm
- ✓ Total tank height = 2,264 mm
- ✓ Top part diameter = 3,500 mm

To simplify the modelling of the tank height in order to determine when manual “fresh FeSi addition” must happen, it was assumed that the effective area of the medium tank does not change with change in medium height in the tank. Thus, the modelling of rate of change of medium level in the tank can be simulated utilising the conservation of mass taking into account the rate of medium flow in and out of the tank as follows:

$$A_t \frac{dh_t}{dt} = Q_{t,med} + Q_{t,dis} - Q_t \quad \dots \text{Equation 6.5}$$

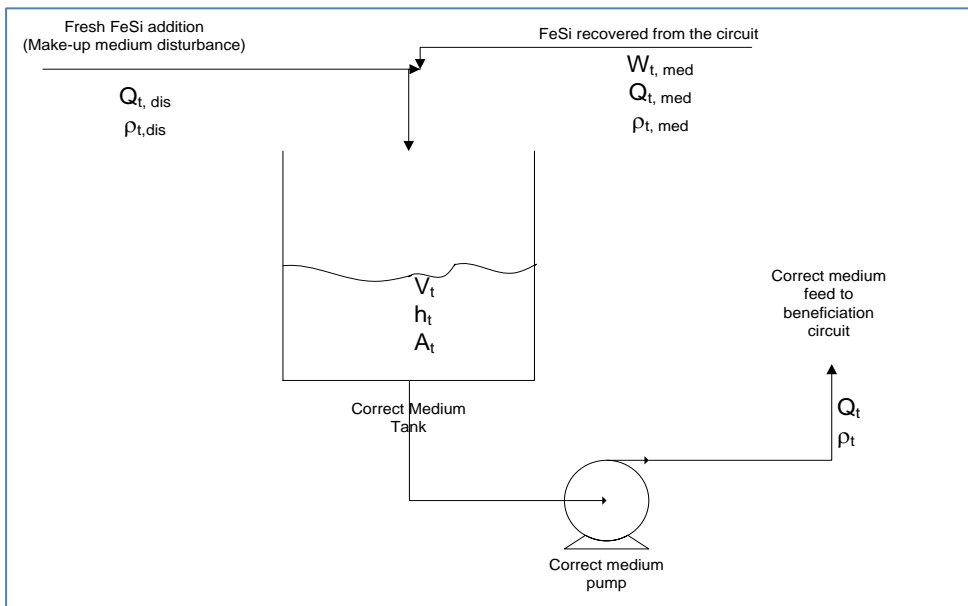


Figure 6.2: Simplified representation of correct medium tank

Figure 6.3 illustrates the internal structure of the Simulink for the modelling of correct medium tank level. The structure shows flow rate of medium recovered back into the circuit by utilising the random flow rate generator, with the average flow of $155 \text{ m}^3/\text{h}$, in order to mimic the plant operating conditions. The parameter selection was selected to denote a mean of 155 representing the average design flow rate for the plant whilst the variance was kept a default value of 1. The out flow stream denotes medium fed to the beneficiation circuit which is inclusive of the FeSi lost via adhesion losses as well as effluent stream of the magnetic separator. A signal builder is incorporated to mimic the disturbance attributed to the addition of the “fresh FeSi powder” via current manual bag breaker system.

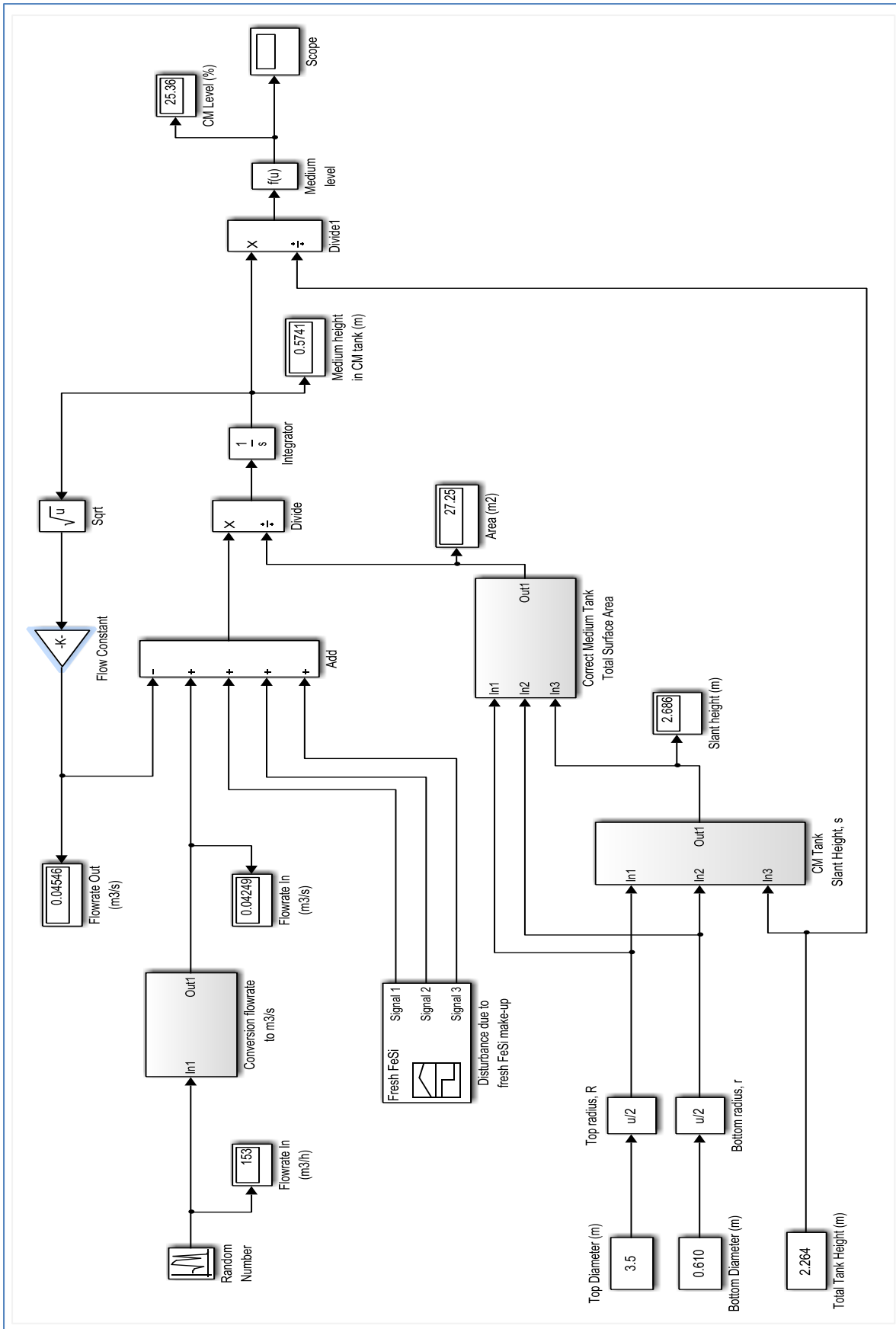


Figure 6.3: Simulink structure for the correct medium tank level control

The simulated output of the correct medium sump level is illustrated in Figure 6.4 whilst the measured sump level is presented in Figure 6.5. The simulation was carried out with loading

a disturbance mimicking the manual addition of “fresh FeSi” powder in the correct medium sump. Point A in Figure 6.5 indicate the period when the module was shut-down which shows an increase in the sump level due to the FeSi medium in the circuit gravitating back to the correct medium sump.

The correct medium sump level control can easily be controlled by proper conventional PID controller. This will ensure that the level control is maintained at a set-point value and able to accept and/or adapt to process disturbances. This can be achieved by automating the “fresh FeSi make-up system. However, the current manual fresh FeSi addition method necessitated that the modelling be done to mimic such disturbance. Thus, the current model set-up will suffices for the indication of when and the frequency of the manual of the “fresh FeSi batch” in the system.

For the system with automated fresh FeSi make-up system, the design of the controller will be similar to that described by (Aslam & Haider, 2011) and (Meyer, 2010). The design model will consist of the controller that will maintain the dense medium level in the sump to a desired set-point as well as at the required operating density while rejecting the disturbance introduced by make-up FeSi and recovered FeSi streams.

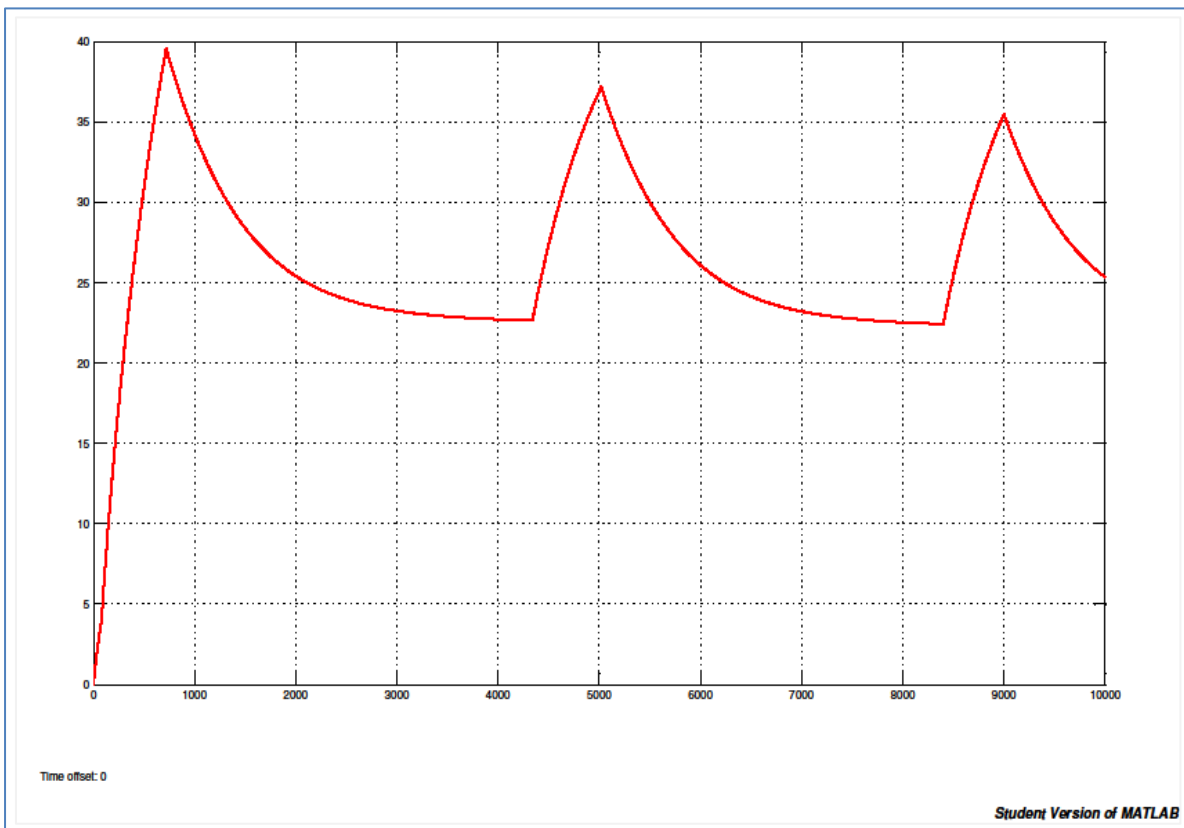


Figure 6.4: Simulated response of the correct medium sump level

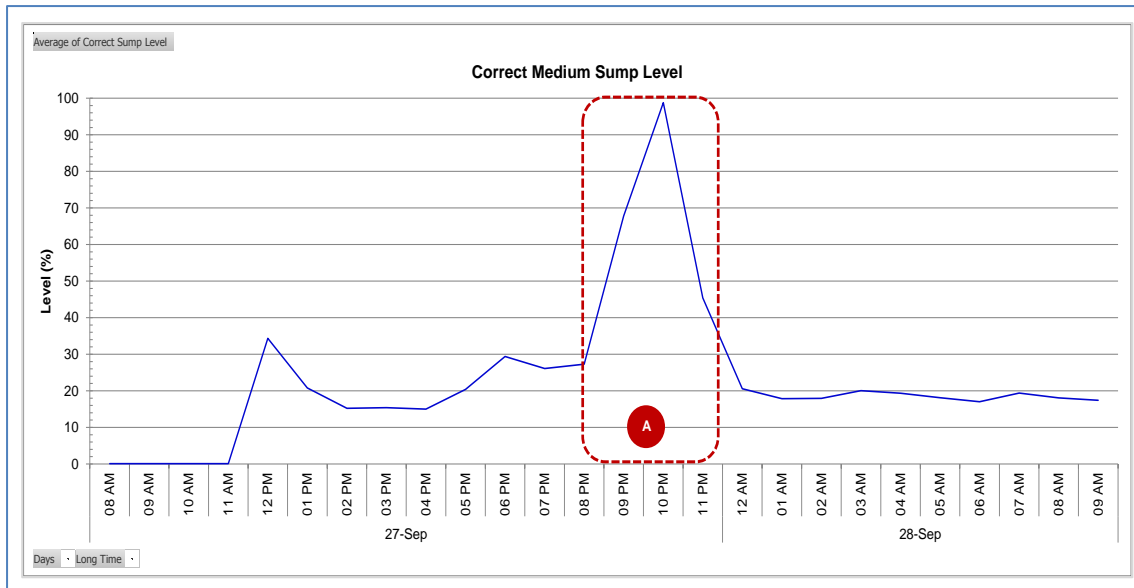


Figure 6.5: Plant measured correct medium sump level

6.2 CYCLONE PERFORMANCE MODELLING

A dense medium cyclone model has been developed for the Sishen iron ore DMS plant, with a specific focus on underflow and overflow medium density, which incorporated the current state of the art model by Woods that relies heavily on calibration constants. The model also incorporates the medium flow split in the cyclone. In view of the difficulty in applying the Woods model, a model structure that has few calibration constants and specifically uses operational state variables has been designed.

The modelling of the cyclone Module 811 is based on the following baseline setup conditions:

- Cyclone diameter (D_c) : 360 mm
- Cone angle : 10 degrees
- Spigot diameter (D_u) : 100 mm
- Vortex diameter (D_o) : 125 mm
- Barrel length : 200 mm
- Cone length : 535 mm

Design operational parameters are:

- Ore feed rate = 180 t/h (average)
- Ore particle density = 4.50 t/m³
- Medium flow rate = 150 m³/h (absolute min)
- Medium operating density = 3.4 t/m³
- Viscosity = 0.02 Pa.s

The Simulink structure to model the performance of the dense medium cyclones based on the total conservation of mass principle and incorporation of the Wood's sub-models is

presented in Figure 6.6. A random number generator was incorporated in the model to mimic the variation if the ore feed rate (t/h) in the cyclone module. The parameter selection was kept at a mean of 180 to denotes the average feed design feed rate whilst the variance was kept at default value of 1. This was done to simulate the actual plant performance around the set-point throughput of 180t/h.

The structure is used to simulate the cyclone underflow and overflow densities. Detailed sub-systems for the Simulink internal structure for modelling the cyclone module's overflow and underflow densities as well as the percentage of medium split to overflow stream are presented in Figure 6.7 and Figure 6.8. A function block to describe the medium behaviour was incorporated in sub-system depicted in Figure 6.7 as adopted from the Wood's sub-model 4, which aim to determine the medium density of the overflow stream as described in equation 2.10 (Section 2.2.4).

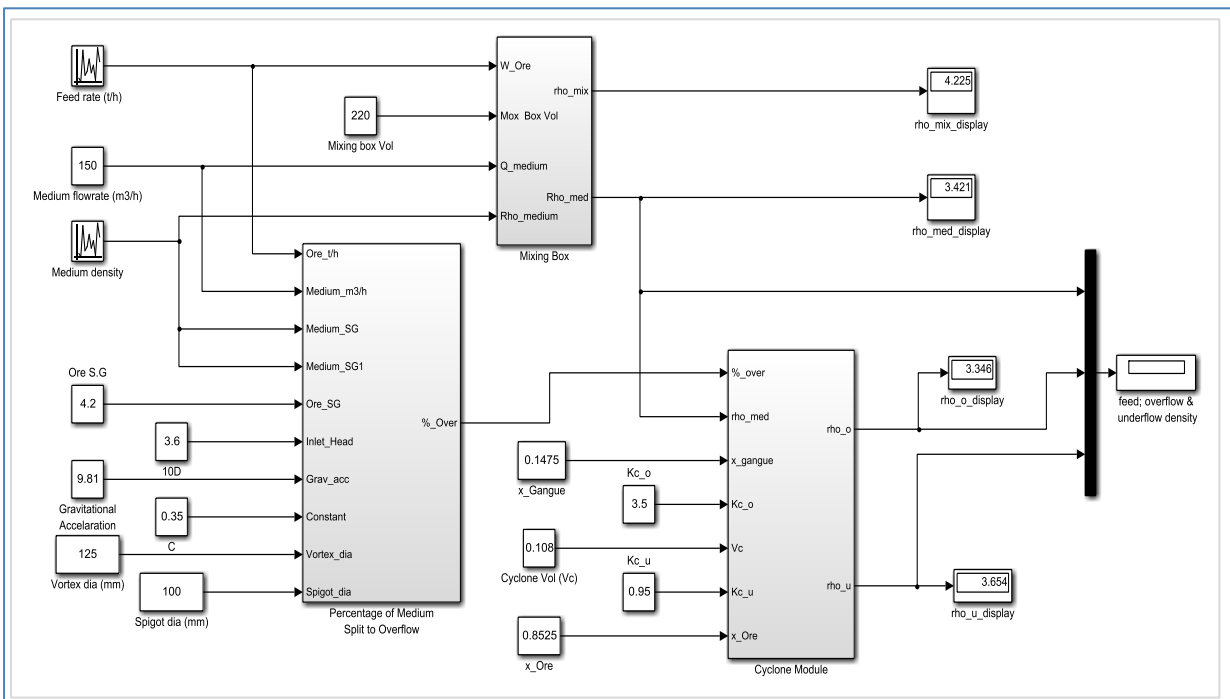


Figure 6.6: Internal structure of the Simulink model for the modelling of the cyclone underflow and overflow density

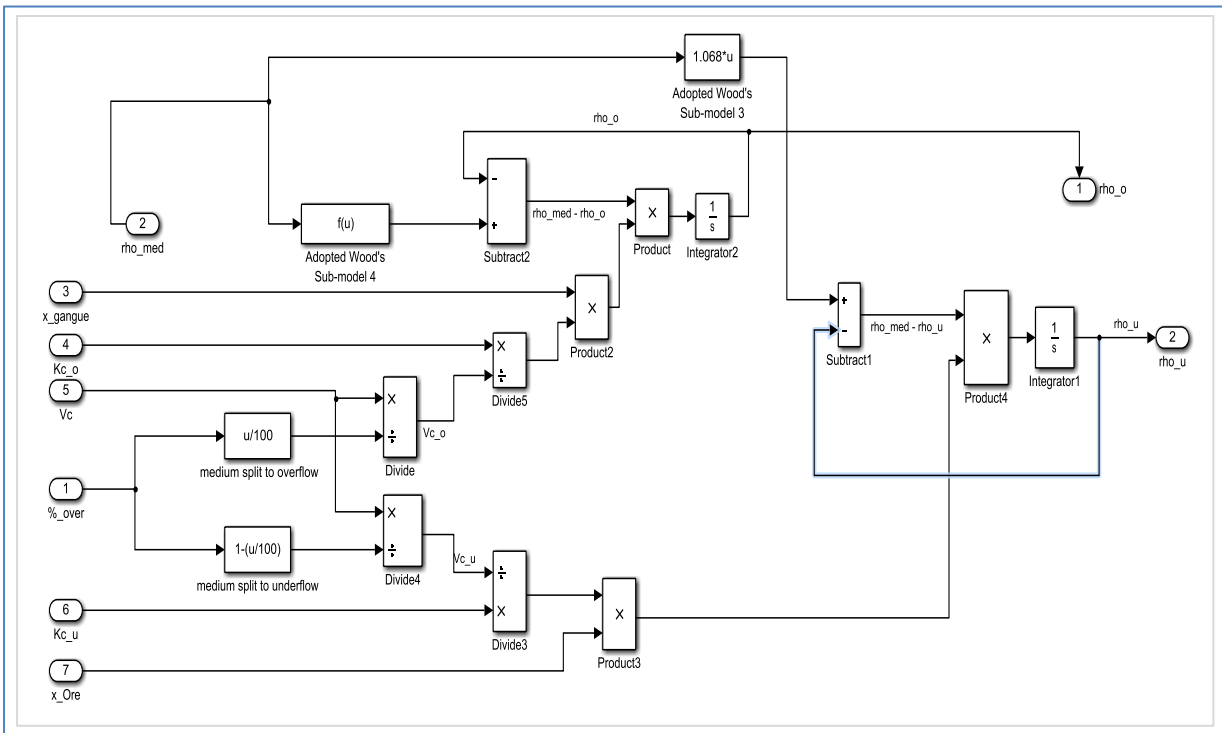


Figure 6.7: Subsystem of the internal structure of modelling of the cyclone underflow and overflow density

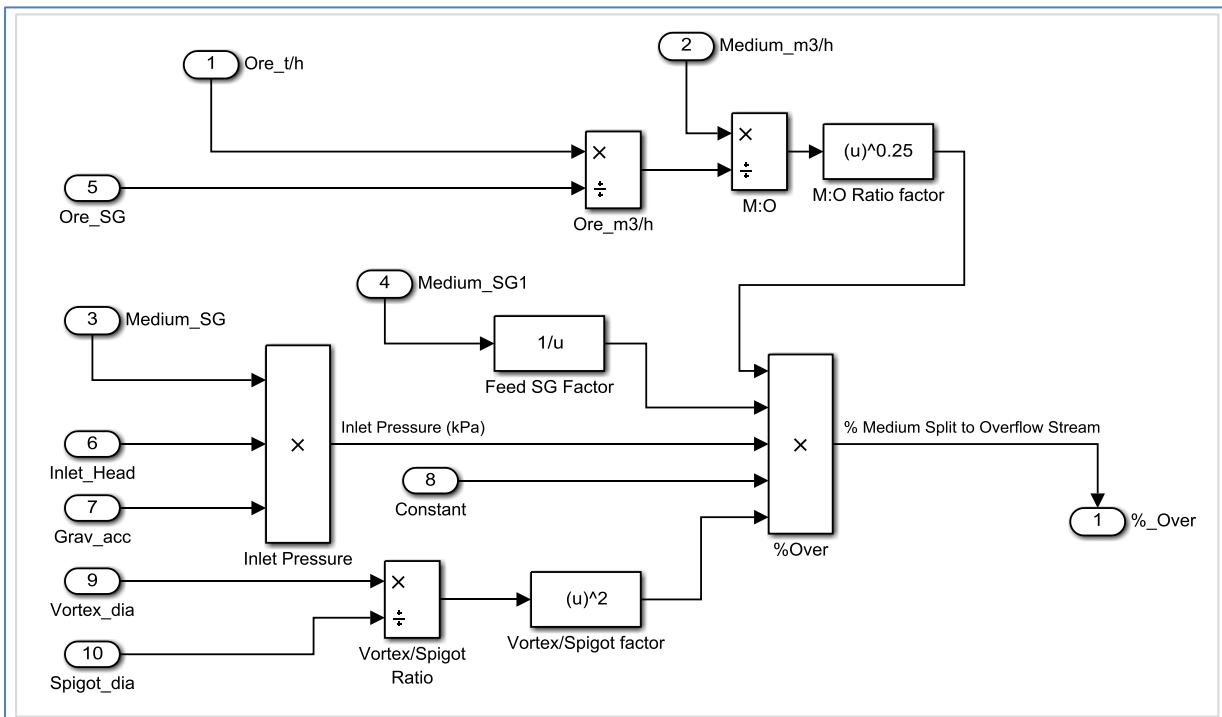


Figure 6.8: Subsystem of the internal structure of modelling of the medium split within the dense medium cyclone

Figure 6.9 illustrates the simulation output for the overflow and underflow density of the dense medium cyclone system. The response gives a clear indication that the underflow density is higher than the overflow density. In addition the simulation show that as expected

the values of the underflow stream is higher than the feed density whilst the overflow stream being lower than feed density.

The model output is the medium density in the spigot, which is underflow density. This can be correlated to the cyclone cut-point density, however, has no explicit reference to sharpness of separation. The model structure has been tested for the sake of diagnosing if the model has all of the salient features that would be required to adequately mimic DMS cyclone operation and the separation of a range of particle densimetric profile. Results show that the model is highly educational, providing specific details as to the reason why separation dynamics would change for any change in operating parameters.

The model output correlate well with the plant measured data under stable condition as depicted in Point B of Figure 5.17, while the plant was operated at feed density of 3.40 SG. Thus this outcome indicates that the model predicts the cyclone underflow and overflow density accurately. The simulated output indicated a density differential of 0.304 SG whilst the plant real-time measurement showed density differential ranging between 0.484 and 1.476 SG (average ~ 0.801SG).

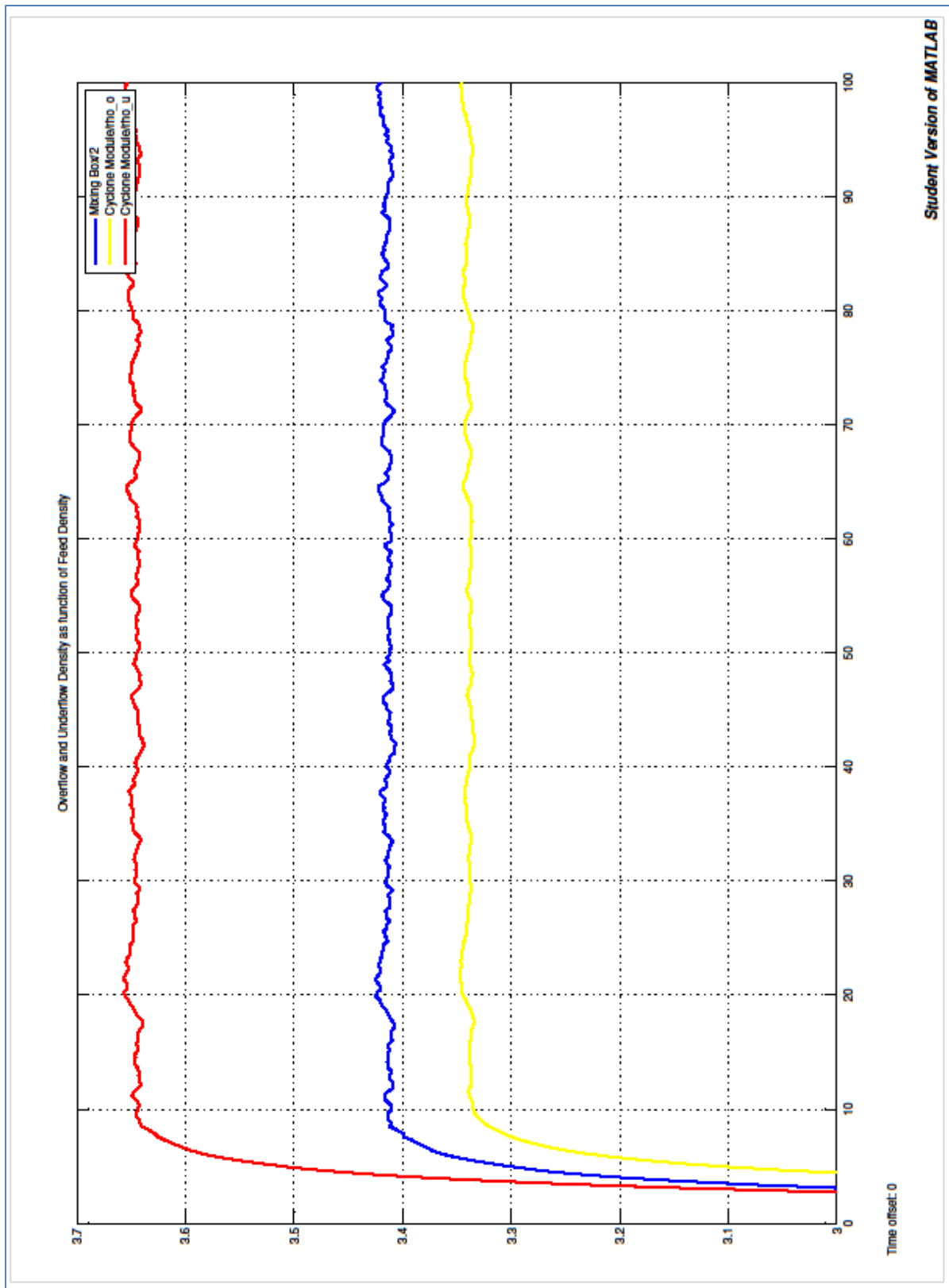


Figure 6.9: Simulated response indicating the result of cyclone underflow & overflow density

Evaluation of the model response when the medium flow rate to the beneficiation cyclone is increased was conducted while the operating density and ore feed rate is kept constant. In addition, the model response when the operating density was very low and very high, while the medium flow rate and ore feed rate were kept constant was evaluated. The model

responses when medium flow rate and operating density are increased are presented in Figure 6.10 and Figure 6.11 respectively.

The simulated response of the underflow and overflow density initially increased with an increase in the medium flow rate, but then declined at medium flow rates higher than 150 m³/h. This was apparently due to the effect of medium-to-ore ratio which has been incorporated in the Simulink model structure by the use of Equation 6.4. The underflow density showed a better correlation to increase in medium flow rate compared with the overflow density. This phenomenon is described by better polynomial fit of the simulated response of the underflow density with an increase in medium flow as shown in Figure 6.10.

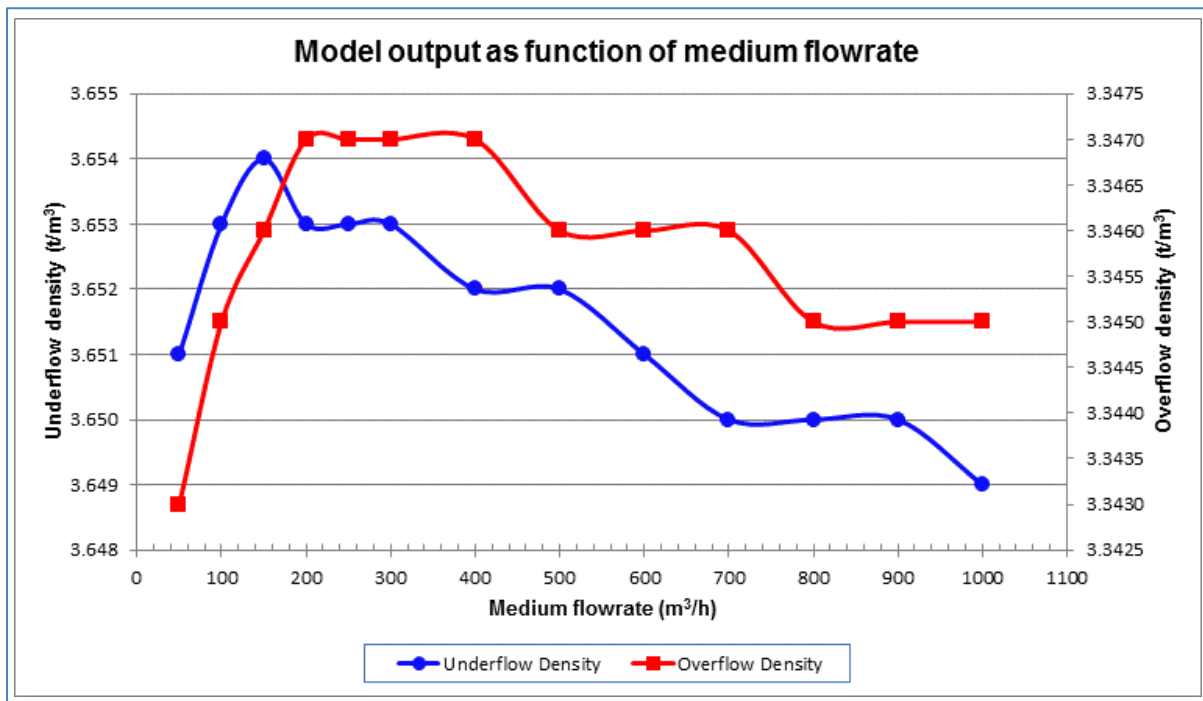
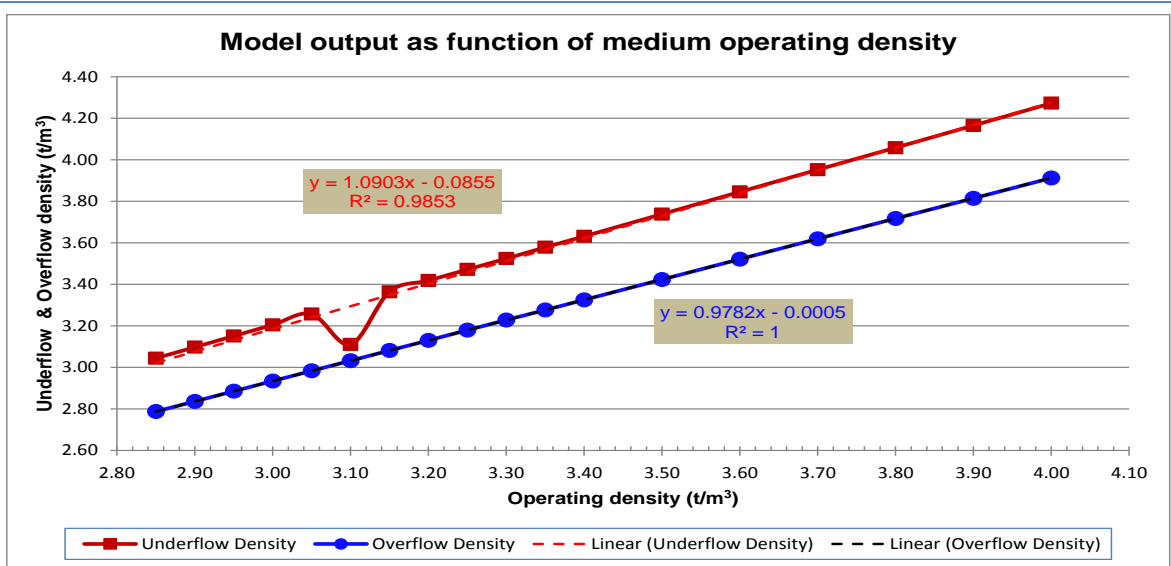


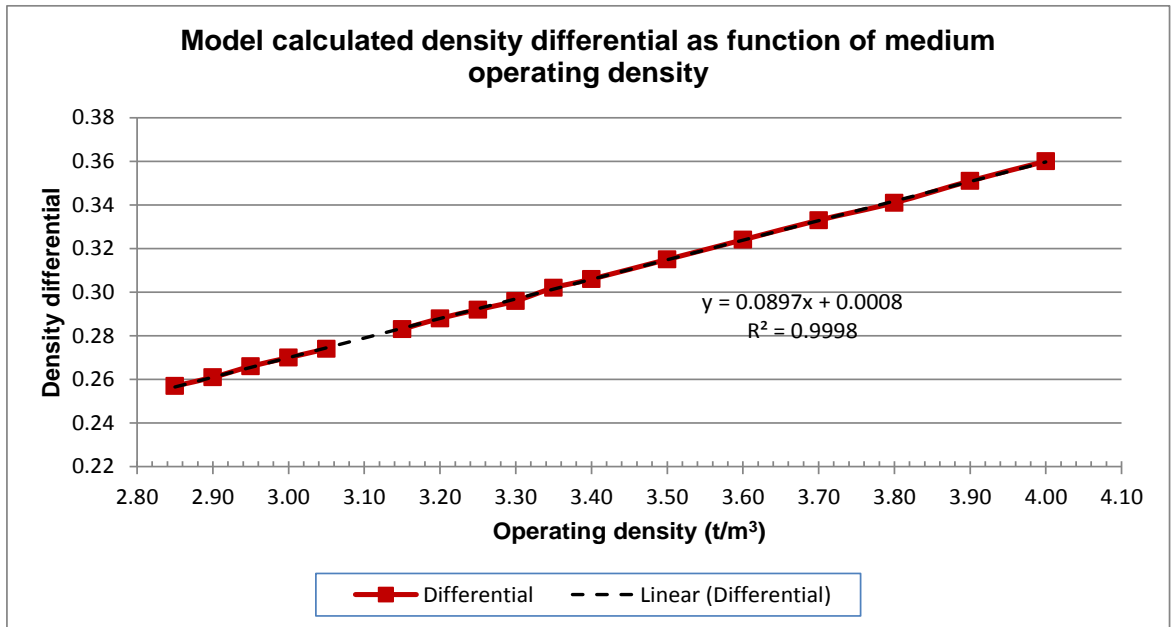
Figure 6.10: Model response for underflow and overflow density as function of medium flow rate

Increasing the operating density showed a steady increase in both the simulated response of the underflow and overflow densities as shown in Figure 6.11(a). This phenomenon is similar to the experimental findings of (He & Laskowski, 1994) for the magnetite heavy medium.

In addition, the calculated density differential showed a constant increase with increasing operating density as shown in Figure 6.11(b). This is in contrast to the findings of (He & Laskowski, 1994) and (Wang, et al., 2009) which indicated that the density differential increase to a maximum and then decreases as the operating density further increase. Thus the continuous increase in the density differential is indicative that the model structure does not take into account the effect of the medium rheology. In practice, it is expected that as the medium density increases, the medium viscosity also increases. Thus an increase in medium viscosity would result in a decrease in density differential.



(a)



(b)

Figure 6.11: Model response for underflow and overflow density as function of operating density

CHAPTER 7: CONCLUSIONS AND RECOMMENDATIONS

7 CONCLUSIONS AND RECOMMENDATIONS

7.1 CONCLUSIONS

7.1.1 Ore and FeSi Characterisation Conclusions

Ore characterisation is mainly focused on understanding the densimetric profile of the ore body, in order to determine the probability to produce a saleable product as well as predicting the expected yields and quality. This is done to utilise the endowment entrusted upon the operating entity by the government and shareholders to treat the mineral resource to its full potential. Understanding of the beneficiation potential of the ore body will assist the mine planning and processing plant to optimise the product tons and quality. This will ensure proper marketing plans that are synchronised to beneficiation plant due whose performance will depend on mining block reserves. Certain mining blocks have potential to produce varying product grades with different recoveries.

Ore characterisation was conducted on the GR80 mining block, low-grade stockpiles (i.e. C-grade ore reserves & Jig discard and dense medium separation (DMS) run-of-mine (ROM) material. The GR80 material was characterised as having low proportion of near-density material and will be easy to beneficiate as well as producing high volumes of high grade product. Furthermore, it was revealed that the 2014 DMS ROM had an increased proportion of low-density material; however this material was also had low proportion of near-density material.

The low-grade stockpiles was characterised by high proportion of near density material, which necessitate the beneficiation process to operate at high density in excess of 3.8 t/m³. Thus with higher operating density, the dense medium might lead to viscosity problems which have to be managed and controlled efficiently. Therefore, characterisation of the FeSi medium was imperative to understand its behaviour and potential influence to beneficiation of low-grade stockpiles and mining blocks with elevated proportion of near-density material. As the proportion of near-density waste material increases in the run-of-mine (ROM), it is necessary to beneficiate the material at elevated operating medium densities. However, when cyclones are operated at high densities, the negative influences of the medium viscosity become more apparent and thus influence the separation efficiency.

Heavy medium, ferrosilicon (FeSi) characterisation looked at identifying the effects of viscosity on the FeSi stability and whether there is a need for viscosity modifier should the need arise. Thus, the importance of controlling the stability, viscosity, and density of the medium must not be under-estimated and can very often override the improvements attainable through better designs of cyclones. Furthermore, the slurry mixture of the heavy medium utilised for the purpose of dense medium separation should be non-detrimental to

the effectiveness of separation in the DMS Fine cyclone plant. Medium characterisation showed that removal of ultra-fines leads to unstable media as indicated by faster settling rates. This would result in medium segregation in the beneficiation cyclone thereby leading to unacceptable high density differential which will negatively impact the cut-point shift and cause high yield losses to waste.

FeSi characterisation looked at various ways of reducing the viscosity of ferrosilicon (FeSi). Coarse and Process FeSi were tested with a portion of fines removed and a viscosity modifier was tested to see how this affects the FeSi flow behaviour. The viscosity modifier used for this test work was DP 725.

The heavy medium stability characteristics were determined through the static and vertical pipe settling tests. The bench top settling tests show that the coarse FeSi with viscosity modifier settles out the fastest whilst the coarse FeSi less fines settles faster than the coarse FeSi without fines removed. Thus, this proves that the content of ultra-fines proportion in the heavy medium improves the medium stability.

Contrary to the bench top settling test, the pipe loop settling tests showed that the coarse FeSi with viscosity modifier was significantly more stable compared to the other slurries tested. The vertical tube viscometer tests proved that removing the fines made no significant difference to the rheology of the coarse FeSi or the process FeSi. The viscosity modifier reduced the viscosity of the coarse FeSi and dispersed the particles in the slurry thus keeping them in suspension longer than otherwise possible.

7.1.2 Automation and Modelling Conclusions

The overall control of the metallurgical processes in Sishen's Cyclone Plant is still done on a manual basis and thus operation still varies from person-to-person and/or from shift-to-shift. This results in some of the process data and trends not being available online as well as being captured inaccurately. Furthermore, this negatively affects the traceability and reproducibility of the production metallurgical key performance indicators (KPI's) as well as process stability and efficiency. However, clear understanding of key operational parameters and being able to figure them out, allows process controllers and metallurgists to implement the control philosophy for the advanced process control.

It has been demonstrated that real-time online measurements are crucial to maintain processing plant stability and efficiency thereby ensuring that the final product grade and its value is not eroded. In addition, online measurement provides feedback to process operators and managers, to allow full control of the process as well as improving reaction time to changes such as variations in the quality of feed ore body. This, in turn, prevents and/or minimizes value losses and improves the economics of the process by controlling finished product specification and optimization of the operating cost.

Modelling and automated control is aimed at maintaining process stability, improving plant throughput as well as processing efficiency. The fundamental mathematical modelling technique is capable of providing detailed information about the dense medium dynamics within the cyclone. In addition, Simulink modelling by incorporating the popular industry Woods' empirical model allows for a better understanding of the performance of dense medium cyclone and can be utilised as a trouble-shooting tool.

Modelling and automation of the key metallurgical parameters for the cyclone plant circuit was achieved by installation of appropriate instrumentation and interlocking to the programmable logic control (PLC). This allowed for the control of the correct medium sump level, cyclone inlet pressure, medium-to-ore ratio as well as online monitoring of density differential as "proxy" for medium rheological characteristics.

The benefit of modelling and simulation allows the virtual investigation and optimisation of the processing plant behaviour as well as analysis of the impact of varying ore characteristics, throughput variations and changing operating parameters. Linking models to automated plant instrumentation would be able to warn abnormal process behaviour as well as identifying bottlenecks. In addition, Modelling and steady-state simulation can be utilised for the prediction of the metallurgical plant efficiency where automated and real-time online measurements cannot be obtained.

7.2 RECOMMENDATIONS FOR FUTURE WORK

Currently the system is only monitoring and trending data, thus activation of the control and interlocking described in this document should be been activated with the roll-out phase of the automation of the entire cyclone plant module.

Kumba Iron Ore is in the process of improving processing stability by the deployment of advanced process control at the DMS plant. Thus, the advanced process control systems can utilise MatLAB Simulink built-in mathematical models as central element in the controllers' calculations for "Model Predictive Control".

Construction of the operational performance monitoring reports will be valuable as these reports will focus on any constraints that can negatively influence process performance as well as highlighting processing opportunities. Furthermore, these reports will assist in keeping track of the processing plant state and also be usable for optimisation work.

REFERENCES AND APPENDICES

REFERENCES

Abu-Khalaf, M., Chen, R. & Turevskiy, A., 2010. *MathWorks*. [Online] Available at: <http://www.mathworks.com/company/newsletters/articles/pid-control-design-made-easy.html> Accessed 23 April 2014].

Anon., n.d. *Principles: Dense Medium Cyclones*. [Online] Available at: http://www.portaclone.co.za/pr_cyclo.htm Accessed 10 Jan 2014].

Aravind, P., Valluvan, M. & Saranya, M., 2013. Simulation based modeling and implementation of adaptive control technique for non linear process tank. *International Journal of Computer Applications*, Vol. 68(No. 16), pp. pp.1-5.

Aslam, F. & Haider, M. Z., 2011. An implementation and comparative analysis of PID controller and their auto tuning method for three tank liquid level control. *International Journal of Computer Applications*, Vol. 21(No. 8), pp. pp.42-45.

Atkinson, B. et al., 2012. *Dense Medium Cyclone Handbook*. s.l.:HMC Processing, ACARP.

Bekker, E., 2012. *Cyclone Design and Application*. Johannesburg: Multotec and Witwatersrand University.

Bekker, E., 2012. *Cyclone Design and Application*. Johannesburg: Multotec and Witwatersrand University.

Björn, A. et al., 2012. *Rheological Characterization*, Sweden: InTech.

Chu, K. W., Wang, B., Yu, A. B. & Vince, A., 2009. CFD-DEM modelling of multiphase flow in dense medium cyclone. *Powder Technology*, Volume 193, pp. 235-247.

de Villiers, R., Muller, D. & van Rooyen, J., 2014. *Presentation: Intergrated Control Strategy for Regulatory, Advanced and Optimisation Control for Mine, Plant and Logistics*. s.l.:Anglo American.

Doll, A., 2014. http://www.codecogs.com/d-ox/engineering/materials/rosin_rammer.php. [Online] Available at: <https://www.sagmilling.com/articles/2/view/?s=1> Accessed 20 September 2014].

Gochin, R. J. & Smith, M. R., 1983. Dense Medium Separation. Part 1: An introduction to the theory and practice. *Mining Magazine*, December, pp. pp. 453-460.

Gupta, A. & Yan, D. S., 2006. *Mineral Processing Design and Operations: An Introduction*. Oxford, UK: Elsevier.

He, Y. B. & Laskowski, J. S., 1994. Effect of dense medium properties on the separation performance of a dense medium cyclone. *Minerals Engineering*, Vol. 7(Nos 2/3), pp. pp. 209-221.

- King, R. P., 2001. *Modeling and Simulation of Mineral Processing Systems*. Linacre House, Jordan Hill, Oxford: Butterworth-Heinemann.
- Magwai, M. K. & Bosman, J., 2008. The effect of cyclone geometry and operating conditions on spigot capacity of dense medium cyclones. *International Journal of Mineral Processing*, Volume Vol. 86, pp. pp. 94-103.
- Meyer, E. J., 2010. *The development of dynamic models for a dense medium separation circuit in coal beneficiation*. Pretoria: Faculty of Engineering, the Built Environment and Information Technology. University of Pretoria.
- Mukherjee, A. K., Sripriya, R., Rao, P. V. & Das, P., 2003. Effect of increase in feed inlet pressure on feed rate of dense media cyclone. *International Journal of Mineral Processing*, Volume Vol. 69, pp. pp. 259-274.
- Myburgh, H. A., 2006. *The influence of the quality of ferrosilicon on the rheology of dense medium and the ability to reach higher densities*. s.l., The Journal of the Southern African Institute of Mining and Metallurgy.
- Nabbie, A., 2012. *Owner's manual for the Dense Medium Controller*. Rev: 1.4 ed. s.l.:De Beers Group Services.
- Napier-Munn, T. J., Dungalson, M. & Shi, F., 1994. *The rheological properties and selection of ferrosilicon dense media*. South Africa, Samancor.
- Narasimha, M., Brennan, M. S. & Holtham, P. N., 2006. Numerical simulation of magnetite segregation in a dense medium cyclone. *Minerals Engineering*, Volume 19, pp. 1034 - 1047.
- Petersen, K. R., 2010. *Understanding inlet pressure in cyclone operation and process design*. s.l., The Southern African Institute of Mining and Metallurgy, pp. pp. 233-240.
- Saad, M., Albagul, A. & Abueejela, Y., 2013. Performance comparison between PI and MRAC for coupled-tank system. *Journal of Automation and Control Engineering*, Vol. 2(No. 3), pp. pp 316-321.
- Shyan, C. W., Padmesh, T. V. N. & Suresh Manic, K., 2013. Controller tuning for a nonlinear liquid level system. *EURECA*, pp. pp 17 - 18.
- Sripriya, R. et al., 2001. Critical evaluation of factors affecting the operation of dense medium cyclones treating medium coking coals. *International Journal of Mineral Processing*, Volume Vol. 63, pp. pp. 191 - 206.
- SRK Consulting Engineers, 2006. *CPR on the material properties which will be incorporated into Exxaro and Kumba Iron Ore*, s.l.: Kumba Resources Limited.
- Stephanopoulos, G., 1984. *Chemical Process Control: An introduction to theory and practice*. Englewood Cliffs, New Jersey 07632: Prentice-Hall International, Inc.

Tom, P., 2014. *Control Philosophy for the automated control and monitoring of dense media circuit for cyclone plant*, s.l.: Anglo American Kumba Iron Ore.

van Sittert, F. & Malloch, R., n.d. *Proposal for FeSi rheology test for Kumba Iron Ore*. s.l.: Paterson and Cooke.

Wang, B., 2009. *PhD Thesis: Modelling the multiphase flow in cyclones*, s.l.: The University of New South Wales.

Wang, B., Chu, K. W., Yu, A. B. & Vince, A., 2009. Numerical studies of the effects of medium properties in dense medium cyclone operations. *Minerals Engineering*, Volume Vol. 22, pp. pp. 931-943.

Wills, B. A. & Napier-Munn, T. J., 2006. *Wills' Mineral Processing Technology: An Introduction to the Practical Aspects of Ore Treatment and Mineral*. 7th ed. s.l.: Elsevier Science & Technology Books.

APPENDICES

APPENDIX A: ORE CHARACTERISATION

7.2.1 Appendix A.1 – Material Type Classification

Material type classifications											
	1/2 bank	b-dms-fe = 61% b-dms-opb = 60%	b-dms-fe = 64.5%	b-dms-fe = 61%	b-jig-fe = 58.5%	b-ins-fe = 40%					
12.5m bench	KL	Light waste	Ert & Ekg	Ert & Ekg	Bif or Heavy waste	Bif or Heavy waste	Bif or Heavy waste	Bif or Heavy waste	Bif or Heavy waste	Bif or Heavy waste	
	801	701	402	401	101	102	201 301	202 302	203 303	501 601	602
First condition in this order	Second condition in this order	Fe Grade or Yield Cut-off	CLAS S	Production Geology & Grade Control description	stock pile	Mining					
Full bench Ore		b_dms_fe >= 64.5	101	Full bench high grade ore (DMS plant)	Bruce A	A					
			102	Full bench ore w ith intermediate w aste lenses (DMS plant)	Bruce A						
Less than full bench ore	High density BIF exclusively (RD >= 3.6)	b_dms_fe >= 61	201	Ore w ith high density Bif (DMS or JIG plant)	BIF	L					
		b_jig_fe >= 58.5	202	Ore w ith high density Bif (JIG plant)	BIF						
		b_ins_fe >= 40	203	Ore w ith high density Bif (JIG plant)	c		C				
	Low density waste including Clay (RD < 3.6)	b_dms_fe >= 61 & b_dms_opb >= 60	401	Ore w ith low density w aste (JIG plant or selectif mining)	SP H4	A					
			402	Ore w ith low density w aste (selective mining)	SP EKG						
	High density waste (RD >= 3.6)	b_dms_fe >= 61	301	Ore w ith high density w aste (JIG or DMS plant)	SP EKG	B					
b_jig_fe >= 58.5		302	Ore w ith high density w aste (JIG plant)	B	B						
b_ins_fe >= 40		303	Ore w ith high density w aste (JIG plant)	c	C						
No ore	More than half bench Clay		801	Half bench or more of clay w ith or w ith out other w aste	E	E					
	BIF (No more than 10% other waste)	b_jig_fe >= 58.5	501	Full bench high density Bif (JIG plant exclusively)	BIF	L					
	Remaining waste (RD >= 3.6) Excluding any possible kk kl lav law kwt mm dol di	b_jig_fe >= 58.5	601	Full bench high density w aste (JIG plant exclusively)	B	B					
		b_ins_fe >= 40	602	Full bench high density w aste (w aste dump)	c	C					
All sterile wastes			701	All sterile w astes	D	D					

7.2.2 Appendix A.2 - Densimetric Analysis Results of DMS Head Grade ROM

Batch 1: 19th – 30th May 2014 Composite Sample

Size and Density Split	Mass (g)	Mass (%)	Fe (%)	SiO ₂ (%)	Al ₂ O ₃ (%)	K ₂ O (%)	P (%)
-90+25mm							
SR-01-ROM (-90+25MM) F3.2	1890.4	5.30	12.8	67.2	8.74	1.04	0.04
SR-01-ROM (-90+25MM) F3.4	1103.6	3.10	30.2	52.7	2.69	0.07	0.03
SR-01-ROM (-90+25MM) F3.6	1088.8	3.06	35.7	41.8	4.16	0.24	0.06
SR-01-ROM (-90+25MM) F3.8	701.3	1.97	41.8	37.4	2.16	0.49	0.04
SR-01-ROM (-90+25MM) F4.0	485.8	1.36	44.4	29.6	4.15	0.33	0.04
SR-01-ROM (-90+25MM) F4.2	272	0.76	55.4	15.5	3.40	0.58	0.02
SR-01-ROM (-90+25MM) F4.4	676.8	1.90	55.7	16.3	1.87	0.16	0.03
SR-01-ROM (-90+25MM) F4.6	2637.1	7.40	64.0	4.47	1.51	0.20	0.09
SR-01-ROM (-90+25MM) S4.6	26779.9	75.15	67.9	1.70	0.59	0.07	0.05
-25+8mm							
SR-02-ROM (-25+8MM) F3.2	1372.8	6.62	10.6	61.3	14.29	2.69	0.06
SR-02-ROM (-25+8MM) F3.4	351.8	1.70	29.7	50.8	4.08	0.79	0.06
SR-02-ROM (-25+8MM) F3.6	432.8	2.09	34.8	43.5	3.49	0.57	0.03
SR-02-ROM (-25+8MM) F3.8	290.3	1.40	40.8	37.9	2.22	0.50	0.03
SR-02-ROM (-25+8MM) F4.0	251.4	1.21	46.2	27.1	3.63	0.71	0.06
SR-02-ROM (-25+8MM) F4.2	454.9	2.19	53.4	20.0	1.88	0.27	0.04
SR-02-ROM (-25+8MM) F4.4	325	1.57	59.0	11.1	2.55	0.43	0.11
SR-02-ROM (-25+8MM) F4.6	1926.9	9.29	64.6	4.1	1.20	0.19	0.06
SR-02-ROM (-25+8MM) S4.6	15327.1	73.93	67.6	1.7	0.66	0.09	0.05
-8+5mm							
SR-03-ROM (-8+5MM) F3.2	832.6	9.11	11.0	60.5	14.12	2.63	0.07
SR-03-ROM (-8+5MM) F3.4	159.8	1.75	28.9	47.3	7.10	1.41	0.06
SR-03-ROM (-8+5MM) F3.6	103.1	1.13	34.7	41.0	5.32	1.07	0.07
SR-03-ROM (-8+5MM) F3.8	97.9	1.07	39.5	33.8	5.46	1.09	0.07
SR-03-ROM (-8+5MM) F4.0	142.3	1.56	45.2	28.2	3.96	0.74	0.06
SR-03-ROM (-8+5MM) F4.2	204.8	2.24	51.7	18.8	3.66	0.61	0.08
SR-03-ROM (-8+5MM) F4.4	314	3.44	60.8	9.6	2.51	0.46	0.10
SR-03-ROM (-8+5MM) F4.6	680.3	7.44	63.7	5.0	1.65	0.29	0.07
SR-03-ROM (-8+5MM) S4.6	6604.2	72.26	67.7	1.5	0.70	0.10	0.05
-5+2mm							
SR-04-ROM (-5+2MM) F3.2	543.7	9.78	10.6	56.6	16.71	3.32	0.09
SR-04-ROM (-5+2MM) F3.4	75.2	1.35	29.8	41.6	9.28	1.92	0.14
SR-04-ROM (-5+2MM) F3.6	80.4	1.45	35.4	37.6	6.89	1.36	0.08
SR-04-ROM (-5+2MM) F3.8	58.1	1.05	40.9	29.3	6.92	1.36	0.12
SR-04-ROM (-5+2MM) F4.0	61.1	1.10	46.4	24.3	5.28	1.00	0.10
SR-04-ROM (-5+2MM) F4.2	166.4	2.99	53.8	14.6	4.37	0.87	0.11
SR-04-ROM (-5+2MM) F4.4	109.8	1.97	57.3	11.6	3.42	0.65	0.09
SR-04-ROM (-5+2MM) F4.6	698.2	12.56	64.8	3.95	1.73	0.31	0.08
SR-04-ROM (-5+2MM) S4.6	3766.7	67.75	68.2	1.31	0.65	0.09	0.04

Batch 2: 31st May – 13th June 2014 Composite Sample

Size and Density Split	Mass (g)	Mass (%)	Fe (%)	SiO2 (%)	Al2O3 (%)	K2O (%)	P (%)
-90 + 25mm							
DMS-ROM -01(-90+25mm)F3.2	1759.5	5.24	10.4	63.8	13.87	2.15	0.04
DMS-ROM -01(-90+25mm)F3.4	336.2	1.00	30.0	56.3	0.45	0.08	0.02
DMS-ROM -01(-90+25mm)F3.6	628.9	1.87	35.5	44.0	3.56	0.95	0.04
DMS-ROM -01(-90+25mm)F3.8	296.1	0.88	40.9	33.7	3.90	0.51	0.18
DMS-ROM -01(-90+25mm)F4.0	274.3	0.82	42.1	31.9	5.32	0.64	0.07
DMS-ROM -01(-90+25mm)F4.2	288.8	0.86	52.7	20.4	1.89	0.48	0.05
DMS-ROM -01(-90+25mm)F4.4	795.2	2.37	57.8	9.5	4.97	0.44	0.04
DMS-ROM -01(-90+25mm)F4.6	1849.5	5.51	65.1	4.61	1.47	0.18	0.08
DMS-ROM -01(-90+25mm)S4.6	27365.1	81.46	68.1	1.63	0.64	0.08	0.05
-25+8mm							
DMS-ROM -02(25+8mm)F3.2	1273.9	6.03	13.1	64.0	10.98	1.65	0.04
DMS-ROM -02(25+8mm) F3.4	432.5	2.05	30.2	50.1	4.00	0.86	0.07
DMS-ROM -02(25+8mm) F3.6	288.2	1.36	35.4	44.9	2.33	0.31	0.03
DMS-ROM -02 (25+8mm) F3.8	400.6	1.90	40.9	33.7	3.90	0.51	0.18
DMS-ROM -02 (25+8mm) F4.0	388	1.84	47.2	29.1	1.96	0.29	0.03
DMS-ROM -02 (25+8mm) F4.2	474.6	2.25	53.9	19.3	2.34	0.42	0.07
DMS-ROM -02 (25+8mm) F4.4	342.3	1.62	58.3	13.6	2.73	0.47	0.05
DMS-ROM -02 (25+8mm) F4.6	1437.7	6.81	64.0	4.7	1.48	0.25	0.08
DMS-ROM -02 (25+8mm) S4.6	16080.4	76.14	67.8	1.5	0.64	0.08	0.06
-8+5mm							
DMS-ROM -03(-8+5mm) F3.2	655.3	7.90	10.7	63.3	13.92	2.29	0.07
DMS-ROM -03(-8+5mm) F3.4	84	1.01	29.9	48.7	5.27	1.10	0.05
DMS-ROM -03(-8+5mm) F3.6	89	1.07	34.7	38.5	6.90	1.02	0.09
DMS-ROM -03(-8+5mm) F3.8	98.3	1.19	41.0	32.3	4.93	0.73	0.09
DMS-ROM -03(-8+5mm) F4.0	91.8	1.11	45.4	24.2	5.92	1.03	0.09
DMS-ROM -03(-8+5mm) F4.2	152.1	1.83	52.5	16.6	4.71	0.79	0.10
DMS-ROM -03(-8+5mm) F4.4	244.1	2.94	60.1	9.0	2.82	0.49	0.12
DMS-ROM -03(-8+5mm) F4.6	425.2	5.13	63.6	4.7	2.01	0.36	0.11
DMS-ROM -03(-8+5mm) S4.6	6454.6	77.82	68.2	1.5	0.72	0.10	0.05
-5+2mm							
DMS-ROM -04(-5+2mm) F3.2	424.3	7.68	9.5	63.2	14.53	2.51	0.06
DMS-ROM -04(-5+2mm) F3.4	79.1	1.43	28.1	47.0	7.79	1.44	0.11
DMS-ROM -04(-5+2mm) F3.6	73.7	1.33	34.2	40.4	6.92	1.28	0.08
DMS-ROM -04(-5+2mm) F3.8	66.4	1.20	40.7	32.0	5.97	1.11	0.09
DMS-ROM -04(-5+2mm) F4.0	57.9	1.05	45.0	25.6	5.38	1.02	0.10
DMS-ROM -04(-5+2mm) F4.2	114.3	2.07	51.4	17.5	4.81	0.92	0.14
DMS-ROM -04(-5+2mm) F4.4	180.4	3.27	57.3	10.5	3.55	0.66	0.13
DMS-ROM -04(-5+2mm) F4.6	494.9	8.96	64.1	4.14	1.84	0.33	0.10
DMS-ROM -04(-5+2mm) S4.6	4030.9	73.00	68.2	1.26	0.69	0.09	0.06

Batch 3: 14th June – 04th July 2014 Composite Sample

Size and Density Split	Mass (g)	Mass (%)	Fe (%)	SiO ₂ (%)	Al ₂ O ₃ (%)	K ₂ O (%)	P (%)
-90+25mm							
DMS-ROM-01(-90+25mm) F3.2	1311.5	4.36	11.3	55.3	16.74	1.67	0.05
DMS-ROM-01(-90+25mm) F3.4	756	2.51	31.5	42.0	7.96	0.82	0.05
DMS-ROM-01(-90+25mm) F3.6	375.6	1.25	37.9	41.1	2.49	0.24	0.05
DMS-ROM-01(-90+25mm) F3.8	210.3	0.70	43.7	35.6	0.50	0.06	0.03
DMS-ROM-01(-90+25mm) F4.0	295.6	0.98	47.0	22.3	6.48	0.67	0.05
DMS-ROM-01(-90+25mm) F4.2	263.7	0.88	51.7	16.4	5.53	1.10	0.07
DMS-ROM-01(-90+25mm) F4.4	296.7	0.99	57.3	11.3	3.92	0.39	0.06
DMS-ROM-01(-90+25mm) F4.6	1936.9	6.44	64.2	4.35	1.35	0.06	0.10
DMS-ROM-01(-90+25mm) S4.6	24632.5	81.89	67.9	1.50	0.62	0.08	0.05
-25+8mm							
DMS-ROM -02 (25+8mm) F3.2	1767.2	5.99	10.0	60.6	16.29	2.26	0.06
DMS-ROM -02 (25+8mm) F3.4	265.3	0.90	29.7	44.1	8.32	1.28	0.06
DMS-ROM -02 (25+8mm) F3.6	415.4	1.41	36.3	36.7	5.59	1.04	0.05
DMS-ROM -02 (25+8mm) F3.8	348	1.18	41.2	31.8	5.83	0.83	0.06
DMS-ROM -02 (25+8mm) F4.0	461.5	1.56	46.7	25.6	4.06	0.65	0.05
DMS-ROM -02 (25+8mm) F4.2	513.5	1.74	52.8	17.4	3.90	0.62	0.10
DMS-ROM -02 (25+8mm) F4.4	746	2.53	57.1	12.2	3.37	0.42	0.13
DMS-ROM -02 (25+8mm) F4.6	2893.6	9.81	64.2	4.44	1.71	0.22	0.11
DMS-ROM -02 (25+8mm) S4.6	22079.7	74.87	67.5	1.58	0.71	0.09	0.06
-8+5mm							
DMS-ROM -03 (-8+5mm) F3.2	599.5	7.07	8.8	61.1	15.95	2.44	0.07
DMS-ROM -03 (-8+5mm) F3.4	141	1.66	28.5	42.6	9.60	1.67	0.10
DMS-ROM -03 (-8+5mm) F3.6	114.4	1.35	36.1	34.8	7.31	1.22	0.09
DMS-ROM -03 (-8+5mm) F3.8	107.1	1.26	41.8	29.1	5.79	0.76	0.08
DMS-ROM -03 (-8+5mm) F4.0	91.3	1.08	46.6	23.2	5.50	1.08	0.11
DMS-ROM -03 (-8+5mm) F4.2	121.2	1.43	51.8	16.5	4.62	0.86	0.18
DMS-ROM -03 (-8+5mm) F4.4	201	2.37	58.0	10.9	3.43	0.63	0.13
DMS-ROM -03 (-8+5mm) F4.6	514.5	6.07	62.7	5.41	2.10	0.35	0.13
DMS-ROM -03 (-8+5mm) S4.6	6590.4	77.71	67.6	1.49	0.80	0.10	0.07
-5+2mm							
DMS-ROM -04 (-5+2mm) F3.2	675.5	7.73	8.9	61.1	16.16	2.52	0.07
DMS-ROM -04 (-5+2mm) F3.4	124.4	1.42	27.6	41.5	11.34	2.01	0.14
DMS-ROM -04 (-5+2mm) F3.6	114.4	1.31	34.4	35.4	9.16	1.57	0.11
DMS-ROM -04 (-5+2mm) F3.8	101.8	1.16	40.3	29.3	7.22	1.16	0.10
DMS-ROM -04 (-5+2mm) F4.0	122.4	1.40	45.8	23.4	6.55	1.14	0.14
DMS-ROM -04 (-5+2mm) F4.2	190.2	2.18	53.5	14.9	4.73	0.86	0.15
DMS-ROM -04 (-5+2mm) F4.4	111.9	1.28	55.0	13.2	4.48	0.83	0.16
DMS-ROM -04 (-5+2mm) F4.6	924.4	10.58	64.0	4.80	2.22	0.40	0.14
DMS-ROM -04 (-5+2mm) S4.6	6375.6	72.94	68.4	1.47	0.79	0.11	0.06

7.2.3 Appendix A.3 - Densimetric Analysis Results of GR80 Mining Block

Sample	Density	RD to Sinks	Mass (g)	Mass (%)	Grade			
					% Fe	% SiO ₂	% P ₂ O ₅	% Al ₂ O ₃
Plant 5: EL+LY	+ 4.0	4.0	250000	99.03	68.00	1.81	0.11	0.64
	- 4.0 + 3.8	3.8	1546.5	0.61	66.00	2.77	0.14	1.44
	- 3.8 + 3.6	3.6	695.1	0.28	52.40	9.46	0.18	4.83
	- 3.6 + 3.4	3.4	54.3	0.02	48.40	11.80	0.25	5.31
	- 3.4 + 3.2	3.2	37.1	0.01	16.50	34.80	0.25	22.70
	- 3.2 + 3.0	3.0	17.2	0.01	25.50	29.90	0.18	15.20
	- 3.0	2.8	86.3	0.03	7.20	50.20	0.09	19.50
Plant 3: Conglomeratic	+ 4.0	4.0	208000	95.60	65.00	3.52	0.16	2.01
	- 4.0 + 3.8	3.8	5134.9	2.36	61.10	7.82	0.32	2.90
	- 3.8 + 3.6	3.6	1460.3	0.67	44.60	28.80	0.11	4.31
	- 3.6 + 3.4	3.4	1917.7	0.88	35.20	46.10	0.02	1.33
	- 3.4 + 3.2	3.2	106.9	0.05	22.20	36.20	0.14	21.00
	- 3.2 + 3.0	3.0	433.4	0.20	30.90	49.20	0.07	4.19
	- 3.0	2.8	530.3	0.24	7.56	50.98	0.09	19.63
Plant 11: EL Laminated Ore	+ 4.0	4.0	209000	94.11	66.50	2.73	0.09	1.84
	- 4.0 + 3.8	3.8	3571	1.61	54.80	10.10	0.02	7.28
	- 3.8 + 3.6	3.6	1189.9	0.54	39.80	20.20	0.09	14.90
	- 3.6 + 3.4	3.4	2025.8	0.91	36.10	22.60	0.09	16.50
	- 3.4 + 3.2	3.2	1560.1	0.70	27.30	27.80	0.09	21.30
	- 3.2 + 3.0	3.0	3445.9	1.55	16.50	34.80	0.07	27.10
	- 3.0	2.8	1278.7	0.58	8.79	41.60	0.09	31.70
Plant 2: EL Laminated Ore	+ 4.0	4.0	239000	95.27	66.60	2.71	0.16	1.63
	- 4.0 + 3.8	3.8	2023	0.81	47.10	15.40	0.05	11.20
	- 3.8 + 3.6	3.6	1215.9	0.48	39.90	20.00	0.09	14.40
	- 3.6 + 3.4	3.4	856.1	0.34	35.80	22.10	0.07	16.50
	- 3.4 + 3.2	3.2	1271.9	0.51	23.30	30.60	0.04	24.40
	- 3.2 + 3.0	3.0	4628	1.84	16.50	34.50	0.07	27.50
	- 3.0	2.8	1863.3	0.74	10.50	40.70	0.09	31.10
Plant 10: EL Laminated Ore	+ 4.0	4.0	211000	98.95	66.00	3.03	0.09	1.47
	- 4.0 + 3.8	3.8	708.8	0.33	56.70	8.84	0.32	5.62
	- 3.8 + 3.6	3.6	234.1	0.11	48.70	14.80	0.32	9.43
	- 3.6 + 3.4	3.4	168.5	0.08	38.80	24.00	0.16	13.00
	- 3.4 + 3.2	3.2	134.3	0.06	26.00	29.00	0.16	22.10
	- 3.2 + 3.0	3.0	395.8	0.19	24.40	30.60	0.09	24.20
	- 3.0	2.8	599.7	0.28	22.40	33.00	0.09	25.00
Plant 6: HL+SH	+ 4.0	4.0	188000	93.97	67.10	2.56	0.14	1.30
	- 4.0 + 3.8	3.8	3863.3	1.93	49.40	13.80	0.14	9.41
	- 3.8 + 3.6	3.6	2904	1.45	39.90	20.00	0.09	14.40
	- 3.6 + 3.4	3.4	678	0.34	35.70	23.90	0.11	15.40
	- 3.4 + 3.2	3.2	624.5	0.31	27.90	29.80	0.06	20.30
	- 3.2 + 3.0	3.0	1154.3	0.58	23.30	32.40	0.09	21.00
	- 3.0	2.8	2850.3	1.42	14.80	39.00	0.06	25.80
Plant 9: HL+BIF	+ 4.0	4.0	131000	72.62	66.40	3.27	0.16	0.78
	- 4.0 + 3.8	3.8	7121.3	3.95	59.30	11.90	0.16	1.22
	- 3.8 + 3.6	3.6	5639.1	3.13	45.30	33.80	0.14	0.84
	- 3.6 + 3.4	3.4	5981.7	3.32	34.70	47.20	0.14	0.54
	- 3.4 + 3.2	3.2	5026.4	2.79	28.90	55.30	0.11	0.88
	- 3.2 + 3.0	3.0	7490.4	4.15	20.60	68.60	0.09	0.90
	- 3.0	2.8	18136.6	10.05	9.56	85.60	0.07	0.72
Plant 8: Laminated ore	+ 4.0	4.0	210000	96.71	67.80	1.91	0.07	0.93
	- 4.0 + 3.8	3.8	837.9	0.39	60.00	6.68	0.14	4.55
	- 3.8 + 3.6	3.6	161.8	0.07	59.10	7.31	0.16	4.83
	- 3.6 + 3.4	3.4	49.2	0.02	46.00	20.30	0.27	9.09
	- 3.4 + 3.2	3.2	1840.4	0.85	36.30	24.90	0.16	15.80
	- 3.2 + 3.0	3.0	4140.4	1.91	32.80	50.80	0.02	0.82
	- 3.0	2.8	109	0.05	1.34	40.60	0.05	40.60

Sample	Density	RD to Sinks	Mass (g)	Mass (%)	Grade			
					% Fe	% SiO ₂	% P ₂ O ₅	% Al ₂ O ₃
Plant 1: HL+BIF	+ 4.0	4.0	182000	82.65	66.40	3.65	0.18	0.46
	- 4.0 + 3.8	3.8	7206.9	3.27	49.70	28.30	0.11	0.27
	- 3.8 + 3.6	3.6	5943.3	2.70	40.40	40.80	0.07	0.19
	- 3.6 + 3.4	3.4	8758.2	3.98	36.30	45.80	0.11	0.16
	- 3.4 + 3.2	3.2	8510	3.86	29.20	57.80	0.07	0.11
	- 3.2 + 3.0	3.0	5677.3	2.58	23.40	65.90	0.09	0.15
	- 3.0	2.8	2100.7	0.95	11.90	82.90	0.07	0.37
Plant 7: Laminated ore + Banded ironstone	+ 4.0	4.0	121000	54.83	64.30	6.35	0.09	0.70
	- 4.0 + 3.8	3.8	14906.8	6.75	52.70	23.60	0.07	0.67
	- 3.8 + 3.6	3.6	20527.4	9.30	50.20	47.50	0.05	0.64
	- 3.6 + 3.4	3.4	28111.4	12.74	45.20	32.60	0.05	0.45
	- 3.4 + 3.2	3.2	11471.8	5.20	39.00	42.80	0.05	0.63
	- 3.2 + 3.0	3.0	13174.9	5.97	22.80	65.40	0.05	0.58
	- 3.0	2.8	11495.6	5.21	11.20	82.00	0.09	1.37

7.2.4 Appendix A.4 - Densimetric Analysis Results of ROM from the Low Grade Stockpiles

-25+6mm material

SG ¹	Mass	Mass %	Fe	Cum Fe	SiO2	Al2O3	K2O
BIF G39 (-25+6mm)							
F3.000	483.1	1.54	11.0102	55.05	80.11	2.48	0.26
F3.200	737.1	2.35	20.3939	55.74	69.31	0.69	0.08
F3.400	1151.5	3.68	29.3525	56.60	57.12	0.29	0.02
F3.600	2140.2	6.83	37.0383	57.69	45.84	0.48	0.03
F3.800	2917.7	9.31	43.4833	59.33	36.52	0.45	0.02
F4.000	2295	7.32	47.23	61.27	30.48	0.62	0.07
F4.200	3615.50	11.54	52.31	62.76	22.73	0.88	0.11
F4.400	2331.7	7.44	56.86	64.86	16.42	1.07	0.14
F4.600	2313.90	7.39	60.92	66.05	10.20	1.41	0.20
F4.800	12321.9	39.33	66.85	66.94	2.33	0.84	0.09
S4.800	1024.8	3.27	68.02	68.02	1.26	0.67	0.07
BIF 16(-25+6mm)							
F3.000	2365.2	9.74	12.58	53.11	76.02	2.93	0.47
F3.200	1041.8	4.29	25.38	57.48	61.44	2.08	0.32
F3.400	1330.2	5.48	30.8	59.08	53.19	1.62	0.24
F3.600	1979.5	8.15	36.4	61.01	43.97	2.00	0.31
F3.800	1157	4.76	44.6	63.78	35.05	0.87	0.13
F4.000	1510.8	6.22	50.44	65.13	26.56	0.82	0.08
F4.200	1075.20	4.43	58.43	66.62	15.59	0.84	0.10
F4.400	2080.8	8.57	63.28	67.26	8.18	0.62	0.07
F4.600	8337.80	34.33	67.6	67.96	2.29	0.40	0.03
F4.800	3346	13.78	68.85	68.85	1.21	0.31	0.02
S4.800	61.20	0.25	68.651	68.65	1.26	0.27	0.01
BIF22 (-25+6mm)							
F3.000	2776.3	9.08	8.5	35.93	86.51	0.69	0.04
F3.200	3718.8	12.16	20.32	38.67	69.07	0.68	0.04
F3.400	4149.7	13.57	29.05	41.51	57.46	0.32	0.01
F3.600	4011.6	13.12	36.07	44.10	47.22	0.27	0.00
F3.800	10772.7	35.23	42.18	46.12	38.21	0.44	0.04
F4.000	964.3	3.15	46.57	54.38	32.83	0.31	0.02
F4.200	1812.70	5.93	50.9583	56.18	26.56	0.27	0.01
F4.400	1284.8	4.20	57.27	60.17	17.61	0.24	0.01
F4.600	980.70	3.21	63.25	63.60	9.07	0.29	0.01
F4.800	104.30	0.34	66.89	66.89	3.30	0.34	0.03
S4.800	0	0.00	0	66.89			
BIF 24 (-25+6mm)							
F3.000	9160.4	34.89	9.086	31.59	85.67	0.40	0.08
F3.200	2407.3	9.17	22.56	43.65	66.53	0.71	0.08
F3.400	3205.3	12.21	31.58	47.11	54.26	0.36	0.07
F3.600	1690.4	6.44	36.87	51.44	47.24	0.20	0.02
F3.800	2290.6	8.73	43.99	53.96	35.99	0.80	0.17
F4.000	1724.7	6.57	48.7	57.01	29.81	0.28	0.04
F4.200	1682.30	6.41	52.85	59.49	24.18	0.27	0.03
F4.400	1858	7.08	58.33	62.22	16.07	0.33	0.04
F4.600	2091.80	7.97	65.28	65.46	5.97	0.50	0.06
F4.800	140.6	0.54	68.09	68.09	2.28	0.37	0.04
S4.800	0.00	0.00	0	68.09			
KGT12 (-25+6mm)							
F3.000	4637.9	19.25	15.0042	46.64	35.99	27.08	0.34
F3.200	1278.5	5.31	27.2431	54.18	26.79	22.37	0.25
F3.400	1533.5	6.37	33.0969	56.08	25.42	17.17	0.35
F3.600	2154.6	8.94	38.9943	58.19	28.21	10.17	0.59
F3.800	2064.1	8.57	44.4174	61.05	25.71	6.98	0.62
F4.000	641.4	2.66	47.07	63.81	19.89	8.60	0.60
F4.200	829.50	3.44	53.9	64.72	12.34	6.80	0.39
F4.400	1146.5	4.76	60.5	65.54	6.18	4.40	0.25
F4.600	1292.00	5.36	63.77	66.13	3.98	2.81	0.18
F4.800	8180.8	33.96	66.44	66.49	1.94	1.35	0.18
S4.800	332.50	1.38	67.81	67.81	1.40	0.93	0.13
SK7 (-25+6mm)							
F3.000	2353.3	9.36	8.82917	52.43	66.20	13.03	1.42
F3.200	885.9	3.52	22.0774	56.93	50.73	10.85	1.75
F3.400	702	2.79	30.9705	58.34	44.32	7.02	1.11
F3.600	1857.7	7.39	38.5927	59.25	37.39	4.52	0.84

¹ F prefix denotes floats whereas the S denotes sinks.

SG ¹	Mass	Mass %	Fe	Cum Fe	SiO2	Al2O3	K2O
F3.800	2035	8.09	43.4046	61.23	31.36	4.07	0.77
F4.000	1457.8	5.80	46.48	63.33	26.69	4.19	0.85
F4.200	1307.50	5.20	54.24	64.88	17.62	2.77	0.49
F4.400	1535.1	6.11	59.0191	65.83	8.54	2.32	0.38
F4.600	2057.80	8.19	64.66	66.64	4.85	1.59	0.24
F4.800	10235.8	40.71	66.93	67.01	1.97	0.84	0.11
S4.800	712.3	2.83	68.11	68.11	1.09	0.51	0.06
SK27 (-25+6mm)							
F3.000	2830.5	14.21	9.40674	52.44	44.84	29.16	0.99
F3.200	525	2.63	22.8105	59.57	36.01	21.84	0.52
F3.400	526.4	2.64	29.716	60.73	28.69	20.06	0.48
F3.600	816.1	4.10	37.0817	61.75	23.26	16.49	0.26
F3.800	795.9	3.99	42.9983	63.07	17.96	13.56	0.20
F4.000	793.5	3.98	49.0555	64.18	14.46	10.49	0.17
F4.200	719.00	3.61	54.23	65.06	11.02	7.79	0.13
F4.400	1385	6.95	59.52	65.66	7.40	5.06	0.13
F4.600	2303.30	11.56	64.18	66.40	4.51	2.49	0.08
F4.800	7691.4	38.60	66.71	66.95	2.37	1.08	0.02
S4.800	1538.90	7.72	68.15	68.15	1.48	0.67	0.01
SK30 (-25+6mm)							
F3.000	158	1.19	16.0913	53.32	37.57	26.54	0.80
F3.200	218	1.65	26.25	53.77	28.66	22.99	0.74
F3.400	402.5	3.04	31.59	54.23	24.43	20.67	0.57
F3.600	629	4.75	38.24	54.96	20.53	17.17	0.43
F3.800	1446.6	10.93	44.23	55.85	16.29	14.26	0.31
F4.000	1731.2	13.09	48.929	57.47	12.80	12.05	0.28
F4.200	2235.00	16.89	55.1662	59.19	9.48	7.69	0.13
F4.400	3790.8	28.66	58.66	60.59	6.82	5.84	0.08
F4.600	2475.50	18.71	63.24	63.38	4.98	3.27	0.03
F4.800	142.5	1.08	65.8	65.80	3.64	1.99	0.02
S4.800	0	0.00	0	65.80			

-6+2mm material

SG	Mass	Mass %	Fe	Cum Fe	SiO2	Al2O3	K2O
BIF G39 (-6+2mm)							
F3.000	768.9	3.79	9.507	53.90	77.22	5.59	0.46
F3.200	921	4.54	19.88	55.65	66.91	2.47	0.28
F3.400	858.4	4.23	30.858	57.42	53.81	0.99	0.11
F3.600	1187.9	5.85	38.920	58.70	42.81	0.66	0.06
F3.800	2502.4	12.33	48.968	60.12	28.21	0.79	0.08
F4.000	1054.4	5.20	44.21	62.11	34.08	0.86	0.10
F4.200	1887	9.30	56.12	63.56	17.05	0.93	0.12
F4.400	2461.6	12.13	60.54	64.83	11.08	0.97	0.12
F4.600	2828.2	13.94	64.71	66.05	4.93	0.91	0.09
F4.800	5116.2	25.22	66.59	66.69	2.69	0.83	0.07
S4.800	703.5	3.47	67.45	67.45	1.90	0.72	0.05
BIF 16 (-6+2mm)							
F3.000	2879.4	13.24	11.2663	51.42	77.07	3.80	0.58
F3.200	1529.3	7.03	25.9033	57.55	57.95	2.66	0.56
F3.400	964.9	4.44	31.6846	60.35	50.11	2.50	0.46
F3.600	977.9	4.50	37.9269	62.04	40.04	3.17	0.38
F3.800	2610.1	12.00	57.0173	63.57	15.13	0.99	0.14
F4.000	883.1	4.06	45.59	64.90	32.50	1.82	0.25
F4.200	1490.7	6.86	60.26	66.34	12.34	0.86	0.11
F4.400	2797.6	12.87	65.5	67.21	4.90	0.58	0.06
F4.600	4831.4	22.22	67.69	67.84	2.27	0.51	0.04
F4.800	2729.8	12.55	68.09	68.09	1.71	0.47	0.04
S4.800	50	0.23	68.08	68.08	1.51	0.57	0.03
BIF22 (-6+2mm)							
F3.000	8346.1	41.68	8.275	27.38	86.78	0.76	0.04
F3.200	2051.2	10.24	20.91	41.03	69.10	0.44	0.02
F3.400	2258.9	11.28	30.58	45.32	56.04	0.38	0.02
F3.600	1856.7	9.27	38.6	49.83	44.47	0.61	0.06
F3.800	1945.2	9.71	44.9	53.62	35.02	0.54	0.02
F4.000	634.6	3.17	51.046	58.37	26.52	0.33	0.01
F4.200	1151.5	5.75	55.33	59.96	19.39	0.41	0.01
F4.400	1199.1	5.99	61.78	62.95	10.83	0.38	0.01
F4.600	571.8	2.86	65.34	65.35	5.51	0.32	0.01
F4.800	10.6	0.05	65.63	65.63	5.57	0.32	0.00
S4.800	0	0.00	0	65.63			
BIF 24 (-6+2mm)							
F3.000	7374.7	35.56	7.79013	33.51	87.42	0.81	0.13
F3.200	1608.5	7.76	21.85	47.70	66.11	0.96	0.16
F3.400	1796.2	8.66	31.21	51.24	53.99	0.83	0.13

SG	Mass	Mass %	Fe	Cum Fe	SiO2	Al2O3	K2O
F3.600	1403.3	6.77	40.05	54.85	40.46	0.72	0.10
F3.800	2265.4	10.92	50.03	57.28	26.38	0.59	0.08
F4.000	838.2	4.04	42.59	59.89	38.17	0.50	0.07
F4.200	1286.9	6.21	55.51	62.55	19.46	0.47	0.07
F4.400	1300.6	6.27	61.34	64.72	11.14	0.60	0.09
F4.600	2803.4	13.52	66.26	66.26	3.95	0.60	0.08
F4.800	59.7	0.29	66.38	66.38	3.19	0.69	0.09
S4.800	0	0.00	0	66.38			
KGT12 (-6+2mm)							
F3.000	3960.6	18.94	13.0709	45.29	36.98	27.31	0.37
F3.200	1367.8	6.54	24.4263	52.81	28.69	22.58	0.35
F3.400	1556.1	7.44	32.9424	55.31	24.76	17.44	0.37
F3.600	2463.8	11.78	40.7674	57.79	25.12	10.09	0.54
F3.800	2103.5	10.06	48.7044	61.42	16.93	8.16	0.39
F4.000	1005.2	4.81	52.7782	64.24	13.96	6.83	0.34
F4.200	1339.4	6.41	60.7629	65.61	6.62	4.25	0.21
F4.400	1889.9	9.04	64.8212	66.52	3.49	2.41	0.18
F4.600	2391.3	11.44	66.7065	67.14	2.15	1.49	0.15
F4.800	2730.8	13.06	67.4903	67.50	1.72	1.18	0.14
S4.800	99.6	0.48	67.7304	67.73	1.48	0.99	0.12
SK7 (-6+2mm)							
F3.000	2844.5	12.00	8.29929	51.70	65.22	14.36	1.51
F3.200	902.2	3.81	22.176	57.62	49.10	12.45	1.93
F3.400	739	3.12	31.7016	59.22	41.83	8.12	1.36
F3.600	1801.3	7.60	39.2213	60.28	33.43	6.53	1.14
F3.800	2201.7	9.29	48.912	62.45	21.99	4.62	0.90
F4.000	1187.8	5.01	50.17	64.41	20.97	4.13	0.75
F4.200	1877.9	7.92	59.97	65.62	9.46	2.48	0.42
F4.400	3206.2	13.52	64.3978	66.49	5.05	1.69	0.25
F4.600	4239.4	17.88	66.6661	67.24	2.58	1.19	0.17
F4.800	4540.7	19.15	67.7479	67.76	1.60	0.83	0.10
S4.800	168.3	0.71	68.0327	68.03	1.46	0.62	0.08
SK27 (-6+2mm)							
F3.000	3361.8	14.60	8.521	52.31	45.25	29.66	0.95
F3.200	673.5	2.92	22.22	59.80	37.04	21.51	0.50
F3.400	602	2.61	32.13	61.13	27.96	18.37	0.33
F3.600	951.6	4.13	40.03	62.08	21.28	15.07	0.27
F3.800	2092.2	9.08	52.7	63.29	12.09	8.48	0.14
F4.000	1503.4	6.53	55.14	64.73	10.80	6.36	0.12
F4.200	1925.3	8.36	60.9	65.77	6.08	3.86	0.07
F4.400	2447.6	10.63	65.248	66.56	3.50	2.02	0.04
F4.600	3594.8	15.61	66.12	66.89	2.93	1.38	0.02
F4.800	5734.9	24.90	67.37	67.37	1.99	1.02	0.03
S4.800	143.2	0.62	67.23	67.23	2.01	1.03	0.03
SK30 (-6+2mm)							
F3.000	336	2.40	12.2947	51.55	40.01	28.38	1.14
F3.200	401.4	2.87	24.83	52.51	29.13	23.89	0.77
F3.400	696.6	4.97	32.43	53.35	23.77	20.48	0.58
F3.600	1735.2	12.39	42.37	54.51	17.32	15.40	0.38
F3.800	1919	13.70	50.2	56.45	12.20	11.31	0.25
F4.000	2202.9	15.73	50.89	57.80	11.39	10.35	0.21
F4.200	2594.2	18.52	56.38	60.06	7.93	7.60	0.13
F4.400	1830.1	13.07	60.53	62.38	5.52	5.16	0.08
F4.600	2241.7	16.01	63.86	63.87	3.83	3.22	0.04
F4.800	48	0.34	64.15	64.15	3.62	2.89	0.04
S4.800	0	0.00	0	64.15			

7.2.5 Appendix A.5 - Chemical and Densimetric Analysis Results of Material Treated through the Ultra-High Density DMS

Low Grade Stockpile Material

14/01 Day Shift Feed	Mass (g)	Mass (%)	Fe	SiO₂	Al₂O₃	K₂O
U1-14DS Feed F3.6 ²	2983.5	25.69	15.3	52.5	16.09	2.56
U1-14DS Feed F3.8	371.4	3.20	38.4	26.0	10.78	1.80
U1-14DS Feed F4.0	544.3	4.69	45.5	19.3	8.93	1.31
U1-14DS Feed F4.2	491.5	4.23	51.3	14.0	7.49	0.99
U1-14DS Feed F4.4	847.8	7.30	55.6	10.0	5.81	0.79
U1-14DS Feed F4.6	1150.5	9.91	60.5	6.0	3.92	0.48
U1-14DS Feed F4.8	2021.9	17.41	64.4	3.4	2.26	0.28
U1-14DS Feed F5.0	2152.4	18.53	67.0	1.76	1.15	0.13
U1-14DS Feed S5.0	1051.3	9.05	68.5	1.08	0.71	0.07
14/01 Day Shift Product	Mass (g)	Mass (%)	Fe	SiO₂	Al₂O₃	K₂O
U2-14DS Product F4.2	124	0.91	48.7	16.9	8.10	1.18
U2-14DS Product F4.4	160.7	1.18	55.9	9.6	5.92	0.79
U2-14DS Product F4.6	695.5	5.12	61.2	5.8	3.70	0.46
U2-14DS Product F4.8	4363	32.11	65.1	3.1	2.08	0.25
U2-14DS Product F5.0	5790.4	42.62	66.9	1.77	1.10	0.12
U2-14DS Product S5.0	2452.7	18.05	68.1	1.06	0.49	0.06
14/01 Day Shift Waste	Mass (g)	Mass (%)	Fe	SiO₂	Al₂O₃	K₂O
U3-14DS Waste F3.6	5478.6	42.67	14.9	52.6	16.71	2.76
U3-14DS Waste F3.8	893.4	6.96	40.3	24.3	10.50	1.65
U3-14DS Waste F4.0	541.6	4.22	45.6	19.0	9.00	1.35
U3-14DS Waste F4.2	1141.5	8.89	50.5	14.3	7.66	1.07
U3-14DS Waste F4.4	1330.6	10.36	56.0	9.9	5.73	0.76
U3-14DS Waste F4.6	2070.2	16.12	61.5	5.3	3.36	0.44
U3-14DS Waste F4.8	1140	8.88	63.1	4.55	2.95	0.38
U3-14DS Waste S4.8	244.7	1.91	66.8	2.06	1.45	0.16
14/01 Night Shift Feed	Mass (g)	Mass (%)	Fe	SiO₂	Al₂O₃	K₂O
U4-14NS Feed F3.6	3293.5	24.73	14.4	51.3	16.04	2.57
U4-14NS Feed F3.8	628.4	4.72	39.8	26.0	10.51	1.68
U4-14NS Feed F4.0	423	3.18	46.0	18.8	8.61	1.33
U4-14NS Feed F4.2	723.4	5.43	51.3	14.3	7.34	1.03
U4-14NS Feed F4.4	836.2	6.28	55.8	10.2	5.82	0.80
U4-14NS Feed F4.6	1104.1	8.29	60.5	6.3	3.96	0.52
U4-14NS Feed F4.8	1846.4	13.86	64.4	3.6	2.31	0.29
U4-14NS Feed F5.0	2850.3	21.40	66.6	2.00	1.32	0.16
U4-14NS Feed S5.0	1614.7	12.12	68.4	1.22	0.79	0.08
14/01 Night Shift Product	Mass (g)	Mass (%)	Fe	SiO₂	Al₂O₃	K₂O
U5-14NS Product F4.2	115	0.81	46.9	18.9	8.60	1.26
U5-14NS Product F4.4	190	1.35	54.9	10.8	6.08	0.76
U5-14NS Product F4.6	1357.7	9.62	63.3	4.6	3.00	0.38
U5-14NS Product F4.8	4326.4	30.65	64.7	3.1	2.08	0.25
U5-14NS Product F5.0	5055.1	35.81	67.6	1.64	1.10	0.12
U5-14NS Product S5.0	3072.3	21.76	68.6	1.17	0.77	0.07
14/01 Night Shift Waste	Mass (g)	Mass (%)	Fe	SiO₂	Al₂O₃	K₂O
U6-14NS Waste F3.6	6103.5	44.77	15.2	52.2	16.59	2.65
U6-14NS Waste F3.8	657.3	4.82	38.8	26.3	10.69	1.66
U6-14NS Waste F4.0	852.6	6.25	45.2	20.0	9.15	1.38
U6-14NS Waste F4.2	1135.9	8.33	51.8	13.6	7.34	1.05
U6-14NS Waste F4.4	1295	9.50	55.0	10.6	6.05	0.81
U6-14NS Waste F4.6	2172	15.93	60.5	6.1	3.81	0.51
U6-14NS Waste F4.8	906.2	6.65	63.9	3.4	2.23	0.30
U6-14NS Waste F5.0	405.1	2.97	66.3	2.47	1.63	0.21
U6-14NS Waste S5.0	105	0.77	67.6	1.79	1.17	0.13

² F prefix on the number denotes float at that particular density, whereas S prefix denotes sinks

Jig Waste Material

15/01 Day Shift Feed	Mass (g)	Mass (%)	Fe	SiO₂	Al₂O₃	K₂O
U7-15DS Feed F3.6	5038.7	38.41	16.5	63.5	8.25	0.99
U7-15DS Feed F3.8	580.2	4.42	40.2	33.5	4.89	0.68
U7-15DS Feed F4.0	543.8	4.15	45.6	26.9	4.15	0.52
U7-15DS Feed F4.2	756.9	5.77	53.1	17.0	3.61	0.46
U7-15DS Feed F4.4	659.4	5.03	58.6	10.3	2.41	0.32
U7-15DS Feed F4.6	1168.8	8.91	60.4	7.9	2.11	0.30
U7-15DS Feed F4.8	1645.8	12.55	66.1	2.7	1.01	0.15
U7-15DS Feed F5.0	1633.7	12.45	66.5	2.11	0.87	0.12
U7-15DS Feed S5.0	1090	8.31	67.5	1.30	0.59	0.07
15/01 Day Shift Product	Mass (g)	Mass (%)	Fe	SiO₂	Al₂O₃	K₂O
U8-15DS Product F4.2	267.3	1.80	46.7	24.5	4.06	0.55
U8-15DS Product F4.4	185.2	1.25	55.5	14.0	3.19	0.41
U8-15DS Product F4.6	541.7	3.65	61.1	7.2	1.97	0.29
U8-15DS Product F4.8	3553.9	23.96	65.5	3.2	1.20	0.18
U8-15DS Product F5.0	7070.5	47.67	67.2	1.54	0.66	0.08
U8-15DS Product S5.0	3212.6	21.66	67.7	1.02	0.49	0.05
15/01 Day Shift Waste	Mass (g)	Mass (%)	Fe	SiO₂	Al₂O₃	K₂O
U9-15DS Waste F3.6	5936.5	52.65	16.8	61.8	8.34	1.00
U9-15DS Waste F3.8	639.8	5.67	40.9	32.8	4.55	0.63
U9-15DS Waste F4.0	564.3	5.00	46.4	25.3	4.19	0.56
U9-15DS Waste F4.2	746.2	6.62	53.2	16.6	3.59	0.48
U9-15DS Waste F4.4	949.8	8.42	56.0	13.3	3.11	0.41
U9-15DS Waste F4.6	879.4	7.80	62.4	5.9	1.80	0.26
U9-15DS Waste F4.8	1144.8	10.15	64.4	4.01	1.36	0.20
U9-15DS Waste S4.8	414.9	3.68	67.3	1.70	0.71	0.09

APPENDIX B: FESI CHARACTERISATION

7.2.6 Appendix B.1 - Viscosity Modifier Specification

LIGNOTECH SOUTH AFRICA

A Borregaard - Sappi joint venture

LignoTech SA
Umkomanzi Drift
P.O. Box 743
Umkomaas 4170
South Africa

Tel: +27 (0) 39 97 36 000
Fax: +27 (0) 39 97 36 015

DP 725
Spec. No.: 013
Effective Date: 12.12.06
Revision Date: 03.08.10
Revision No. : 03

DP 725

Product Description

DP 725 is a purified grade calcium lignosulphonate product with low insoluble content and with near neutral pH.

Typical application: As plasticizer or water reducing admixture for good grade concrete and mortar. When used as admixture, it reduces water demand, improves workability and produce low air entrained concrete, mortar.

CAS No. 8061-52-7 (Calcium lignosulphonate)

Specifications

		Test Method
Dry matter %	52.0 ± 2.0	LAB TEST 001
pH (10% Solution)	7.0 ± 0.8	LAB TEST 008
Insolubles %	Max 0.5	LAB TEST 004

Active customers would be notified of changes where any.

Chemical Data

Parameter	Typical values*
pH	6.8
Calcium	6.0%
Total Sulphur	4.0%
Reducing Sugars	2.0%
HPLC Sugars	<1.0%
Alkaline Content	≤ 0.50% m/m
Chloride Content	≤ 0.10% m/m

Physical Data

Parameter	Typical values*
Colour	Brown
Dry Matter	51%
Density(51% DS, 25 °C)	1270 kg/m ³

*The above analyses are not formal specifications and values may change. All values calculated on solids where applicable.

Storage Stability:

As this is a liquid product, shelf life may vary from a few months to about 6 months dependent upon the storage condition when kept in the original sealed packaging or tank. No preservative has been added additionally.

Compatibility:

Lignosulphonates are compatible with anionic and non-ionic dispersants, wetting agents and most organic and inorganic materials.

Delivery Form:

Liquid product is available in flowbins or bulk truckloads. Alternative forms available upon further discussion.

Lead Time:

2 weeks lead time is typical for local.
6 to 8 weeks lead time for international.

Material Safety Data Sheets are available upon request.

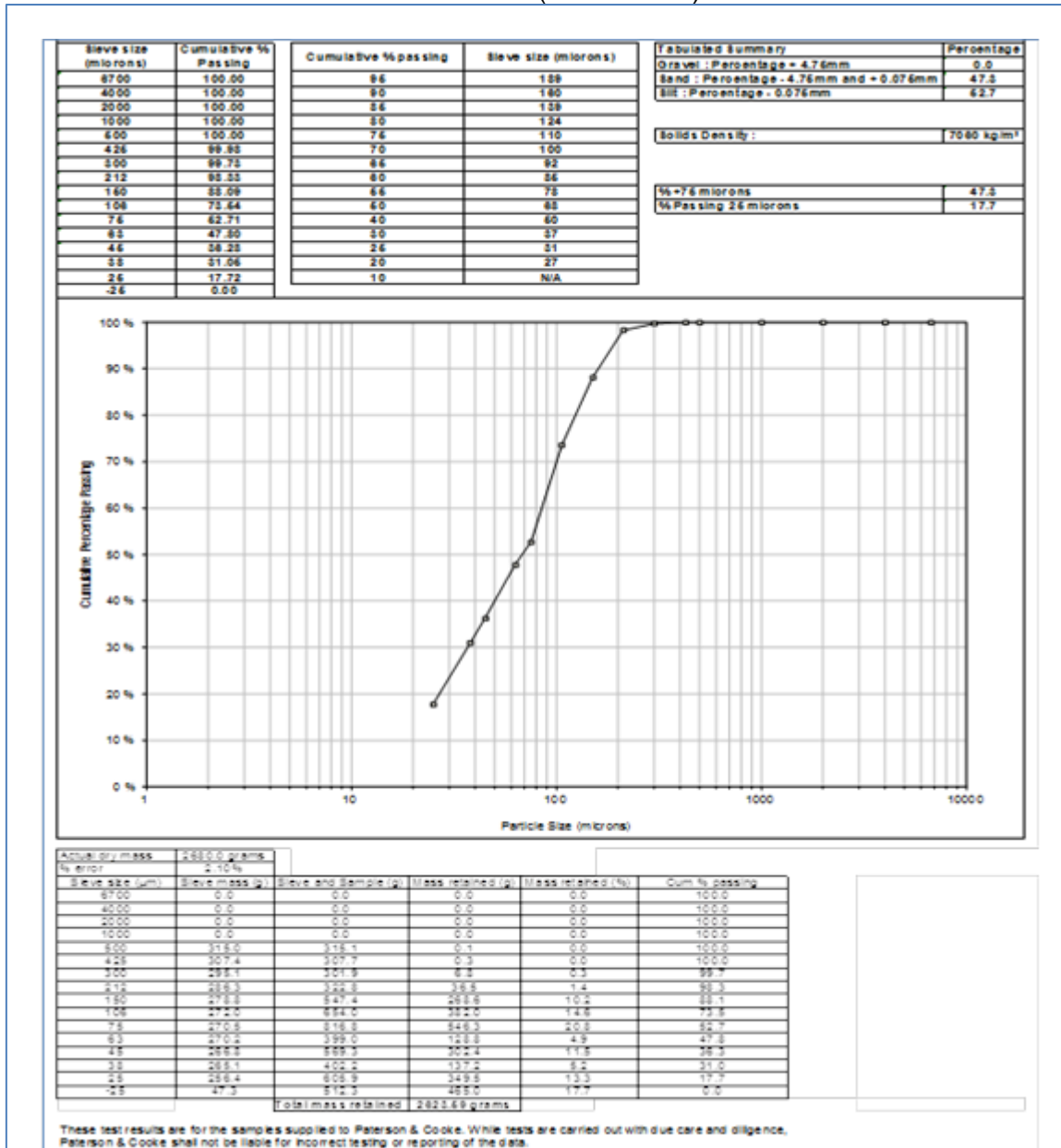
UNCONTROLLED COPY

Please contact your LignoTech Sales Representative for additional product information.

The information given here is based on our best knowledge and we believe it to be true and accurate. However, LignoTech South Africa does not warrant or guarantee in any manner whatsoever, including the warranty of merchant-ability or fitness for the end user the accuracy of the information and procedures listed herein and will not be responsible for any damage resulting from their use.

7.2.7 Appendix B.2 - Particle Size Analysis of FeSi

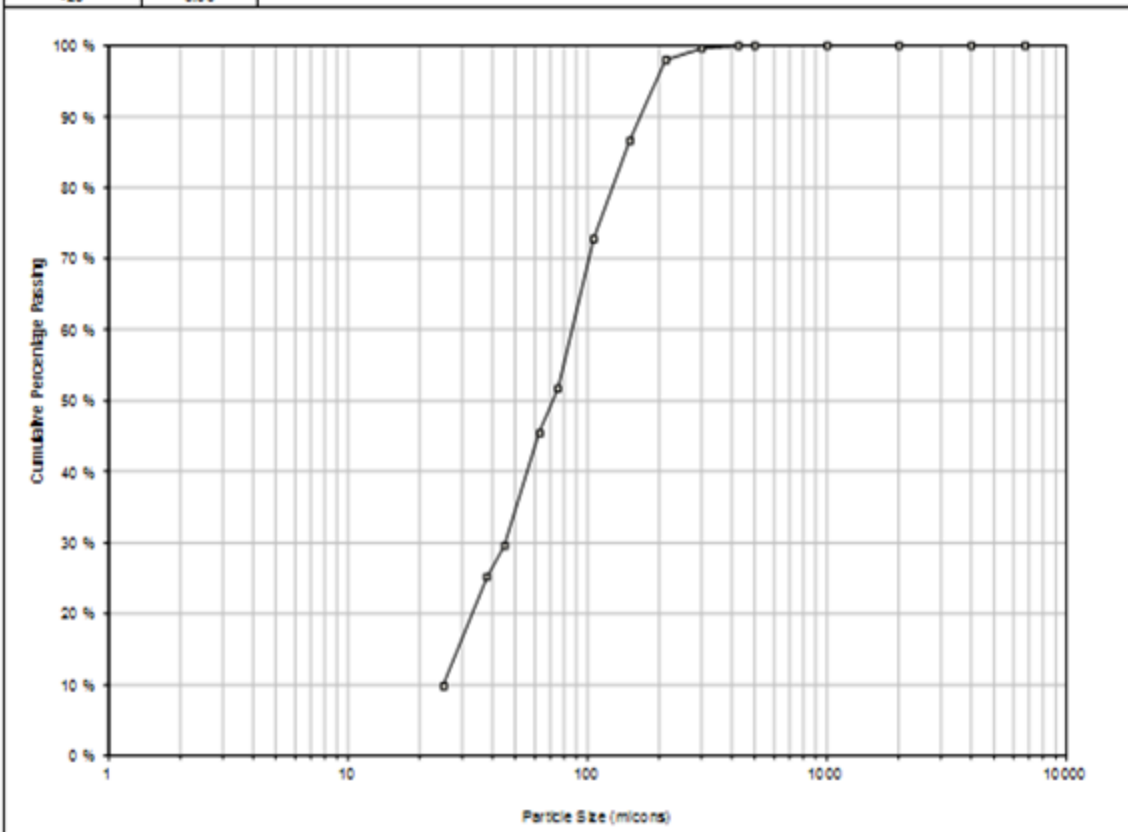
Coarse FeSi (as delivered)



Coarse FeSi less Fines

Sieve size (microns)	Cumulative % Passing	Cumulative % passing	Sieve size (microns)
8700	100.00	96	193
4000	100.00	90	188
2000	100.00	86	144
1000	100.00	80	127
600	100.00	76	112
425	99.99	70	101
300	99.88	66	93
212	98.03	60	88
160	88.88	66	78
106	72.37	60	71
76	61.72	40	68
60	46.60	30	46
46	29.67	26	38
38	26.20	20	33
26	9.84	10	26
-26	0.00		

Tabulated Summary		Percentage
Gravel : Percentage - 4.76mm		0.0
Sand : Percentage - 4.76mm and +0.076mm		48.3
Silt : Percentage - 0.076mm		61.7
Solids Density:		7080 kg/m ³
%+75 microns		48.3
% Passing 26 microns		9.8



Actual dry mass	1920.8 grams				
% error	-1.90%				
Sieve size (µm)	Sieve mass (g)	Sieve and Sample (g)	Mass retained (g)	Mass retained (%)	Cum % passing
8700	0.0	0.0	0.0	0.0	100.0
4000	420.2	420.2	0.0	0.0	100.0
2000	408.8	408.8	0.0	0.0	100.0
1000	388.2	388.2	0.0	0.0	100.0
600	317.8	317.7	0.1	0.0	100.0
425	307.8	307.7	0.2	0.0	100.0
300	294.2	300.7	6.4	0.3	99.7
212	287.7	319.7	32.0	1.6	98.0
160	268.8	491.8	223.1	11.4	86.6
106	273.8	642.8	269.2	13.8	72.8
75	268.7	679.7	414.0	21.2	61.7
60	266.8	388.5	121.7	6.2	48.5
46	268.0	580.0	311.9	15.9	29.6
38	268.2	380.6	95.4	4.4	25.2
26	248.4	549.0	300.6	15.4	9.8
-26	55.3	247.9	192.6	9.8	0.0
Total mass retained			1967.20 grams		

These test results are for the samples supplied to Paterson & Cooke. While tests are carried out with due care and diligence, Paterson & Cooke shall not be liable for incorrect testing or reporting of the data.

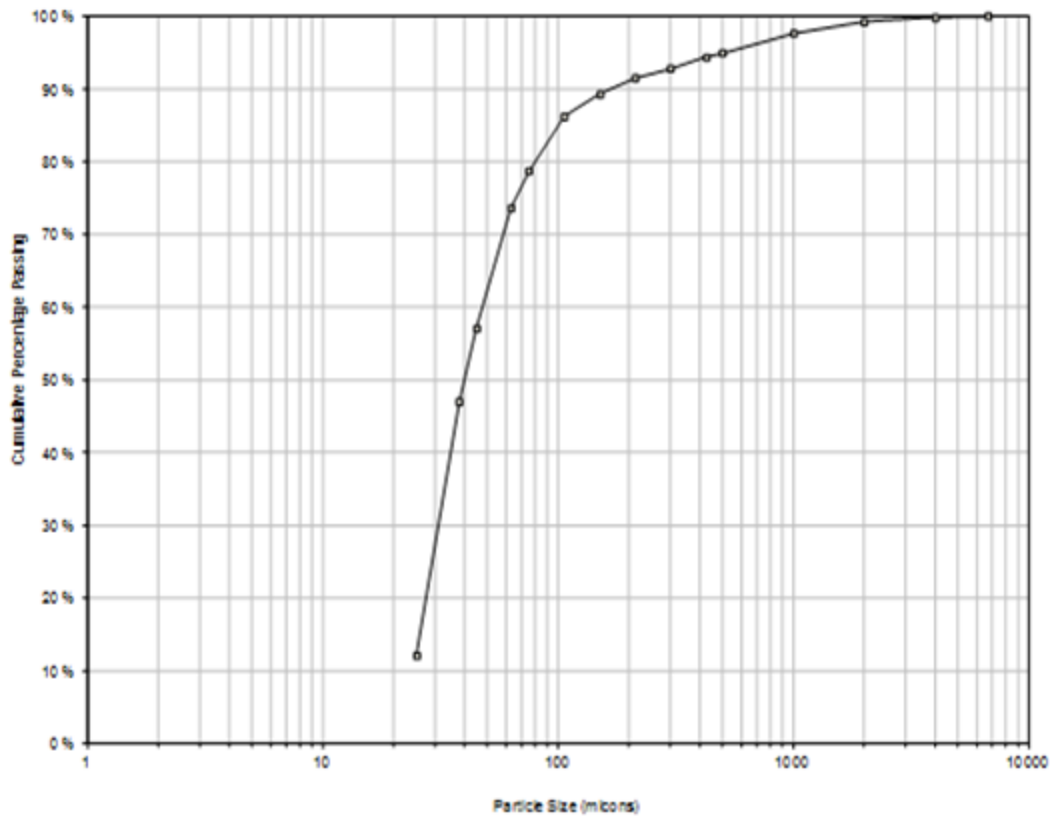
Process FeSi (as delivered)

Sieve size (microns)	Cumulative % Passing	Cumulative % passing	Sieve size (microns)
8700	100.00	96	608
4000	99.34	90	187
2000	99.24	86	100
1000	97.88	80	80
600	94.96	76	88
425	94.38	70	69
300	92.31	66	63
212	91.62	60	43
160	89.31	66	43
108	88.23	60	40
75	78.70	40	36
63	73.69	30	31
45	67.11	26	29
38	47.04	20	27
26	12.12	10	N/A
-26	0.00		

Tabulated Summary		Percentage
Gravel : Percentage - 4.76mm		0.1
Sand : Percentage - 4.76mm and + 0.075mm		21.2
Blitt : Percentage - 0.075mm		78.7

Solids Density:	6601 kg/m ³
-----------------	------------------------

% +75 microns	21.3
% Passing 26 microns	12.1



Actual dry mass	1924.6 grams
% error	61.09%

Sieve size (µm)	Sieve mass (g)	Sieve and Sample (g)	Mass retained (g)	Mass retained (%)	Cum % passing
8700	306.9	306.9	0.0	0.0	100.0
4000	435.8	437.0	1.2	0.2	99.8
2000	405.5	410.0	4.5	0.6	99.2
1000	355.2	367.1	11.9	1.6	97.7
500	317.6	337.8	20.2	2.7	95.0
425	307.5	311.9	4.4	0.6	94.4
300	294.2	305.8	11.7	1.6	92.8
212	287.7	297.3	9.7	1.3	91.5
160	268.7	286.2	16.6	2.2	89.3
108	273.8	296.9	23.1	3.1	86.2
75	266.7	323.0	56.3	7.5	78.7
63	257.6	303.9	38.3	5.1	73.6
45	259.0	392.4	133.4	16.5	57.1
38	264.5	340.0	75.5	10.1	47.0
26	247.9	509.4	261.5	34.9	12.1
-26	56.4	147.1	90.7	12.1	0.0
Total mass retained			748.86 grams		

These test results are for the samples supplied to Paterson & Cooke. While tests are carried out with due care and diligence, Paterson & Cooke shall not be liable for incorrect testing or reporting of the data.

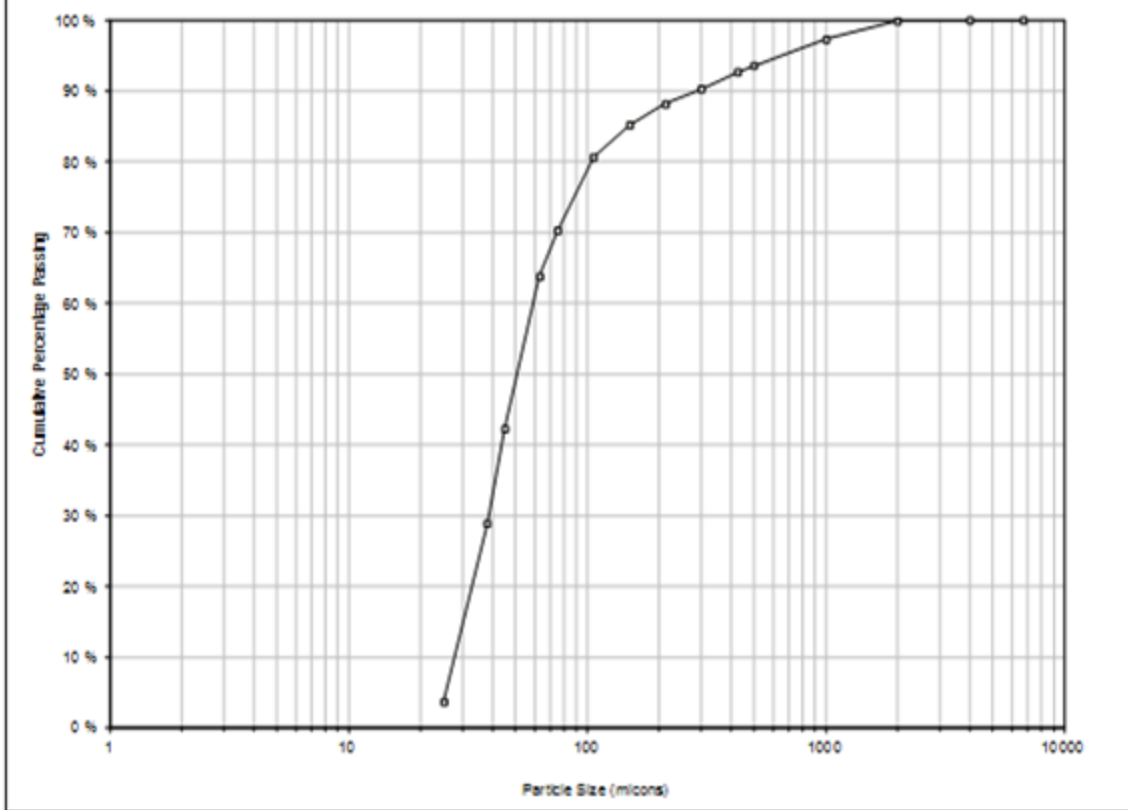
Process FeSi less Fines

Sieve size (microns)	Cumulative % Passing	Cumulative % passing	Sieve size (microns)
8700	100.00	96	848
4000	100.00	90	254
2000	99.97	86	147
1000	97.34	80	104
600	93.60	76	88
425	92.88	70	74
300	90.33	66	66
212	88.23	60	61
150	86.23	56	56
106	80.88	60	61
75	70.37	40	44
63	63.87	30	38
45	42.23	26	38
38	28.88	20	33
25	3.88	10	25
-25	0.00		

Fabricated Summary		Percentage
Gravel : Percentage - 4.76mm		0.0
Sand : Percentage - 4.76mm and + 0.075mm		28.8
Silt : Percentage - 0.075mm		70.4

Solids Density :	8601 kg/m ³
------------------	------------------------

% +75 microns	28.8
% Passing 25 microns	3.7



Actual dry mass	1820.4 grams				
% error	0.32%				
Sieve size (µm)	Sieve mass (g)	Sieve and Sample (g)	Mass retained (g)	Mass retained (%)	Cum % passing
8700	0.0	0.0	0.0	0.0	100.0
4000	435.9	435.9	0.0	0.0	100.0
2000	408.8	408.0	0.8	0.0	100.0
1000	355.2	402.8	47.6	2.6	97.3
600	317.6	385.5	67.9	3.7	93.6
425	307.6	324.6	17.0	0.9	92.7
300	294.2	336.7	42.5	2.3	90.3
212	287.7	325.7	38.0	2.1	88.2
150	268.6	323.0	54.4	3.0	85.2
106	273.8	386.4	62.6	4.5	80.7
75	268.8	483.0	187.2	10.3	70.4
63	268.9	384.8	117.9	6.5	63.9
45	260.2	660.9	392.7	21.6	42.2
38	265.3	607.4	242.1	13.3	28.9
25	248.8	706.0	457.3	25.2	3.7
-25	63.4	130.2	66.8	3.7	0.0
Total mass retained			1814.63 grams		

These test results are for the samples supplied to Paterson & Cooke. While tests are carried out with due care and diligence, Paterson & Cooke shall not be liable for incorrect testing or reporting of the data.

7.2.8 Appendix B.3 - Pipe Loop Settling Data

Material	Density
Coarse FeSi Less Fines	3604 kg/m ³
	3938 kg/m ³
	4135 kg/m ³
	4233 kg/m ³
Process FeSi	3991 kg/m ³
	3898 kg/m ³
	3822 kg/m ³
	3609 kg/m ³
	3609 kg/m ³
Process FeSi Less Fines	3991 kg/m ³
	3898 kg/m ³
	3822 kg/m ³
	3609 kg/m ³
Coarse FeSi with Rheology Modifier	3704 kg/m ³
	3915 kg/m ³
	4085 kg/m ³
	4251 kg/m ³

NB! Appended data for only a single density for each dense medium type tested, however, detailed data available for all density range tested.

Coarse FeSi Less Fines 3604 kg/m³

Data point	Pressure Bottom - kPa (abs)	Pressure Top - kPa (abs)	Density Calc	Duration
8	167.748	132.396	3604 kg/m ³	00:00:00
9	167.484	132.114	3606 kg/m ³	00:00:04
10	167.391	131.906	3617 kg/m ³	00:00:08
11	167.246	131.801	3613 kg/m ³	00:00:12
12	167.112	131.656	3614 kg/m ³	00:00:16
13	167.009	131.461	3624 kg/m ³	00:00:20
14	166.921	131.338	3627 kg/m ³	00:00:24
15	166.784	131.228	3624 kg/m ³	00:00:28
16	166.726	131.027	3639 kg/m ³	00:00:32
17	166.620	130.887	3642 kg/m ³	00:00:37
18	166.470	130.688	3648 kg/m ³	00:00:41
19	166.405	130.556	3654 kg/m ³	00:00:46
20	166.299	130.495	3650 kg/m ³	00:00:50
21	166.219	130.315	3660 kg/m ³	00:00:54
22	166.176	130.114	3676 kg/m ³	00:00:59
23	166.083	130.025	3676 kg/m ³	00:01:03
24	166.057	129.940	3682 kg/m ³	00:01:07
25	165.826	129.757	3677 kg/m ³	00:01:12
26	165.632	129.644	3669 kg/m ³	00:01:16
27	165.288	129.470	3651 kg/m ³	00:01:20
28	165.118	129.342	3647 kg/m ³	00:01:25
29	164.669	129.238	3612 kg/m ³	00:01:29
30	164.333	129.112	3590 kg/m ³	00:01:33
31	164.090	129.015	3576 kg/m ³	00:01:37
32	163.869	128.907	3564 kg/m ³	00:01:41
33	163.536	128.795	3541 kg/m ³	00:01:45
34	163.224	128.657	3524 kg/m ³	00:01:49
35	162.928	128.514	3508 kg/m ³	00:01:53
36	162.684	128.456	3489 kg/m ³	00:01:57

Data point	Pressure Bottom - kPa (abs)	Pressure Top - kPa (abs)	Density Calc	Duration
37	162.411	128.273	3480 kg/m ³	00:02:01
38	162.128	128.168	3462 kg/m ³	00:02:05
39	161.842	128.080	3442 kg/m ³	00:02:09
40	161.521	127.998	3417 kg/m ³	00:02:13
41	161.248	127.896	3400 kg/m ³	00:02:17
42	160.962	127.797	3381 kg/m ³	00:02:21
43	160.672	127.628	3368 kg/m ³	00:02:25
44	160.394	127.566	3346 kg/m ³	00:02:29
45	160.202	127.442	3339 kg/m ³	00:02:33
46	159.862	127.421	3307 kg/m ³	00:02:37
47	159.579	127.311	3289 kg/m ³	00:02:41
48	159.318	127.164	3278 kg/m ³	00:02:45
49	159.061	127.083	3260 kg/m ³	00:02:49
50	158.762	126.943	3243 kg/m ³	00:02:53
51	158.467	126.894	3218 kg/m ³	00:02:57
52	158.210	126.765	3205 kg/m ³	00:03:01
53	157.917	126.683	3184 kg/m ³	00:03:05
54	157.691	126.597	3170 kg/m ³	00:03:09
55	157.362	126.470	3149 kg/m ³	00:03:14
56	157.084	126.361	3132 kg/m ³	00:03:18
57	156.800	126.250	3114 kg/m ³	00:03:23
58	156.478	126.160	3091 kg/m ³	00:03:27
59	156.161	126.060	3068 kg/m ³	00:03:31
60	155.916	125.985	3051 kg/m ³	00:03:35
61	155.641	125.889	3033 kg/m ³	00:03:39
62	155.431	125.789	3022 kg/m ³	00:03:43
63	155.131	125.752	2995 kg/m ³	00:03:47
64	154.857	125.643	2978 kg/m ³	00:03:51
65	154.641	125.583	2962 kg/m ³	00:03:55
66	154.356	125.460	2946 kg/m ³	00:03:59
67	154.076	125.384	2925 kg/m ³	00:04:03
68	153.854	125.287	2912 kg/m ³	00:04:07
69	153.587	125.210	2893 kg/m ³	00:04:11
70	153.291	125.158	2868 kg/m ³	00:04:15
71	153.055	125.040	2856 kg/m ³	00:04:19
72	152.807	125.008	2834 kg/m ³	00:04:23
73	152.551	124.809	2828 kg/m ³	00:04:27
74	152.308	124.801	2804 kg/m ³	00:04:31
75	152.068	124.732	2787 kg/m ³	00:04:35
76	151.795	124.713	2761 kg/m ³	00:04:39
77	151.574	124.589	2751 kg/m ³	00:04:43
78	151.287	124.558	2725 kg/m ³	00:04:47
79	151.069	124.441	2714 kg/m ³	00:04:51
80	150.799	124.367	2694 kg/m ³	00:04:55
81	150.534	124.219	2682 kg/m ³	00:04:59
82	150.308	124.141	2667 kg/m ³	00:05:03
83	150.093	124.112	2648 kg/m ³	00:05:07
84	149.799	124.044	2625 kg/m ³	00:05:11
85	149.583	124.002	2608 kg/m ³	00:05:15
86	149.360	123.947	2591 kg/m ³	00:05:19
87	149.099	123.900	2569 kg/m ³	00:05:23
88	148.826	123.747	2556 kg/m ³	00:05:27
89	148.630	123.725	2539 kg/m ³	00:05:31
90	148.416	123.663	2523 kg/m ³	00:05:35

Data point	Pressure Bottom - kPa (abs)	Pressure Top - kPa (abs)	Density Calc	Duration
91	148.221	123.578	2512 kg/m ³	00:05:39
92	147.948	123.503	2492 kg/m ³	00:05:43
93	147.724	123.445	2475 kg/m ³	00:05:47
94	147.472	123.353	2459 kg/m ³	00:05:51
95	147.233	123.287	2441 kg/m ³	00:05:55
96	147.062	123.254	2427 kg/m ³	00:05:59
97	146.795	123.145	2411 kg/m ³	00:06:03
98	146.566	123.114	2391 kg/m ³	00:06:07
99	146.391	123.009	2384 kg/m ³	00:06:11
100	146.195	122.933	2371 kg/m ³	00:06:15
101	145.939	122.903	2348 kg/m ³	00:06:19
102	145.754	122.858	2334 kg/m ³	00:06:23
103	145.522	122.781	2318 kg/m ³	00:06:27
104	145.306	122.673	2307 kg/m ³	00:06:31
105	145.091	122.660	2286 kg/m ³	00:06:35
106	144.819	122.566	2268 kg/m ³	00:06:39
107	144.620	122.544	2250 kg/m ³	00:06:43
108	144.455	122.496	2238 kg/m ³	00:06:47
109	144.270	122.418	2228 kg/m ³	00:06:51
110	144.064	122.361	2212 kg/m ³	00:06:55
111	143.862	122.295	2199 kg/m ³	00:06:59
112	143.671	122.274	2181 kg/m ³	00:07:03
113	143.523	122.180	2176 kg/m ³	00:07:07
114	143.323	122.127	2161 kg/m ³	00:07:11
115	143.126	122.099	2143 kg/m ³	00:07:15
116	143.072	122.019	2146 kg/m ³	00:07:19
117	142.915	121.976	2134 kg/m ³	00:07:23
118	142.852	121.897	2136 kg/m ³	00:07:27
119	142.693	121.864	2123 kg/m ³	00:07:31
120	142.537	121.790	2115 kg/m ³	00:07:35
121	142.397	121.772	2102 kg/m ³	00:07:39
122	142.304	121.740	2096 kg/m ³	00:07:43
123	142.030	121.651	2077 kg/m ³	00:07:47
124	141.718	121.624	2048 kg/m ³	00:07:51
125	141.477	121.589	2027 kg/m ³	00:07:55
126	141.175	121.479	2008 kg/m ³	00:07:59
127	140.877	121.464	1979 kg/m ³	00:08:03
128	140.584	121.434	1952 kg/m ³	00:08:07
129	140.360	121.340	1939 kg/m ³	00:08:11
130	140.088	121.311	1914 kg/m ³	00:08:15
131	139.852	121.263	1895 kg/m ³	00:08:19
132	139.692	121.233	1882 kg/m ³	00:08:23
133	139.499	121.214	1864 kg/m ³	00:08:27
134	139.209	121.161	1840 kg/m ³	00:08:31
135	139.060	121.046	1836 kg/m ³	00:08:35
136	138.860	121.030	1818 kg/m ³	00:08:39
137	138.630	120.993	1798 kg/m ³	00:08:43
138	138.455	120.933	1786 kg/m ³	00:08:47
139	138.275	120.895	1772 kg/m ³	00:08:51
140	138.104	120.870	1757 kg/m ³	00:08:55
141	137.953	120.806	1748 kg/m ³	00:08:59
142	137.747	120.726	1735 kg/m ³	00:09:03
143	137.594	120.716	1720 kg/m ³	00:09:07
144	137.459	120.670	1711 kg/m ³	00:09:11

Data point	Pressure Bottom - kPa (abs)	Pressure Top - kPa (abs)	Density Calc	Duration
145	137.243	120.667	1690 kg/m ³	00:09:15
146	137.095	120.594	1682 kg/m ³	00:09:19
147	136.946	120.593	1667 kg/m ³	00:09:23
148	136.815	120.516	1661 kg/m ³	00:09:27
149	136.664	120.505	1647 kg/m ³	00:09:31
150	136.620	120.463	1647 kg/m ³	00:09:35
151	136.530	120.419	1642 kg/m ³	00:09:39
152	136.735	120.389	1666 kg/m ³	00:09:43
153	147.855	120.337	2805 kg/m ³	00:09:47
154	155.313	120.308	3568 kg/m ³	00:09:51
155	156.121	120.222	3659 kg/m ³	00:09:55
156	156.016	120.172	3654 kg/m ³	00:09:59
157	155.069	120.108	3564 kg/m ³	00:10:03

Process FeSi
3350 kg/m³

Data point	Pressure Bottom - kPa (abs)	Pressure Top - kPa (abs)	Density Calc	Duration
7	166.999	134.138	3350 kg/m ³	00:00:00
8	167.688	134.403	3393 kg/m ³	00:00:04
9	168.059	134.513	3420 kg/m ³	00:00:08
10	168.151	134.540	3426 kg/m ³	00:00:12
11	168.135	134.481	3431 kg/m ³	00:00:16
12	168.205	134.490	3437 kg/m ³	00:00:20
13	168.244	134.480	3442 kg/m ³	00:00:24
14	168.236	134.456	3443 kg/m ³	00:00:28
15	168.303	134.410	3455 kg/m ³	00:00:32
16	168.319	134.395	3458 kg/m ³	00:00:36
17	168.237	134.390	3450 kg/m ³	00:00:40
18	168.244	134.358	3454 kg/m ³	00:00:44
19	168.228	134.395	3449 kg/m ³	00:00:48
20	168.287	134.368	3458 kg/m ³	00:00:52
21	168.255	134.358	3455 kg/m ³	00:00:56
22	168.251	134.354	3455 kg/m ³	00:01:00
23	168.238	134.348	3455 kg/m ³	00:01:04
24	168.270	134.318	3461 kg/m ³	00:01:08
25	168.296	134.250	3471 kg/m ³	00:01:12
26	168.279	134.237	3470 kg/m ³	00:01:16
27	168.262	134.193	3473 kg/m ³	00:01:20
28	168.222	134.194	3469 kg/m ³	00:01:24
29	168.234	134.129	3477 kg/m ³	00:01:28
30	168.363	134.159	3487 kg/m ³	00:01:32
31	167.974	134.034	3460 kg/m ³	00:01:36
32	168.154	134.080	3473 kg/m ³	00:01:40
33	168.274	134.103	3483 kg/m ³	00:01:44
34	168.176	134.027	3481 kg/m ³	00:01:48
35	168.101	134.005	3476 kg/m ³	00:01:52
36	168.110	134.059	3471 kg/m ³	00:01:56
37	168.111	134.118	3465 kg/m ³	00:02:00
38	168.128	134.095	3469 kg/m ³	00:02:04
39	168.115	134.164	3461 kg/m ³	00:02:08
40	168.082	134.066	3467 kg/m ³	00:02:12
41	168.048	134.054	3465 kg/m ³	00:02:16
42	167.987	134.065	3458 kg/m ³	00:02:20
43	168.013	134.043	3463 kg/m ³	00:02:24

Data point	Pressure Bottom - kPa (abs)	Pressure Top - kPa (abs)	Density Calc	Duration
44	167.950	134.074	3453 kg/m ³	00:02:28
45	167.926	133.984	3460 kg/m ³	00:02:32
46	167.922	133.961	3462 kg/m ³	00:02:36
47	167.891	133.926	3462 kg/m ³	00:02:40
48	167.824	133.888	3459 kg/m ³	00:02:44
49	167.858	133.864	3465 kg/m ³	00:02:48
50	167.813	133.919	3455 kg/m ³	00:02:52
51	167.807	133.836	3463 kg/m ³	00:02:56
52	167.810	133.844	3462 kg/m ³	00:03:00
53	167.774	133.803	3463 kg/m ³	00:03:04
54	167.783	133.746	3470 kg/m ³	00:03:08
55	167.792	133.716	3474 kg/m ³	00:03:12
56	167.758	133.681	3474 kg/m ³	00:03:16
57	167.793	133.653	3480 kg/m ³	00:03:20
58	167.766	133.707	3472 kg/m ³	00:03:24
59	167.799	133.608	3485 kg/m ³	00:03:28
60	167.741	133.638	3476 kg/m ³	00:03:32
61	167.726	133.663	3472 kg/m ³	00:03:36
62	167.728	133.638	3475 kg/m ³	00:03:40
63	167.676	133.664	3467 kg/m ³	00:03:44
64	167.655	133.751	3456 kg/m ³	00:03:48
65	167.589	133.754	3449 kg/m ³	00:03:52
66	167.601	133.748	3451 kg/m ³	00:03:56
67	167.596	133.712	3454 kg/m ³	00:04:00
68	167.509	133.711	3445 kg/m ³	00:04:04
69	167.509	133.659	3451 kg/m ³	00:04:08
70	167.455	133.666	3444 kg/m ³	00:04:12
71	167.428	133.642	3444 kg/m ³	00:04:16
72	167.419	133.591	3448 kg/m ³	00:04:20
73	167.349	133.661	3434 kg/m ³	00:04:24
74	167.344	133.617	3438 kg/m ³	00:04:28
75	167.288	133.587	3435 kg/m ³	00:04:32
76	167.284	133.499	3444 kg/m ³	00:04:36
77	167.220	133.506	3437 kg/m ³	00:04:40
78	167.229	133.489	3439 kg/m ³	00:04:44
79	167.140	133.479	3431 kg/m ³	00:04:48
80	167.104	133.455	3430 kg/m ³	00:04:52
81	167.023	133.448	3423 kg/m ³	00:04:56
82	166.961	133.442	3417 kg/m ³	00:05:00
83	166.918	133.382	3418 kg/m ³	00:05:04
84	166.867	133.383	3413 kg/m ³	00:05:08
85	166.837	133.329	3416 kg/m ³	00:05:12
86	166.741	133.350	3404 kg/m ³	00:05:16
87	166.714	133.299	3406 kg/m ³	00:05:20
88	166.609	133.335	3392 kg/m ³	00:05:24
89	166.545	133.285	3390 kg/m ³	00:05:28
90	166.555	133.294	3391 kg/m ³	00:05:32
91	166.490	133.225	3391 kg/m ³	00:05:36
92	166.490	133.234	3390 kg/m ³	00:05:40
93	166.447	133.226	3386 kg/m ³	00:05:44
94	166.338	133.221	3376 kg/m ³	00:05:48
95	166.265	133.247	3366 kg/m ³	00:05:52
96	166.227	133.179	3369 kg/m ³	00:05:56
97	166.181	133.183	3364 kg/m ³	00:06:00
98	166.072	133.224	3348 kg/m ³	00:06:04

Data point	Pressure Bottom - kPa (abs)	Pressure Top - kPa (abs)	Density Calc	Duration
99	166.028	133.210	3345 kg/m ³	00:06:08
100	165.996	133.143	3349 kg/m ³	00:06:12
101	165.925	133.148	3341 kg/m ³	00:06:16
102	165.887	133.175	3335 kg/m ³	00:06:20
103	165.806	133.108	3333 kg/m ³	00:06:24
104	165.699	133.083	3325 kg/m ³	00:06:28
105	165.687	133.097	3322 kg/m ³	00:06:32
106	165.680	133.049	3326 kg/m ³	00:06:36
107	165.552	132.996	3319 kg/m ³	00:06:40
108	165.484	132.984	3313 kg/m ³	00:06:44
109	165.409	132.974	3306 kg/m ³	00:06:48
110	165.339	132.969	3300 kg/m ³	00:06:52
111	165.272	132.957	3294 kg/m ³	00:06:56
112	165.203	132.952	3288 kg/m ³	00:07:00
113	165.178	132.911	3289 kg/m ³	00:07:04
114	165.046	132.909	3276 kg/m ³	00:07:08
115	165.053	132.861	3282 kg/m ³	00:07:12
116	164.944	132.887	3268 kg/m ³	00:07:16
117	164.837	132.874	3258 kg/m ³	00:07:20
118	164.821	132.847	3259 kg/m ³	00:07:24
119	164.756	132.859	3251 kg/m ³	00:07:28
120	164.680	132.796	3250 kg/m ³	00:07:32
121	164.616	132.820	3241 kg/m ³	00:07:36
122	164.553	132.825	3234 kg/m ³	00:07:40
123	164.525	132.817	3232 kg/m ³	00:07:44
124	164.401	132.783	3223 kg/m ³	00:07:48
125	164.329	132.753	3219 kg/m ³	00:07:52
126	164.339	132.685	3227 kg/m ³	00:07:56
127	164.183	132.686	3211 kg/m ³	00:08:00
128	164.150	132.671	3209 kg/m ³	00:08:04
129	164.122	132.639	3209 kg/m ³	00:08:08
130	163.943	132.650	3190 kg/m ³	00:08:12
131	163.914	132.584	3194 kg/m ³	00:08:16
132	163.860	132.592	3187 kg/m ³	00:08:20
133	163.797	132.561	3184 kg/m ³	00:08:24
134	163.693	132.608	3169 kg/m ³	00:08:28
135	163.696	132.549	3175 kg/m ³	00:08:32
136	163.590	132.525	3167 kg/m ³	00:08:36
137	163.544	132.637	3151 kg/m ³	00:08:40
138	163.502	132.549	3155 kg/m ³	00:08:44
139	163.462	132.444	3162 kg/m ³	00:08:48
140	163.350	132.461	3149 kg/m ³	00:08:52
141	163.312	132.454	3146 kg/m ³	00:08:56
142	163.224	132.454	3137 kg/m ³	00:09:00
143	163.154	132.492	3126 kg/m ³	00:09:04
144	163.074	132.530	3114 kg/m ³	00:09:08
145	163.057	132.490	3116 kg/m ³	00:09:12
146	163.016	132.492	3112 kg/m ³	00:09:16
147	162.980	132.511	3106 kg/m ³	00:09:20
148	162.899	132.472	3102 kg/m ³	00:09:24
149	162.861	132.395	3106 kg/m ³	00:09:28
150	162.737	132.394	3093 kg/m ³	00:09:32
151	162.720	132.420	3089 kg/m ³	00:09:36
152	163.333	132.461	3147 kg/m ³	00:09:40
153	163.302	132.379	3152 kg/m ³	00:09:44

Data point	Pressure Bottom - kPa (abs)	Pressure Top - kPa (abs)	Density Calc	Duration
154	163.113	132.351	3136 kg/m ³	00:09:48
155	162.972	132.315	3125 kg/m ³	00:09:52
156	162.825	132.370	3104 kg/m ³	00:09:56
157	162.784	132.303	3107 kg/m ³	00:10:00
158	162.629	132.298	3092 kg/m ³	00:10:04

Process FeSi Less Fines

3991 kg/m³

Data point	Pressure Bottom - kPa (abs)	Pressure Top - kPa (abs)	Density Calc	Duration
8	177.984	138.828	3991 kg/m ³	00:00:00
9	177.796	138.631	3992 kg/m ³	00:00:04
10	177.520	138.547	3973 kg/m ³	00:00:08
11	177.225	138.403	3957 kg/m ³	00:00:12
12	176.938	138.262	3942 kg/m ³	00:00:16
13	176.682	138.160	3927 kg/m ³	00:00:20
14	176.387	138.005	3913 kg/m ³	00:00:24
15	176.195	137.899	3904 kg/m ³	00:00:28
16	176.007	137.801	3895 kg/m ³	00:00:32
17	175.816	137.658	3890 kg/m ³	00:00:36
18	175.590	137.547	3878 kg/m ³	00:00:40
19	175.502	137.463	3878 kg/m ³	00:00:44
20	175.308	137.363	3868 kg/m ³	00:00:48
21	175.202	137.276	3866 kg/m ³	00:00:52
22	175.079	137.207	3861 kg/m ³	00:00:56
23	175.007	137.223	3852 kg/m ³	00:01:00
24	174.822	137.121	3843 kg/m ³	00:01:04
25	174.617	137.048	3830 kg/m ³	00:01:08
26	174.564	136.974	3832 kg/m ³	00:01:12
27	174.432	136.990	3817 kg/m ³	00:01:16
28	174.280	136.923	3808 kg/m ³	00:01:20
29	174.079	136.889	3791 kg/m ³	00:01:24
30	173.923	136.905	3774 kg/m ³	00:01:28
31	173.706	136.917	3750 kg/m ³	00:01:32
32	173.528	136.895	3734 kg/m ³	00:01:36
33	173.313	136.834	3719 kg/m ³	00:01:40
34	173.109	136.790	3702 kg/m ³	00:01:44
35	172.880	136.758	3682 kg/m ³	00:01:48
36	172.552	136.716	3653 kg/m ³	00:01:52
37	172.336	136.745	3628 kg/m ³	00:01:56
38	172.024	136.679	3603 kg/m ³	00:02:00
39	171.723	136.721	3568 kg/m ³	00:02:04
40	171.423	136.728	3537 kg/m ³	00:02:08
41	171.072	136.694	3504 kg/m ³	00:02:12
42	170.749	136.697	3471 kg/m ³	00:02:16
43	170.531	136.667	3452 kg/m ³	00:02:20
44	170.244	136.621	3427 kg/m ³	00:02:24
45	170.012	136.595	3406 kg/m ³	00:02:28
46	169.782	136.602	3382 kg/m ³	00:02:32
47	169.483	136.526	3359 kg/m ³	00:02:36
48	169.167	136.533	3327 kg/m ³	00:02:40

Data point	Pressure Bottom - kPa (abs)	Pressure Top - kPa (abs)	Density Calc	Duration
49	168.877	136.508	3300 kg/m ³	00:02:44
50	168.533	136.377	3278 kg/m ³	00:02:48
51	168.257	136.292	3258 kg/m ³	00:02:52
52	168.002	136.296	3232 kg/m ³	00:02:56
53	167.719	136.291	3204 kg/m ³	00:03:00
54	167.451	136.254	3180 kg/m ³	00:03:04
55	167.101	136.179	3152 kg/m ³	00:03:08
56	166.695	136.101	3119 kg/m ³	00:03:12
57	166.362	136.018	3093 kg/m ³	00:03:16
58	166.176	136.094	3066 kg/m ³	00:03:20
59	165.985	136.110	3045 kg/m ³	00:03:24
60	165.792	135.949	3042 kg/m ³	00:03:28
61	165.181	135.865	2988 kg/m ³	00:03:32
62	164.665	135.794	2943 kg/m ³	00:03:36
63	164.222	135.692	2908 kg/m ³	00:03:40
64	163.683	135.550	2868 kg/m ³	00:03:44
65	163.247	135.488	2830 kg/m ³	00:03:48
66	162.755	135.466	2782 kg/m ³	00:03:52
67	162.320	135.351	2749 kg/m ³	00:03:56
68	161.793	135.218	2709 kg/m ³	00:04:00
69	161.342	135.130	2672 kg/m ³	00:04:04
70	160.890	135.122	2627 kg/m ³	00:04:08
71	160.444	135.019	2592 kg/m ³	00:04:12
72	159.977	135.054	2541 kg/m ³	00:04:16
73	159.592	134.974	2510 kg/m ³	00:04:20
74	159.156	134.913	2471 kg/m ³	00:04:24
75	158.720	134.915	2427 kg/m ³	00:04:28
76	158.359	134.911	2390 kg/m ³	00:04:32
77	158.032	134.895	2358 kg/m ³	00:04:36
78	157.999	134.855	2359 kg/m ³	00:04:40
79	157.794	134.910	2333 kg/m ³	00:04:44
80	157.242	134.923	2275 kg/m ³	00:04:48
81	156.859	134.831	2246 kg/m ³	00:04:52
82	156.495	134.775	2214 kg/m ³	00:04:56
83	156.148	134.822	2174 kg/m ³	00:05:00
84	156.023	135.075	2135 kg/m ³	00:05:04
85	156.033	135.263	2117 kg/m ³	00:05:08
86	155.862	135.370	2089 kg/m ³	00:05:12
87	155.542	135.188	2075 kg/m ³	00:05:16
88	155.123	135.023	2049 kg/m ³	00:05:20
89	154.671	134.818	2024 kg/m ³	00:05:24
90	154.135	134.596	1992 kg/m ³	00:05:28
91	153.615	134.500	1949 kg/m ³	00:05:32
92	153.157	134.457	1906 kg/m ³	00:05:36
93	152.796	134.334	1882 kg/m ³	00:05:40
94	152.292	134.316	1832 kg/m ³	00:05:44
95	151.838	134.288	1789 kg/m ³	00:05:48
96	151.369	134.232	1747 kg/m ³	00:05:52
97	150.937	134.173	1709 kg/m ³	00:05:56

Data point	Pressure Bottom - kPa (abs)	Pressure Top - kPa (abs)	Density Calc	Duration
98	150.476	134.120	1667 kg/m ³	00:06:00
99	150.078	134.103	1629 kg/m ³	00:06:04
100	149.688	134.048	1594 kg/m ³	00:06:08
101	149.261	133.951	1561 kg/m ³	00:06:12
102	148.856	133.909	1524 kg/m ³	00:06:16
103	148.415	133.898	1480 kg/m ³	00:06:20
104	148.048	133.875	1445 kg/m ³	00:06:24
105	147.676	133.663	1428 kg/m ³	00:06:28
106	147.273	133.547	1399 kg/m ³	00:06:32
107	146.860	133.465	1365 kg/m ³	00:06:36
108	146.507	133.383	1338 kg/m ³	00:06:40
109	146.134	133.368	1301 kg/m ³	00:06:44
110	145.968	133.242	1297 kg/m ³	00:06:48
111	145.845	132.965	1313 kg/m ³	00:06:52
112	145.422	132.679	1299 kg/m ³	00:06:56
113	144.910	132.369	1278 kg/m ³	00:07:00
114	144.461	132.012	1269 kg/m ³	00:07:04
115	144.010	131.654	1259 kg/m ³	00:07:08
116	143.571	131.241	1257 kg/m ³	00:07:12
117	143.109	130.784	1256 kg/m ³	00:07:16
118	142.665	130.373	1253 kg/m ³	00:07:20
119	142.191	130.071	1235 kg/m ³	00:07:24
120	141.770	129.805	1220 kg/m ³	00:07:28
121	141.388	129.529	1209 kg/m ³	00:07:32
122	140.938	129.268	1190 kg/m ³	00:07:36
123	140.706	129.124	1181 kg/m ³	00:07:40
124	140.437	128.640	1203 kg/m ³	00:07:44
125	140.077	128.207	1210 kg/m ³	00:07:48
126	139.712	127.703	1224 kg/m ³	00:07:52
127	139.332	127.230	1234 kg/m ³	00:07:56
128	138.931	126.992	1217 kg/m ³	00:08:00
129	138.533	126.559	1221 kg/m ³	00:08:04
130	138.141	126.172	1220 kg/m ³	00:08:08
131	137.720	125.652	1230 kg/m ³	00:08:12
132	137.287	125.139	1238 kg/m ³	00:08:16
133	136.915	124.693	1246 kg/m ³	00:08:20
134	136.456	124.247	1245 kg/m ³	00:08:24
135	136.085	123.790	1253 kg/m ³	00:08:28
136	135.632	123.415	1245 kg/m ³	00:08:32
137	135.239	123.105	1237 kg/m ³	00:08:36
138	134.889	122.835	1229 kg/m ³	00:08:40
139	134.514	122.441	1231 kg/m ³	00:08:44
140	134.222	122.061	1240 kg/m ³	00:08:48
141	133.861	121.772	1232 kg/m ³	00:08:52
142	133.536	121.451	1232 kg/m ³	00:08:56
143	133.201	121.135	1230 kg/m ³	00:09:00
144	132.946	120.865	1232 kg/m ³	00:09:04
145	132.617	120.528	1232 kg/m ³	00:09:08
146	132.316	120.208	1234 kg/m ³	00:09:12

Data point	Pressure Bottom - kPa (abs)	Pressure Top - kPa (abs)	Density Calc	Duration
147	132.012	119.946	1230 kg/m ³	00:09:16
148	131.673	119.622	1228 kg/m ³	00:09:20
149	131.352	119.401	1218 kg/m ³	00:09:24
150	131.027	119.056	1220 kg/m ³	00:09:28
151	130.732	118.763	1220 kg/m ³	00:09:32
152	130.455	118.525	1216 kg/m ³	00:09:36
153	130.164	118.299	1209 kg/m ³	00:09:40
154	129.854	118.043	1204 kg/m ³	00:09:44
155	129.621	117.857	1199 kg/m ³	00:09:48
156	129.307	117.612	1192 kg/m ³	00:09:52
157	129.031	117.440	1182 kg/m ³	00:09:56
158	132.468	119.015	1371 kg/m ³	00:10:00

7.2.9 Appendix B.4 - Vertical Pipe loop Test Data

Coarse FeSi less Fines

Data Point	Velocity	Pseudo shear rate	Wall shear stress	Temperature	Coriolis Density
41	1.426 m/s	582 1/s	32.3 Pa	20.0 °C	4277 kg/m ³
42	1.230 m/s	502 1/s	28.2 Pa	19.9 °C	4277 kg/m ³
43	1.013 m/s	413 1/s	22.8 Pa	19.8 °C	4277 kg/m ³
44	0.727 m/s	297 1/s	18.3 Pa	19.6 °C	4277 kg/m ³
52	1.332 m/s	544 1/s	39.6 Pa	19.1 °C	4373 kg/m ³
53	0.954 m/s	389 1/s	28.0 Pa	18.8 °C	4373 kg/m ³
54	0.851 m/s	347 1/s	23.3 Pa	18.7 °C	4373 kg/m ³
55	1.145 m/s	467 1/s	33.0 Pa	18.4 °C	4373 kg/m ³
67	1.169 m/s	477 1/s	43.5 Pa	22.2 °C	4462 kg/m ³
68	0.941 m/s	384 1/s	36.7 Pa	22.1 °C	4462 kg/m ³
69	0.742 m/s	303 1/s	31.5 Pa	22.0 °C	4462 kg/m ³
78	1.387 m/s	566 1/s	52.0 Pa	23.0 °C	4568 kg/m ³
79	1.215 m/s	496 1/s	45.8 Pa	22.9 °C	4568 kg/m ³
80	0.922 m/s	376 1/s	38.9 Pa	22.7 °C	4568 kg/m ³
81	0.574 m/s	234 1/s	29.3 Pa	22.6 °C	4568 kg/m ³
82	2.563 m/s	1046 1/s	111.1 Pa	25.3 °C	4625 kg/m ³
83	2.364 m/s	965 1/s	101.2 Pa	25.5 °C	4625 kg/m ³
84	2.133 m/s	870 1/s	89.2 Pa	25.6 °C	4625 kg/m ³
85	1.974 m/s	806 1/s	81.5 Pa	25.7 °C	4625 kg/m ³
86	1.776 m/s	725 1/s	73.0 Pa	25.8 °C	4625 kg/m ³
87	1.569 m/s	640 1/s	64.6 Pa	25.8 °C	4625 kg/m ³
88	1.340 m/s	547 1/s	55.3 Pa	25.8 °C	4625 kg/m ³
89	1.167 m/s	476 1/s	49.2 Pa	25.6 °C	4625 kg/m ³
90	1.015 m/s	414 1/s	43.3 Pa	25.5 °C	4625 kg/m ³
91	0.853 m/s	348 1/s	36.2 Pa	25.3 °C	4625 kg/m ³
92	2.477 m/s	1011 1/s	88.2 Pa	27.7 °C	4665 kg/m ³
93	2.251 m/s	919 1/s	104.4 Pa	28.0 °C	4665 kg/m ³
94	2.076 m/s	847 1/s	91.9 Pa	28.2 °C	4665 kg/m ³
95	1.934 m/s	789 1/s	84.4 Pa	28.5 °C	4665 kg/m ³
96	1.777 m/s	725 1/s	77.5 Pa	28.5 °C	4665 kg/m ³
97	1.581 m/s	645 1/s	68.8 Pa	28.5 °C	4665 kg/m ³
98	1.337 m/s	546 1/s	58.7 Pa	28.4 °C	4665 kg/m ³
99	1.146 m/s	468 1/s	51.6 Pa	28.1 °C	4665 kg/m ³
100	0.912 m/s	372 1/s	41.8 Pa	28.0 °C	4665 kg/m ³

Process FeSi less Fines

Data Point	Velocity	Pseudo shear rate	Wall shear stress	Temperature	Coriolis Density
4	2.246 m/s	917 1/s	55.5 Pa	26.5 °C	3670 kg/m ³
5	1.992 m/s	813 1/s	49.7 Pa	26.1 °C	3670 kg/m ³
6	1.755 m/s	716 1/s	43.1 Pa	25.5 °C	3670 kg/m ³
7	1.395 m/s	569 1/s	34.7 Pa	25.2 °C	3670 kg/m ³
8	1.049 m/s	428 1/s	26.6 Pa	24.9 °C	3670 kg/m ³
9	1.223 m/s	499 1/s	31.4 Pa	24.6 °C	3670 kg/m ³
10	1.568 m/s	640 1/s	38.2 Pa	24.3 °C	3670 kg/m ³
11	0.800 m/s	327 1/s	20.7 Pa	23.8 °C	3670 kg/m ³
14	2.349 m/s	959 1/s	92.1 Pa	21.9 °C	3812 kg/m ³
15	2.211 m/s	902 1/s	84.8 Pa	22.1 °C	3812 kg/m ³
16	1.999 m/s	816 1/s	74.6 Pa	22.1 °C	3812 kg/m ³
17	1.850 m/s	755 1/s	68.4 Pa	22.2 °C	3812 kg/m ³
18	1.627 m/s	664 1/s	59.8 Pa	22.1 °C	3812 kg/m ³
19	1.387 m/s	566 1/s	50.9 Pa	22.0 °C	3812 kg/m ³
20	1.123 m/s	458 1/s	42.7 Pa	21.9 °C	3812 kg/m ³
23	2.213 m/s	903 1/s	132.8 Pa	23.1 °C	3910 kg/m ³
24	2.065 m/s	843 1/s	120.0 Pa	23.4 °C	3910 kg/m ³
25	1.950 m/s	796 1/s	110.1 Pa	23.8 °C	3910 kg/m ³
26	1.834 m/s	749 1/s	101.4 Pa	24.1 °C	3910 kg/m ³
27	1.693 m/s	691 1/s	91.5 Pa	24.2 °C	3910 kg/m ³
28	1.565 m/s	639 1/s	83.6 Pa	24.4 °C	3910 kg/m ³
29	1.418 m/s	579 1/s	74.4 Pa	24.3 °C	3910 kg/m ³
30	1.259 m/s	514 1/s	65.2 Pa	24.3 °C	3910 kg/m ³
31	1.131 m/s	462 1/s	57.8 Pa	24.2 °C	3910 kg/m ³
32	1.009 m/s	412 1/s	51.5 Pa	24.0 °C	3910 kg/m ³
33	0.796 m/s	325 1/s	42.2 Pa	23.8 °C	3910 kg/m ³
34	0.582 m/s	237 1/s	33.4 Pa	23.7 °C	3910 kg/m ³
37	2.082 m/s	850 1/s	129.1 Pa	34.0 °C	3994 kg/m ³
38	1.979 m/s	808 1/s	116.7 Pa	34.4 °C	3994 kg/m ³
39	1.838 m/s	750 1/s	105.3 Pa	34.7 °C	3994 kg/m ³
40	1.676 m/s	684 1/s	98.1 Pa	34.9 °C	3994 kg/m ³
41	1.587 m/s	648 1/s	90.6 Pa	34.8 °C	3994 kg/m ³
42	1.432 m/s	585 1/s	82.2 Pa	34.7 °C	3994 kg/m ³
43	1.247 m/s	509 1/s	71.6 Pa	34.5 °C	3994 kg/m ³
44	1.101 m/s	449 1/s	64.4 Pa	34.3 °C	3994 kg/m ³
45	1.046 m/s	427 1/s	59.1 Pa	33.8 °C	3994 kg/m ³
46	0.898 m/s	367 1/s	53.6 Pa	33.5 °C	3994 kg/m ³
47	0.685 m/s	280 1/s	42.1 Pa	33.3 °C	3994 kg/m ³
1	2.264 m/s	924 1/s	109.7 Pa	45.5 °C	3980 kg/m ³
2	2.045 m/s	835 1/s	101.0 Pa	45.5 °C	3980 kg/m ³
3	1.878 m/s	767 1/s	91.9 Pa	45.3 °C	3980 kg/m ³
4	1.773 m/s	724 1/s	86.3 Pa	45.0 °C	3980 kg/m ³
5	1.678 m/s	685 1/s	80.5 Pa	44.6 °C	3980 kg/m ³
6	1.553 m/s	634 1/s	76.2 Pa	44.5 °C	3980 kg/m ³
7	1.394 m/s	569 1/s	68.8 Pa	44.2 °C	3980 kg/m ³
8	1.280 m/s	523 1/s	62.7 Pa	43.9 °C	3980 kg/m ³
9	1.069 m/s	436 1/s	52.7 Pa	43.6 °C	3980 kg/m ³

Coarse FeSi with Rheology Modifier

Data Point	Velocity	Pseudo shear rate	Wall shear stress	Temperature	Coriolis Density	Rheology Modifier
16	2.346 m/s	958 1/s	69.1 Pa	24.0 °C	4506 kg/m ³	not added
17	2.050 m/s	837 1/s	60.1 Pa	24.1 °C	4506 kg/m ³	not added
18	1.759 m/s	718 1/s	51.7 Pa	24.1 °C	4506 kg/m ³	not added
19	1.508 m/s	616 1/s	45.0 Pa	24.1 °C	4506 kg/m ³	not added
20	1.207 m/s	493 1/s	37.3 Pa	24.1 °C	4506 kg/m ³	not added
21	0.996 m/s	407 1/s	32.1 Pa	24.0 °C	4506 kg/m ³	not added
22	0.702 m/s	286 1/s	25.1 Pa	24.0 °C	4506 kg/m ³	not added
33	2.264 m/s	924 1/s	54.9 Pa	28.7 °C	4500 kg/m ³	added
34	2.037 m/s	832 1/s	49.9 Pa	28.2 °C	4500 kg/m ³	added
35	1.654 m/s	675 1/s	41.6 Pa	27.9 °C	4500 kg/m ³	added
36	1.452 m/s	593 1/s	36.6 Pa	27.5 °C	4500 kg/m ³	added
37	1.116 m/s	456 1/s	30.1 Pa	27.1 °C	4500 kg/m ³	added
38	0.834 m/s	340 1/s	24.9 Pa	26.8 °C	4500 kg/m ³	added
39	0.597 m/s	244 1/s	20.1 Pa	26.4 °C	4500 kg/m ³	added
48	2.372 m/s	968 1/s	39.5 Pa	23.4 °C	4357 kg/m ³	added
49	2.205 m/s	900 1/s	36.4 Pa	23.2 °C	4357 kg/m ³	added
50	2.039 m/s	832 1/s	33.9 Pa	23.0 °C	4357 kg/m ³	added
51	1.792 m/s	731 1/s	30.5 Pa	22.8 °C	4357 kg/m ³	added
52	1.492 m/s	609 1/s	30.7 Pa	22.6 °C	4357 kg/m ³	added
53	1.124 m/s	459 1/s	25.4 Pa	22.5 °C	4357 kg/m ³	added
54	0.758 m/s	309 1/s	21.0 Pa	22.3 °C	4357 kg/m ³	added
64	2.204 m/s	900 1/s	26.8 Pa	20.9 °C	4170 kg/m ³	added
65	1.980 m/s	808 1/s	24.9 Pa	20.6 °C	4170 kg/m ³	added
66	1.788 m/s	730 1/s	22.4 Pa	20.4 °C	4170 kg/m ³	added
67	1.496 m/s	611 1/s	19.9 Pa	20.3 °C	4170 kg/m ³	added
68	1.300 m/s	531 1/s	18.1 Pa	20.0 °C	4170 kg/m ³	added
69	1.096 m/s	447 1/s	16.3 Pa	19.8 °C	4170 kg/m ³	added
83	1.576 m/s	643 1/s	15.2 Pa	18.0 °C	3947 kg/m ³	added
84	1.392 m/s	568 1/s	13.6 Pa	17.7 °C	3947 kg/m ³	added
85	1.104 m/s	450 1/s	12.5 Pa	17.6 °C	3947 kg/m ³	added
86	0.809 m/s	330 1/s	10.7 Pa	17.5 °C	3947 kg/m ³	added
87	0.516 m/s	210 1/s	9.2 Pa	17.4 °C	3947 kg/m ³	added
13	1.478 m/s	603 1/s	15.9 Pa	22.9 °C	3944 kg/m ³	not added
14	1.280 m/s	522 1/s	15.2 Pa	22.7 °C	3944 kg/m ³	not added
15	0.982 m/s	401 1/s	12.5 Pa	22.6 °C	3944 kg/m ³	not added
16	1.094 m/s	446 1/s	12.4 Pa	21.9 °C	3944 kg/m ³	not added
17	0.643 m/s	263 1/s	10.1 Pa	21.8 °C	3944 kg/m ³	not added
25	1.542 m/s	629 1/s	14.6 Pa	23.2 °C	3967 kg/m ³	added
26	1.264 m/s	516 1/s	13.6 Pa	23.1 °C	3967 kg/m ³	added
27	0.980 m/s	400 1/s	10.8 Pa	23.0 °C	3967 kg/m ³	added
28	0.529 m/s	216 1/s	9.3 Pa	22.9 °C	3967 kg/m ³	added
4	2.171 m/s	886 1/s	31.7 Pa	26.5 °C	4262 kg/m ³	not added
5	1.792 m/s	732 1/s	28.5 Pa	26.3 °C	4262 kg/m ³	not added
6	1.576 m/s	643 1/s	24.2 Pa	26.2 °C	4262 kg/m ³	not added
7	1.074 m/s	438 1/s	19.2 Pa	26.1 °C	4262 kg/m ³	not added
8	0.393 m/s	160 1/s	10.8 Pa	26.0 °C	4262 kg/m ³	not added
9	1.364 m/s	557 1/s	21.8 Pa	25.3 °C	4262 kg/m ³	not added
10	0.869 m/s	355 1/s	14.7 Pa	25.2 °C	4262 kg/m ³	not added
11	0.495 m/s	202 1/s	12.4 Pa	25.2 °C	4262 kg/m ³	not added
25	2.390 m/s	975 1/s	32.0 Pa	24.3 °C	4262 kg/m ³	added
26	1.923 m/s	785 1/s	25.8 Pa	24.1 °C	4262 kg/m ³	added
27	1.480 m/s	604 1/s	20.6 Pa	24.0 °C	4262 kg/m ³	added
28	1.070 m/s	437 1/s	17.3 Pa	24.0 °C	4262 kg/m ³	added
29	0.521 m/s	213 1/s	11.7 Pa	23.9 °C	4262 kg/m ³	added

APPENDIX C: CITECT SCADA DISPLAY

